HYDROXY CRUCIFORMS AND BIS(HYDROXYSTYRYL)BENZENES: SYNTHESIS, STRUCTURE, AND PHOTOPHYSICAL PROPERTIES OF NOVEL π-SYSTEMS

A Dissertation
Presented to
The Academic Faculty

By

Psaras Lamar McGrier

In Partial Fulfillment
Of the Requirements for the Degree
Doctor of Philosophy in Chemistry

Georgia Institute of Technology

December, 2010

HYDROXY CRUCIFORMS AND BIS(HYDROXYSTYRYL)BENZENES: SYNTHESIS, STRUCTURE, AND PHOTOPHYSICAL PROPERTIES OF NOVEL π-SYSTEMS

Dr. Uwe H. F. Bunz, Advisor
School of Chemistry and Biochemistry
Georgia Institute of Technology

Dr. Laren M. Tolbert
School of Chemistry and Biochemistry
Georgia Institute of Technology

Dr. Mostafa El-Sayed
School of Chemistry and Biochemistry
Georgia Institute of Technology

Dr. David M. Collard
School of Chemistry and Biochemistry
Georgia Institute of Technology

Dr. Anselm Griffin
School of Polymer, Textile, and Fiber Engineering
Georgia Institute of Technology

Date Approved: May 6th, 2010

ACKNOWLEDGEMENTS

First, I would like to thank my advisor, Dr. Uwe Bunz, for his continued support and friendship. Your passion to achieve the highest quality of science possible has been a true inspiration to me. Without your guidance and tough love, none of the work presented in this dissertation would be possible.

Next, I would like to thank the members of my committee – Dr. Laren Tolbert, Dr. David Collard, Dr. Mostafa El-Sayed, and Dr. Anselm Griffin- for dedicating their time, energy, and advice whenever needed. To Dr. Collard, thank you for being very supportive of me from the beginning to the end. I would like to send a special thank you to Dr. Laren Tolbert, Dr. Kyril Solntsev, and Dr. Christoph Fahrni for their help in understanding and interpreting the photophysical properties of my materials. It has been fun collaborating with all of you to accomplish some amazing science, and I will miss our conversations together. I would also like to thank Dr. Vincent Rotello and Oscar Miranda for their help with the statistical analysis of my data. Thanks to Rebecca Shiels and Dr. Chris Jones for providing the silica materials for the cruciform-hybrid sensory investigations.

I would like to thank (some of the smartest people I have ever had the priviledge of working with) the past and present members of the Bunz Group: Dr. James Wilson, Dr. Anthony Zucchero, Dr. Ronnie Phillips, Dr. Shaobin Miao, Dr. Ik-Bum Kim, Dr. Juan Tolosa, Bradley Carson, Jake Leech, Scott Brombosz, Drew Zappas, Chris Kub, Ewelina Kieley, Jonny Bryant, Steven Hayden, Anthony Appleton, Nancy Berger, and Imani Jones. I would like to send a special thanks to Dr. James Wilson and Dr. Anthony

Zucchero for the advancements they have made with their exploration of cruciform fluorophores. Without your contributions, my work would not be possible. I also would like to thank Scott Brombosz. We came into the Bunz group together, and now we will graduate together. Thank you for being a competitive inspiration and a good friend.

I would also like to thank the chemistry department at the University of South Carolina-Aiken for their help and support: in particular Dr. Monty Fetterolf, Dr. Kutty Pariyadath, Dr. Ann Willbrand, Dr. Jack Goldsmith, and Dr. Bill Pirkle. Each one of you have touched my life as an undergraduate student, and have encouraged me to further my education. That encouragement has led me to this point. I thank you all for the time, inspiration, and support that you have given me over the years.

I would like to thank my parents, Melvin and Barbara, for their love and support. Both of you have stood behind me no matter the cause or situation, and I am truly grateful. Your support has pulled me through some rough times, and I am truly blessed to have parents as wonderful as you.

Finally, I would like to thank my fiancée Brishundra Berry and our baby girl Breana. We have endured a lot over the years, but our love for one another has always pulled us through. Thank you both for always being there for me no matter what, and providing me with the strength and encouragement to accomplish my goals. I look forward to our life together, and being as supportive of you as you have been of me.

TABLE OF CONTENTS

LIST OF TABLES

LIST OF FIGURES

LIST OF SCHEMES

LIST OF ABBREVIATIONS

Å	angstrom
Abs	absorbance
AcOH	acetic acid
Ar	aryl
°C	degrees Celsius
cm^{-1}	wavenumber
δ	chemical shift
d	days
DBU	1,8-diaza-bicyclo[5.4.0]undec-7-ene
DCM	dichloromethane
DI	deionized
DMF	dimethylformamide
DMSO	dimethylsulfoxide
EI	electrospray ionization
ε	molar absorptivity
Et_2O	diethyl ether
EtOAc	ethyl acetate
EtOH	ethanol
Eq	equivalents
ESPT	excited state proton transfer
ex	excitation
Δf	polarizability

FAB	fast atom bombardment
FMO	frontier molecular orbital
g	gram
HOMO	highest occupied molecular orbital
h	hour
HCSH	Heck-Cassar-Sonogashira-Hagihara
Hz	hertz
IPA	isopropyl alcohol
IR	infrared
ISC	intersystem crossing
J	coupling constant
K_a	association constant
KOH	potassium hydroxide
KT	Kamlet-Taft
L	liter
LED	light emitting device
LDA	linear discriminant analysis
LUMO	lowest unoccupied molecular orbital
m/z	mass-to-charge ratio
MP	melting point
MeOH	methanol
mg	milligram
MHz	megaHertz

min	minute
mL	milliliter
mmol	millimole
μL	microliter
μm	micrometer
M	molaity
mM	millimolar
MP	melting point
MO	molecular orbital
NaH	sodium hydride
NaOH	sodium hydroxide
nm	nanometer
NBS	*N*-Bromosuccinimide
NMR	nuclear magnetic resonance
OTf	trifluoromethanesulfonate
%	percent
Φ_F	fluorescence quantum yield
pH	potentiometric hydrogen ion concentration
pK_a	acid dissociation constant
Ppb	parts per billion
PPE	poly(*para*-phenyleneethynylene)
Ppm	parts per million
PPV	poly(*para*-phenylenevinylene)

RGB	red, green blue
rt	room temperature
TBAF	tetrabutylammonium fluoride
TBAOH	tetrabutylammonuim hydroxide
TD-DFT	time dependent-density functional theory
TEA	triethylamine
TFA	trifluoroacetic acid
THF	tetrahydrofuran
THP	tetrahydropyranyl
TIPS	triisopropylsilane
TLC	thin layer chromatography
TMS	trimethylsilane
TS	trans-stilbene
TTSB	trans,trans-distyrylbenzene
Triflate	trifluoromethanesulfonate
UV	ultra-violet
VOC	volatile organic compound
XF	cruciform

SUMMARY

This thesis examines the synthesis, photophysical properties, and sensory responses of hydroxy-substituted 1,4-distyryl-2,5-bis(arylethynyl)benzenes (Cruciforms, XFs). These two-dimensional cross-conjugated materials possess spatially separated frontier molecular orbitals (FMOs). This spatial separation allows the HOMO and LUMO to be addressed independently by analytes, which leads to significant changes in their absorption and emission. These properties allow XFs to be utilized for the detection of various analytes. These studies highlight the benefits of utilizing XFs for the development of advanced functional solid state materials for sensory applications.

Chapter 1

Cruciform Fluorophores: Background and Focus of Dissertation

1.1 Introduction

Conjugated organic materials have attracted much attention as fluorescent sensors and components in organic electronics. In order for dyes to exhibit ratiometric sensory responses, the interaction of the analyte must elicit a change in the fluorophore's HOMO-LUMO gap. This implies that one frontier molecular orbital (FMO) must be disportionally affected by analyte interaction. The HOMO and LUMO of a majority of organic fluorophores are "congruent", i.e. their orbital coefficients are of similar magnitude. As a consequence, one would not expect large spectral shifts in color or emission wavelengths upon binding to an analyte. The position of the HOMO and LUMO should be more or less equally affected, resulting in only small changes in the HOMO-LUMO gap.

A seductive strategy to develop responsive fluorophores is to design molecular architectures possessing spatially separated FMOs. Due this design, electronic information becomes spatially encoded as recognition elements can be incorporated into the fluorophore such that analyte binding independently influences the FMOs. Interest in materials possessing spatially separated FMOs has prompted the exploration of new two-dimensional conjugated materials[1] ; including spiro compounds,[2] paracyclophanes,[3] swivel-type dimers,[4] bisoxazole derived cruciforms,[5] tetraethynylethenes,[6] and tetrasubstituted tolanes.[7] Subsets of these compounds are constructed from two perpendicular pi-conjugated linear arms connected through a central aromatic core;

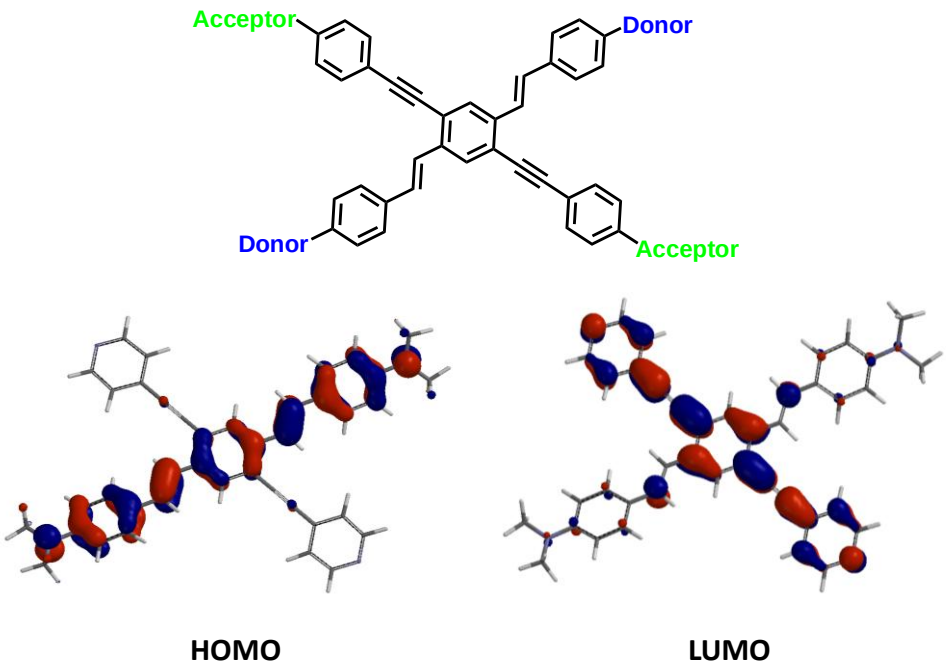

Figure 1.1. General structure of an XF (top). The bottom depicts the FMO distribution of a donor-acceptor substituted XF, illustrating the FMO separation induced upon donor-acceptor substitution of the XF.

examples include tetrakis(arylethynyl)benzenes,[8] tetrakis(styryl)benzenes,[9] and tetrasubstituted thiophenes.[10]

Motivated by the desire to design new two-dimensional molecular architectures, the Bunz group has actively investigated the photophysical properties of 1,4-distyl-2,5-bisarylethynylbenzenes (cruciforms, XFs).[11] XFs are composed of two linear π-conjugated arms, a perpendicular distyryl branch and an arylethynyl branch, connected to a central benzene core. Analysis of the electronic structure of XFs has revealed that donor and acceptor substitution results in compounds possessing spatially disjoint molecular orbitals; in these cases the HOMO and LUMO localize on the "orthogonal" arms of the XFs (Figure 1.1). This separation of the FMOs has significant consequences for the photophysics of XFs and has led to their use as building blocks in supramolecular

assemblies,[12] components in molecular electronics,[13] and most notably as responsive cores in sensory schemes.[14]

1.2 Origin of Cruciforms

XFs have emerged from the Bunz groups extensive research in poly(para-phenyleneethynylene)s (PPEs), a class of conjugated polymers related to poly(phenylenevinylene)s (PPVs).[15] Although their chemical and thermal properties make them attractive candidates for many devices, PPEs do not share the balanced performance of PPVs in organic device applications; hole injection is a particular problem. Attempts to solve this problem by introducing vinyl groups into the main chain did not improve performance as **1.3** resembles **1.1** much more than **1.2** with respect to its optical and solid state semiconducting properties.[16] In a second attempt to introduce PPV character in to PPE architectures, we synthesized polymers of type **1.4a-c** incorporating styryl groups in the side chain.[17] In these systems, the solution and solid state band gap shrinks from **1.4a** to **1.4c**. Hole injection is considerably facilitated, particularly in **1.4c**, which was explored in a photodiode-type application; **1.4c** is more electron rich than PPV .[17] Cyclic voltammetry revealed that increasing donor strength in the distyrylbenzene arms (from **1.4a** to **1.4c**) exclusively affects the HOMO position. Only later would we come to understand the significance of this discovery; *these cross-conjugated architectures permit the spatial separation of FMOs.*

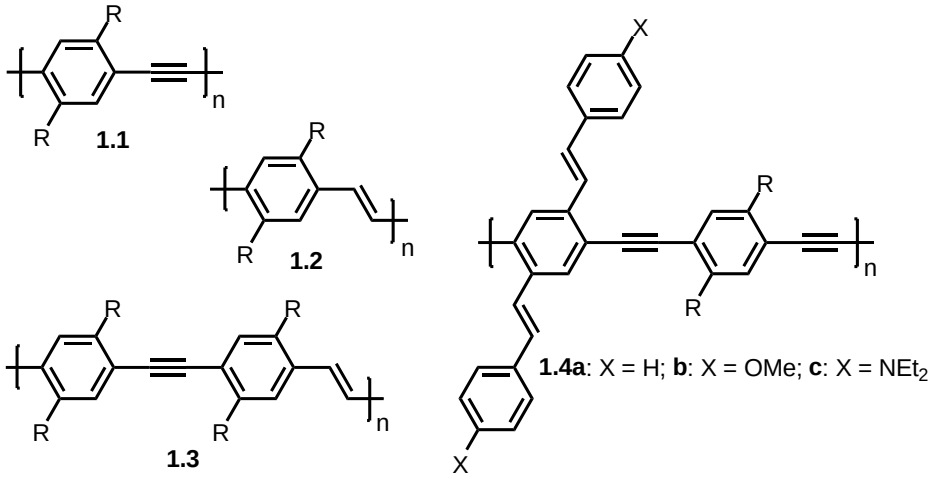

Figure 1.2. Structure of several classes of conjugated polymers, including PPEs (**1.1**), PPVs (**1.2**), and hybrid polymers **1.3** and **1.4a**-**c**.

1.3 Synthetic Methodology

XFs are constructed from a common tetrahalide precursor, 2,5-bis(bromomethyl)-1,4-diiodobenzene (**1.7**, Scheme **1.1**). This compound is produced in a two step synthetic sequence from *para*-xylene. Iodination of **1.5** following bromination of **1.6** with N-bromosuccinimide produces the tetrahalide precursor **1.7**.[18] This radical bromination typically produces an inseparable mixture of 2,5-bis(bromomethyl)-1,4-diiodobenzene (90%) and the halogen exchanged 1-iodo-4-bromo-2,5-bis (bromomethyl)benzene (10%). Although this halogen exchange material is present, this mixture can still successfully be utilized in the synthesis of XFs.

1.7 can be reacted with triethylphosphite in an Arbuzov reaction to form the bisphosphonate **1.8**. A Horner[19] olefination of bisphosphonate **1.8** with any suitable aromatic aldehyde and potassium tert-butoxide in THF can produce the diiodide **1.9**. These diiodides are typically obtained as brilliant yellow-to-orange crystalline powders. Subsequently, a Sonogashira-Hagihara[15,20] coupling with any suitable alkyne can be performed to complete the synthetic sequence to give the XFs. This can be achieved by

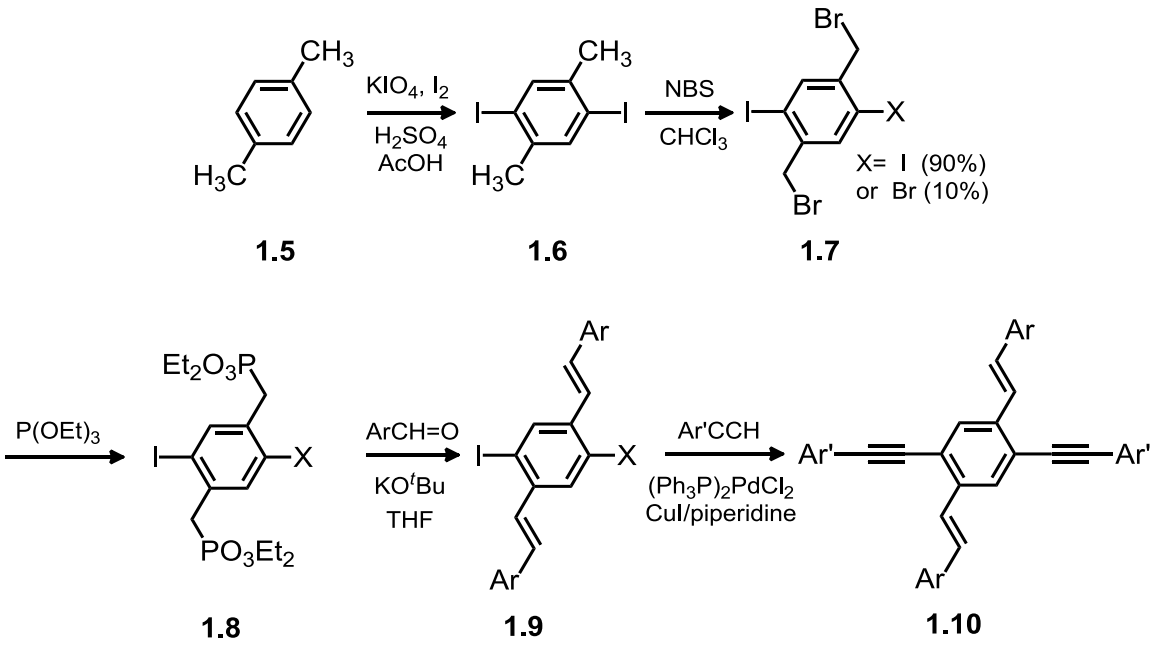

Scheme 1.1. General synthesis of XFs.

utilizing a $(Ph_3P)_2PdCl_2$/CuI catalyst system with piperidine as the base and THF as the solvent. Due to the versatility of both Horner and Sonogashira reactions, this synthetic sequence allows for the construction of any conceivable XF (**1.10**) so long as the desired aldehydes and alkynes are available.

1.4 Photophysical Properties

Utilizing the synthetic scheme shown in the previous section, we have prepared and studied the photophysics of XFs **1.11-1.16** (Figure 1.3).[11j] We discovered that the photophysical properties of these XFs can be tuned by varying the substitution of the XF traverses. When dissolved in dichloromethane, XFs **1.11-1.16** display distinct emission colors ranging from blue to orange (Figure 1.4).

XFs **1.11-1.13** display strong absorptions in hexanes at approximately 325 nm with a second feature appearing as shoulder at roughly 350 to 360 nm. Introducing donor

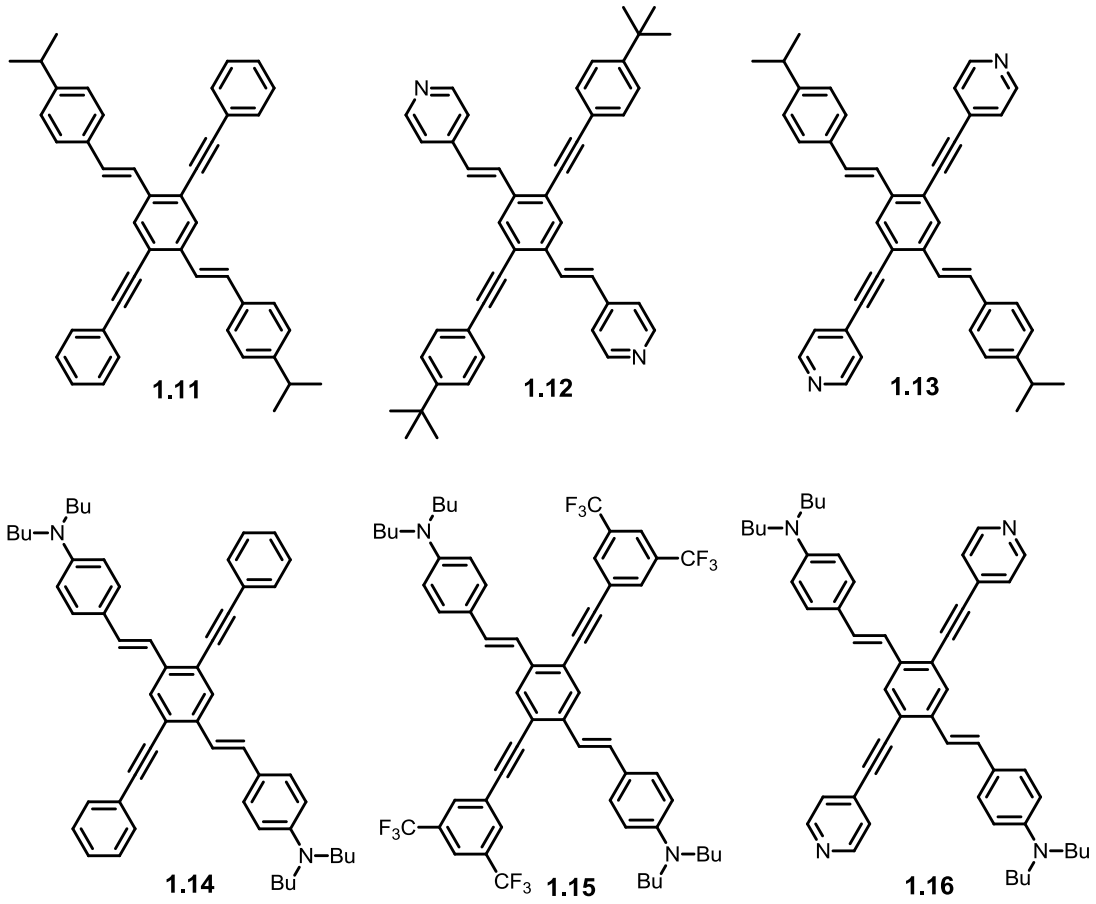

Figure 1.3. Structure of XFs **1.11-1.16.**

Figure 1.4. Emission of XFs **1.11-1.16** in dichloromethane under blacklight irradiation (λ_{max} =365 nm)

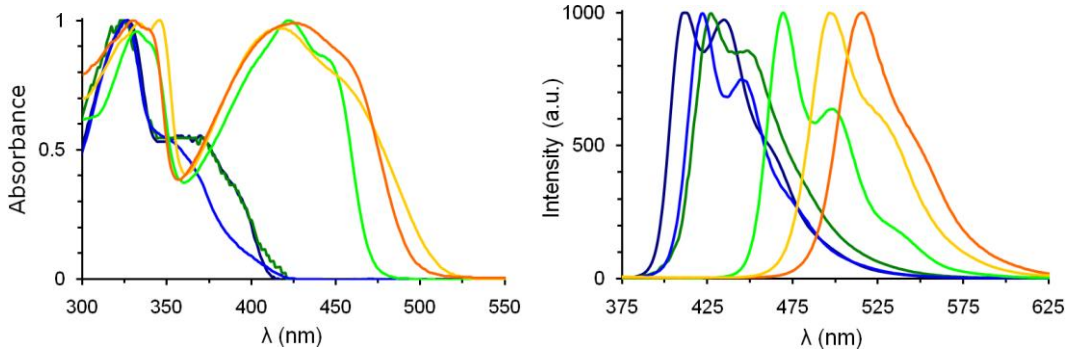

Figure 1.5. Normalized absorption (left) and emission (right) of XFs **1.11**(dark blue), **1.12**(light blue), **1.13**(dark green), **1.14**(light green), **1.15**(yellow), and **1.16**(orange) in hexanes.

(**1.14**) or donor-acceptor (**1.15** and **1.16**) substituition, we observe a charge transfer band at lower energy around 430 nm (Figure 1.5). In the emission spectra, XFs **1.11-1.13** display vibrant blue emissions with well defined vibronic structure. Dibutylamino substituted **1.14** displays a similar vibronic structure but with a red-shifted emission maximum around 469 nm. Upon donor-acceptor substituition (**1.15** and **1.16**), the emission becomes increasingly red-shifted and the vibronic coupling disappears. The quantum yields for these XFs are robust and range from 0.09 to 0.70 in halogenated solvents. XFs are considered to be distyrylbenzene derivatives. However, the emissive lifetimes are usually no longer than $\tau \approx 4$ ns, atypical for distyrylbenzene derivatives, which normally display shorter lifetimes of approximately $\tau \approx 1$ ns.[21]

FMO Structure of XFs

Varying substitution of the XF framework results in differentiated spectroscopic properties. In effort to rationalize their optical properties, we performed quantum chemical calculations on simplified analogues of XFs **1.17** and **1.18**. B3LYP 6-31G**//6-31G** calculations provide an understanding of ground state properties and

HOMO-LUMO gaps when examining trends in a series of related compounds. In the unsubstituted parent XF **1.17**, the HOMO and LUMO are evenly distributed over the π-system, with larger coefficients on the central benzene ring and smaller ones on the peripheral phenyl rings (Figure 1.6). This distribution is typical of π-conjugated hydrocarbons. Donor-acceptor substitution of the XF framework elicits a large change in the coefficient distribution of the FMOs. In the case of **1.18**, possessing donor substituents on the distyryl axis of the XF and acceptor substituents on the arylethynyl axis of the XF, HOMO and LUMO show a spatially *disjoint* distribution. *The donor and acceptor substituents localize the FMOs on the respective arylethynyl and styryl branches*.

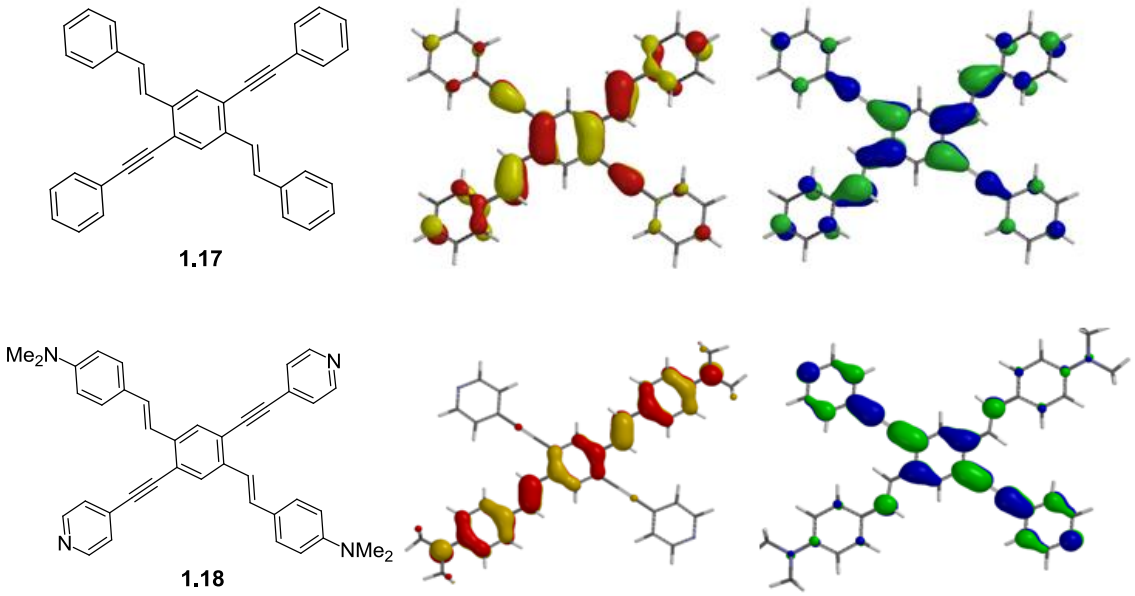

Figure 1.6. Top: Frontier molecular orbitals of **1.17** (Spartan, B3LYP 6-31G**//6-31G**); left: HOMO (-5.17 eV), right: LUMO (-2.00 eV). Bottom: Frontier orbitals of **1.18** (Spartan, B3LYP 6-31G**//6-31G**); left: HOMO (-4.63 eV) and right: LUMO (-2.07 eV) are now localized on the different branches of the molecule.

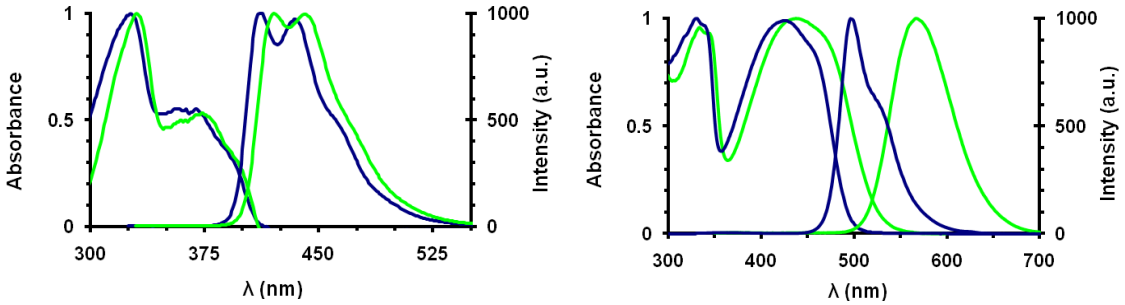

Figure 1.7. Normalized absorption and emission spectra of Class C XF **1.11** (left) and Class D XF **1.16** (right) in hexanes (blue trace) and dichloromethane (green trace).

The ability of substitution to tune the FMO distribution, and as a result the optical properties, of XFs allows us to divide these chromophores into two subsets. *Class D* XFs show a *disjoint* FMO structure as a consequence of donor-acceptor substitution of the framework. On the other hand, cruciforms that are not significantly donor/acceptor substituted possess spatially superimposable FMOs; we propose to call these *Class C* XFs in reference to their spatially *congruent* FMO arrangement. The distinction between Class C and Class D XFs is rigidly defined; however, the gradual transition between the two coincides with the appearance of a charge transfer band in the absorption spectra and a loss of vibronic features in the emission spectra (Figure 1.7).

1.6 Focus of Dissertation

This dissertation comprises an extensive examination of hydroxy-substituted XFs, including their synthesis, investigation of their photophysical properties, and evaluation of their sensory responses upon exposure to aliphatic amines. In an effort to fully understand the spectroscopic responses generated by hydroxy XFs, this dissertation also explores the fundamental photophysical properties of hydroxy-substituted

distyrylbenzenes and bisarylethynylbenzenes. The following distinct projects will form the body of my thesis:

- Photophysical properties of hydroxycruciforms
- Anomalous photophysics of bis(hydroxystyryl)benzenes
- Hydroxycruciforms: amine responsive fluorophores
- Cruciform-silica hybrid materials
- Acidochromicity of bisarylethynylbenzenes: hydroxy versus dialkylamino substituents
- Hydroxy-dialkylamino cruciforms: dual reponse to protons, base, selected metal ions and aliphatic amines

These research endeavors have uncovered the spectroscopic responses of hydroxy XFs towards various analytes, highlighting their ability to be used to create functional solid state materials for sensory applications.

1.7 References and Notes

1. (a) Opsitnick, E.; Lee, D. *Chem. Eur. J.* **2007**, *13*, 7040-7049. (b) Galbrecht, F.; Bönnagel, T.; Bilge, A.; Scherf, U.; Farrell, T. Cruciform-Conjugated Oligomers. In *Functional Organic Materials – Syntheses, Strategies, and Applications;* Müller, T. J. J., Bunz, U. H. F., Eds.; Wiley-VCH: Heidelberg, **2007**, 83-118.

2. (a) Saragi, T. P. I.; Spehr, T.; Siebert, A.; Fuhrmann-Lieker, T.; Salbeck, J. Spiro compounds for organic optoelectronics. *Chem. Rev.* **2007**, *107*, 1011-1065. (b) Shirota, Y.; Kageyama, H.. *Chem. Rev.* **2007**, *107*, 953-1010.

3. (a) Bartholomew, G. P.; Bazan, G. C. Acc. Chem. Res. **2001,** 34, 30-39. (b) Bartholomew, G. P.; Rumi, M.; Pond, S. J. K.; Perry, J. W.; Tretiak, S.; Bazan, G. C. *J. Am. Chem. Soc.* **2004**, *126*, 11529-11542. (c) Bartholomew, G. P.; Bazan, G. C. *J. Am. Chem. Soc.* **2002**, *124*, 5183-5196.

4. (a) Zen, A.; Pingel, P.; Jaiser, F.; Neher, D.; Grenzer, J.; Zhuang, W.; Rabe, J. P.; Bilge, A.; Galbrecht, F.; Nehls, B. S.; Farrell, T.; Scherf, U.; Abellon, R. D.; Grozema,F. C.; Siebbeles, L. D. A. *Chem. Mater.* **2007,** *19*, 1267-1276. (b) Bilge,

A.; Zen, A.; Forster, M.; Li, H.; Galbrecht, F.; Nehls, B. S.; Farrell, T.; Neher, D.; Scherf, U. *J. Mater. Chem.*, **2006**, *16*, 3177–3182.

5. (a) Klare, J. E.; Tulevski, G. S.; Sugo, K.; de Picciotto, A.; White, K. A.; Nuckolls, C. *J. Am. Chem. Soc.* **2003**, *125*, 6030-6031. (b) Klare, J. E.; Tulevski, G. S.; Nuckolls, C. *Langmuir.* **2004**, *20*, 10068-10072. (c) Florio, G. M.; Klare, J. E.; Pasamba, M. O.; Werblowsky, T. L.; Hyers, M.; Berne, B. J.; Hybertsen, M. S.; Nuckolls, C.; Flynn, G. W. . *Langmuir.* **2006**, *22*, 10003-10008.

6. (a) Nielsen, M. B.; Diederich, F. *Chem. Rev.* **2005**, *105*, 1837-1867. (b) Kivala, M.; Diederich, F. *Acc. Chem. Res.* **2009**, *42*, 235-248.

7. (a) Tolosa, J.; Díez-Barra, E.; Sánchez-Verdú, P.; Rodríguez-López, J. *Tetrahedron Lett*. **2006**, *47*, 4647-4651.

8. (a) Marsden, J. A.; Miller, J. J.; Shirtcliff, L. D.; Haley, M. M. *J. Am. Chem. Soc.* **2005**, *127*, 2464-2476. (b) Spitler, E. L.; Shirtcliff, L. D.; Haley, M. M. *J. Org. Chem.* **2007**, *72*, 86-96. (c) Slepkov, A. D.; Hegmann, F. A.; Tykwinski, R. R.; Kamada, K.; Ohta, K.; Marsden, J. A.; Spitler, E. L.; Miller, J. J.; Haley, M. H. *Opt. Lett.* **2006**, *31*, 3315-3317. (d) Spitler, E. L.; Haley, M. M. *Tetrahedron.* **2008**, *64*, 11469-11474.

9. (a) Fratiloiu, S.; Senthilkumar, K.; Grozema, F. C.; Christian-Pandya, H.; Niazimbetova, Z. I.; Bhandari, Y. J.; Galvin, M. E.; Siebbeles, L. D. *Chem. Mater.* **2006**, *18*, 2118-2129. (b) Niazimbetova, Z. I.; Christian, H. Y.; Bhandari, Y. j.; Beyer, F. L.; Galvin, M. E. *J. Phys. Chem. B.* **2004**, *108*, 8673-8681. (c) Christian-Pandya, H. K.; Niazimbetova, Z. I.; Beyer, F. L.; Galvin, M. E. *Chem. Mater.* **2007**, *19*, 993-1001.

10. (a) Hsu, H.-F.; Kuo, C.-H.; Chen, C.-F.; Lin, Y.-H.; Huang, L.-Y.; Chen, C.-H.; Cheng, K.-C.; Chen, H.-H. *Chem. Mater.* **2004**, *16*, 2379-2385. (b) Sun, X. B.; Zhou, Y. H.; Wu, W. C.; Liu, Y. Q.; Tian, W. J.; Yu, G.; Qiu, W. F.; Chen, S. Y.; Zhu, D. B. *J. Phys. Chem. B.* **2006**, *110*, 7702-7707. (c) Sun, X. B.; Liu, Y. Q.; Chen, S. Y.; Qiu, W. F.; Yu, G.; Ma, Y. Q.; Qi, T.; Zhang, H. J.; Xu, X. J.; Zhu, D. B. *Adv. Funct. Mater.* **2006**, *16*, 917-925.

11. (a) Wilson, J. N.; Hardcastle, K. I.; Josowicz, M.; Bunz, U. H. F. *Tetrahedron.* **2004**, *60*, 7157-7167. (b) Wilson, J. N.; Bunz, U. H. F. *J. Am. Chem. Soc.* **2005**, *127*, 4124-4125. (c) Zucchero, A. J.; Wilson, J. N.; Bunz, U. H. F. *J. Am. Chem. Soc.* **2006**, *128*, 11872-11881. (d) Tolosa, J.; Zucchero, A. J.; Bunz, U. H. F. *J. Am. Chem. Soc.* **2008**, *130*, 6498-6506. (e) Wilson, J. N.; Smith, M. D.; Enkelmann, V.; Bunz, U. H. F. *Chem. Commun.* **2004**, 1700-1701. (f) Brombosz, S. M.; Zucchero, A. J.; Phillips, R. L.; Vazquez, D.; Wilson, A.; Bunz, U. H. F. *Org. Lett.* **2007**, *22*, 4519-4522. (g) Hauck, M.; Schönhaber, J.; Zucchero, A. J.; Hardcastle, K. I.; Müller, T. J. J.; Bunz, U. H. F. *J. Org. Chem.* **2007**, *72*, 6714-6725. (h) McGrier, P. L.; Solntsev, K. M.; Schönhaber, J.; Brombosz, S. M.; Tolbert, L. M.; Bunz, U. H. F. *Chem. Commun.*

2007, 2127 –2129. (i) McGrier, P. L.; Solntsev, K. M.; Miao, S.; Tolbert, L. M.; Miranda, O. R.; Rotello, V. M.; Bunz, U. H. F. *Chem. Eur. J.* **2008**, 14, 4503-4510. (j) Zucchero, A.J; McGrier, P. L.; Bunz, U. H. F. *Acc. Chem. Res.* **2010**, *43*, 397-408.

12. (a) Gerhardt, W. W.; Zucchero, A. J.; Wilson, J. N.; South, C. R.; Bunz, U. H. F.; Weck, M. *Chem. Commun.* **2006**, 2141-2143. (b) Gerhardt, W. W.; Zucchero, A. J.; South, C. R.; Bunz, U. H. F.; Weck, M. *Chem. Eur. J.* **2007**, *13*, 4467-4474.

13. (a) Grunder, S.; Huber, R.; Horhoiu, V.; González, M. T.; Schönenberger, C.; Calame, M.; Mayor, M. *J. Org. Chem.* **1997**, *72*, 8337-8344.

14. (a) Wilson, J. N.; Bunz, U. H. F. *J. Am. Chem. Soc.* **2005**, *127*, 4124-4125. (b) Zucchero, A. J.; Wilson, J. N.; Bunz, U. H. F. *J. Am. Chem. Soc.* **2006**, *128*, 11872-11881. (c) Tolosa, J.; Zucchero, A. J.; Bunz, U. H. F. *J. Am. Chem. Soc.* **2008**, *130*, 6498-6506. (d) Brombosz, S. M.; Zucchero, A. J.; Phillips, R. L.; Vazquez, D.; Wilson, A.; Bunz, U. H. F. *Org. Lett.* **2007**, *22*, 4519-4522. (e) Hauck, M.; Schönhaber, J.; Zucchero, A. J.; Hardcastle, K. I.; Müller, T. J. J.; Bunz, U. H. F. *J. Org. Chem.* **2007**, *72*, 6714-6725. (f) McGrier, P. L.; Solntsev, K. M.; Schönhaber, J.; Brombosz, S. M.; Tolbert, L. M.; Bunz, U. H. F. *Chem. Commun.* **2007**, 2127 – 2129. (g) McGrier, P. L.; Solntsev, K. M.; Miao, S.; Tolbert, L. M.; Miranda, O. R.; Rotello, V. M.; Bunz, U. H. F. *Chem. Eur. J.* **2008**, *14*, 4503-4510.

15. Bunz, U. H. F. *Chem. Rev.* **2000**, *100*, 1605-1644.

16. Tekin, E.; Egbe, D. A. M.; Kranenburg, J. M.; Ulbricht, C.; Rathgeber, S.; Birckner, E.; Rehmann, N.; Meerholz, K.; Schubert, U. S. *Chem. Mater*. **2008**, *20*, 2727-2735.

17. (a) Wilson, J. N.; Windscheif, P. M.; Evans, U.; Myrick, M. L.; Bunz, U. H. F. *Macromolecules* **2002**, *35*, 8681-8683. (b) Wilson, J. N.; Josowicz, M.; Wang, Y.; Bunz, U. H. F. *Chem. Commun.* **2003**, 2962-2963.

18. Wheland, R. C.; Martin, E. L. *J. Org. Chem.* **1975**, *40*, 3101-3109.

19. (a) Horner, L.; Hoffmann, H.; Wippel, H. G.; Klahre, G. *Chem. Ber.* **1959**, *92*, 2499-2505. (b) Horner, L.; Klink, W. *Tetrahedron Lett.* **1964**, *36*, 2467-2473.

20. (a) Sonogashira, K. *J. Organomet. Chem.* **2002**, *653*, 46-49.

21. (a) Marri, E.; Pannacci, D.; Galiazzo, G.; Mazzucato, U.; Spalletti, A. *J. Phys. Chem. A.* **2003**, *107*, 11231-11238. (b) Sancho-Garcia, J. C.; Bredas, J. L.; Beljonne, D.; Cornil, J.; Martinez-Alvarez, R.; Hanack, M.; Poulsen, L.; Gierschner, J.; Mack, H. G.; Egelhaaf, H. J.; Oelkrug, D. *J. Phys. Chem. B.* **2005**, *109*, 4872-4880. (c) Pond, S. J. K.; Tsutsumi, O.; Rumi, M.; Kwon, O.; Zojer, E.; Bredas, J. L.; Marder, S. R.; Perry, J. W. *J. Am. Chem. Soc.* **2004**, *126*, 9291-9306. (d) Hong, J. W.; Woo, H. Y.; Liu, B.; Bazan, G. C. *J. Am. Chem. Soc.* **2005**, *127*, 7435-7443.

Chapter 2

Photophysical Properties of Hydroxy Cruciforms

2.1 Introduction

Cruciform fluorophores (tetra-1,2,4,5-vinyl- or -ethynyl-substituted benzenes, XFs) are π -systems with unusual frontier molecular orbitals (FMOs). If one of the axes is donor substituted and the other axis is acceptor substituted, species with *spatially separated* FMOs can result. The HOMO is localized on the donor part of the molecule, while the LUMO is localized on the acceptor part of the molecule. This FMO arrangement leads to a situation in which electronic information can be addressed spatially and for which HOMO and LUMO are manipulated by metal cations or by protons. We[1] and others[2-5] have shown that dialkylaniline- and pyridine-containing XFs display unusually large bathochromic or hypsochromic shifts when exposed to zinc, magnesium, calcium and manganese salts or protons.[1,2] The reason for the large shifts in absorption and emission is the independently addressable HOMO and LUMO, enforcing large changes in the HOMO–LUMO gap.[3] Up to now, HOMO–LUMO of XF-types have been addressed by cationic species, binding to the free electron pairs of pyridines and dialkylanilines. In this chapter, we demonstrate that XFs carrying strategically placed phenol functionalities show unusual photophysical effects upon deprotonation and exposure to amines.

2.2 Results and Discussion

2.2.1 Synthesis of Hydroxy XFs

The synthesis of hydroxy-XFs starts with the reaction of phosphonate **2.1**[6] with either the protected aldehyde **2.2** or **2.3** to give the distyrylbenzene derivatives **2.4** and **2.5** in 77% and 68% yield, respectively, after chromatography and recrystallization. Coupling of **2.4** or **2.5** with 4-tert-butylphenylacetylene in the presence of CuI–$(Ph_3P)_2PdCl_2$ under standard Heck–Cassar–Sonogashira–Hagihara conditions[7] in piperidine furnished the target XFs **2.7** and **2.8**, after aqueous workup, chromatography and subsequent deprotection with trifluoroacetic acid at -78 °C in dichloromethane, as yellow or yellowish–brown solids in 41% and 40% yield respectively (Scheme 1). The relatively low coupling yield (44 and 48% respectively) is due to losses during the chromatography of the intermediate. Nevertheless, the target XFs are easily available on a 100–200 mg scale. If **2.4** is coupled to **2.9**, we obtain an intermediate in 53% yield, which is deprotected in 85% yield to give **2.10**.

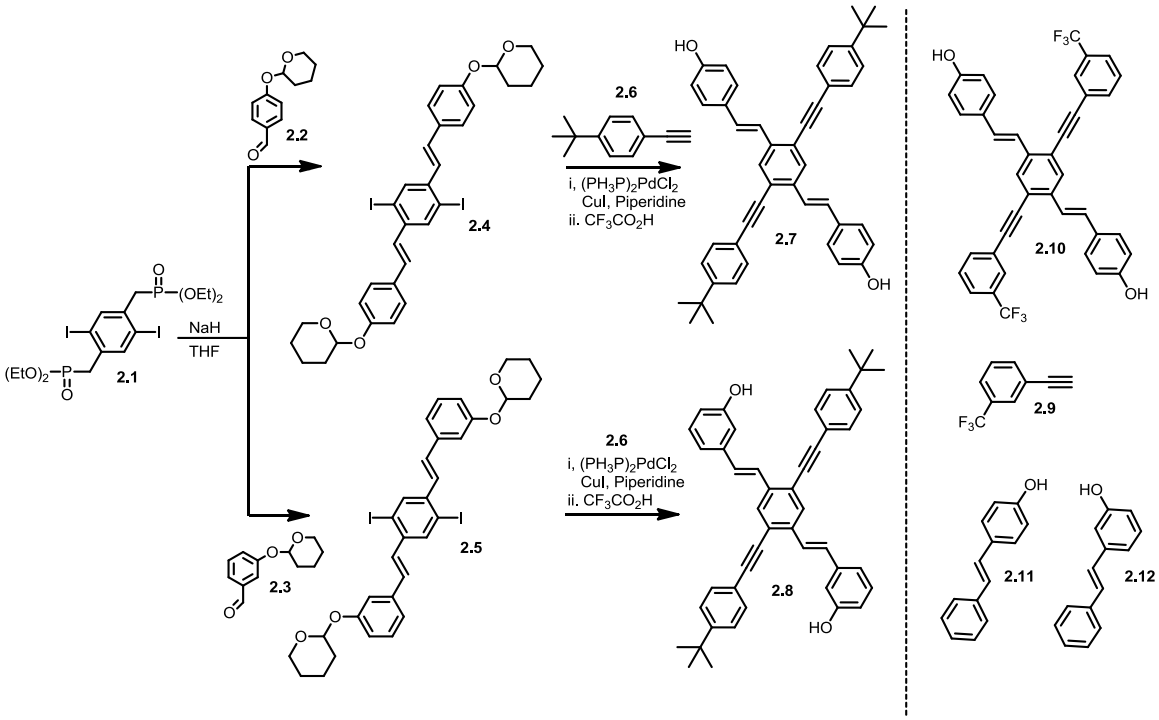

Scheme 2.1. Synthesis of hydroxy XFs **2.7**, **2.8**, and **2.10**.

2.2.2 Spectroscopic Properties and Titration Studies of Hydroxy XFs

Table 2.1 shows the pertinent photophysical data of **2.7**, **2.8** and **2.10**. The XFs **2.7** and **2.8** are similar to each other, as they show blue emission with robust quantum yields. Attachment of $-CF_3$ groups on the aryleneethynylene axis in **2.10** decreases the band gap and leads to significantly red-shifted absorption and emission. The Stokes shifts in these XFs are similar and around 3000 cm^{-1}. The vibronic progression of **2.8** is in the expected range, while that of **2.7** is smaller. The fluorescence spectrum of **2.10** does not show any vibronic bands, suggesting that its excited state is structurally different from its ground state.[8]

Table 2.1. Photophysical data of XFs **2.7**, **2.8**, and **2.10** in dichloromethane

Compound	**2.7**	**2.8**	**2.10**
Absorption (nm)	380	376	404
Emission (nm)	432	423	456
Vibronic Progression (cm^{-1})	876	1219	None
Stokes Shift (cm^{-1})	3167	2955	2822
Φ_{fl} (quantum yields)	0.41	0.72	0.57
T (ns)	1.42	2.99	Na

We titrated (see Figures 2.1 & 2.2) **2.7** and **2.8** in a methanol–water mixture with aqueous base (KOH). Figure 1 shows absorption and emission for **2.8**. Upon addition of hydroxide, *there is no significant change in the absorption spectrum of* **2.8**; the emission of the phenolate of **2.8** is largely quenched. A very weak emission band for the deprotonated form of **2.8** is observed at 515 nm. The invariance of the absorption spectrum is surprising and persists upon addition of a large excess of hydroxide. In the

case of **2.7**, upon deprotonation (Figure 2.2), the absorption spectrum shows an appreciable red shift, as would be expected for a phenolate, with a prominent absorption appearing at 416 nm. At the same time, the emission changes from 476 nm (blue) to 580 nm (yellow). Addition of an excess of KOH solution does not change the emission wavelength further. From the titrations, the pK_a values for **2.7** and **2.8** were determined to be 9.9 and 10.0, respectively.

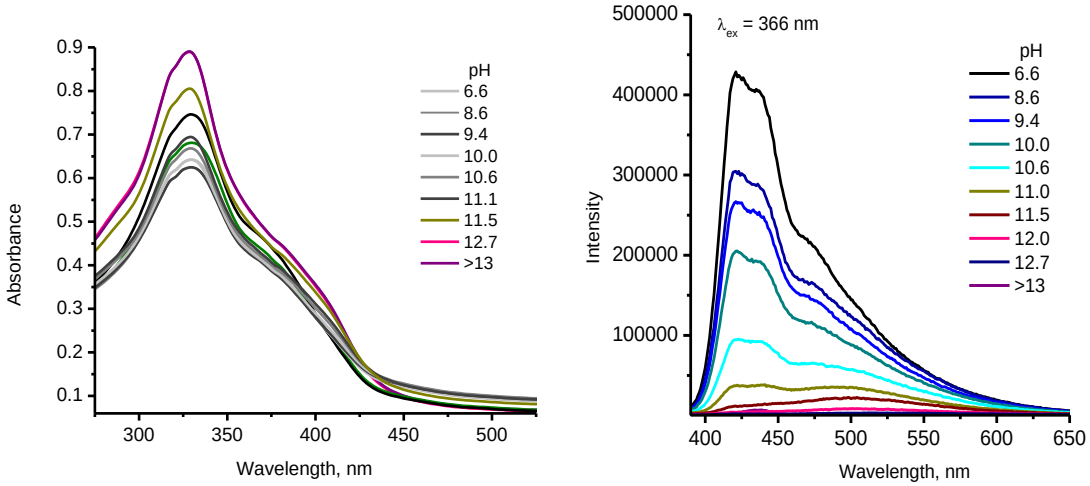

Figure 2.1. Uv-vis (left) and emission (right) spectra of XF **2.8** in a 2:1 vol. methanol-water mixture at different pH-values.

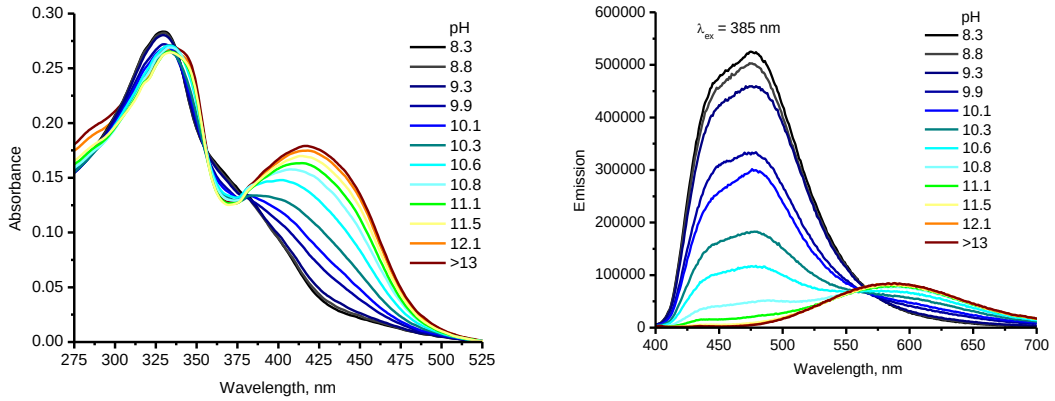

Figure 2.2. Uv-vis (left, 417 nm λ_{max} deprotonated form) and emission (right, 474 nm, 596 nm λ_{max}) spectra of XF **2.7** in a 2:1 vol. methanol-water mixture at different pH-values.

Changes in spectroscopic properties are not only observed upon deprotonation of the XFs **2.7** and **2.8** in methanol–water mixtures, but also when solutions of XFs in dichloromethane are exposed to amines. Figure 2.3 shows a photograph of the XFs **2.7**,

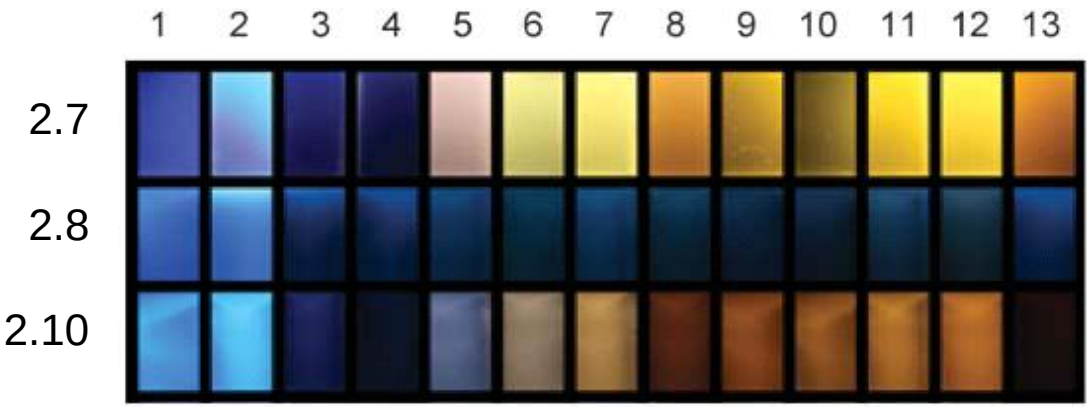

Figure 2.3. Photograph of the cruciforms **2.7, 2.8,** and **2.10** in DCM: 1) reference; exposure to 2) pyrrole (-), 3) quinoline (4.90), 4) pyridine (5.25), 5) imidazole (6.96; $\lambda_{max.\ 7}$ = 551 nm), 6) morpholine (8.33; 555 nm), 7) piperazine (9.83; 556 nm), 8) ethylenediamine (10.7; 579 nm), 9) piperidine (10.8; 564 nm), 10) triethylamine (10.8; 555 nm), 11) diethylamine (11.0; 562 nm), 12) diisopropylamine (11.1; 558 nm), and 13) 1,8-diaza-bicyclo-[5.4.0]undec-7-ene (DBU, ~12; 572). The numbers in parenthesis are the pK_a values of the corresponding ammonium ions.

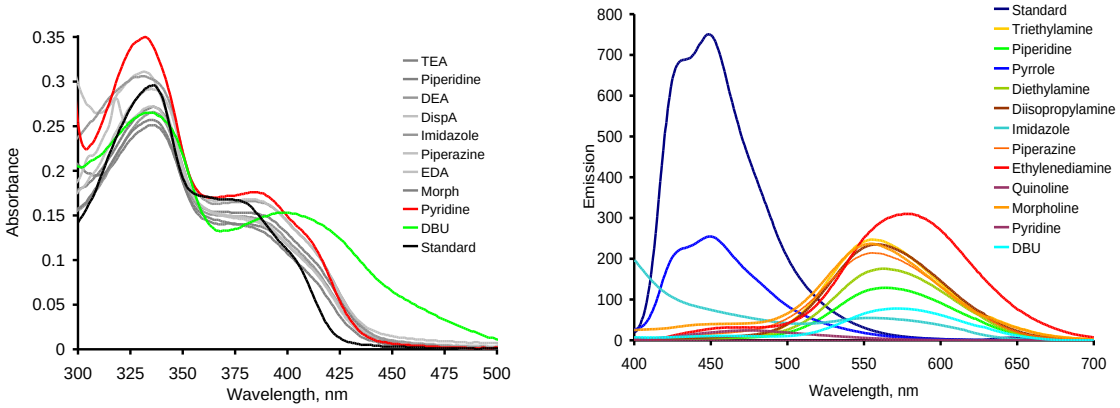

Figure 2.4. Absorption spectra (left) of solutions of **2.7** in DCM upon addition of amine (0.1 mL). Emission spectra (right) of solutions of **2.7** in dichloromethane (DCM, 15 mL, vial) upon addition of amine (0.1 mL).

2.8 and **2.10** exposed to a panel of different amines, ordered by their increasing pK_a values, while Figure 2.4 shows the corresponding emission spectra for **2.7**.

Interestingly, the magnitude in shift and the pK_a-values of the amines do not correlate particularly well, as ethylenediamine (pK_a = 10.7), i.e. not the most basic amine, displays the largest red shift. In the case of the exposure of **2.7** to quinoline or to pyridine, fluorescence is quenched, possibly due to a back electron transfer following proton transfer to the basic nitrogen.[9] If the amine under consideration is not very basic, such as pyrrole and imidazole, either there is no change in the emission or a mixed color (imidazole) is observed. Similar trends are observed for XF **2.10**, even though the emission intensities are much lower, as expected from the energy gap law.[10]

Exposure of the XF **2.8** to amines in dichloromethane results in quenching (see experimental for spectra) of the emission, similar to that observed on exposure of **2.8** to KOH. The above observations demonstrate that **2.7** and **2.8** are different from hydroxystilbenes **2.11** and **2.12**. The phenolate of stilbene **2.11** is weakly fluorescent, while that of the meta-compound **12** is quite fluorescent.[11] In **2.11** and **2.12** the excited state acidity of the phenolic function is significantly enhanced, that of **2.12** more so than that of **2.11**. Neither the XF **2.7** nor **2.8**, on the other hand, shows dramatically enhanced photoacidity in methanol–water mixtures with up to 50% vol. water,[11] which makes them comparable to the weak photoacid 2-naphthol with a pK_a* of 2.8.[12]

The absorption and emission spectra of **2.7** show a more complex behavior in the presence of amines (Figure 4). On the one hand, except for 1,8-diaza[5.4.0]bicycloundecene (DBU, pK_a ~ 12), the absorption maxima show a shift of ca. 20 nm and are consistent with a hydrogen-bonded complex.[13] Upon addition of DBU a

red-shifted feature is observed, which we attribute to the fully bisdeprotonated ground state species, as it is identical to that observed in the KOH-promoted deprotonation of **2.7**. On the other hand, all of the amine complexes exhibit efficient emission from the fully deprotonated (ion pair) state. From these observations, we conclude that in dichloromethane solutions the difference in pK_a (or ΔG of the proton transfer) between **2.7*** and amines is sufficient to produce solvent-separated ion pairs.[14] In the ground state, the observed ΔpK_a results in the formation of hydrogen-bonded complexes.

The observation of different amine-dependent emission characteristics is of potential importance since Lavigne *et al.*[15] have shown that carboxylate-substituted polythiophenes can discern biogenic amines when the absorption spectra of the complexes are compared. Our approach is complementary as we use more sensitive fluorescence spectroscopy.

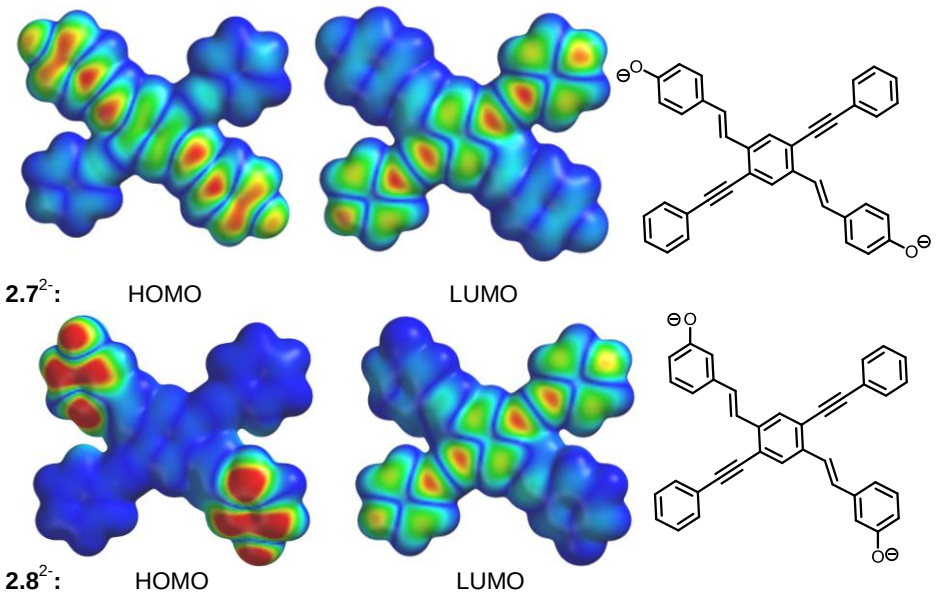

Figure 2.5. Density of the frontier molecular orbitals (HOMO and LUMO) of the bisphenolate anions of models of **2.7** and of **2.8** as calculated by B3LYP-6-31G**//B3LYP-6-31G** using SPARTAN.

What is the reason for the dramatic differences in the optical properties of **2.7** and **2.8** upon interaction with bases, i.e. proton dissociation induced red shift vs. quenching? A DFT calculation (Figure 2.5) of the FMO-distribution of **2.7** and **2.8** sheds light on this issue. In the dianion of **2.7**, HOMO and LUMO show spatial overlap in the central ring and both absorption and emission is Franck–Condon allowed. In the case of **2.8** the situation is different. Due to the disjoint orbital structure *in which the HOMO is localized only on the two phenolate rings, while the LUMO is strictly localized on the bisarylethynyl axis, there is a vanishingly small spatial overlap between the two frontier molecular orbitals, resulting in a Franck–Condon forbidden transition. Without the quantum chemical calculations, the different spectroscopic properties of* ***2.7***$^{2-}$ *and* ***2.8***$^{2-}$ *would be very hard to rationalize.* Since the 340 nm transition is both invariant with respect to deprotonation and strongly allowed, we conclude that this is a HOMO–LUMO transition in **2.8** but a HOMO–LUMO + n-transition in the deprotonated form of **2.8**, while the weaker HOMO–LUMO transition of the dianion of **2.8** is hidden in the baseline.[3] The allowed transition in the dianion must have a similar gap to the HOMO–LUMO-transition in the neutral compound, explaining the lack of change in the absorption spectra.

2.3 Conclusions

In conclusion, we have prepared the two XFs **2.7** and **2.8** and investigated their photophysical properties upon deprotonation and exposure to amines. We see dramatic differences between the *para* (**2.7**) and the *meta* (**2.8**) XF as a consequence of the different FMO distribution. The dianion **2.8** suffers from a Franck–Condon disallowed HOMO–LUMO-transition, which is responsible for the observed fluorescence quenching.

Potential applications of such materials with separated FMOs include exciton collection and splitting in photovoltaic devices and fluorescence sensors in cases where the XFs are equipped with additional binding elements.

2.4 Experimental

Materials and Methods: All chemicals were purchased from Aldrich Chemical, Acros, TCI America, or Fisher Scientific and used without purification unless otherwise specified. Column chromatography was performed using Standard Grade silica gel 60 Å, 32-63 μm (230 x 450 mesh) from Sorbent Technologies and the indicated eluent. Elution of cruciforms was readily monitored using a handheld UV lamp (365 nm). Melting points were obtained using a Mel-Temp apparatus fitted with a Fluke 51K/J digital thermometer. All IR spectra were obtained using a Simadzu FTIR-8400s spectrometer. Unless otherwise specified, NMR spectra were recorded at 298 K on a Bruker (500 MHz) or Varian Mercury spectrometer (300 MHz). Chemical shifts are reported in parts per million (ppm), using residual solvents (chloroform-*d*) or (THF-*d5*) as an internal standard. Data are reported as follows: chemical shift, multiplicity (s = singlet, d = doublet, t = triplet, q = quartet, m = multiplet), coupling constant, and integration. Mass spectral analyses were provided by the Georgia Institute of Technology Mass Spectrometry Facility.

All absorption spectra were collected using a Shimadzu UV-2401PC spectrophotometer. All emission spectra were acquired using a Shimadzu RF-5301PC spectrofluorophotometer. Lifetime data were collected using a Lifespec-ps (Edinburgh Instruments), pulsed diode laser (PicoQuant, 372 nm excitation), and PMT detector

(Hamamatsu). Data were fit to single exponential decay so as to optimize chi-squared values. Quantum yields for all cruciforms were measured using standard procedures.[16] In all cases, quinine sulfate was used as a standard.

Synthesis of THP Aldehydes

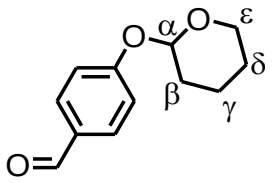

Synthesis of 2.2: 4-hydroxybenzaldehyde (5.8, 47.5 mmol) and 3,4-dihydro-2H-pyran (6.4 g, 76.1 mmol) was dissolved in dichloromethane (100 mL) in a 250 mL round bottom flask. Para-toluenesulfonic acid (0.43 g, 2.5 mmol) was added to the reaction mixture along with pyridine (1 mL). The pyridine was added drop wise over a 5 min period. The crude reaction mixture was washed three times with water, dried with magnesium sulfate and reduced until a dark brown oil was obtained. The product was washed with a solution of dilute NaOH and water to remove the starting material. The final product was obtained as a dark brown oil. Yield: 84%. *^{1}H NMR (500 MHz, $CDCl_3$):* δ = 9.90 (s, 1H, Ar-CHO), 7.84 (d, 2H, Ar-H, $J_{H,H}$ = 9 Hz), 7.17 (d, 2H, Ar-H, $J_{H,H}$ = 8.5 Hz), 5.55 (s, 1H, α-C-H), 3.85 (m, 1H, ε-CH), 3.64 (m, 1H, ε-C-H), 2.01 (m, 1H, β-C-H), 1.90 (m, 2H, γ-C-H) 1.71 (m, 2H, δ-C-H), 1.62 (m, 1H, β-C-H). *^{13}C NMR (125MHz, $CDCl_3$):* δ = 191.19, 162.48, 132.11, 130.77, 116.82, 96.41, 62.34, 30.36, 25.35, 18.77.

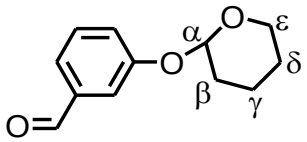

Synthesis of 2.3: 3-hydroxybenzaldehyde (5.8, 47.5 mmol) and 3,4-dihydro-2H-pyran (6.4 g, 76.1 mmol) was dissolved in dichloromethane (100 mL) in a 250 mL round

bottom flask. Para-toluenesulfonic acid (0.43 g, 2.5 mmol) was added to the reaction mixture along with pyridine (1 mL). The pyridine was added drop wise over a 5 min period. The crude reaction mixture was washed three times with water, dried with magnesium sulfate and reduced until a light brown oil was obtained. The product was washed with a solution of dilute NaOH and water to remove the starting material. The final product was obtained as a light brown oil. Yield: 85%. *^{1}H NMR (500 MHz, $CDCl_3$):* δ = 9.97 (s, 1H, Ar-CHO), 7.56 (s, 1H, Ar-H,), 7.50 (dt, 1H, Ar-H, $J_{H,H}$ = 7.5 Hz, *with long range coupling*), 7.44 (t, 1H, Ar-H, $J_{H,H}$ = 8 Hz), 7.31 (md, 1H, Ar-H, $J_{H,H}$ = 8 Hz, *with long range coupling*), 5.49 (s, 1H, α-C-H), 3.88 (m, 1H, ε-CH), 3.63 (m, 1H, ε-C-H), 2.01 (m, 1H, β-C-H), 1.90 (m, 2H, γ-C-H) 1.71 (m, 2H, δ-C-H), 1.62 (m, 1H, β-C-H). *^{13}C NMR (500 MHz, $CDCl_3$)*: δ = 192.19, 157.90, 138.10, 130.10, 123.63, 123.18, 116.59, 96.59, 62.21, 30.47, 25.40, 18.92.

General procedure for compounds 2.4 and 2.5: An oven dried Schlenk flask cooled under nitrogen was charged with **1**, NaH (2.5 eq), and dry THF. The flask was closed with a septum, a nitrogen-filled balloon was fitted to the arm and the stopcock was opened. With mild heating (40°C), the solution turned a vivid purple-red. The aldehyde was introduced in small portions over 1 h with a syringe as a pure oil. The reaction was allowed to stir overnight before work-up. The small excess of NaH was quenched with water and the mixture was extracted three times with dichloromethane. The organic layer was washed three times with water, dried with magnesium sulfate, filtered and reduced until a precipitate was formed. The precipitate was recrystallized from chloroform and collected by suction filtration and dried under vacuum.

Note: Compounds **2.4** and **2.5** both contain traces of previously reported halogen exchange material (**2.4a** and **2.5a**) from the precursor **2.1,** which is inseparable but can be used for further reactions.

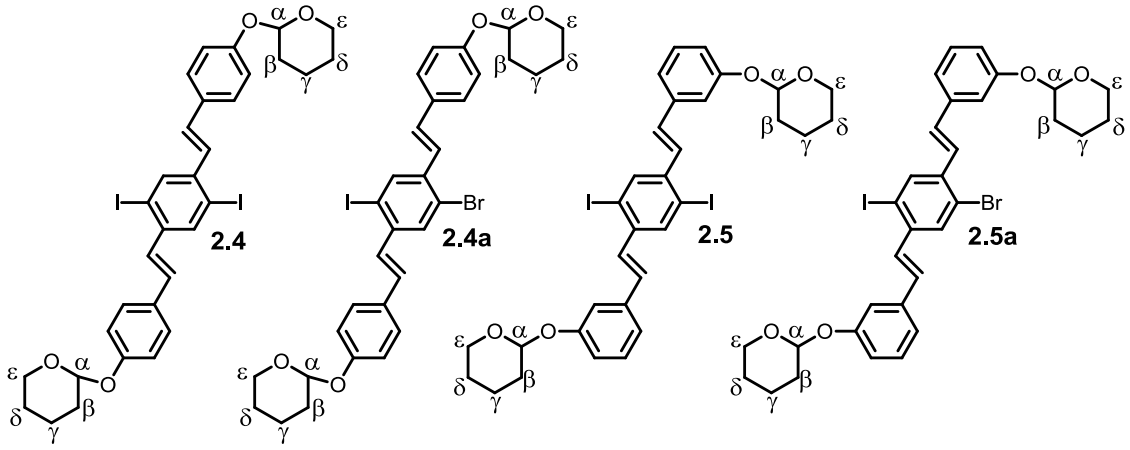

Synthesis of 2.4: Following the general procedure, **2.4** (0.500 g, 0.681 mmol), NaH (60 mg, 2.50 mmol), and THF (50 mL) were combined. 4-(tetrahydropyran-2-yloxy)-benzaldehyde (0.409 g, 1.98 mmol) was then added. Work up and recrystallization yielded (0.448 g, 77%) of bright yellow crystals. *MP:* 268-270 ºC. *IR:* 2933, 2869, 1600, 1508, 1234, 1170, 1107, 1035, 970, 810. *^{1}H NMR (500 MHz, $CDCl_3$):* δ = 8.07 (s, 2H, Ar-H), 7.58 (d, 4H, Ar-H, $J_{H,H}$ = 8.5 Hz), 7.10 (d, 4H, Ar-H, $J_{H,H}$ = 8.5 Hz), 7.09 (d, 2H, C=C-H, $J_{H,H}$ = 16.5 Hz), 6.95 (d, 2H, CH=CH, $J_{H,H}$ = 16.5 Hz), 5.49 (s, 2H, α-C-H), 3.95 (m, 2H, ε-CH), 3.65 (m, 2H, ε-C-H), 2.04 (m, 2H, β-C-H), 1.91 (m, 4H, γ-C-H) 1.71 (m, 4H, δ-C-H), 1.64 (m, 2H, β-C-H). *^{13}C NMR (125 MHz, $CDCl_3$):* δ = 157.73, 141.10, 136.44, 132.17, 130.63, 129.05, 128.57, 117.14, 100.62, 96.69, 62.47, 30.70, 25.59, 19.13.

Synthesis of 2.5: Following the general procedure, **2.5** (0.500 g, 0.681 mmol), NaH (60 mg, 2.50 mmol), and THF (50 mL) were combined. 3-(tetrahydropyran-2-yloxy)-

benzaldehyde (0.409 g, 1.98 mmol) was then added. Work up and recrystallization yielded (0.399 g, 68%) of pale yellow crystals. *MP:* 216-218 ºC. *IR:* 2947, 2873, 1581, 1488, 1251, 1120, 1037, 1014, 970, 904, 869, 777. *^{1}H NMR (500 MHz, $CDCl_3$):* 8.09 (s, 2H, Ar-H), 7.33 (t, 2H, Ar-H, $J_{H,H}$ = 8 Hz), 7.27 (s, 2H, Ar-H), 7.22 (d, 2H, Ar-H, $J_{H,H}$= 5 Hz), 7.20 (d, 2H, C=C-H, $J_{H,H}$ =16 Hz), 7.05 (d, 2H, Ar-H, $J_{H,H}$ = 8.5 Hz), 6.97 (d, 2H, C=C-H, $J_{H,H}$ = 16 Hz), 5.49 (s, 2H, α-C-H), 3.95 (m, 2H, ε-C-H), 3.65 (m, 2H, ε-C-H), 2.04 (m, 2H, β-C-H), 1.91 (m, 4H, γ-C-H) 1.71 (m, 4H, δ-C-H), 1.64 (m, 2H, β-C-H). *^{13}C NMR (125 MHz, $CDCl_3$):* δ = 157.86, 141.18, 138.36, 136.78, 132.70, 131.10, 130.13, 120.87, 116.94, 115.39, 100.69, 96.90, 62.59, 30.81, 25.62, 19.25.

Compounds 4a-4b

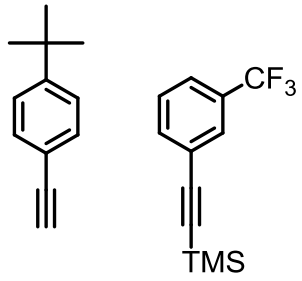

2.6 **2.9a**

Compound **2.6** has been previously reported. [17]

Compound 2.9a: *^{1}H NMR (300 MHz, $CDCl_3$):* δ = 7.72 (s, 1H, Ar-H), 7.62 (d, 1H, Ar-H, $J_{H,H}$ = 7.7 Hz), 7.56 (d, 1H, Ar-H, $J_{H,H}$ = 8.4 Hz), 7.42 (t, 1H, Ar-H, $J_{H,H}$ = 7.3 Hz), 0.26 (s, 9H, -CH_3). *^{13}C NMR (125 MHz, $CDCl_3$):* δ = 134.98, 130.90(m), 128.73, 125.52, 124.93(m), 124.14, 121.91, 118.30, 103.28, 96.20. *MS (EI, 70-SE) ($C_{12}H_{13}F_3Si$):* m/z = 242.

Compounds **2.13-2.15** were produced by the Sonogashira coupling of either the free alkyne **4a,b** or by in-situ deprotection of TMS with potassium hydroxide and ethanol

as a co-solvent. The reaction progress could be monitored by the development of the fluorescent products which were isolated by precipitating twice in non solvents.

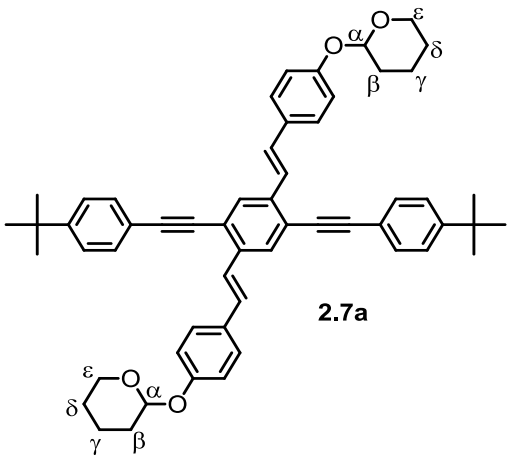

2.7a

Synthesis of XF 2.7a: 2.4 (0.297 g, 0.404 mmol) was combined with **2.6** (0.192, g, 1.21 mmol), $(PPh_3)_2PdCl_2$ (5 mg, 7.1 μmol), CuI (5 mg, 33 μmol) and dissolved in THF (50 mL) and piperidine (5 mL) in a nitrogen purged Schlenk flask. The solution was degassed, capped with a septum and allowed to stir at room temperature for 24 h. The product was extracted with dichloromethane, washed three times with water and dried with magnesium sulfate and reduced until a yellow powder was formed, which was purified by chromotagraphy eluting with 70:30 dichloromethane and hexanes yielding 150 mg of yellow crystals. Yield: 47%. *MP:* 186-188 ºC. *IR:* 2939, 2866, 2250, 1602, 1508, 1236, 1170, 1035, 1018, 960, 919, 831, 813. *^{1}H NMR (500 MHz, $CDCl_3$):* δ = 7.90 (s, 2H, Ar-H), 7.59 (d, 2H, C=C-H, $J_{H,H}$ = 16.5 Hz), 7.57 (d, 4H, Ar-H, $J_{H,H}$ = 8 Hz), 7.54 (d, 4H, Ar-H, $J_{H,H}$ = 8 Hz), 7.45 (d, 4H, Ar-H, $J_{H,H}$ = 8.5 Hz), 7.25 (d, 2H, C=C-H, $J_{H,H}$ = 16.5 Hz), 7.10 (d, 4H, Ar-H, $J_{H,H}$ = 8.5 Hz), 5.49 (s, 2H, α-C-H), 3.95 (m, 2H, ε-C-H), 3.65 (m, 2H, ε-C-H), 2.04 (m, 2H, β-C-H), 1.91 (m, 4H, γ-C-H) 1.71 (m, 4H, δ-C-H), 1.64 (m, 2H, β-C-H), 1.37 (s, 18H, t-butyl). *^{13}C NMR (125 MHz, $CDCl_3$):* δ = 156.97,

151.80, 137.22, 131.29, 130.97, 129.91, 128.43, 127.90, 125.50, 123.89, 122.06, 120.18, 116.67, 96.24, 95.47, 87.38, 62.01, 34.85, 31.18, 30.29, 25.18, 18.70. *MS (FAB, 70-SE) ($C_{56}H_{58}O_4$):* m/z = 794.

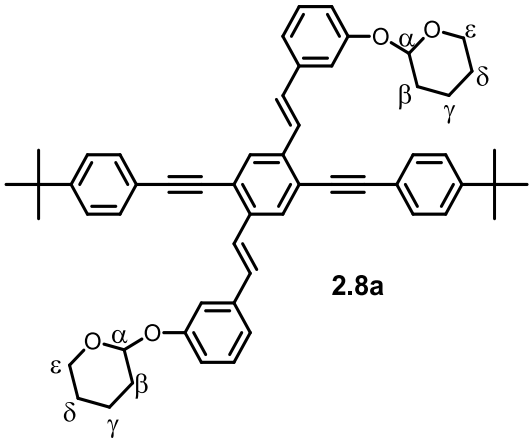

2.8a

Synthesis of XF 2.8a: 2.5 (0.399 g, 0.543 mmol) was combined with **2.6** (0.258 g, 1.63 mmol), $(PPh_3)_2PdCl_2$ (5 mg, 7.1 μmol), CuI (5 mg, 33 μmol) and dissolved in THF (50 mL) and piperidine (5 mL) in a nitrogen purged Schlenk flask. The solution was degassed, capped with a septum and allowed to stir at room temperature for 24 h. The product was extracted with dichloromethane, washed three times with water and dried with magnesium sulfate and reduced until a yellow powder was formed, which was purified by chromotagraphy eluting with 70:30 dichloromethane and hexanes yielding 190 mg of yellow crystals. Yield: 44%. *MP:* 266-268 ºC. *IR:* 2947, 2869.8, 2220. 1, 1583.4, 1512.1, 1452.3, 1257.5, 1157.21, 1020.27, 956.6, 831.2, 775.3 *^{1}H NMR (500 MHz, $CDCl_3$):* δ = 7.93 (s, 2H, Ar-H), 7.72 (d, 2H, C=C-H, $J_{H,H}$ = 16.5 Hz), 7.60 (d, 4H, Ar-H, $J_{H,H}$ = 8.5), 7.45 (d, 4H, Ar-H, $J_{H,H}$ = 8.5), 7.36 (s, 2H, Ar-H), 7.32 (t, 2H, Ar-H, $J_{H,H}$ = 8 Hz), 7.27 (d,2H, $J_{H,H}$ = 16.5 Hz, CH=CH), 7.23 (d, 2H, $J_{H,H}$ = 8 Hz Ar-H), 7.02 (d, 2H, $J_{H,H}$ = 8 Hz, Ar-H), 5.49 (s, 2H, α-C-H), 3.95 (m, 2H, ε-C-H), 3.65 (m, 2H, ε-C-H), 2.04 (m, 2H, β-C-H), 1.91 (m, 4H, γ-C-H) 1.71 (m, 4H, δ-C-H), 1.64 (m, 2H, β-C-H),

1.37 (s, 18H, t-butyl). *^{13}C NMR (125 MHz, $CDCl_3$):* δ = 157.92, 152.27, 139.17, 137.68, 131.68, 130.82, 130.08, 129.06, 126.40, 125.93, 122.85, 120.99 120.62, 116.83, 114.74, 96.82, 96.82, 87.73, 62.41, 35.30, 31.65, 30.90, 25.73, 19.26. *MS (FAB, 70-SE) ($C_{56}H_{58}O_4$):* m/z = 794.

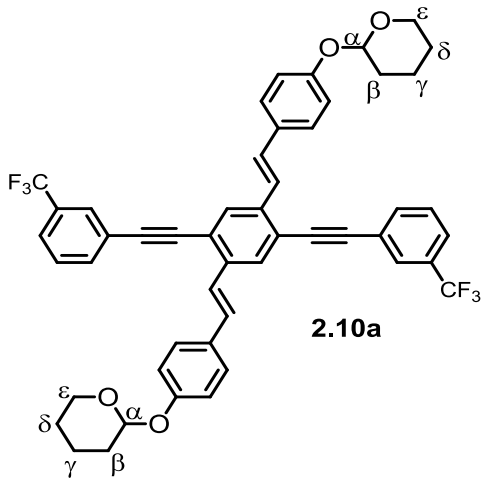

2.10a

Synthesis of XF 2.10a: 2.4 (0.403 g, 0.549 mmol) was combined with **2.9a** (0.399 g, 1.64 mmol), $(PPh_3)_2PdCl_2$ (5 mg, 7.1 μmol), CuI (5 mg, 33 μmol), KOH (0.500 g, 8.90 mmol) and dissolved in piperidine (5 mL), EtOH (10 mL) and THF (25 mL) in a nitrogen purged Schlenk flask. The solution was degassed, capped with a septum and allowed to stir at room temperature for 24 h. The product was extracted with dichloromethane, washed three times with water and dried with magnesium sulfate and reduced until a yellow powder was formed, which was purified by chromotagraphy eluting with 60:40 dichloromethane and hexanes yielding 280 mg of yellow crystals. Yield: 53%. *MP:* 246-248 ºC. *IR:* 3035, 2943, 2875, 2235, 1600, 1508, 1330, 1240, 1164, 1122, 958, 919, 800. *^{1}H NMR (500 MHz, $CDCl_3$):* δ = 7.92 (s, 2H, Ar-H), 7.90 (s, 2H, Ar-H), 7.79 (d, 2H, Ar-H, $J_{H,H}$ = 8 Hz), 7.66 (d, 2H, Ar-H, $J_{H,H}$ = 8 Hz), 7.56 (t, 2H, Ar-H, $J_{H,H}$ = 8 Hz), 7.54 (d, 2H, C=C-H, $J_{H,H}$ = 16.5 Hz), 7.54 (d, 4H, Ar-H, $J_{H,H}$ = 9 Hz), 7.26 (d, 2H, C=C-H, $J_{H,H}$ =

16.5 Hz), 7.11 (d, 4H, Ar-H, $J_{H,H}$ = 9 Hz), 5.49 (s, 2H, α-C-H), 3.95 (m, 2H, ε-C-H), 3.65 (m, 2H, ε-C-H), 2.04 (m, 2H, β-C-H), 1.91 (m, 4H, γ-C-H) 1.71 (m, 4H, δ-C-H), 1.64 (m, 2H, β-C-H). *^{13}C NMR (125 MHz, $CDCl_3$):* δ = 157.66, 138.01, 134.97, 131.70, 131.42, 131.09, 129.51, 129.14, 128.78 (m), 128.39, 125.49 (m), 125.21, 124.51, 123.76, 123.06, 122.13, 117.18, 96.75, 94.27, 89.88, 30.73, 25.61, 19.15. *MS (FAB, 70-SE) ($C_{50}H_{40}F_6O_4$):* m/z = 818.

General procedure for deprotection of XFs 2.7a, 2.8a, and 2.10a: XFs **2.7a, 2.8a, and 2.10a** were deprotected by trifluoroacetic acid in a dry ice acetone bath. The products were obtained by extracting with dichloromethane or ethyl ether. The yields reported reflect the amount of pure material that was recovered after deprotection and recrystallization.

Synthesis of XF 2.7: **2.7a** (0.080 g, 0.128 mmol) was dissolved in dichloromethane (30 mL) and trifluoroacetic acid (1 mL) was added into a 100-mL round bottom flask kept in a dry ice acetone bath. The solution was allowed to stir at -78 °C for 2 h. The crude reaction mixture was washed three times with water, dried with magnesium sulfate, filtered and reduced until a brown powder was formed. The resulting brown powder was recrystallized by dissolving in hot chloroform and adding an excess amount of hexanes yielding brown crystals. Yield: 88%. *MP:* 236-238 ºC. *IR:* 3321, 2956, 2852, 2195, 1604, 1512, 1440 1168, 1016, 958, 833, 815. *^{1}H NMR (500 MHz, $CDCl_3$):* δ = 7.89 (s, 2H, Ar-H), 7.57 (d, 4H, Ar-H, $J_{H,H}$ = 8.5 Hz), 7.56 (d, 2H, C=C-H, $J_{H,H}$ = 16.5 Hz), 7.50 (d, 4H, Ar-H, $J_{H,H}$ = 9 Hz), 7.45 (d, 4H, Ar-H, $J_{H,H}$ = 8.5 Hz), 7.24 (d, 2H, C=C-H, $J_{H,H}$ = 16.5 Hz), 6.88 (d, 4H, Ar-H, $J_{H,H}$ = 9 Hz***).*** *^{13}C NMR (125 MHz, $CDCl_3$):* δ = 155.97, 152.30,

137.64, 131.72, 130.82, 130.29, 128.93, 128.65, 125.93, 124.14, 122.50, 120.61, 116.15, 95.89, 87.80, 35.30, 31.30. *MS (FAB, 70-SE) ($C_{46}H_{42}O_2$):* m/z = 626.

Synthesis of XF 2.8: **2.8a** (0.102 g, 0.163 mmol) was dissolved in dichloromethane (30 mL) and trifluoroacetic acid (1 mL) was added into a 100-mL round bottom flask kept in a dry ice acetone bath. The solution was allowed to stir at -78 °C for 2 h. The crude reaction mixture was washed three times with water, dried with magnesium sulfate and reduced until a green powder was formed. The resulting green powder was recrystallized by dissolving in hot chloroform and adding an excess amount of hexanes yielding green crystals. Yield: 90%. *MP:* 238-240 ºC. *IR:* 3319, 2954, 2862, 1784, 1683, 1591, 1506, 1450, 1265, 1151, 1016, 962, 833, 775. *^{1}H NMR (500 MHz, $CDCl_3$):* δ = 7.89 (s, 2H, Ar-H), 7.65 (d, 4H, C=C-H, $J_{H,H}$ = 16.5 Hz), 7.57 (d, 4H, Ar-H, $J_{H,H}$ = 8.5 Hz), 7.45 (d, 4H, Ar-H, $J_{H,H}$ = 8.5 Hz), 7.26 (t, 2H, Ar-H, $J_{H,H}$ = 8.5 Hz), 7.22 (d, 2H, C=C-H, $J_{H,H}$ = 16.5 Hz), 7.16 (d, 2H, Ar-H, $J_{H,H}$ = 7 Hz), 7.07 (s, 2H, Ar-H), 6.82 (d, 4H, Ar-H, $J_{H,H}$ = 7 Hz). *^{13}C NMR (125 MHz, $CDCl_3$):* δ = 156.41, 152.40, 139.40, 137.59, 131.78, 130.67, 130.37, 129.30, 126.56, 125.96, 122.81, 120.47, 119.97, 115.57, 113.77, 96.21, 87.57, 35.30, 31.61. *MS (FAB, 70-SE) ($C_{46}H_{42}O_2$):* m/z = 626.

Synthesis of XF 2.10: **2.10a** (0.120 g, 0.184 mmol) was dissolved in dichloromethane (30 mL) and trifluoroacetic acid (1 mL) was added into a 100-mL round bottom flask kept in a dry ice acetone bath. The solution was allowed to stir at -78 °C for 2 h. The product was extracted with ethyl ether and washed three times with water, dried with magnesium sulfate and reduced until a yellow powder was formed. The resulting yellow powder was recrystallized from methanol yielding yellow crystals. Yield: 85% *MP:* 236-

238 ºC. *IR:* 3309, 2923, 2852, 1784, 1697, 1604, 1512, 1328, 1245, 1166, 1122, 962, 806. *^{1}H NMR (500 MHz, THF-d_8)* δ = 8.57 (s, 2H, Ar-OH), 7.99 (s, 2H, Ar-H), 7.97 (s, 2H, Ar-H), 7.87 (d, 2H, Ar-H, $J_{H,H}$ = 8 Hz), 7.72 (d, 2H, Ar-H, $J_{H,H}$ = 8 Hz), 7.64 (t, 2H, Ar-H, $J_{H,H}$ = 8 Hz), 7.52 (d, 2H, C=C-H, $J_{H,H}$ = 16.5 Hz), 7.46 (d, 4H, Ar-H, $J_{H,H}$ = 8.5 Hz), 7.34 (d, 2H, C=C-H, $J_{H,H}$ = 16.5 Hz), 6.77 (d, 4H, Ar-H, $J_{H,H}$ = 8.5 Hz). *^{13}C NMR (125 MHz, THF-d_8):* δ = 156.86, 136.23, 133.27, 129.77, 129.46, 129.21, 127.99, 127.09, 126.95, 126.61 (m), 123.55 (m), 122.83, 121.46, 120.05, 119.95, 114.05, 91.96, 87.94. *MS (FAB, 70-SE) ($C_{40}H_{24}F_6O_2$)*: m/z = 650.

Absorption and emission spectra of XFs 2.8 and 2.10 with amines. To investigate the sensory ability of hydroxy cruciforms towards amines, XFs **2.8 and 2.10** were tested. Approximately 0.1 mL of amine was added to each 15 mL vial and its optical properties were measured. The absorption and emission data are shown in Figures 2.6-2.9**.**

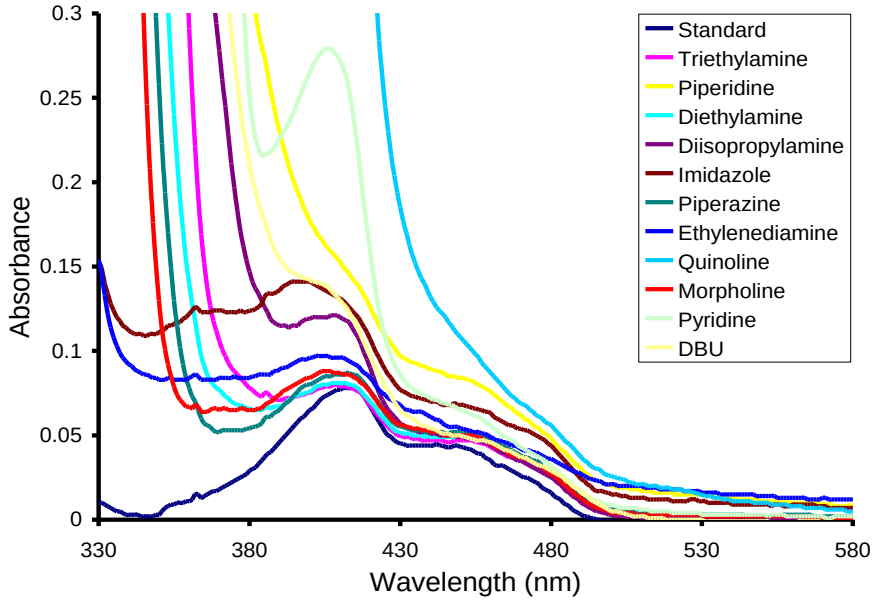

Figure 2.6. Absorption spectrum of **2.8** with amines in dichloromethane.

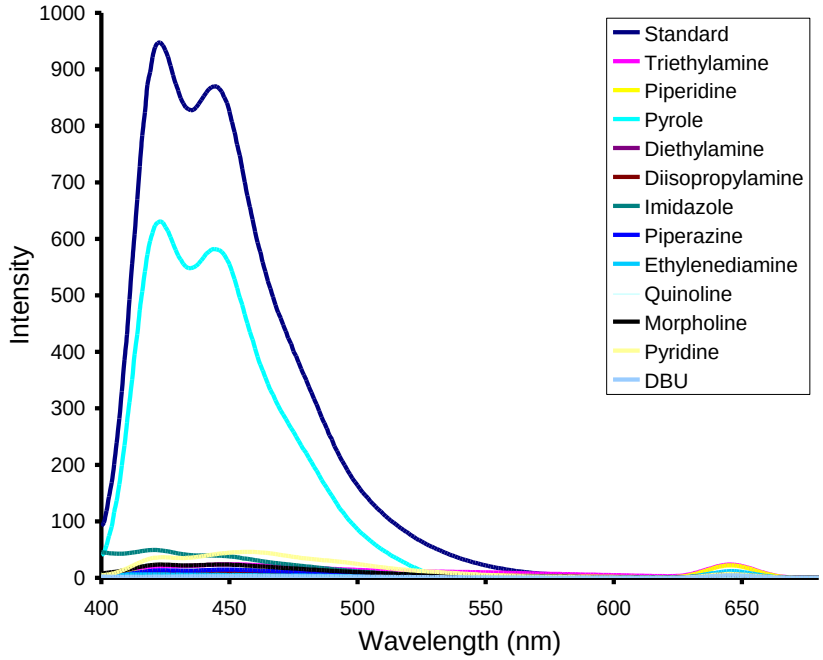

Figure 2.7. Emission spectrum of **2.8** with amines in dichlomethane**.**

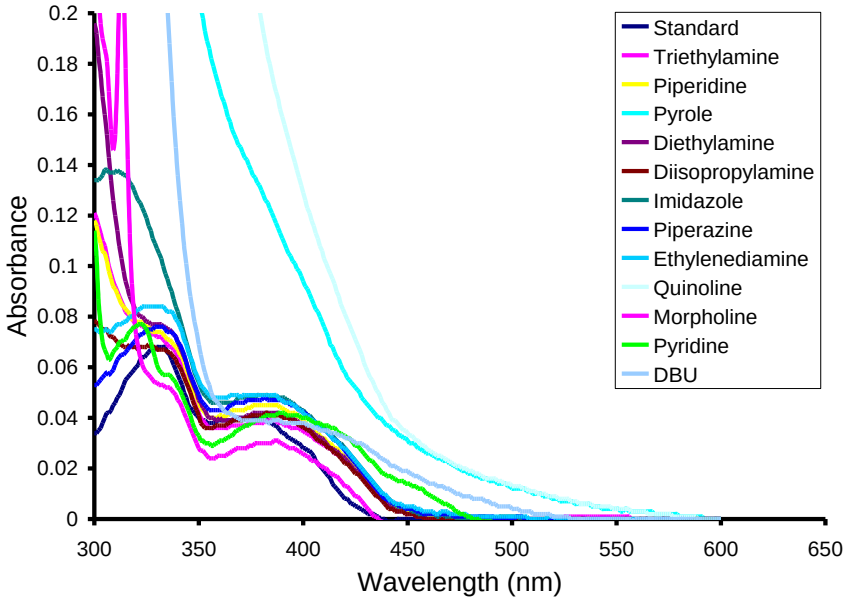

Figure 2.8. Absorption spectrum of **2.10** with amines in dichloromethane**.**

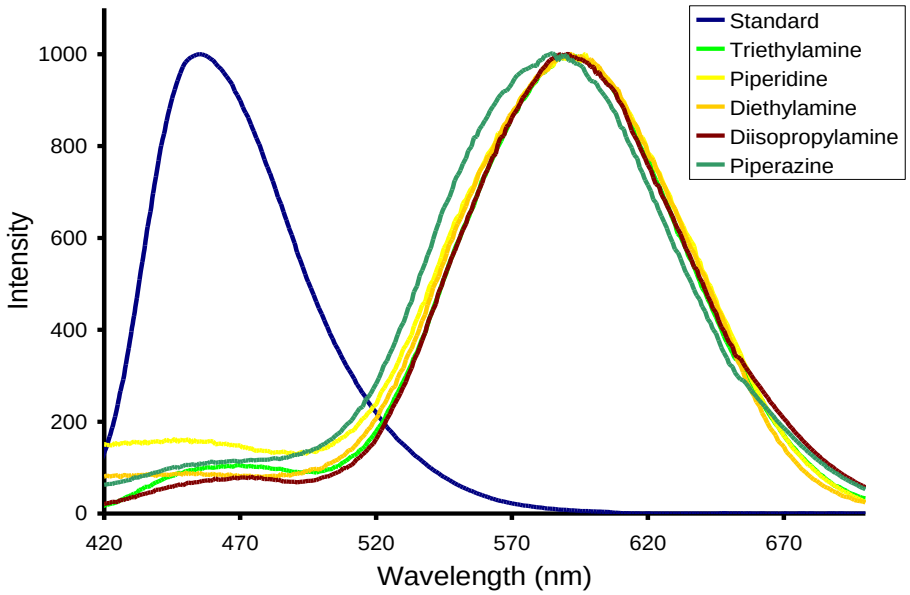

Figure 2.9. Normalized emission spectrum of **2.10** with amines in dichloromethane**.**

2.5 References and Notes

1. (a) Wilson, J. N. ; Bunz, U. H. F., *J. Am. Chem. Soc.* **2005**, *127*, 4124–4125. (b) Wilson, J. N.; Josowicz, M.; Wang, Y. Q ; Bunz, U. H. F. *Chem. Commun.*, **2003**, 2962– 2963. (c) Zucchero, A. J.; Wilson, J. N. ; Bunz, U. H. F. *J. Am. Chem. Soc.*, **2006**, *128*, 11872-11881. (d) Gerhardt, W. W.; Zucchero, A. J.; Wilson, J. N.; South, C. R.; Bunz, U. H. F.; Weck, M. *Chem. Commun.*, **2006**, 2141–2142.

2. (a) Spiteler, E. L.; Shirtlcliff, L. D.; Haley, M. M. *J. Org. Chem.* **2007**, *72*, 86–96. (b) Marsden, J. A.; Miller, J. J.; Shirtcliff, L. D.; Haley, M. M. *J. Am. Chem. Soc.* **2005**, *127*, 2464–2476.

3. (a) Zen, A.; Bilge, A.; Galbrecht, F.; Alle, R.; Meerholz, K.; Grenzer, J.; Neher, D.; Scherf, U.; Farrell, T. *J. Am. Chem. Soc.* **2006**, 128, 3914–3915. (b) Thompson, A. L.; Ahn, T. S.; Thomas, K. R. J. ; Thayumanavan, S.; Martinez, T. J.; Bardeen, C. J. *J. Am. Chem. Soc.* **2005**, *125*, 16348–16349. (c) Meier, H.; Mühling, B.; Kolshorn, H. *Eur. J. Org. Chem.* **2004**, 1033–1042.

4. (a) Kang, H.; Evmenenko, G.; Dutta, P.; Clays, K.; Song, K.; Marks, T. J. *J. Am. Chem. Soc.* **2006**, *128*, 6194–6205. (b) Hu, K.; Zhu, P. W.; Yu, Y.; Facchetti, A.; Marks, T. J. *J. Am. Chem. Soc.* **2004**, *126*, 15974–15975.

5. (a) Sorensen, J. K.; Vestergaard, M.; Kadziola, A.; Kilsa, K.; Nielsen, M. B. *Org. Lett.* **2006**, *8*, 1173–1176.

6. (a) Wilson, J. N.; Windscheif, P. M.; Evans, U.; Myrick, M. L.; Bunz, U. H. F. *Macromolecules*, **2002**, *35*, 8681–8683.

7. (a) Bunz, U. H. F. *Chem. Rev.* **2000**, *100*, 1605–1644. Sonogashira, K. *J. Organomet. Chem.* **2002**, *653*, 46–49. Negishi, E.; Anastasia, L. *Chem. Rev.* **2003**, *103*, 1979–2017.

8. Yang, J. S.; Chiou, S. Y.; Liau, K. L. *J. Am. Chem. Soc.* **2002**, *124*, 2518–2527.

9. (a) Zhou, Q.; Swager, T. M. *J. Am. Chem. Soc.* **1995**, *117*, 12593–12602. (b) Müller, J. G.; Atas, E.; Tan, C.; Schanze, K. S.; Kleiman, V.D. *J. Am. Chem. Soc.* **2006**, *128*, 4007–4016.

10. (a) Caspar, J. V.; Meyer, T. J.; *J. Phys. Chem.* **1983**, 87, 952–957. (b) Tolbert, L. M.; Nesselroth, S. M.; Netzel, T. L.; Raya, N.; Stapleton, M.; *J. Phys. Chem.* **1992**, *96*, 4492–4496.

11. (a) Lewis, F. D.; Crompton, E. M. *J. Am. Chem. Soc.* **2003**, 125, 4044–4045, Lewis, F. D.; Sinks, L. E.; Weigel, W.; Sajimon, M. C.; Crompton, E. M. *J. Phys. Chem. A*, **2005**, *109*, 2443–2451.

12. Tolbert, L. M.; Solntsev, K. M. *Acc. Chem. Res.* **2002**, *35*, 19–27.

13. Baba, H.; Suzuki, S. J. *Chem. Phys.* **1961**, *35*, 1118–1127.

14. Zaitsev, N. K.; Demyashkevich, A. B.; Kuzmin, M. G.; *High Energy Chem.* **1980**, *14*, 116–120.

15. Nelson, T. L.; O'Sullivan, C.; Greene, N. T.; Maynor, M. S.; Lavigne, J. J. *J. Am. Chem. Soc.* **2006**, *128*, 5640–5641.

16. "A Guide to Recording Fluorescence Quantum Yields." Horiba Jobin Yvon Ltd. Available online: http://www.jobinyvon.co.uk/ukdivisions/Fluorescence/plqy.htm. Accessed 06/14/2010.

17. Perttu, E.K.; Arnold, M.; Iovine, P.M. *Tetaheron Lett.* **2005**, *46*, 8753-8756.

Chapter 3

Anomalous Photophysics of Bis(hydroxystyryl)benzenes

3.1 Introduction

In an effort to better understand the photophysical properties of hydroxy XFs, we elected to prepare and examine hydroxy-substituted distytrylbenzenes. Stilbenes and distyrylbenzenes represent the first two oligomers leading to poly(*p*-phenylenevinylene) (PPV) and thus are important model compounds for conjugated polymers.[1] As a consequence, there is a significant fundamental interest in the excited-state behavior of these materials. Curiously, *trans*-stilbene (**TS**) is poorly fluorescent, the result of its well known propensity for isomerization in the excited state.[2] In contrast, *trans,trans*-distyrylbenzene (**TTSB**) and certain derivatives resist isomerization and are strongly fluorescent.[3,4] Recently, Lewis *et al.*[5] investigated the photoinduced processes for 4-hydroxystilbene (**3.8**), 3-hydroxystilbene (**3.9**), and several of their derivatives. The authors observed strikingly different behavior upon excitation concluding that **3.9** is a strong photoacid in water, while **3.8** does not undergo efficient excited-state proton transfer (ESPT) because of much faster photoisomerization. As a result, both compounds exhibit very weak fluorescence in aqueous solutions.

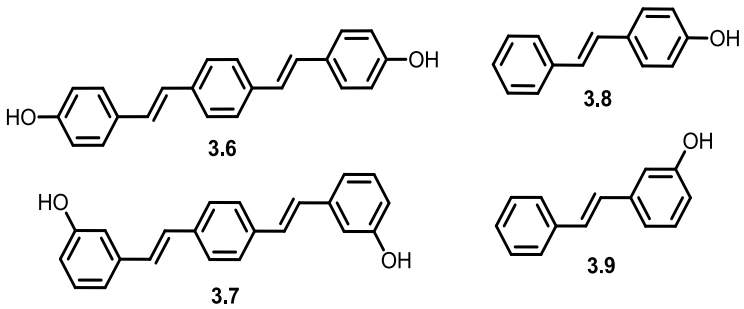

Figure 3.1. Structures of bis(hydroxystyryl)benzenes and hydroxystilbenes.

Given the stronger emissive properties of **TTSB** vs. **TS**, we speculated that hydroxyarenes based upon the former might show interesting ESPT properties. In this chapter, we demonstrate that the excited-state properties of the homologues **3.6** and **3.7** are different both from each other *and* from those of **3.8** and of **3.9**, coinciding with the differences between **TS** and **TTSB** in some respects but not in others. Specifically, we show that neither **3.6** nor **3.7** is a photoacid. Surprisingly, there is no published literature on the spectroscopy and photoinduced phenomena of either **3.6** or **3.7**.

3.2 Results and Discussion

3.2.1 Synthesis of Bis(hydroxystyryl)benzenes

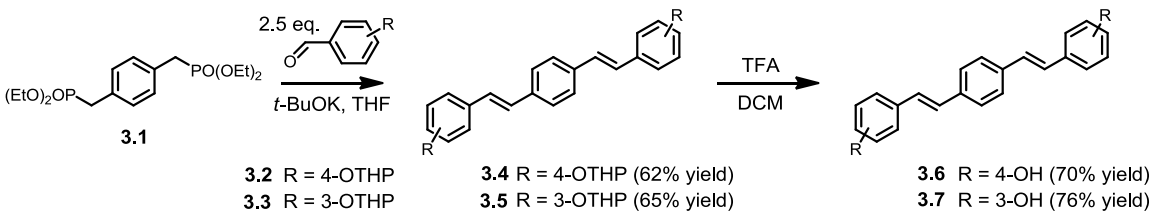

Scheme 3.1. Synthesis of bis(hydroxystyryl)benzenes **3.6** and **3.7**.

3.4 and **3.5** were readily synthesized by a Horner reaction of the 4-(tetrahydropyran-2-yloxy) (**3.2**) and 3-(tetrahydropyran-2-yloxy)-benzaldehyde (**3.3**) with tetraethyl-*para*-xylene-diphosphonate (**3.1**). Both **3.4** and **3.5** were then deprotected using trifluoroacetic acid in dichloromethane (DCM) to produce **3.6** and **3.7**. The resulting dyes were readily isolated by recrystallization yielding pale yellow crystalline solids.

3.2.2 Spectroscopic Properties and Titration Studies of Bis(hydroxystyryl)benzenes

In methanol, both **3.6** and **3.7** display intensive, single peak blue fluorescence with a Φ_{fl} of 0.37 and 0.62, respectively. Upon preparative photolysis with 355 nm light for one hour, 3% of the compound **3.6** interconverted into its cis, trans-isomer, while **3.7** remained unchanged. Similar to hydroxystilbenes, the bis-para isomer **3.6** has somewhat red-shifted spectroscopic features in absorption and emission compared to the *meta* derivative **3.7** (see Table 3.1). Both **3.6** and **3.7** are soluble in methanol but begin to aggregate in solutions with more than 50 vol % of water. To obtain pK_a values, all measurements were performed in a 2:1 methanol/water (v/v) mixture,[6] in which both compounds were soluble without apparent aggregation. Figure 3.2 shows the absorption and emission spectra of **3.6** and **3.7**. Upon addition of KOH, the absorption maximum of **3.6** shifts from 362 nm in the neutral compound to 393 nm in the bis-deprotonated form of **3.6** (**3.6**$^{2-}$) while λ_{max} of **3.7** shifted from 355 to 363 nm.

Table 3.1. Thermodynamic and photophysical properties of **3.6** and **3.7** in methanol/water (2:1 v/v) at 298 K.

Compound	**3.6**	**3.7**
pK_{a1}, pK_{a2}	10.1 ± 0.1, 12.0 ± 0.1	10.6 ± 0.1, 11.2 ± 0.1
Species	H_2A, HA^-, A^{2-}	H_2A, HA^-, A^{2-}
Absorption maxima (nm)	362, 388, 393	355, 359, 363
Emission maxima (nm)	428, 575, 533	412, quenched
Φ_{fl} (quantum yields)	0.34, n/d, 0.26	0.46 < 0.001
τ (ns)	0.91, n/d, 1.0	0.91, n/d, 1.0

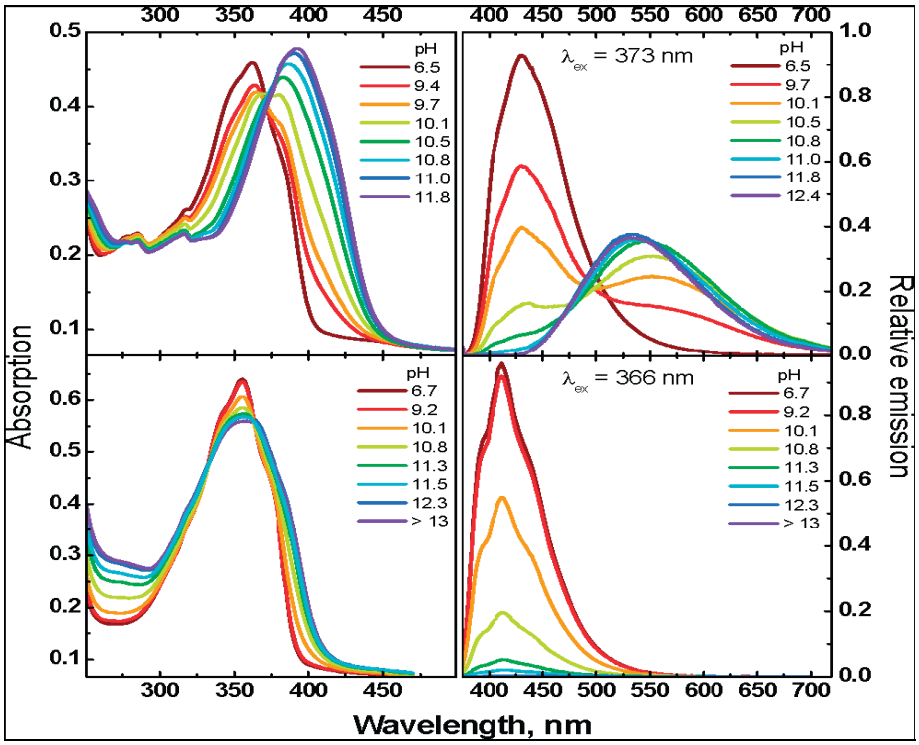

Figure 3.2. Absorption (left column) and emission (right column) spectra of **3.6** (top row) and **3.7** (bottom row) in the 2:1 mixture of MeOH/H_2O (v/v) at different pH values.

To obtain more information about the deprotonation dependent properties of the two distyrylbenzenes **3.6** and **3.7**, we analyzed the obtained absorption data (**3.6** and **3.7**) using the principal component analysis program SPECFIT.[7] Figure 3.3 shows the results. The pK_a values for **3.6** are pK_{a1}=10.1 ± (0.1) and pK_{a2} = 12.0 ± (0.1), while those for **3.7** are pK_{a1}= 10.6 ± (0.1) and pK_{a2} = 11.2 ± (0.3). The absorption data show that the first deprotonation of **3.6** is easier than that of **3.7**, however, the second pK_a of **3.6** is almost 0.8 units higher than that of **3.7**. The difference must be due to the conjugative, mesomeric interactions effective in **3.6** and its anions, as opposed to the purely electrostatic interactions in **3.7**, which render its two pK_a's more alike.

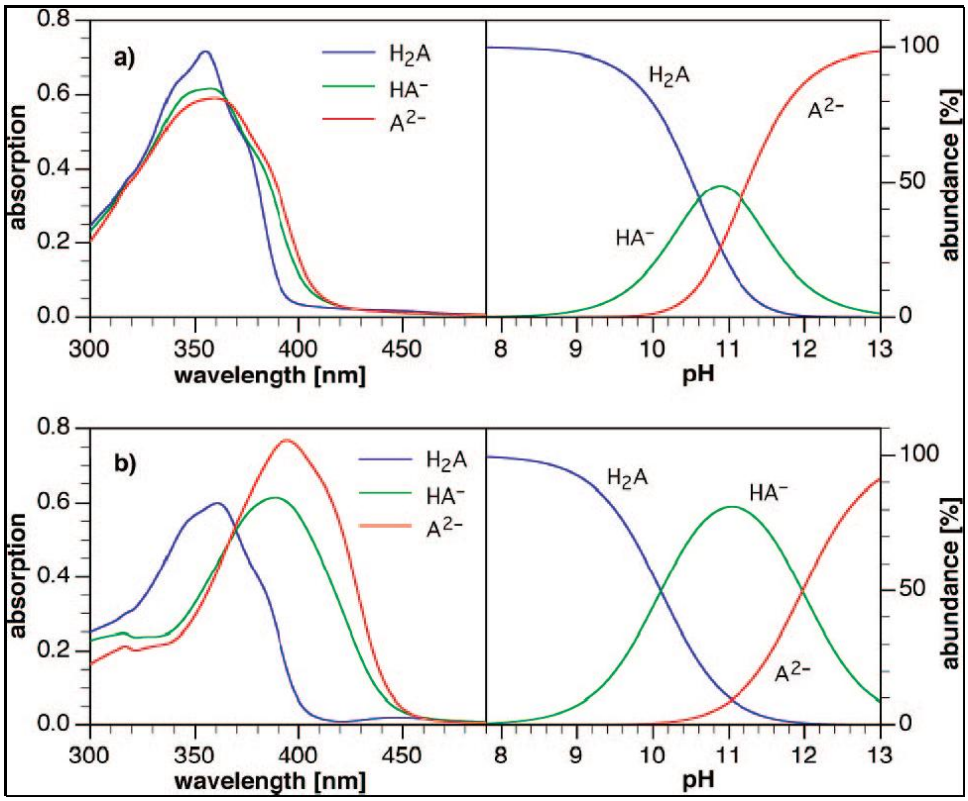

Figure 3.3. Deconvoluted absorption spectra (left) and species distribution diagram (right) for compounds **3.7** (row a) and **3.6** (row b).

The pK_{a1}* of **3.6** estimated using a modified Forster method,[8] however, is *1.9*, and unlike in more condensed hydroxyarenes, such moderate thermodynamic photoacidity does not lead to detectable ESPT in neutral methanol/water solutions that can compete effectively with the 0.91 ns decay.[9] Therefore, for **3.6** we do not see any appreciable ESPT, and the pK_a's determined from the fluorescence pH-titration simply reflects the ground-state acid-base equilibrium. From Figure 3.2, it is clear that upon the first deprotonation of **3.6** an absorption spectrum results that is close in appearance to that of the dianion **3.6**$^{2-}$. However, in the emission, the monoanion **3.6**$^{-}$ emission is red-shifted (575 nm) from both the neutral compound (428 nm) and the dianion **3.6**$^{2-}$ (533 nm). In contrast to the emission, the monoanion of **3.6** exhibits a blue-shifted absorption from

that of **3.6**$^{2-}$. We assume that the anion experiences and intramolecular charge transfer stabilization in the excited-state as the monodeprotonated species is formally a donor-acceptor system, leading to the observed red-shifted emission.

The same experiment, i.e. deprotonation of **3.7** (λ_{max} 355 nm) to **3.7**$^{2-}$ leads to a broadening of the absorption and a slight red shift to 363 nm with a red-shifted absorption edge. The emission of neutral **3.7** is centered at 412 nm. *Upon deprotonation its fluorescence is not shifted but quenched.* A reliable determination of pK_a* for **3.7** is problematic due to the complete absence of anion fluorescence. These observations, i.e., the quenching of the fluorescence of **3.7** upon deprotonation and the large red-shift of the fluorescence of **3.6** upon exposure to aqueous base are in stark contrast to the effects visible upon deprotonation of **3.8** and **3.9**.[5] On the one hand, **3.6** shows a much larger red–shift upon deprotonation and its dianion **3.6**$^{2-}$ is highly fluorescent. On the other hand, dianion **3.7**$^{2-}$ is weakly fluorescent but its absorption spectrum does not show a significant shift upon exposure to base, similar to the observation for other *m*-hydroxybenzylidene derivatives (*m*-hydroxystilbene[5a] and *m*-hydroxybenzylideneimidazolinone[10]). It is tempting to conclude that the reason for the fluorescence quenching involves twisting about the formal double bond. However, Sandros[3] and Motoyoshiya[4] have observed that distyrylbenzenes undergo adiabatic one-way cis/trans isomerization, producing emission spectra corresponding to the *E*/*E* forms only. More recently, time-resolved studies indicate the formation of an intermediate but largely planar excited state.[11] Thus, we conclude that twisting leading to quenching does not occur. In the case of stilbenes, twisting leads to such decay pathways.

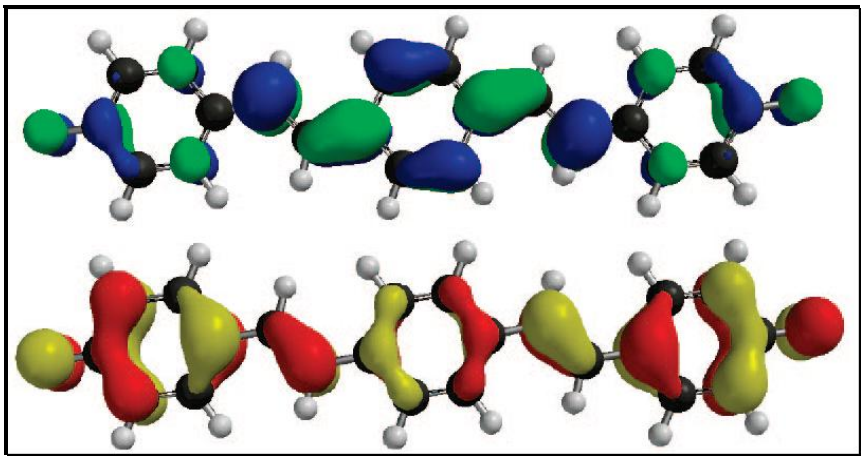

Figure 3.4. LUMO (top) and HOMO (bottom) of **3.6**$^{2-}$.

In order to investigate this phenomenon further, we performed quantum chemical calculations (B3LYP/6-311+G(2d,2p)// B3LYP//6-311+G(2d,2p)) upon **3.6**, **3.7**, and their respective dianions **3.6**$^{2-}$ and **3.7**$^{2-}$. Figures 3.4, 3.5 and Table 3.2 show the most salient results. While the neutral compounds **3.6** and **3.7** show frontier molecular orbitals (FMO) that are similar to those calculated for distyrylbenzenes, the FMOs for **3.6**$^{2-}$ show larger amplitudes in the two peripheral rings, as a consequence of the delocalized phenolate moieties. According to these calculations, the HOMO-LUMO gap decreases upon deprotonation from 3.27 to 2.48 eV.

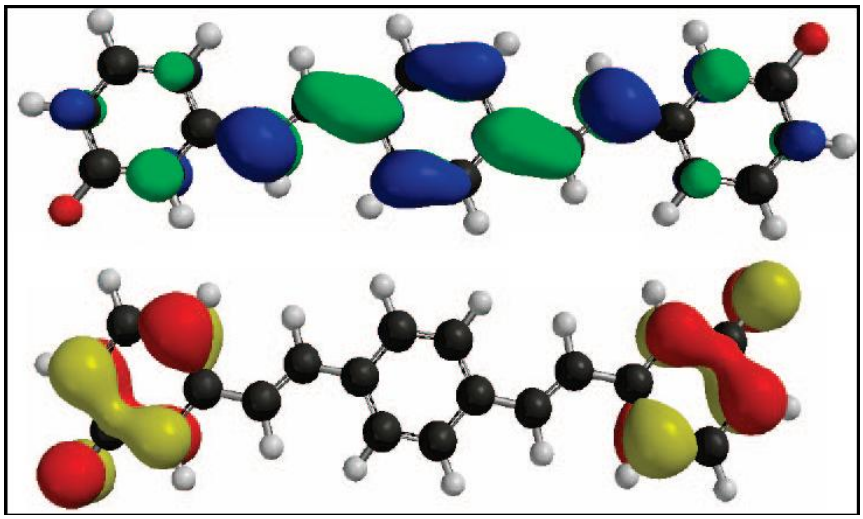

Figure 3.5. LUMO (top) and HOMO (bottom) of **3.7**$^{2-}$.

Table 3.2. Gas-phase computational data for compounds. [a] TDDFT/B3LYP/6 311+G(2d,2p)//B3LYP/6-311+G(2d,2p) level of theory. [b] Oscillator strength in parentheses. [c] Major component of the CI description. [d] Experimental vertical absorption energy. [e] From excitation spectrum.

Compound	**3.6**	**3.7**
Species	H_2A, A^{2-}	H_2A, A^{2-}
S_1 (eV)	3.18, 2.48	3.25, 1.91
$7B_g \rightarrow 7\ A_u$ [c]	$(2.33)^b$, $(2.39)^b$	$(2.21)^b$, $(0.061)^b$
S_6 (eV)	-	-, 3.13
$6B_g \rightarrow 7A_u$ [c]	-	-, $(1.74)^b$
Exp (eV)[d]	3.42 (S_1), 3.15(S_1)	3.49(S_1), 3.04(S_1)[e]-3.42(S_6)
HOMO (eV) ($7B_g$)	-5.22, 0.73	-5.50,0.44
LUMO (eV) ($7A_u$)	-1.96, 3.21	-2.18, 2.69
HOMO-LUMO Gap (eV)	3.27, 2.48	3.32, 2.26

In the case of **3.7**, the situation is dramatically different. The HOMO and the HOMO-1 are almost degenerate and localized on the two phenolate rings. In valence bond terms, the two phenolates are disjoint[12] and are electronically only weakly coupled, while the LUMO is extended over the whole π-system but has larger coefficients in the central ring.[13] Given the poor orbital overlap, the HOMO-LUMO transition leading to the lowest singlet excited-state S_1 is expected to exhibit a negligible oscillator strength despite the fact that a B_g -> A_u transition is symmetry allowed in the C_{2h} point group.

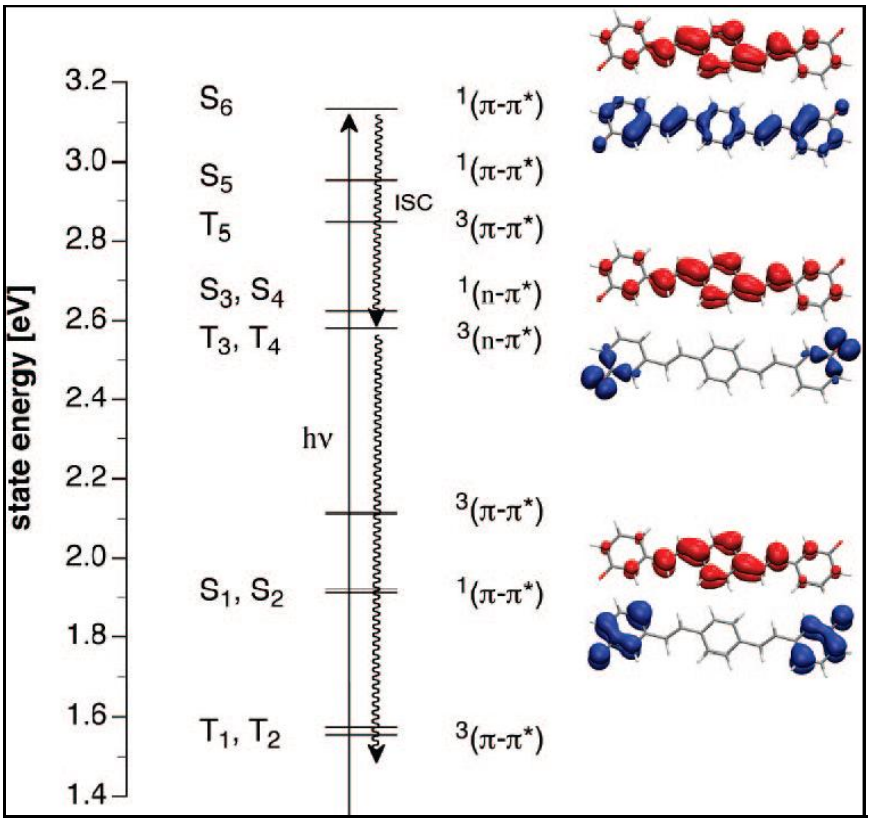

Figure 3.6. Excited-state manifold for dianion **3.7**$^{2-}$ based on TD-DFTcalculations (B3LYP/6-311+G(2d,2p)//B3LYP/6-311+G(2d,2p)).Upon excitation into S_6, nonradiative deactivation may occur through rapid intersystem crossing (ISC) to the ^{3}(n-π*) states T_3 and T_4. The surface plots to the right illustrate the π-π* and n-π* nature of S_1, S_3, and S_6 with the corresponding electron detachment (blue) and attachment (red) densities.

A closer inspection of the excited-state manifold obtained from time-dependent density functional theory (TD-DFT) calculations indeed revealed a strong S_1 oscillator strength for neutral **3.6** and **3.7** as well as **3.6**$^{2-}$ but not the *meta*-substituted dianion **3.7**$^{2-}$ (Table 3.2). The latter is preferentially excited into S_6, while all the lower states exhibit neglible oscillator strengths. Although the quantum chemical calculations offer only estimates for gas phase vertical excitation energies at 0 K, the dominant lowest energy transitions scale linearly with the solution phase experimental data (correlation coefficient 0.994, mean unsigned error 0.01 eV). In agreement with the experiment, the

calculations predict a strong bathochromic shift upon deprotonation of **3.6**, but only a small shift for **3.7** due to excitation into S^6 rather S^1 (Table 3.2). The TD-DFT results furthermore indicate a possible nonradiative deactivation pathway through a lower lying triplet $^3(n\text{-}\pi^*)$ state (Figure 3.6). According to the El-Sayed rule,[14] intersystem crossing from $^1(\pi\text{-}\pi^*)$ to $^3(n\text{-}\pi^*)$ is rapid and typically results in fluorescence quenching due to an increased nonradiative deactivation rate.[15] As illustrated with the electron detachment-attachment densities[16] in Figure 3.6, the triplet states T_3 and T_4 together with their parent states S_3 and S_4 exhibit $n\text{-}\pi^*$ character involving excitation of a nonbonding oxygen lone-pair electron, thus offering an efficient nonradiative deactivation channel from S_6 through T_3 and T_4. Because the calculations indicate that the two $^3(n\text{-}\pi^*)$ states lie above the lowest energy $^1(\pi\text{-}\pi^*)$ state, this nonradiative pathway should not be accessible upon excitation into S_1. Excitation at the red-edge in the absorption spectrum of $\mathbf{3.7}^{2-}$ revealed indeed a weak emission band centered around 541 nm, which was not visible with excitation at the absorption maximum. The corresponding excitation trace acquired at 541 nm peaked at 407 nm and lacked the major higher energy band visible in the absorption spectrum, thus confirming that excitation into S_6 results in nonradiative deactivation without detectible emission from S_1.

3.3 Conclusions

In conclusion, we have demonstrated that the two bis(hydroxystyryl)benzenes **3.6** and **3.7** show photophysical properties that are distinct from each other and also distinct from the smaller 3- and 4-hydroxystilbenes **3.8** and **3.9**. It is remarkable that the dianion of **3.6** is highly fluorescent, while the dianion of its isomer **3.7** is completely non

fluorescent. The large quantum yield of fluorescence of **3.6**, and its dianion presumably reflects a planarized and quite rigid excited-state with quinoidal resonance contributions, [3] while the quenching of the dianion of **3.7** may be explained by the presence of an intermediate ^{3}(n-π*) state combined with a poor Franck-Condon overlap between the HOMO and LUMO of this double phenolate. Overall, we find it remarkable that a consanguine group of styryl-based phenols **3.6**-**3.9** display such disparate-and fundamentally interesting-photoinduced effects, not easily predicted by simply examining the structural motifs involved. Such effects, when understood, help illuminate the rather unusual properties of the related hydroxy cruciforms[17] and may aid in the design of other conjugated fluorophores.[18]

3.4 Experimental

Materials and Methods: All chemicals were purchased from Aldrich Chemical, Acros, TCI America, or Fisher Scientific and used without purification unless otherwise specified. Column chromatography was performed using standard grade silica gel 60 Å, 32-63 μm (230 x 450 mesh) from Sorbent Technologies (Atlanta, GA) and the indicated eluent. Elution of the fluorophores was readily monitored using a handheld UV lamp (365 nm). Melting points were obtained using a Mel-Temp apparatus fitted with a Fluka 51K/J digital thermometer. All IR spectra were obtained using a Shimadzu FTIR-8400s spectrometer. Unless otherwise specified, NMR spectra were recorded at 298 K on a Bruker (500 MHz/400 MHz) or Varian Mercury spectrometer (300 MHz). Chemical shifts are reported in parts per million (ppm), using residual solvents (chloroform-*d*) or (THF-*d5*) as an internal standard. Data are reported as follows: chemical shift,

multiplicity (s = singlet, d = doublet, t = triplet, q = quartet, m = multiplet), coupling constant, and integration. Mass spectral analyses were provided by the Georgia Institute of Technology Mass Spectrometry Facility.

All absorption spectra were collected using a Shimadzu UV-2401PC spectrophotometer. All emission spectra were acquired using a Shimadzu RF-5301PC spectrofluorophotometer. Lifetime data were collected using a Lifespec-ps (Edinburgh Instruments), pulsed diode laser (PicoQuant, 372 nm excitation), and PMT detector (Hamamatsu). Data were fit to single exponential decay so as to optimize chi-squared values. Quantum yields for all cruciforms were measured using standard procedures.[19] In all cases, quinine sulfate was used as a standard.

Synthesis of intermediates 3.4 and 3.5:

General Procedure: An oven dried Schlenk flask cooled under nitrogen was charged with **3.1** (0.500 g, 1.32 mmol), potassium *tert*-butoxide (60 mg, 2.5 mmol), and THF (50 mL). The flask was closed with a septum, a nitrogen-filled balloon was fitted to the arm and the stopcock was opened. Upon addition of the potassium *tert*-butoxide, the solution turned purple-red. 4-(Tetrahydropyran-2-yloxy)benzaldehyde (**3.2**) (0.409 g, 1.98 mmol) or 3-(tetrahydropyran-2-yloxy)-benzaldehyde (**3.3**) (0.409 g, 1.98 mmol) was then added dropwise over a 10 min period. The reaction was allowed to stir overnight before work-up. The small excess potassium *tert*-butoxide was quenched with water and the mixture was extracted three times with dichloromethane. The organic layer was washed three times with water and dried with magnesium sulfate and reduced until a pale yellow precipitate was formed. The yellow precipitate was purified by chromotagraphy eluting with 80:20 dichloromethane/hexanes to give yellow crystals.

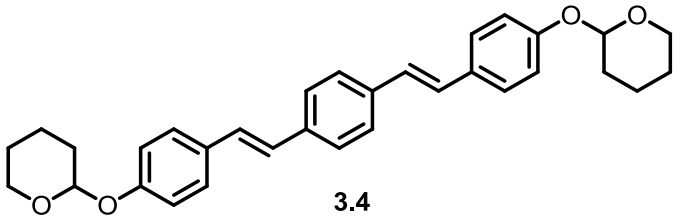

3.4

Compound 3.4: Yield: 62%. *MP:* 270-272 ºC. *IR:* 2923, 2867, 1600, 1514, 1234, 1174, 1108, 964, 837. *^{1}H NMR (500 MHz, $CDCl_3$):* δ = 7.50 (s, 4H, Ar-H), 7.48 (d, 4H, Ar-H, $J_{H,H}$ = 8.5 Hz), 7.11 (d, 2H, C=C-H, $J_{H,H}$ = 16.5 Hz), 7.08, (d, 4H, Ar-H, $J_{H,H}$ = 8.5 Hz), 7.01 (d, 2H, C=C-H, $J_{H,H}$ = 16.5 Hz), 5.49 (s, 2H, α-C-H), 3.95 (m, 2H, ε-C-H), 3.65 (m, 2H, ε-C-H), 2.04 (m, 2H, β-C-H), 1.91 (m, 4H, γ-C-H) 1.71 (m, 4H, δ-C-H), 1.64 (m, 2H, β-C-H). *^{13}C NMR (125 MHz, $CDCl_3$):* δ = 156.9, 136.9, 131.3, 128.4, 128.2, 127.8, 126.8, 116.9, 96.56, 62.2, 30.1, 25.5, 18.9.

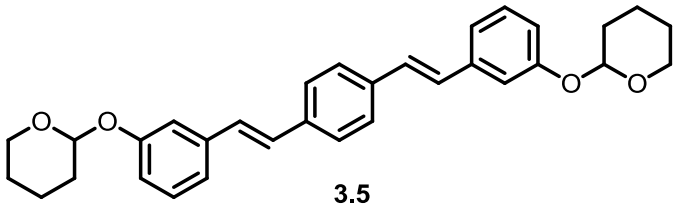

3.5

Compound 3.5: Yield: 65%. *MP:* 248-250 ºC. *IR:* 2924.8, 2871.8, 1593.5, 1574.7, 1446.9, 1201.1, 1158.1, 1108.9, 1003.4, 964.3. . *^{1}H NMR (500 MHz, $CDCl_3$):* δ = 7.52 (s, 4H, Ar-H), 7.30 (t, 2H, Ar-H, $J_{H,H}$ = 8 Hz), 7.26 (s, 2H, Ar-H), 7.18 (d, 2H, Ar-H, $J_{H,H}$ = 8 Hz), 7.12 (s, 4H, C=C-H), 7.00 (d, 2H, Ar-H, $J_{H,H}$ = 8.5 Hz), 5.51 (s, 2H, α-C-H), 3.97 (m, 2H, ε-C-H), 3.67 (m, 2H, ε-C-H), 2.06 (m, 2H, β-C-H), 1.91 (m, 4H, γ-C-H) 1.73 (m, 4H, δ-C-H), 1.65 (m, 2H, β-C-H). ^{13}C NMR (*125 MHz,* $CDCl_3$): δ = 157.8, 139.1, 137.1, 129.9, 128.9, 127.2, 120.5, 116.2, 114.7, 96.7, 62.4, 30.8, 25.6, 19.1

Synthesis of bis(hydroxystyryl)benzenes 3.6 and 3.7:

Compounds **3.4** and **3.5** were deprotected by trifluoroacetic acid in dichloromethane. The products were obtained by extracting with ethyl ether or ethyl acetate. The yields reported reflect the amount of pure material that was recovered after deprotection and recrystallization.

1,4-Bis(*p*-hydroxystyryl)benzene 3.6: **3.4** (0.200 g, 0.414 mmol) was dissolved in dichloromethane (30 mL) and trifluoroacetic acid (1 mL) was added into a 100-mL round bottom flask. The solution was allowed to stir for 2 h. The product was extracted with ethyl ether, washed three times with water, dried with magnesium sulfate and reduced until a dark green powder was formed. The powder was washed with dichloromethane and collected by suction filtration and dried under vacuum. Yield: 70%. *MP:* 300 ºC. *IR:* 3278, 3010, 1676, 1602, 1514, 1448, 1377, 1249, 960, 831. *^{1}H NMR (500 MHz, THF-d5):* δ = 8.36 (s, 2H, Ar-OH), 7.45 (s, 4H, Ar-H), 7.36 (d, 4H, Ar-H, $J_{H,H}$ = 8.5 Hz), 7.08 (d, 2H, C=C-H, $J_{H,H}$ = 16.5 Hz), 6.94 (d, 2H, C=C-H, $J_{H,H}$ = 16.5 Hz), 6.72 (d, 2H, Ar-H, $J_{H,H}$ = 8.5 Hz). *^{13}C NMR (125 MHz, THF-d_8):* δ = 159.7, 138.8 131.1, 130.1, 129.6, 128.3, 127.07, 117.4. *MS (EI, 70-SE) ($C_{22}H_{18}O_2$)*: m/z = 314.

1,4-Bis(*m*-hydroxystyryl)benzene 3.7: **3.5** (0.200 g, 0.414 mmol) was dissolved in dichloromethane (30 mL) and trifluoroacetic acid (1 mL) was added into a 100-mL round bottom flask. The solution was allowed to stir for 2 h. The product was extracted with ethyl ether, washed three times with water, dried with magnesium sulfate and reduced until a yellow powder was formed. The powder was recrystallized by dissolving in hot

ethyl acetate and adding an excess amount of hexanes. Yield: 76%. MP: 240 ºC IR: 3345.7, 3025.4, 1645.2, 1590.2, 1447.4, 1301.2 1157.6, 962.4, 800.3. *^{1}H NMR (400 MHz, DMSO-d_6):* δ = 9.43 (s, 2H, Ar-OH), 7.61 (s, 4H, Ar-H), 7.21 (d, 2H, C=C-H, $J_{H,H}$ = 16.5 Hz), 7.18 (t, 2H, Ar-H, $J_{H,H}$ = 8.5 Hz), 7.16 (d, 2H, C=C-H, $J_{H,H}$ = 16.5 Hz), 7.05 (d, 2H, Ar-H, $J_{H,H}$ = 7.5 Hz), 6.99 (s, 2H, Ar-H), 6.70 (d, 2H, Ar-H, $J_{H,H}$ = 8.5 Hz). ^{13}C NMR (*125 MHz, THF-d_8*): δ= 158.4, 139.2, 137.23, 129.5, 128.9, 128.2, 126.9, 118.0, 114.9, 113.3. *MS (EI, 70-SE) ($C_{22}H_{18}O_2$)*: m/z = 314.

Determination of p*K*a Values: Measurements were performed with a combination glass microelectrode (Orion, Thermo Electron Corp, Waltham). The electrode was precalibrated in aqueous buffers at pH 4, 7, and 10. Solution pH measurements were performed in 2/1 v/v methanol-water mixtures. For the determination of the pK_a's, a series of UV-vis spectra were acquired for which –log[H_3O^+] was varied between 5 and 12. It was demonstrated[20] that the pH can be measured directly in alcohol-water mixtures using glass electrodes precalibrated in aqueous buffers. In this case for 2/1 v/v methanol/water mixtures the observed pH values are 0.18 pH units higher than the real ones for this mixture. The raw spectral data were processed via non-linear least squares fit analysis using the SPECFIT software package,[7] providing deconvoluted spectra for each species present as well as the acidity constants for the relevant protonation equilibria.

Computational Methods: Quantum chemical calculations were performed using the Q-Chem computational package.[21] Ground state (S_0) equilibrium geometries for each compound were optimized using density functional theory with the B3LYP functional

and the triple split valence polarized basis set 6-311+G(2d,2p) with added diffuse functions for improved accuracy of the di-anion structures.

Table 3.3. Cartesian atomic coordinates for neutral **3.6** (S_0, B3LYP/6-311+G(2d,2p), C_{2h}, E = –999.91745779 a.u.)

Atom	X (Å)	Y (Å)	Z (Å)
H	8.190388	-2.027408	0.000000
C	7.537830	-1.162661	0.000000
C	5.852421	1.039759	0.000000
C	6.159437	-1.334101	0.000000
C	8.075818	0.120288	0.000000
C	7.222379	1.224806	0.000000
C	5.278915	-0.243655	0.000000
H	5.755633	-2.338069	0.000000
O	9.421003	0.366356	0.000000
H	7.649409	2.217519	0.000000
C	3.839281	-0.491297	0.000000
H	5.216231	1.912979	0.000000
C	2.853885	0.424400	0.000000
H	3.571002	-1.542231	0.000000
H	3.120898	1.475555	0.000000
C	1.415964	0.175381	0.000000
C	-1.415964	-0.175381	0.000000
C	0.838568	-1.103817	0.000000
C	0.534075	1.270723	0.000000
C	-0.838568	1.103817	0.000000
C	-0.534075	-1.270723	0.000000
H	1.469432	-1.981180	0.000000
H	0.944386	2.272408	0.000000
H	-1.469432	1.981180	0.000000
H	-0.944386	-2.272408	0.000000
C	-2.853885	-0.424400	0.000000
C	-3.839281	0.491297	0.000000
H	-3.120898	-1.475555	0.000000
H	-3.571002	1.542231	0.000000
C	-5.278915	0.243655	0.000000
C	-8.075818	-0.120288	0.000000
C	-5.852421	-1.039759	0.000000
C	-6.159437	1.334101	0.000000
C	-7.537830	1.162661	0.000000
C	-7.222379	-1.224806	0.000000
H	-5.216231	-1.912979	0.000000
H	-5.755633	2.338069	0.000000
H	-8.190388	2.027408	0.000000
H	-7.649409	-2.217519	0.000000
O	-9.421003	-0.366356	0.000000
H	-9.907432	0.463425	0.000000
H	9.907432	-0.463425	0.000000

Table 3.4. Cartesian atomic coordinates for bis-deprotonated **3.6**$^{2-}$ (S_0, B3LYP/6-311+G(2d,2p), C_{2h}, E = –998.77466211 a.u.)

Atom	X (Å)	Y (Å)	Z (Å)
H	8.202461	-2.053109	0.000000
C	7.558534	-1.181180	0.000000
C	5.912279	1.057413	0.000000
C	6.187937	-1.321974	0.000000
C	8.202498	0.110293	0.000000
C	7.277020	1.224496	0.000000
C	5.300876	-0.219936	0.000000
H	5.760865	-2.321038	0.000000
O	9.458358	0.262081	0.000000
H	7.707866	2.219344	0.000000
C	3.874781	-0.442546	0.000000
H	5.281360	1.939095	0.000000
C	2.862560	0.464247	0.000000
H	3.598983	-1.494805	0.000000
H	3.117790	1.519514	0.000000
C	1.432478	0.197043	0.000000
C	-1.432478	-0.197043	0.000000
C	0.853651	-1.087804	0.000000
C	0.518261	1.272336	0.000000
C	-0.853651	1.087804	0.000000
C	-0.518261	-1.272336	0.000000
H	1.494125	-1.959865	0.000000
H	0.912553	2.282531	0.000000
H	-1.494125	1.959865	0.000000
H	-0.912553	-2.282531	0.000000
C	-2.862560	-0.464247	0.000000
C	-3.874781	0.442546	0.000000
H	-3.117790	-1.519514	0.000000
H	-3.598983	1.494805	0.000000
C	-5.300876	0.219936	0.000000
C	-8.202498	-0.110293	0.000000
C	-5.912279	-1.057413	0.000000
C	-6.187937	1.321974	0.000000
C	-7.558534	1.181180	0.000000
C	-7.277020	-1.224496	0.000000
H	-5.281360	-1.939095	0.000000
H	-5.760865	2.321038	0.000000
H	-8.202461	2.053109	0.000000
H	-7.707866	-2.219344	0.000000
O	-9.458358	-0.262081	0.000000

Table 3.5. Cartesian atomic coordinates for neutral **3.7** (S_0, B3LYP/6-311+G(2d,2p), C_{2h}, E = –999.91750715 a.u.)

Atom	X (Å)	Y (Å)	Z (Å)
H	-1.604277	-1.876594	0.000000
C	-0.913069	-1.045581	0.000000
C	0.913069	1.045581	0.000000
C	0.444978	-1.305180	0.000000
C	-1.397647	0.271181	0.000000
C	-0.444978	1.305180	0.000000
C	1.397647	-0.271181	0.000000
H	0.790118	-2.331721	0.000000
H	-0.790118	2.331721	0.000000
H	1.604277	1.876594	0.000000
C	-2.815610	0.615632	0.000000
C	-3.857395	-0.234014	0.000000
H	-3.014612	1.680827	0.000000
H	-3.663218	-1.300048	0.000000
C	2.815610	-0.615632	0.000000
C	3.857395	0.234014	0.000000
H	3.014612	-1.680827	0.000000
H	3.663218	1.300048	0.000000
C	5.276894	-0.121179	0.000000
C	8.034079	-0.677247	0.000000
C	5.740870	-1.447650	0.000000
C	6.220172	0.912961	0.000000
C	7.584061	0.639344	0.000000
C	7.099788	-1.711613	0.000000
H	5.042114	-2.270996	0.000000
H	5.896697	1.945374	0.000000
H	7.446984	-2.735884	0.000000
H	9.094634	-0.895843	0.000000
C	-5.276894	0.121179	0.000000
C	-8.034079	0.677247	0.000000
C	-5.740870	1.447650	0.000000
C	-6.220172	-0.912961	0.000000
C	-7.584061	-0.639344	0.000000
C	-7.099788	1.711613	0.000000
H	-5.042114	2.270996	0.000000
H	-5.896697	-1.945374	0.000000
H	-7.446984	2.735884	0.000000
H	-9.094634	0.895843	0.000000
O	-8.434834	-1.713118	0.000000
O	8.434834	1.713118	0.000000
H	-9.346301	-1.406724	0.000000
H	9.346301	1.406724	0.000000

Table 3.6. Cartesian atomic coordinates for bis-deprotonated **3.7**$^{2-}$ (S_0, B3LYP/6-311+G(2d,2p), C_{2h}, E = –998.75867344 a.u.).

Atom	X (Å)	Y (Å)	Z (Å)
H	-1.593934	-1.882857	0.000000
C	-0.907323	-1.047007	0.000000
C	0.907323	1.047007	0.000000
C	0.454670	-1.297360	0.000000
C	-1.411849	0.264387	0.000000
C	-0.454670	1.297360	0.000000
C	1.411849	-0.264387	0.000000
H	0.804517	-2.323551	0.000000
H	-0.804517	2.323551	0.000000
H	1.593934	1.882857	0.000000
C	-2.832891	0.602387	0.000000
C	-3.882571	-0.243920	0.000000
H	-3.035988	1.667582	0.000000
H	-3.685018	-1.311460	0.000000
C	2.832891	-0.602387	0.000000
C	3.882571	0.243920	0.000000
H	3.035988	-1.667582	0.000000
H	3.685018	1.311460	0.000000
C	5.306983	-0.099107	0.000000
C	8.064326	-0.633663	0.000000
C	5.763484	-1.433798	0.000000
C	6.235826	0.944660	0.000000
C	7.665446	0.749973	0.000000
C	7.137377	-1.666594	0.000000
H	5.069243	-2.262166	0.000000
H	5.882261	1.970686	0.000000
H	7.494337	-2.692940	0.000000
H	9.127716	-0.845638	0.000000
C	-5.306983	0.099107	0.000000
C	-8.064326	0.633663	0.000000
C	-5.763484	1.433798	0.000000
C	-6.235826	-0.944660	0.000000
C	-7.665446	-0.749973	0.000000
C	-7.137377	1.666594	0.000000
H	-5.069243	2.262166	0.000000
H	-5.882261	-1.970686	0.000000
H	-7.494337	2.692940	0.000000
H	-9.127716	0.845638	0.000000
O	-8.492208	-1.713939	0.000000
O	8.492208	1.713939	0.000000

3.5 References and Notes

1. Benfaremo, N.; Sandman, D. J.; Tripathy, S.; Kumar, J.; Yang, K.; Rubner, M. F.; Lyons, C. *Macromolecules* **1998**, *31*, 3595–3599.

2. (a) Saltiel, J.; Sun, Y. P. *J. Phys. Chem.***1989**, *93*, 6246– 6250. (b) Meier, H. *Angew. Chem., Int. Ed.* **1992**, *31*, 1399–1440. (c) Waldeck, D. H. *J. Mol. Liq.* **1993**, *57*, 127–148.

3. Sandros, K.; Sundahl, M.; Wennerstro¨m, O.; Norinder, U. *J. Am. Chem. Soc.* **1990**, *112*, 3082–3086.

4. Fengqiang, Z.; Motoyoshiya, J.; Nakamura, J.; Nishii, Y.; Aoyama, H. *Photochem. Photobiol.* **2006**, *82*, 1645–1650.

5. (a) Lewis, F. D.; Crompton, E. M. *J. Am. Chem. Soc.* **2003**, *125*, 4044–4045. (b) Crompton, E. M.; Lewis, F. D. *Photochem. Photobiol. Sci.* **2004**, *3*, 660–668. (c) Lewis, F. D.; Sinks, L. E.; Weigel, W.; Sajimon, M. C.; Crompton, E. M. *J. Phys. Chem. A* **2005**, *109*, 2443–2451.

6. Canals, I.; Oumada, F. Z.; Roses, M.; Bosch, E. *J. Chromatogr. A* **2001**, *911*, 191–202.

7. Binstead, R. A.; Zuberbu¨hler, A. D.; Jung, B. *SPECFIT* V. *3.0.40*; Spectrum Software Associates: Marlborough, MA, 2007.

8. Grabowski, Z. R.; Grabowska, A. *Z. Phys. Chem. N.F.* **1976**, *101*, 197–208.

9. Tolbert, L. M.; Solntsev, K. M. *Acc. Chem. Res.* **2002**, *35*, 19–27.

10. Solntsev, K. M.; Poizat, P.; Dong, J.; Rehault, J.; Lou, Y.; Burda, C.; Tolbert, L. M. *J. Phys. Chem. B* **2008**, *112*, 2700–2711.

11. Hsu, F.-C.; Hayashi, M.; Wang, H.-W.; Lin, S. H.; Wang, J.-K. *J. Phys. Chem.* **2007**, *111*, 759–763.

12. (a) Borden, W. T.; Davidson, E. R. *J. Am. Chem. Soc.* **1977**, *99*, 4587–4594. (b) Properly speaking, "disjoint" refers to diradicals, but the description applies to radical anions and dianions as well.

13. (a) Wilson, J. N.; Bunz, U. H. F. *J. Am. Chem. Soc.* **2005**, *127*, 4124–4125. (b) Zucchero, A. J.; Wilson, J. N.; Bunz, U. H. F. *J. Am. Chem. Soc.* **2006**, *128*, 11872–11881.

14. (a) Lower, S. K.; El-Sayed, M. A. *Chem. Rev.* **1966**, *66*, 199–241. (b) El-Sayed, M. A. *Acc. Chem. Res.* **1968**, *1*, 8–16.

15. (a) Brederek, K.; Forster, T.; Oesterlin, H. G. *Luminescence of Organic and Inorganic Materials*; Kallman, H. P., Sprunch, G. M.; Eds.; Wiley: New York, 1962; p. 161. (b) Young, V, Jr.; Quiring, H. L.; Sykes, A. G. *J. Am. Chem. Soc.* **1997**, *119*, 12477–12480. (c) Leray, I.; Lefevre, J. P.; Delouis, J. F.; Delaire, J.; Valeur, B. *Chem. Eur. J.* **2001**, *7*, 4590–4598. (d) Zhou, Z.; Fahrni, C. J. *J. Am. Chem. Soc.* **2004**, *126*, 8862–8863.

16. Head-Gordon, M.; Grana, A. M.; Maurice, D.; White, C. A. *J. Phys. Chem.* **1995**, *99*, 14261–14270.

17. McGrier, P. L.; Solntsev, K. M.; Scho¨nhaber, J.; Brombosz, S. M.; Tolbert, L. M.; Bunz, U. H. F. *Chem. Commun.* **2007**, 2127–2129.

18. Hudson, B.; Kohler, B. *Synth. Met.* **1984**, *9*, 241–53.

19. "A Guide to Recording Fluorescence Quantum Yields." Horiba Jobin Yvon Ltd. Available online: http://www.jobinyvon.co.uk/ukdivisions/Fluorescence/plqy.htm Accessed 06/14/2010.

20. (a) Bosch, E.; Bou, P.; Allemann, H.; Roses, M. *Anal. Chem*. **1996**, *68*, 3651-3657. (b) Avdeef, A.; Box, K. J.; Comer, J. E. A.; Gilges, M.; Hadley, M.; Hibbert, C.; Patterson, W.; Tam, K. Y. *J. Pharm. Biomed. Anal.* **1999**, *20*, 631-641. (c) Canals, I.; Portal, J. A.; Bosch, E.; Roses, M. *Anal. Chem*. **2000**, *72*, 1802-1809. (d) Canals, I.; Valko, K.; Bosch, E.; Hill, A. P.; Rose´s, M. *Anal. Chem*. **2001**, *73*, 4937-4945. (e) Canals, I.; Oumada, F. Z.; Rose´s, M.; Bosch, E. *J. Chromatogr., A* **2001**, *911*, 191-202.

21. Kong, J.; White, C. A.; Krylov, A. I.; Sherrill, D.; Adamson, R. D.; Furlani, T. R.; Lee, M. S.; Lee, A. M.; Gwaltney, S. R.; Adams, T. R.; Ochsenfeld, C.; Gilbert, A. T. B.; Kedziora, G. S.; Rassolov, V. A.; Maurice, D. R.; Nair, N.; Shao, Y. H.; Besley, N. A.; Maslen, P. E.; Dombroski, J. P.; Daschel, H.; Zhang, W. M.; Korambath, P. P.; Baker, J.; Byrd, E. F. C.; Van Voorhis, T.; Oumi, M.; Hirata, S.; Hsu, C. P.; Ishikawa, N.; Florian, J.; Warshel, A.; Johnson, B. G.; Gill, P. M. W.; Head-Gordon, M.; Pople, J. A. *J. Comput. Chem.* **2000**, *21*, 1532-1548.

Chapter 4

Hydroxycruciforms: Amine Responsive Fluorophores

4.1 Introduction

In this chapter, we investigate the synthesis, photophysics and amine responsive optical properties in absorption and emission of three uniquely designed cruciform (XF) chromophores **4.6**-**4.8**. The detection and quantification of low-molecular-weight amines is critical in the medical field, in environmental science, and in food safety. The enhanced presence of low-molecular-weight amines in breath can mark disease states in patients and in foods it indicates spoilage. The detection and quantification of amines has been achieved by antibodies,[1] molecularly imprinted polymers,[2] enzymes,[3] single-molecule and array sensors,[4] and chromatographic methods.[5] Recently Lavinge, at the University of South Carolina, elegantly demonstrated that the interplay of planarization and aggregate formation in a water soluble polythiophene derivative is a powerful colorimetric tool to detect histamine in food, predicting spoilage in fish samples.[6] Inspired by Lavignes work, we have tailored a novel class of cruciform fluorophores/chromophores (XF), 1,4-distyryl-2,5-bis(arylethynyl)benzenes, containing strategically placed phenol functionalities as model probes for amines.[7] While these small XF-fluorophores do not display aggregation or distinct planarization behavior,[8] their specifically engineered frontier molecular orbitals (FMOs) should allow signal generation and amplification of amine-probing functions such as phenols. The phenols exhibit either full or partial proton transfer to the amine nitrogen atom, resulting in observable spectroscopic changes.

4.1.2 Chromophore Design

Chromophore design centers around different fundamental paradigms: 1) Choose or construct a suitable (aromatic) carbocyclic or heterocyclic skeleton, then 2) attach the necessary auxochromic groups, that is, electron-accepting or electron releasing substituents to the skeleton to tune the absorption and emission. In most chromophores donor and acceptor substituents are attached to the skeleton into positions in which both FMOs have their largest orbital nodes, ensuring the maximum conjugative effect of the auxochromes to the dye skeleton.[9] Auxochromes enlarge the π-system and stabilize/destabilize both the HOMO and LUMO, but to a different degree, leading to red-shifted absorption.

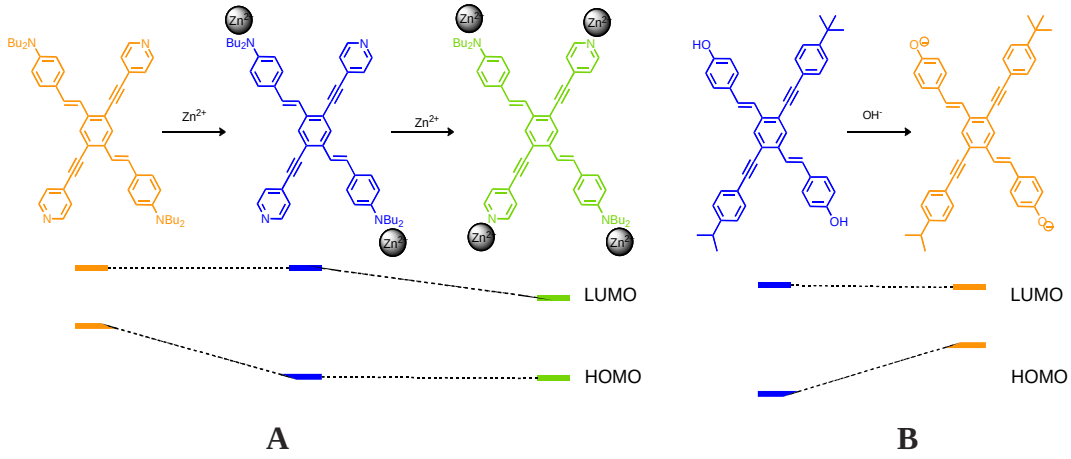

Scheme 4.1. Modulation of the HOMO-LUMO gap in cruciform fluorophores by interaction with metal cations (**A**) and pH change (**B**).

We and others have designed dyes in which the geometric overlap of HOMO and LUMO is minimized. These dyes, XFs, consist of two independent but centrally connected molecular axes, which carry electron-donating and electron-withdrawing substituents respectively; this arrangement leads to a situation in which the HOMO is spatially confined on the electron-rich branch, while the LUMO is confined on the branch that carries the electron-withdrawing substituents. One consequence of the spatially

localized FMOs is a surprisingly large auxochromic effect; that is, absorption and emission are more strongly influenced by substituents than would be generally expected, allowing to tune the emission of a carbocyclic skeleton from blue to red. These FMO-separated fluorophores should allow biomolecular or environmental sensing as XFs might be able to probe metal cations in cell compartments.[10] Outlined in Scheme 4.1 is a two stage metalloresponsive, orange-emitting model fluorophore **A**. Upon exposure to magnesium or zinc ions the fluorescence of **A** changes to blue, but upon further increasing the amount of metal salt the fluorescence color changes from blue to yellow-green. The unusual color changes are explained by a consecutive stabilization of first the HOMO and then the LUMO of the metal-complexed XF (Scheme 4.1).

While we have investigated the stabilization of the FMOs, we can also induce destabilization of the HOMO by introduction of negative charges as in the hydroxy XFs **B** (Scheme 4.1), and indeed, deprotonation led to a red-shift in emission.[11] The LUMO of **B** is not affected according to DFT calculations. In this contribution we examine the emissive properties of three different hydroxy-substituted XFs **4.6**–**4.8** and their emissive properties upon deprotonation and upon exposure to a panel of amines in different solvents. These studies are of interest as it is possible, just by changing the solvent, to identify specific amines by the analysis of the fluorescence color of a single XF, **4.8**.

4.2 Results and Discussion

4.2.1 Synthesis of Hydroxy XFs

The synthesis of hydroxy XFs **4.6-4.8** begins with a Horner reaction of **4.1** with the aldehydes **4.2a** or **4.2b** to furnish the distyrylbenzene derivatives **4.3a** and **4.3b** in 77

and 64 % yield, respectively, after chromotagraphy (Scheme 4.2). Subsequently, a Sonogashira coupling with either **4.4a** or **4.4b** gave rise to the formation of **4.5 a-c** in yields from 61 to 77%. At a temperature of – 78 °C, trifluoroacetic acid (TFA) neatly deprotected **4.5 a-c** in dichloromethane to give XFs **4.6-4.8** in yields around 88-92 % as air and water stable yellow powders.

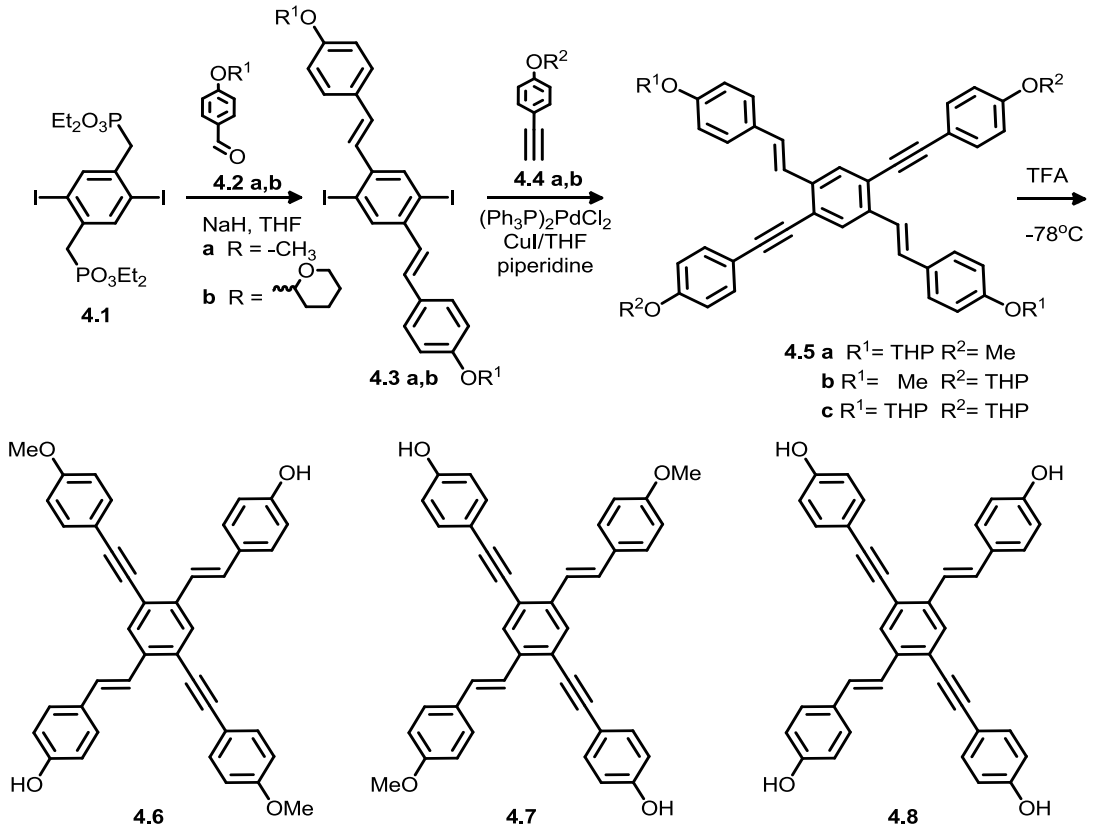

Scheme 4.2. Synthesis of hydroxy XFs **4.6-4.8**

4.2.2 Spectroscopic Properties and Titration Studies of Hydroxy XFs

Figure 4.1 displays the absorption and emission spectra of **4.6–4.8** in different solvents (see also Tables 4.1–4.3). The spectra of tetra-ether **8c** are given for comparison. Solvatochromic behavior of **4.6-4.8** and **4.5c** was investigated.[12] Kamlet–Taft solvent

parameters can account for the contribution of selective (such as point-to-point hydrogen-bonding interactions) versus nonselective (solute–solvent dipole interactions) solvation to

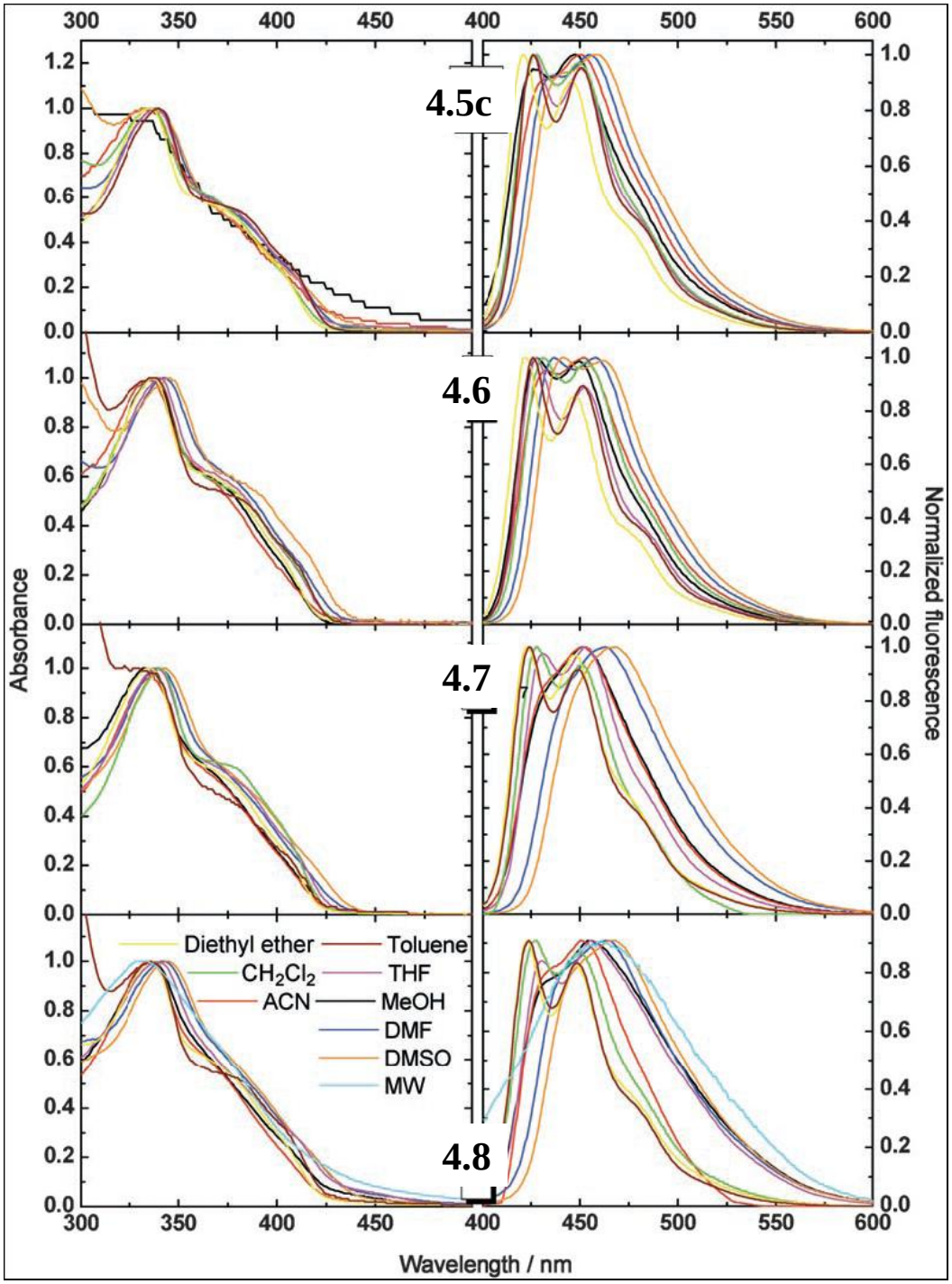

Figure 4.1. Absorption and emission spectra of **4.5c** and **4.6-4.8** in different solvents. The color coding is the identical for all graphs. MW is 1:9 vol. methanol/water.

the electronic spectra of the hydroxyaromatic molecules. For **4.5c** the absorbance spectra depend weakly on solvent polarity, indicating a small ground-state dipole moment. The emission spectra of **4.5c** exhibit stronger bathochromic shifts in polar solvents due to the increase in dipole moment upon excitation (Table 4.4). All four compounds (**4.5c**, **4.6-4.8**) are isoelectronic. We assume that their dipole moments in the ground and the excited states are similar. Therefore, additional bathochromic shifts in the di- and tetrahydroxy cruciforms are related to hydrogen-bonding between the hydroxy groups of the chromophores and basic solvents, such as DMSO or DMF. However, these shifts are small, indicating weak acidity of phenol moieties in both ground and excited states. A weak shoulder located at 530 nm in the emission of **4.8** in 90 % water/methanol solvent mixtures might be associated with the excited state proton-transfer product. For all dyes the fluorescence quantum yield in methanol was in the range of 16-37 % (Table 4.5). Compound **4.7** has the highest quantum yield and the longest emissive lifetime (τ = 1.6 ns). It is not clear what the reason is for the differences in structurally similar XFs.

Table 4.1. Absorption and emission maxima for **4.6** in different solvents.

Solvent	$\lambda_{max\ abs}$	$\lambda_{max\ em}$	Stokes Shift [cm^{-1}]	Vibronic Progression [cm^{-1}]
Methanol	336, 365 sh	451	7589, 5224	-
Acetonitrile	337, 370 sh	451	7501, 4854	-
DMF	340, 375 sh	463	7813, 5068	-
DMSO	343, 380 sh	468	7787, 4948	-
THF	339, 370 sh	431, 453	6297, 3825	1127
DCM	342, 380 sh	428, 451	5875, 2951	1192
Ether	336, 370 sh	423, 447	6121, 3386	1269
Toluene	339, 375 sh	424, 449	5914, 3082	1313

Table 4.2. Absorption and emission maxima for **4.7** in different solvents.

Solvent	$\lambda_{max\ abs}$	$\lambda_{max\ em}$	Stokes Shift [cm^{-1}]	Vibronic Progression [cm^{-1}]
Methanol	338, 370 sh	428, 450	6221, 3663	1142
Acetonitrile	337, 370 sh	433, 452	6579, 3932	971
DMF	344, 375 sh	437, 458	6186, 3783	1049
DMSO	346, 380 sh	441, 462	6226, 3640	1031
THF	341, 370 sh	428, 453	5961, 3663	1289
DCM	339, 375 sh	431, 453	6297, 3465	1127
Ether	338, 370 sh	422, 448	5889, 3330	1375
Toluene	339, 380 sh	426, 452	6024, 2842	1350

Table 4.3. Absorption and emission maxima for **4.8** in different solvents.

Solvent	$\lambda_{max\ abs}$	$\lambda_{max\ em}$	Stokes Shift [cm^{-1}]	Vibronic Progression [cm^{-1}]
90:10 H_3COH/H_2O	334	458	8106	-
Methanol	337	435, 456	6685	1059
Acetonitrile	335	438, 450	7020	609
DMF	343	464	7602	-
DMSO	345	467	7572	-
THF	340	432, 456	6264	1218
DCM	332	428, 450	6756	1142
Ether	337, 370 sh	424, 449	6089, 3442	1313
Toluene	336	424, 448	6177	1263

Table 4.4. Absorption and emission maxima for **4.5c** in different solvents.

Solvent	$\lambda_{max\ abs}$	$\lambda_{max\ em}$	Stokes Shift [cm^{-1}]	Vibronic Progression [cm^{-1}]
Methanol	insoluble	427, 448	-	-
Acetonitrile	331, 370 sh	433, 451	7116, 4854	922
DMF	338, 385 sh	436, 455	6650, 4689	958
DMSO	332, 370 sh	441, 458	7445, 5193	842
THF	338, 375 sh	427, 451	6167, 4494	1246
DCM	336, 370 sh	428, 450	6397, 4805	1142
Ether	335, 375 sh	421, 446	6098, 4245	1331
Toluene	340, 380 sh	426, 451	5938, 4143	1301

Table 4.5. Photophysical data of **4.6-4.8** in methanol.

Compound	4.6	4.7	4.8
Abs (nm)	336, 365	338, 370	337
Em (nm)	433, 451	430, 451	435, 456
Φ_{fl} (quantum yields)	0.17	0.37	0.16
τ (ns)	0.80	1.60	0.89

The compounds **4.6** and **4.7** were poorly soluble in pure water at neutral pH, demonstrating formation of red-shifted aggregates in the absorbance spectra. A comparative study of the acid-base behavior of **4.6-4.8** was performed in a 2:1 volume ratio of methanol/water (Figure 4.2). However, the absorbance spectra of **4.7** in these solvents at neutral pH differed from that in various organic solvents. Thus the absorbance titration data of **4.7** should be evaluated with caution, since it reflects not only deprotonation, but also the dissolution of its aggregates. This aggregation phenomenon at neutral pH is observed also for **4.6**, but to a much lesser extent. The three compounds respond differently towards hydroxide ions in absorption and emission. In the case of **4.6** a new band emerges (416 nm, UV/Vis), which is fully developed at pH 12. Visually, the almost colorless solution turns yellow. Simultaneously, a new band at 600 nm appears in the emission spectra, similar to that described by us for **B** (Scheme 4.1), while the emission at 460 nm disappears due to full ground state deprotonation. At higher pH the long-wavelength emission exhibits a small hypsochromic shift. The titration of XF **4.7** did not lead to the formation of the characteristic red-shifted phenolate band in the absorbance spectra, and the fluorescence spectra were quenched without appearance of a new low-energy band. On the basis of MO calculations we have demonstrated that the HOMO and LUMO orbitals of such molecules have a vanishing overlap, which makes the S_0–S_1 electronic transition forbidden. As a result, bathochromic shifts in the

absorbance spectra were not observed upon deprotonation; the emission from the deprotonated species is so weak that it can not be recorded. The XF **4.8**, with four hydroxy groups, features a diffuse isosbestic point around 346 nm; upon deprotonation a prominent feature develops at 370 nm. We assumed that the terminal spectra at the highest pH value for each XF belong to the fully deprotonated form of the respective chromophore. The absorbance spectra of the tetra-anion of **4.8** can be viewed as a superposition of **4.6** and **4.7** dianion bands. To understand these effects, we analyzed the photometric absorption data using the SPECFIT software.[13] Figure 4.3 displays the relative amounts of the corresponding deprotonated species present and the deconvoluted spectra of the neutral compound and all of the phenolate anions up to the tetra-anion for **4.8**. Upon increasing the pH the absorption profiles of the formed mono-, di-, tri-, and tetra-anion are deconvoluted. Their absorption maximum is consecutively red-shifted from 335 to 370 nm.

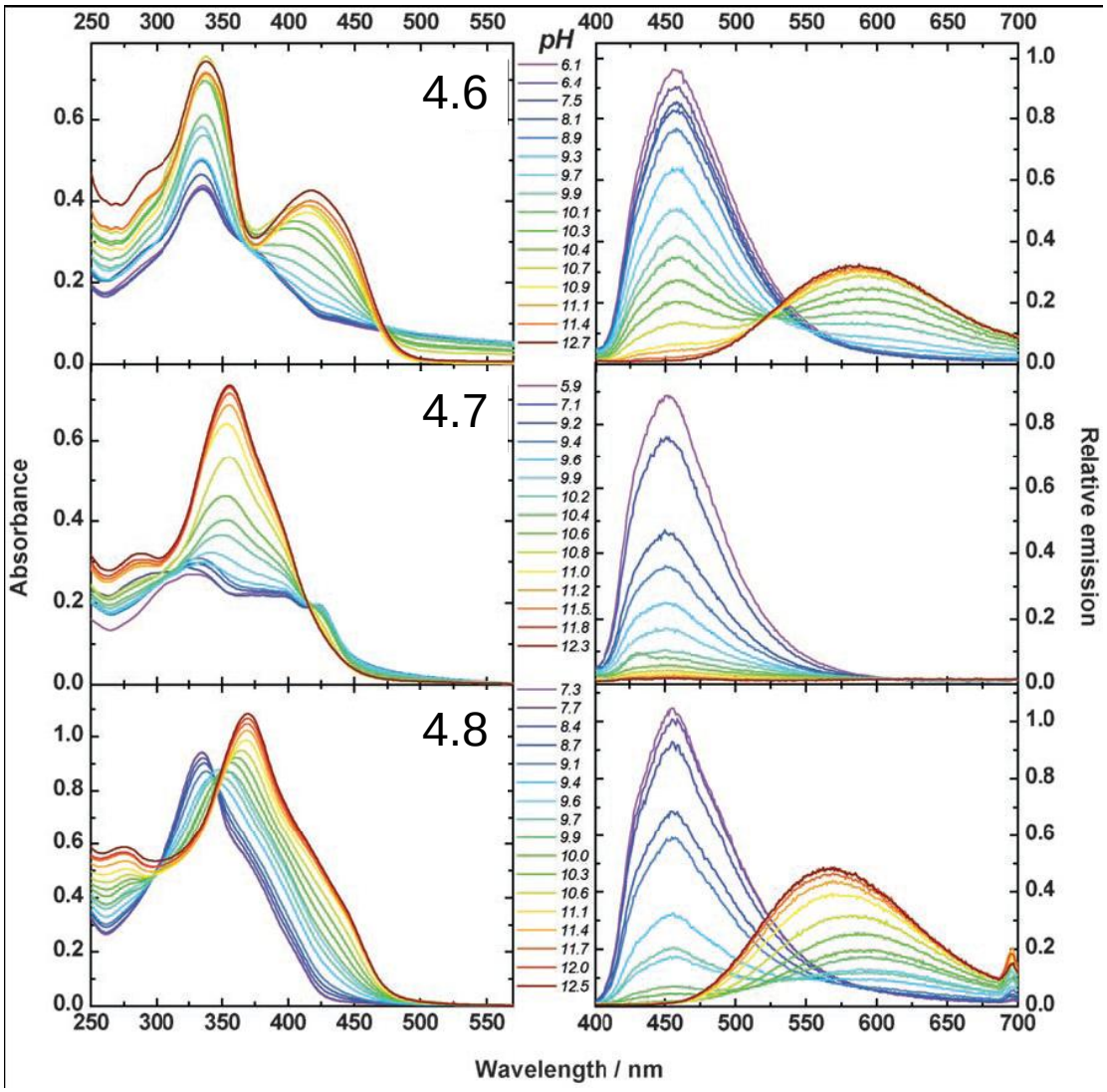

Figure 4.2. Absorption and emission spectra of **4.6-4.8** in 2:1 vol. methanol/water mixtures at different pH. The band at 690 nm in the emission titration of **4.8** is a scattering peak and represents double the excitation wavelength.

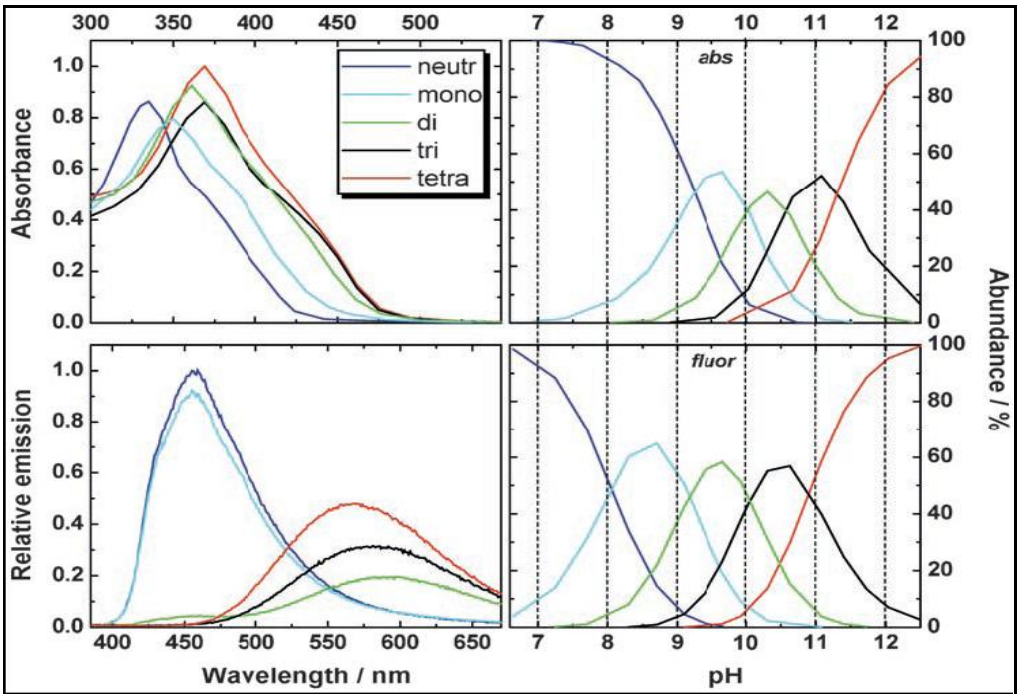

Figure 4.3. Deconvolution absorption and emission spectra of the anions of **4.8** with relative pK_a values: pK_{a1} = 9.2 (± 0.1) ; pK_{a2} = 10.0 (± 0.1); pK_{a3} = 10.6 (± 0.3); pK_{a4} = 11.3 (± 0.2).

When traversing from pH 7 to pH 10 we observe a significantly red-shifted (588 nm) emission band of lower intensity in **4.8**. Upon further increase of the pH, the fluorescence intensity of **4.8** increases again and the emission maximum blueshifts to 565 nm. The results of the fit demonstrate the coexistence of several polyanions of **4.8** at different pH regimes. It is surprising that in contrast to polyphenols[14] the pK_as of four hydroxyl groups differ by not more than one unit. A possible explanation for this phenomenon is the weak electronic interaction between two pairs of hydroxyls located on the distyrylbenzene and arylethynyl axes of the molecules. Another important observation from the data fitting is the pH mismatch in the existence areas of the different acid–base species for the ground- and the excited-state titrations. Such spectral behavior is a classical example of the photoacidity in the hydroxyaromatic molecules.[15] We note

that the apparent shifts between the ground- and excited-state pK_as are only about one unit, demonstrating a small but detectable increase of the photoacidity in aqueous solutions.

4.2.3 Amine Sensing Using XFs 4.6-4.8

With these results in hand, we set out to explore the fluorescence change of the XFs **4.6–4.8** upon exposure towards different amines. We prepared 10 micromolar solutions of the respective XFs in eight different solvents. These were then distributed into 13 vials each to obtain a matrix of 12 amines plus reference in 8 solvents to give 104 samples per XF. The amine (0.1 mL per sample, an excess, corresponding to a 0.7–7.2 mM concentration range) was then added and a picture of the 13 samples with 12 different amines for each of the eight solvents was taken (Figure 4.4). These real-color photographs were taken in the dark upon irradiation with a hand-held UV-lamp at an emission wavelength of 366 nm.

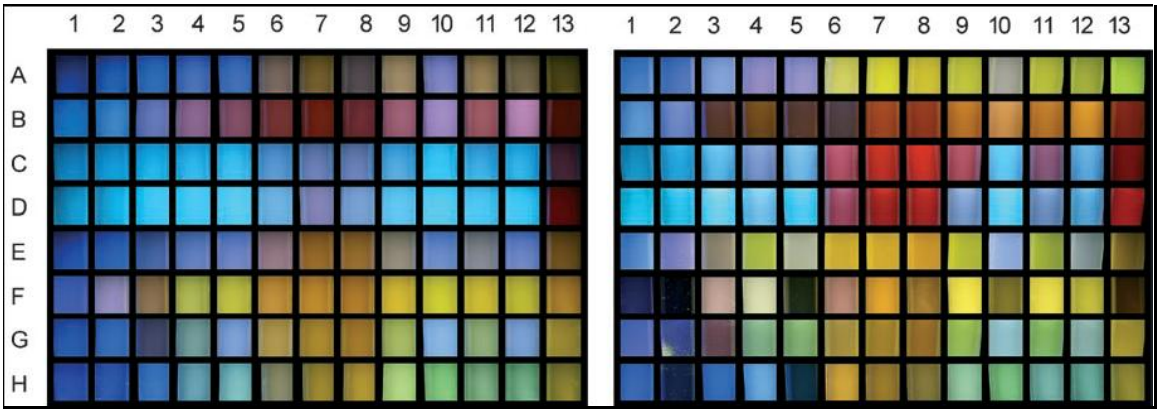

Figure 4.4. Photographs of solutions of **4.6** (left), and **4.8** (right) upon addition of amines 1-13 (left to right) 1) XF, 2) histamine (6.9), 3) imidazole (6.9), 4) morpholine (8.3), 5) piperazine (9.8), 6) putrescine (9.9), 7) 1,3-diaminopropane (10.5), 8) ethylenediamine (10.7), 9) piperidine (10.8), 10) triethylamine (10.8), 11.) diethylamine (11.0), 12.) diisopropylamine (11.1), 13.) 1,8-diazabicyclo[5.4.0]undec-7-ene (DBU~12; numbers in parentheses are the pKa values of the corresponding ammonium ions in water) in different solvents (top to bottom): A) methanol, B) acetonitrile, C) DMF, D) DMSO, E) THF, F) DCM, G) ether, and H) toluene. The samples were

excited by using a hand-held UV-lamp at an emission wavelength of 366 nm.

While the XF **4.6** gives color changes in emission, the XF **4.7** mostly experiences quenching (see 4.4 experimental), similar to the titration in a methanol/water mixture. The XF **4.8**, however, experienced spectacular changes in fluorescence upon the combination of amines, with the emission colors ranging from blue to red traversing yellow and green, covering the full visible spectral range. Ground- and excited-state acid–base interactions between dihydroxycruciforms and various amines in dichloromethane were studied and the fluorophores exhibit emission from the fully deprotonated (ion pair) state. From these observations we concluded that in dichloromethane the difference in pK_a (or ΔG of the proton transfer) between the excited dihydroxycruciforms and amines are sufficient to produce the solvent-separated ion pair with the emission around 550 nm.[11] In the ground state the observed ΔpK_a results in the formation of the hydrogen-bonded complexes.

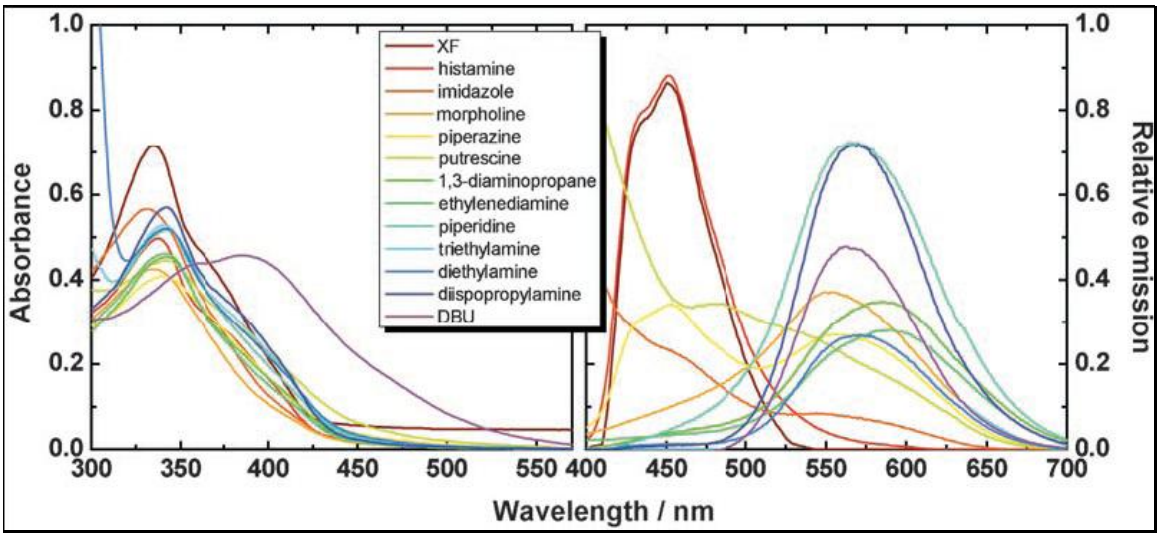

Figure 4.5. Absorption and emission of XF **4.8** in acetonitrile upon addition of different amines. Note that only DBU gives a significant red shift in absorption, while almost all amines give a significant shift in emission.

Generally, a similar behavior of **4.6** and **4.8** is observed in the present work for an array of solvents and amines. The only amine that quantitatively deprotonates the XFs in the ground state is the most basic DBU; significant changes occur both in absorption as well as in emission (Figure 4.5). While only DBU leads to a significant shift in absorption, almost all amines lead to a red-shift in the emission of **4.8**.

We were successful in utilizing the Kamlet-Taft method[16] to analyze the solvatochromic behavior of the ESPT product emission maxima, which are the vertical columns in Figure 4.4. For XF **4.8** the solvent dependence of the emission maxima (υ) of the long-wavelength ban in the presence of ethylenediamine can be presented as equation (1):

$$\upsilon(10^3\ cm^{-1}) = 19.8 - 2.7\pi^* - 0.9\beta + 0.7\alpha\ (r = 0.95) \qquad (1)$$

In this equation, π^*, β, and α are Kamlet-Taft solvents parameters reflecting the polarity, basicity, and acidity, respectively, of the solvent (r = residual). From this analysis one can see that the increase of solvent polarity and basicity causes the bathochromic shift of the emission, while the acidity of the solvent works in the opposite direction. The magnitudes of the coefficients demonstrate the dominating role of the polarity in the solvatochromic behavior of the fluorescence. Interestingly, the data from the horizontal rows in Figure 4.4 did not have a straight forward correlation with the pK_a.

While the photographs give a good indication to discern 12 amines by **4.8**, we converted the color into RGB values and subtracted the RGB value of the reference using the program Contrast Analyzer.[17] Two independent readings yielded RGB values for the XF **4.8** that were subjected to an LDA analysis with the program SYSTAT (Figure 4.6).[18]

With 24 different data points for each amine, SYSTAT reduces the data into a 2D LDA plot containing only two factors. The 12 amines are cleanly separated according to the analysis of their RGB values, allowing us to discern diethylamine and triethylamine or diethylamine and diisopropylamine. Interestingly, the amines are not grouped in this LDA plot according to their pK_a values; however, the di-amines (green) with exception of piperazine are grouped together, and secondary amines such as piperidine, diethylamine, and diisopropylamine (yellow-orange) are also grouped together at the bottom of the plot.

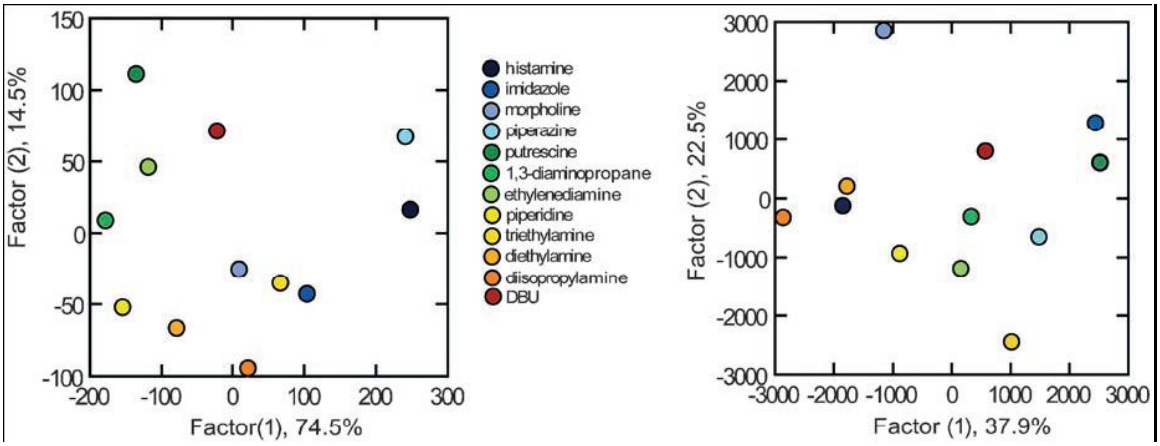

Figure 4.6. Linear discriminant analysis (LDA) of the differential RGB values (left) and ratio intensities (right) of **4.8** obtained from the righ-hand side Figure 4.4. The data on the left were extracted from the matrix generated by the RGB values measured for the photographs of the XF **4.8** dissolved in eight solvents in the presence of each different amine. The data on the right were extracted from the ratio of the intensities of each amine from the emission data. All of the amines are separated when in the 2D LDA. The two factors do not seem to represent a specific chemical property of the amines, such as pK_a value, chemical structure or other obvious chemical properties in either case.

4.3 Conclusions

In conclusion, we have synthesized three phenolic XFs **4.6-4.8**. XFs **4.6** and **4.8** display red-shifted absorption and emission upon deprotonation in methanol/water mixtures and were investigated for amine sensing. A series of 12 different amines could

be discerned by the specific fluorescence response of **4.8** based on excited-state proton transfer in eight different solvents. These experiments imply that one can create a "chemical nose" by using only one sensor molecule, but in different environments, that is, solvents. The emission wavelength of XF **4.8** is exquisitely sensitive towards different amines, and that in a solvent dependent fashion. The selectivity and responsivity of one fluorophore suffices to constitute a small sensor array just by changing the solvent. Using solutions of **4.8** would not be the most effective way to design a strip sensor or a similar application-oriented gadget, but the proof of principle is important, as XFs could easily be incorporated into grafted, conjugated polymers, in which the appended, non-conjugated polymer chains should be able to substitute for the solvent. Such materials could be spin cast onto silanized silica gel and their color response be observed upon exposure towards amines in air or water. The herein described experiments serve as a valuable guide for the design and execution of such polymeric materials, upon which we will report in the future. The colorful hydroxy XFs **4.6** and **4.8** display large and unique ratiometric shifts upon exposure to amines and are fascinating objects, fit for further evaluation exploiting the principles of spatial separation of FMOs and the mechanisms of the photoinduced proton transfer.

4.4 Experimental

Materials and Methods: All chemicals were purchased from Aldrich Chemical, Acros, TCI America, or Fisher Scientific and used without purification unless otherwise specified. Column chromatography was performed using Standard Grade silica gel 60 Å, 32-63 μm (230 x 450 mesh) from Sorbent Technologies and the indicated eluent. Elution

of cruciforms was readily monitored using a handheld UV lamp (365 nm). Melting points were obtained using a Mel-Temp apparatus fitted with a Fluke 51K/J digital thermometer. All IR spectra were obtained using a Simadzu FTIR-8400s spectrometer. Unless otherwise specified, NMR spectra were recorded at 298 K on a Bruker (500 MHz) or Varian Mercury spectrometer (300 MHz). Chemical shifts are reported in parts per million (ppm), using residual solvents (chloroform-*d*) or (THF-*d5*) as an internal standard. Data are reported as follows: chemical shift, multiplicity (s = singlet, d = doublet, t = triplet, q = quartet, m = multiplet), coupling constant, and integration. Mass spectral analyses were provided by the Georgia Institute of Technology Mass Spectrometry Facility.

All absorption spectra were collected using a Shimadzu UV-2401PC spectrophotometer. All emission spectra were acquired using a Shimadzu RF-5301PC spectrofluorophotometer. Lifetime data were collected using a Lifespec-ps (Edinburgh Instruments), pulsed diode laser (PicoQuant, 372 nm excitation), and PMT detector (Hamamatsu). Data were fit to single exponential decay so as to optimize chi-squared values. Quantum yields for all cruciforms were measured using standard procedures.[19] In all cases, quinine sulfate was used as a standard.

Compounds 3a-b:

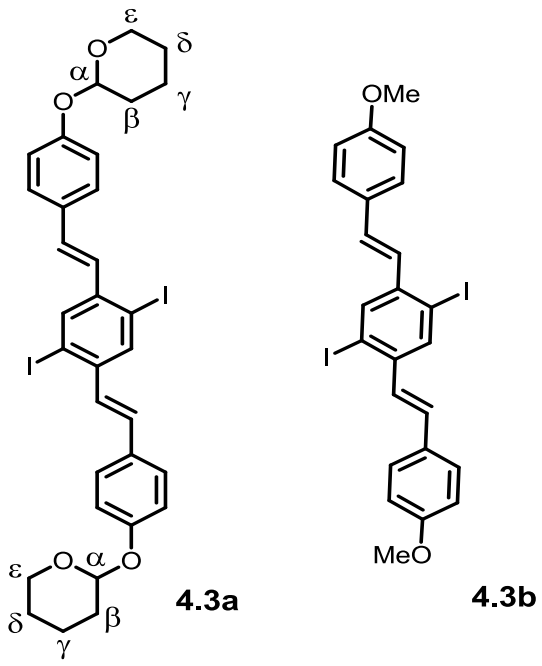

4.3a **4.3b**

The general procedure for compounds **4.3a** and **4.3b** has been previously reported.[11,20]

Compounds 4.4a and 4.4b

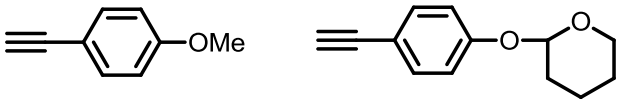

4.4a **4.4b**

Compound **4.4a** has been previously reported.[20]

Synthesis of 4.4b: To the mixture of 2-(4-iodophenoxy)tetrahydro-2H-pryan (3.12 g, 0.0103 mol) with trimethylsilyl acetylene (4.35 mL, 0.0308 mol) in Et_3N (5 mL) and THF (10 mL) was added catalytic amount $Pd(PPh_3)_2Cl_2$ (5 mg, 7.1 μmol), and CuI (5 mg, 33 μmol) under the N_2 atmosphere. The mixture was stirred at room temperature under N_2 atmosphere for 18 h and then filtered. The filtrate was dried by vacuum to yield the light yellow solid. The light yellow solid was dissolved in methanol (20 mL) and K_2CO_3 (6.00 g, 0.0434 mol) was added. The mixture was stirred at room temperature for 6 hours.

Water (100 mL) was added to the mixture and extracted with dichloromethane (150 ml). The organic layer was dried over magnesium sulfate and the residue was isolated by a column on silica gel using hexane and dichloromethane (v/v, 1:1) solvent mixture to give a colorless solid (1.30 g). Yield 63%. *^{1}H NMR (300 MHz, $CDCl_3$):* δ = 7.43 (d, 2H, Ar-H, $J_{H,H}$ = 8 Hz), 7.01 (d, 2H, Ar-H, $J_{H,H}$ = 8 Hz), 5.42 (s, 1H, α-C-H), 3.86 (m, 1H, ε-C-H), 3.61 (m, 1H, ε-C-H), 2.04 (m, 1H, β-C-H), 1.91 (m, 2H, γ-C-H) 1.71 (m, 2H, δ-C-H), 1.64 (m, 1H, β-C-H). *^{13}C NMR (125 MHz, $CDCl_3$):* δ = 157.26, 133.30, 116.15, 114.82, 95.97, 83.53, 75.82, 61.78, 30.04, 24.96, 18.47.

Compounds 4.5a-c:

Compounds **4.5a-c** were produced by the Sonogashira coupling of **4.4a** or **4.4b**. The reaction progress could be monitored by the development of the fluorescent products which were isolated by precipitating twice in non solvents.

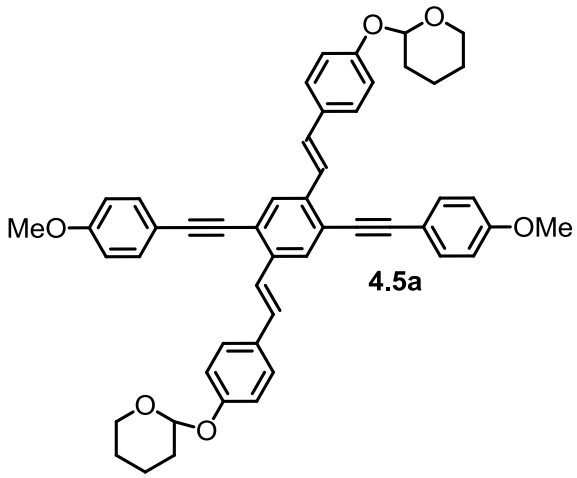

4.5a

Synthesis of 4.5a: 4.3a (0.335 g, 0.456 mmol) was combined with **4.4a** (0.181 g, 1.37 mmol), $(PPh_3)_2PdCl_2$ (5 mg, 7.1 μmol), CuI (5 mg, 33 μmol) and dissolved in THF (50 mL) and piperidine (5 mL) in a nitrogen purged schlenk flask. The solution was degassed, capped with a septum and allowed to stir at room temperature for 24 h. The

product was extracted with dichloromethane (100 mL), washed three times with water (100 mL), dried with magnesium sulfate and reduced until a yellow powder formed, which was purified by recrystallization adding hot chloroform and an excess of hexanes, yielding a yellow powder. Yield: 77%. *MP:* 209 ºC. *IR:* 2933, 2847, 2206, 1603, 1512, 1244, 1172, 1035, 961 cm^{-1}. *^{1}H NMR (500 MHz, $CDCl_3$):* δ = 7.87 (s, 2H, Ar-H), 7.57 (d, 4H, Ar-H, $J_{H,H}$ = 9 Hz), 7.56 (d, 2H, C=C-H, $J_{H,H}$ = 16.5 Hz), 7.53 (d, 4H, Ar-H, $J_{H,H}$ = 9 Hz), 7.24 (d, 2H, C=C-H, $J_{H,H}$ = 16.5 Hz), 7.11 (d, d, 4H, Ar-H, $J_{H,H}$ = 9 Hz), 6.95 (d, 4H, Ar-H, $J_{H,H}$ = 9 Hz), 5.49 (s, 2H, α-C-H), 3.94 (m, 2H, ε-C-H), 3.88 (s, 6H, Ar-OMe), 3.66 (m, 2H, ε-C-H), 2.04 (m, 2H, β-C-H), 1.91 (m, 4H, γ-C-H) 1.71 (m, 4H, δ-C-H), 1.64 (m, 2H, β-C-H). *^{13}C NMR (125 MHz, $CDCl_3$):* δ = 160.24, 157.41, 137.54, 133.46, 131.45, 130.29, 128.80, 128.31, 124.42, 122.48, 117.13, 115.79, 114.57, 96.72, 95.75, 87.23, 62.47, 55.77, 30.74, 25.62, 19.15.

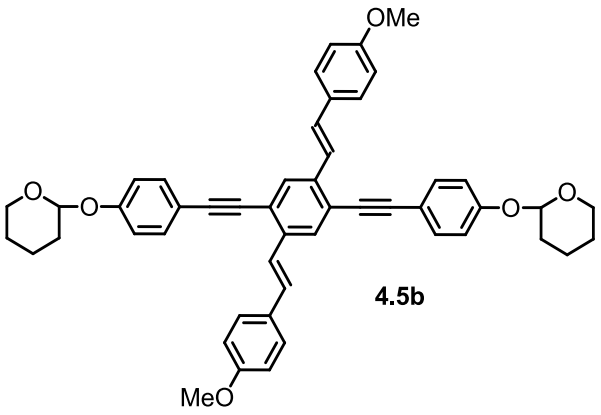

4.5b

Synthesis of 4.5b: 4.3b (0.345 g, 0.581 mmol) was combined with **4.4b** (0.352 g, 1.74 mmol), $(PPh_3)_2PdCl_2$ (5 mg, 7.1 μmol), CuI (5 mg, 33 μmol) and dissolved in THF (50 mL) and piperidine (5 mL) in a nitrogen purged schlenk flask. The solution was degassed, capped with a septum and allowed to stir at room temperature for 24 h. The product was extracted with dichloromethane (100 mL), washed three times with water

(100 mL), dried with magnesium sulfate and reduced until a green powder formed, which was purified by recrystallization adding hot dichloromethane and an excess of hexanes, yielding a light green powder. Yield: 61%. *MP:* 198 ºC. *IR:* 2916, 2847, 2201, 1602, 1511, 1242, 1172, 1035, 957, 919 cm^{-1}. *^{1}H NMR (500 MHz, $CDCl_3$):* δ = 7.87 (s, 2H, Ar-H), 7.55 (d, 2H, C=C-H, $J_{H,H}$ = 16.5 Hz), 7.55 (d, 4H, Ar-H, $J_{H,H}$ = 9 Hz), 7.54 (d, 4H, Ar-H, $J_{H,H}$ = 9 Hz), 7.24 (d, d, 2H, C=C-H, $J_{H,H}$ = 16.5 Hz), 7.10 (d, 4H, Ar-H, $J_{H,H}$ = 9 Hz), 6.95 (d, 4H, Ar-H, $J_{H,H}$ = 9 Hz), 5.51 (s, 2H, α-C-H), 3.94 (m, 2H, ε-C-H), 3.87(s, 6H, Ar-OMe), 3.66 (m, 2H, ε-C-H), 2.04 (m, 2H, β-C-H), 1.91 (m, 4H, γ-C-H) 1.71 (m, 4H, δ-C-H), 1.64 (m, 2H, β-C-H). *^{13}C NMR (125 MHz, $CDCl_3$):* δ = 159.95, 157.74, 137.55, 133.34, 130.65, 130.26, 128.80, 128.41, 124.15, 122.45, 116.95, 116.60, 114.66, 96.68, 95.74, 87.29, 62.49, 55.76, 30.67, 25.56, 19.07.

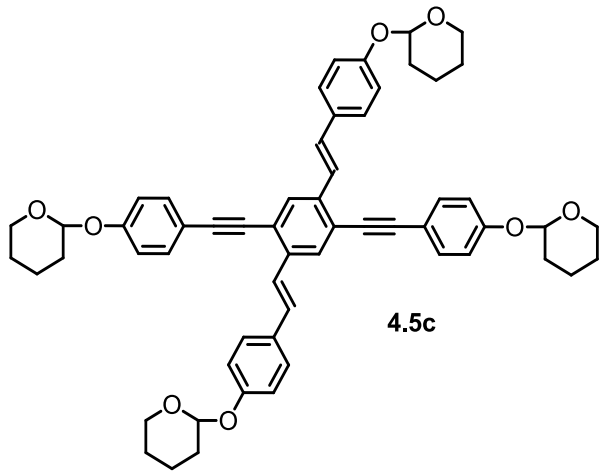

4.5c

Synthesis of 4.5c: 4.3a (0.302 g, 0.411 mmol) was combined with **4.4b** (0.250, g, 1.24 mmol), $(PPh_3)_2PdCl_2$ (5 mg, 7.1 μmol), CuI (5 mg, 33 μmol) and dissolved in THF (50 mL) and piperidine (5 mL) in a nitrogen purged schlenk flask. The solution was degassed, capped with a septum and allowed to stir at room temperature for 24 h. The product was extracted with dichloromethane (100 mL), washed three times with water

(100 mL), dried with magnesium sulfate and reduced until a yellow powder formed, which was purified by recrystallization adding hot dichloromethane and an excess of hexane, yielding a bright yellow powder. Yield: 61%. *MP:* 201 ºC. *IR:* 2941, 2872, 2206, 1604, 1514, 1239, 1201, 1173, 1050, 961 cm $^{-1}$. *^{1}H NMR (500 MHz, $CDCl_3$):* δ = 7.88 (s, 2H, Ar-H), 7.56 (d, 2H, C=C-H, $J_{H,H}$ = 16.5 Hz), 7.55 (d, 4H, Ar-H, $J_{H,H}$ = 9 Hz), 7.53 (d, 4H, Ar-H, $J_{H,H}$ = 9 Hz), 7.24 (d, d, 2H, C=C-H, $J_{H,H}$ = 16.5 Hz), 7.11 (d, d, 4H, Ar-H, $J_{H,H}$ = 4 Hz), 7.09 (d, 4H, Ar-H, $J_{H,H}$ = 4 Hz), 5.50 (s, 4H, α-C-H), 3.94 (m, 4H, ε-C-H), 3.66 (m, 4H, ε-C-H), 2.04 (m, 4H, β-C-H), 1.91 (m, 8H, γ-C-H) 1.71 (m, 8H, δ-C-H), 1.64 (m, 4H, β-C-H). *^{13}C NMR (125 MHz, $CDCl_3$):* δ = 157.73, 157.40, 137.54, 133.36, 131.45, 130.27, 128.79, 128.33, 124.40, 122.48, 117.14, 116.96, 116.61, 96.68, 95.80, 87.33, 62.52, 30.69, 25.63, 19.19. *MS (FAB, 70-SE) ($C_{58}H_{58}O_8$):* m/z = 882.

Compounds 4.6-4.8

Compounds **4.6-4.8** were deprotected by trifluoroacetic acid in a dry ice acetone bath. The products were obtained by extracting with dichloromethane or ethyl ether. The yields reported reflect the amount of pure material that was recovered after deprotection and recrystallization.

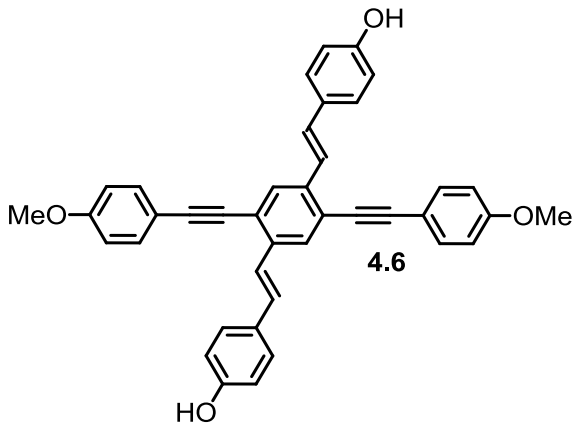

4.6

Synthesis of 4.6: **4.5a** (0.095 g, 0.166 mmol) was dissolved in dichloromethane (50 mL) and trifluoroacetic acid (2 mL) was added into a 100-mL round bottom flask kept in a dry ice acetone bath. The solution was allowed to stir at -78 °C for 2h and then thawed to room temperature. The reaction mixture was washed three times with water (100 mL), dried with magnesium sulfate, filtered and reduced until a dark green powder was formed. The powder was recrystallized by dissolving in hot chloroform and adding an excess amount of hexanes, yielding dark green crystals (83.6 mg). Yield: 88%. *MP:* 228 ºC. *IR:* 3357, 2915, 2834, 2198, 1603, 1512, 1244, 1170, 958 cm $^{-1}$. *^{1}H NMR (500 MHz ,THF-d_8):* δ = 8.42 (s, 2H, Ar-OH), 7.88 (s, 2H, Ar-H), 7.53 (d, 4H, Ar-H, $J_{H,H}$ = 9 Hz), 7.51 (d, 2H, C=C-H, $J_{H,H}$ = 16.5 Hz), 7.44 (d, 4H, Ar-H, $J_{H,H}$ = 9 Hz), 7.29 (d, 2H, C=C-H, $J_{H,H}$ = 16.5 Hz), 6.96 (d, 4H, Ar-H, $J_{H,H}$ = 8.5 Hz), 6.75 (d, 4H, Ar-H, $J_{H,H}$ = 8.5 Hz), 3.82 (s, 6H, Ar-OMe)**.** *^{13}C NMR (125 MHz, THF-d_8):* δ = 160.59, 158.42, 137.53, 133.13, 130.77, 129.30, 128.35, 128.30, 122.52, 122.33, 115.86, 115.67, 114.43, 95.51, 86.92, 54.99. *MS (EI, 70-SE) ($C_{40}H_{30}O_4$):* m/z = 574.

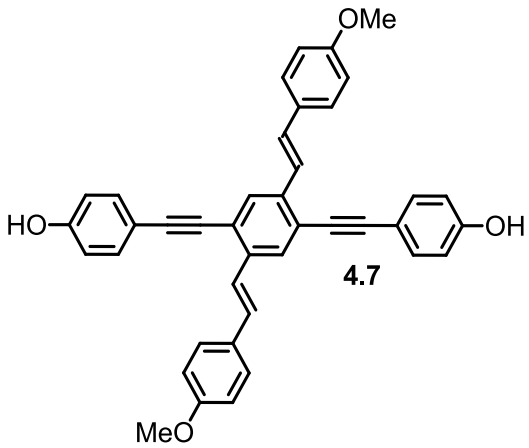

4.7

Synthesis of 4.7: **4.5b** (0.070 g, 0.111 mmol) was dissolved in dichloromethane (50 mL) and trifluoroacetic acid (2 mL) was added into a 100-mL round bottom flask kept in a dry

ice acetone bath. The solution was allowed to stir at -78 °C for 2h and then thawed to room temperature. The reaction mixture was washed three times with water (100 mL), dried with magnesium sulfate, filtered and reduced until a orange powder was formed. The powder was recrystallized by dissolving in hot chloroform and adding an excess amount of hexanes, yielding orange crystals (64.0 mg). Yield: 91%. *MP:* 198 ºC. *IR:* 3380, 2916, 2837, 2185, 1603, 1512, 1248, 1173 1029, 955 cm $^{-1}$. *^{1}H NMR (500 MHz ,THF-d_8):* δ =8.77 (s (broad), 2H, Ar-OH), 7.88 (s, 2H, Ar-H), 7.56 (s d, 2H, C=C-H, $J_{H,H}$ = 16.5 Hz), 7.53 (d, 4H, Ar-H, $J_{H,H}$ = 8.5 Hz), 7.43 (d, 4H, Ar-H, $J_{H,H}$ = 8.5 Hz), 7.33 (d, 2H, C=C-H, $J_{H,H}$ = 16.5 Hz), 6.92 (d, 4H, Ar-H, $J_{H,H}$ = 8.5 Hz), 6.79 (d, 4H, Ar-H, $J_{H,H}$ = 8.5 Hz), 3.79(s, 6H, Ar-OMe)**.** *^{13}C NMR (125 MHz, THF-d_8):* δ = 158.44, 156.97, 135.55, 131.36, 128.74, 128.46, 126.49, 126.29, 121.63, 120.67, 114.01, 112.53, 112.33, 94.20, 84.40, 53.02.

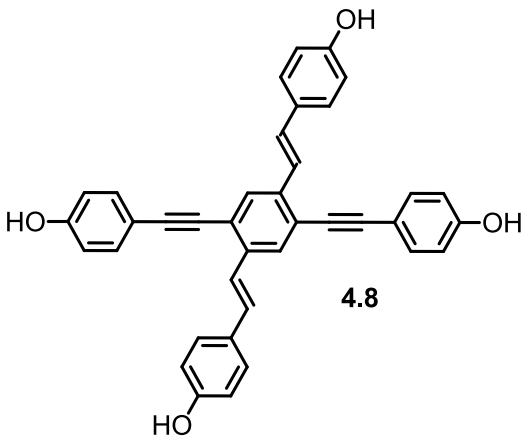

4.8

Synthesis of 4.8: **4.5c** (0.090 g, 0.102 mmol) was dissolved in dichloromethane (50 mL) and trifluoroacetic acid (2 mL) was added into a 100-mL round bottom flask kept in a dry ice acetone bath. The solution was allowed to stir at -78 °C for 2h and then thawed to room temperature. The reaction mixture was washed three times with water (100 mL),

dried with magnesium sulfate, filtered and reduced until a dark brown powder was formed. The powder was rinsed with dichloromethane and dried yielding dark brown crystals (82.8 mg). Yield: 92%. *MP:* 212 ºC. *IR:* 3383, 2136, 1601, 1362, 1221, 1091, 901 cm $^{-1}$. *^{1}H NMR (500 MHz ,THF-d_8):* δ = 8.69 (s, 2H, Ar-OH), 8.40 (s, 2H, Ar-OH), 7.86 (s, 2H, Ar-H), 7.50 (d, 2H, C=C-H, $J_{H,H}$ = 16.5 Hz), 7.43 (d, 8H, Ar-H, $J_{H,H}$ = 9 Hz), 7.28 (d, 2H, C=C-H, $J_{H,H}$ = 16.5 Hz), 6.79 (d, 4H, Ar-H, $J_{H,H}$ = 8.5 Hz), 6.75 (d, 4H, Ar-H, $J_{H,H}$ = 8.5 Hz) . *^{13}C NMR (125 MHz, THF-d_8):* δ = 158.77, 158.38, 137.43, 133.22, 130.61, 129.34, 128.26, 122.63, 122.40, 115.86, 114.28, 95.90, 86.36. *MS (EI, 70-SE) ($C_{38}H_{26}O_4$):* m/z = 546.

General experimental procedure for 4.7: To investigate the sensory ability of hydroxy cruciforms towards amines, a solvatochromism study was conducted using 10 micromolar solutions the following solvents: methanol, acetonitrile, dimethylformamide, dimethylsulfoxide, tetrahydrofuran, dichloromethane, ether, and toluene. Approximately 0.1 mL (0.7-1.5 mM range) of amine was added to each 15 mL vial and its optical properties were measured. A picture of the fluorescent response of **4.7** with amines irradiated under a UV lamp is also shown below (see Figure 4.7). The emission and absorption spectra for all hydroxy XFs **4.6-4.8** can be found in the supporting information .[21]

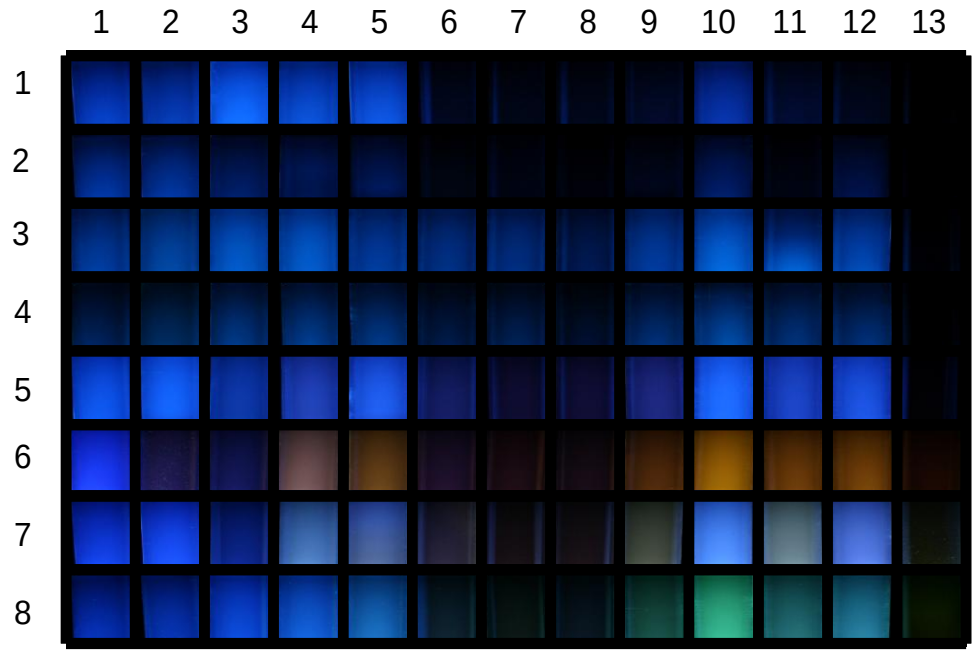

Figure 4.7. Exposure of **4.7** to different amines in various solvents. **Top to bottom:** 1.) methanol, 2.) acetonitrile, 3.) DMF, 4.) DMSO, 5.) THF, 6.) DCM, 7.) ether, and 8.) toluene. **Left to right:** 1.) **4.7**, 2.) histamine (6.90), 3.) imidazole (6.90), 4.) morpholine (8.33), 5.) piperazine (9.83), 6.) putrescine (9.90), 7.) 1,3-diaminopropane (10.47), 8.) ethylenediamine (10.70) , 9.) piperidine (10.80), 10.) triethylamine (10.80), 11.) diethylamine (11.00), 12.) diisopropylamine (11.10), 13.) 1,8-diazabicyclo[5.4.0]undec-7-ene (DBU~12). The numbers in parentheses are the pK_a values of the corresponding ammonium ions.

Titration Spectra and determination of p*K*a Values: Measurements were performed with a combination glass microelectrode (Orion, Thermo Electron Corp, Waltham). The electrode was precalibrated in aqueous buffers at pH 4, 7, and 10. Solution pH measurements were performed in 2/1 v/v methanol-water mixtures. For the determination of the pK_a's, a series of UV-vis spectra were acquired for which $-\log[H_3O^+]$ was varied between 5 and 12. It was demonstrated[22] that the pH can be measured directly in alcohol-water mixtures using glass electrodes precalibrated in aqueous buffers. In this case for 2/1 v/v methanol/water mixtures the observed pH values are 0.18 pH units higher than the real ones for this mixture. The raw spectral data were

processed via non-linear least squares fit analysis using the SPECFIT software package,[23] providing deconvoluted spectra for each species present as well as the acidity constants for the relevant protonation equilibria.

Results from principal component analysis:

1,4-bis(4'-hydroxystyryl)-2,5-bis(4"-hydroxyphenylethynyl)benzene) 4.6: pK_{a1}= 8.67 +/- 0.39; pK_{a2}= 10.02 +/- 0.01

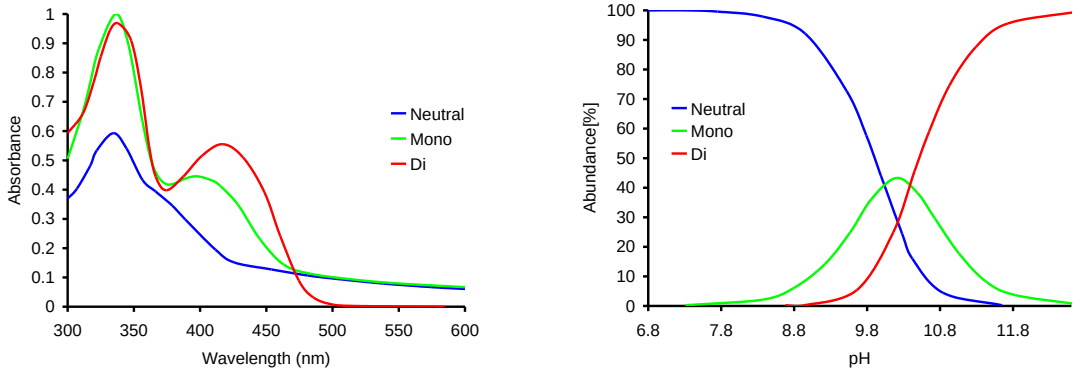

Figure 4.8. Spectrophotometric pH titration of fluorophore **4.6** in MeOH/H_2O (2:1, v/v). Left: deconvoluted UV-vis spectra for the neutral (blue), monoprotonated (green) and fully deprotonated (red) species. Right: Calculated species distribution diagram.

1,4-bis(4'-methoxystyryl)-2,5-bis(4"-hydroxyphenylethynyl)benzene) 4.7: pK_{a1}= 10.8 +/- 0.1; pK_{a2}= 10.8 +/- 0.3

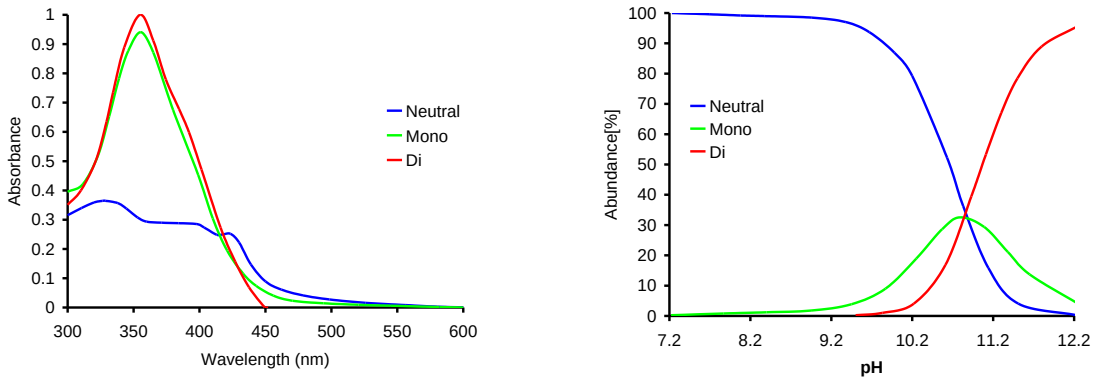

Figure 4.9. Spectrophotometric pH titration of fluorophore **4.7** in MeOH/H_2O (2:1, v/v). Left: deconvoluted UV-vis spectra for the neutral (blue), monoprotonated (green) and fully deprotonated (red) species. Right: Calculated species distribution diagram.

Table 4.6. Linear discriminant analysis (LDA) data set obtained from the RGB values of **4.8** with amines.

	R	G	B
A2	21	-11	-36
B2	37	-21	0
C2	11	-34	-21
D2	-18	60	-23
E2	55	-13	-54
F2	0	4	-64
G2	-36	-21	-142
H2	-18	-41	-202
A3	65	47	0
B3	14	-100	-227
C3	49	-9	1
D3	27	104	0
E3	77	-3	-169
F3	187	151	58
G3	4	-20	-198
H3	-2	8	-32
A4	95	18	-57
B4	42	-84	-252
C4	80	-49	-37
D4	46	65	-10
E4	107	52	-220
F4	213	217	83
G4	34	89	-150
H4	41	93	3
A5	94	26	-45
B5	13	-100	-228
C5	74	1	21
D5	4	82	-2
E5	110	49	-121
F5	22	26	-63
G5	37	91	-170
H5	-21	-29	-201
A6	166	98	-181
B6	8	-97	-211
C6	132	-130	-158
D6	82	-75	-189
E6	143	39	-255
F6	175	117	13
G6	79	57	-225
H6	164	85	-224
A7	173	106	-240
B7	94	-93	-255
C7	160	-159	-231
D7	95	-108	-252
E7	148	33	-255
F7	225	151	-71

G7	72	42	-255
H7	108	38	-243
A8	141	81	-246
B8	40	-100	-255
C8	163	-153	-231
D8	120	-111	-255
E8	91	13	-255
F8	157	106	-57
G8	98	21	-255
H8	104	39	-214
A9	144	80	-236
B9	124	-43	-255
C9	139	-125	-160
D9	55	16	-67
E9	122	56	-255
F9	248	227	-22
G9	61	104	-202
H9	107	127	-106
A10	113	47	-123
B10	136	-14	-207
C10	51	13	24
D10	20	98	0
E10	72	44	0
F10	122	100	-67
G10	49	114	-60
H10	71	108	-158
A11	137	72	-237
B11	117	-46	-255
C11	92	-117	-133
D11	40	7	-73
E11	91	33	-251
F11	231	211	-32
G11	39	96	-186
H11	66	96	-105
A12	106	48	-243
B12	146	-13	-248
C12	52	-29	-19
D12	17	24	-53
E12	57	7	-127
F12	191	177	-52
G12	42	91	-105
H12	54	90	-118
A13	113	81	-233
B13	48	-117	-255
C13	71	-176	-231
D13	93	-114	-255
E13	44	-51	-255
F13	44	21	-78
G13	75	60	-252
H13	98	53	-252

Table 4.7. Linear discriminant analysis (LDA) values of **4.8** obtained from the λ_{max} of the emission and relative fluorescence intensities in the prescence of amines.

histamine	-3	1	-2	0	-2	0	1	0
histamine	-3.2	1.11	-1.7	-0.33	-1.87	-0.44	0.63	0.41
imidazole	-6	0	-4	0	0	97	1	6
imidazole	-6.1	-0.3	-3.75	0.01	-0.21	96.72	0.23	5.9
morpholine	-1	100	-3	-1	91	91	83	10
morpholine	-1.5	99.96	-2.63	-0.98	90.69	90.47	83.05	10.0 1
piperazine	-3	109	-2	0	-3	0	85	0
piperazine	-3.25	109.01	-1.65	0.01	-3.21	-0.16	84.64	0.26
putrescine	89	29	0	0	93	106	88	82
putrescine	88.7	29.25	0.55	-0.47	92.57	105.3 3	87.78	82.4
1,3-diaminopropane	96	134	137	142	103	108	100	90
1,3-diaminopropane	95.6	134.26	137.3	142.0 1	102.7 1	107.3 9	100.1 1	90.0 1
ethylenediamine	100	140	142	141	104	108	101	93
ethylenediamine	99.9	140.01	142.1 4	141.2 7	103.7 9	108.1 2	100.4 3	93.3 1
piperidine	94	116	-3	-1	90	98	86	73
piperidine	94.23	116.21	-2.7	-0.99	89.78	97.61	85.63	73.0 1
triethylamine	-3	113	-4	-1	-1	100	74	65
triethylamine	-2.8	112.9	-3.56	-1.154	-1.21	99.72	73.63	64.9 3
diethylamine	90	122	-3	-2	90	100	83	71
diethylamine	89.9	122.01	-2.7	-1.99	89.54	99.91	82.25	70.6 3
diisopropylamine	91	120	-2	-1	90	97	80	60
diisopropylamine	91.1	119.63	-1.88	-1.2	89.79	96.65	79.63	60.1 8
DBU	86	113	141	136	97	111	97	85
DBU	85.9	112.96	141.7 1	136.0 1	96.48	110.7 2	96.91	85.0 1

4.5 References and Notes

1. Merchant, S. G. Z. M.; Cheng, G. *Characterization of Foods: Emerging Methods* (Ed.: A. G. Gaonkar), Elsevier Science, New York, 1995, Chapter 15.

2. (a) Greene, N. T.; Shimizu, K. D. *J. Am. Chem. Soc.* **2005**, *127*, 5695 – 5700. (b)

Mertz, E.; Zimmerman, S. C. *J. Am. Chem. Soc.* **2003**, *125*, 3424 – 3425.

3. Yeh, C.; Lin, S.; Hwang, D. *J. Food Drug Anal.* **2004**, *12*, 128 –132.

4. (a) Rakow, N. A.; Sen, A.; Janzen, M. C.; Ponder, J. B.; Suslick, K. S. *Angew. Chem.* **2005**, *117*, 4604 –4608; *Angew. Chem. Int. Ed.* **2005**, *44*, 4528 –4532. (b) Suslick, K. S.; Rakow, N. A.; Sen, A. *Tetrahedron* **2004**, *60*, 11133 –11138. (c) Rakow, N. A.; Suslick, K. S. *Nature* **2000**, *406*, 710 – 713. (d) Freund, M. S.; Lewis, N. S. *Proc. Natl. Acad. Sci. USA* **1995**, *92*, 2652 –2656. (e) Wright, A. T.; Anslyn, E. V. *Chem. Soc. Rev.* **2006**, *35*, 14– 28. (f) Vlasov, Y.; Legin, A.; Rudnitskaya, A. *Pure Appl. Chem.* **2005**, *77*, 1965 –1983. (g) Deisingh, A.; Stone, K.; Thompson, D. C. *Int. J. Food Sci. Tech.* **2004**, *39*, 587 –604. (h) Lavigne, J. J.; Anslyn, E. V. *Angew. Chem.* **2001**, *113*, 3212 –3225; *Angew. Chem. Int. Ed.* **2001**, *40*, 3118 – 3130.

5. (a) Rossi, S.; Lee, C.; Ellis, P. C.; Pivarnlik, L. F. *J. Food Sci.* **2002**, *67*, 2056 – 2060. (b) Ruiz-Capillas, C.; Moral, A. *J. Food Sci*. **2001**, *66*, 1030 – 1032. (c) Ritchie, A. H.; Mackie, I. M. *Advances in Fish Science and Technology* (Ed.: J. J. Connell), Fishing News , Farnham (UK), **1980** pp. 489 – 494.

6. (a) Nelson, T. L.; Tran, I.; Ingallinera, T. G.; Maynor, M. S.; Lavigne, J. J. *Analyst* **2007**, *132*, 1024 –1030. b) Maynor, M. S.; Nelson, T. L.; O.Sullivan, C.; Lavigne, J. J. *Org. Lett.* **2007**, *9*, 3217 – 3220. c) Nelson, T. L.; O.Sullivan, C.; Greene, N. T.; Maynor, M. S.; Lavigne, J. J. *J. Am. Chem. Soc.* **2006**, *128*, 5640 – 5641.

7. Wilson, J. N.; Josowicz, M.; Wang, Y. Q.;. Bunz, U. H. F. *Chem. Commun.* **2003**, 2962 – 2963.

8. (a) Halkyard, C. E.; Rampey, M. E.; Kloppenburg, L.; Studer-Martinez, S. L.; Bunz, U. H. F. *Macromolecules* **1998**, *31*, 8655 –8659. b) J. Kim, T. M. Swager, *Nature* **2001**, *411*, 1030 –1034.

9. Zollinger, H. *Color Chemistry*, 3rd ed., Wiley-VCH, Weinheim (Germany), 2003.

10. (a) Henary, M. M.; Wu, Y. G.; Fahrni, C. J. *Chem. Eur. J.* **2004**, *10*, 3015 – 3025. (b) Wang, B.; Wasielewski, M. R. *J. Am. Chem. Soc.* **1997**, *119*, 12–21. (c) Bangcuyo, C. G.; Rampey-Vaughn, M. E.; Quan, L. T.; Angel, S. M.; Smith, M. D.; Bunz, U. H. F. *Macromolecules* **2002**, *35*, 1563 – 1568. (d) Pautzsch, T.; Klemm, E. *Macromolecules* **2002**, *35*, 1569 – 1575. (e) Pond, S. J. K.; Tsutsumi, O.; Rumi, M.; Kwon, O.;Zojer, E.; Bredas, J. L.; Marder, S. R.; Perry, J. W. *J. Am. Chem. Soc.* **2004**, *126*, 9291 –9306. (f) Yang, L. C.; McRae, R.; Henary, M. M.; Patel, R.; Lai, B.; Vogt, S.; Fahrni, C. J. *Proc. Natl. Acad. Sci. USA* **2005**, *102*, 11179 –11184; (g) Cody, J.; Fahrni, C. J. *Tetrahedron* **2004**, *60*, 11099 – 11107. (h) Corradini, R.; Dossena, A.; Galaverna, G.; Marchelli, R.; Panagia, A.; Sartor, G. *J. Org. Chem.* **1997**, *62*, 6283 – 6289. (i) Thomas III, S. W.; Joly, G. D.; Guy, D.; Swager, T. M. *Chem. Rev.* **2007**, *107*, 1339 –1386. (j) Ono, A.; Togashi, H. *Angew. Chem.* **2004**,

116, 4400 –4402; *Angew. Chem. Int. Ed.* **2004**, *43*, 4300 –4302; (k) Nolan, E. M.; Lippard, S. J. *J. Am. Chem. Soc.* **2003**, *125*, 14270 –14271.

11. McGrier, P. L.; Solntsev, K. M.; Schçnhaber, J.; Brombosz, S. M.; Tolbert, L. M.; Bunz, U. H. F. *Chem. Commun.* **2007**, 2127 –2129.

12. (a) Solntsev, K. M.; Huppert, D.; Tolbert, L. M.; Agmon, N. *J. Am.Chem. Soc.* **1998**, *120*, 7981 – 7982. (b) Solntsev, K. M.; Huppert, D.; Agmon, N. *J. Phys. Chem. A* **1998**, *102*, 9599 –9606. (c) Solntsev, K. M.; Huppert, D.; Agmon, N. *J. Phys. Chem. A* **1999**, *103*, 6984 –6997.

13. (a) Tolbert, L. M.; Solntsev, K. M. *Acc. Chem. Res.* **2002**, *35*, 19 –27. (b) R. A. Binstead, A. D. ZuberbRhler, B. Jung, SPECIFIT version 3.0.40, Spectrum Software Associates, Marlborough, MA, **2007**.

14. (a) Slabbert, N. P. *Tetrahedron* **1977**, 33, 821 – 824. (b) Erdemgil, F. Z.; Sanli, S.; Sanli, N.; Oezkan, G.; Barbosa, J.; Guiteras, J.;. Beltran, J. L *Talanta* **2007**, *72*, 489 – 496.

15. Weller, A. *Prog. React. Kinet.* **1961**, *1*, 189 –214.

16. Kamlet, M. J.; Abboud, J. L. M.; Abraham, M. H.; Taft, R.W. *J. Org.Chem.* **1983**, *48*, 2877 –2887.

17. The Contrast Colour Analyzer program is freeware and can be downloaded from http://www.visionaustralia.org.au/info.aspx?page=1985. Accessed 06/14/2010.

18. (a) Brereton, R. G. *Chemometrics: Data Analysis for the Laboratory and Chemical Plant*, Wiley, New York, 2003; (b) Albert, K. J.; Lewis, N. S.; Schauer, C. L.; Sotzing, G. A.; Stitzel, S. E.; Vaid, T. P.; Walt, D. R. *Chem. Rev.* **2000**, *100*, 2595 –2626.

19. "A Guide to Recording Fluorescence Quantum Yields." Horiba Jobin Yvon Ltd. Available online: http://www.jobinyvon.co.uk/ukdivisions/Fluorescence/plqy.htm. Accessed 06/14/2010.

20. Wilson, J.N.; Windscheif, P.M.; Evans, U.; Myrick, M. L.; Bunz, U. H. F. *Macromolecules*. **2002**, *35*, 8681-8683.

21. McGrier, P. L.; Solntsev, K. M.; Miao, S.; Tolbert, L.; Miranda, O. R.; Rotello, V. M. Bunz, U. H. F. *Chem. Eur. J.* **2008**, *14*, 4503-4510.

22. (a) Bosch, E.; Bou, P.; Allemann, H.; Roses, M. *Anal. Chem.* **1996**, *68*, 3651-3657. (b) Avdeef, A.; Box, K. J.; Comer, J. E. A.; Gilges, M.; Hadley, M.; Hibbert, C.; Patterson, W.; Tam, K. Y. *J. Pharm. Biomed. Anal.* **1999**, *20*, 631-641. (c) Canals, I.; Portal, J. A.; Bosch, E.; Roses, M. *Anal. Chem.* **2000**, *72*, 1802-1809. (d) Canals, I.;

Valko, K.; Bosch, E.; Hill, A. P.; Rose´s, M. *Anal. Chem*. **2001**, *73*, 4937-4945. (e) Canals, I.; Oumada, F. Z.; Rose´s, M.; Bosch, E. *J. Chromatogr., A* **2001**, *911*, 191-202.

23. Kong, J.; White, C. A.; Krylov, A. I.; Sherrill, D.; Adamson, R. D.; Furlani, T. R.; Lee, M. S.; Lee, A. M.; Gwaltney, S. R.; Adams, T. R.; Ochsenfeld, C.; Gilbert, A. T. B.; Kedziora, G. S.; Rassolov, V. A.; Maurice, D. R.; Nair, N.; Shao, Y. H.; Besley, N. A.; Maslen, P. E.; Dombroski, J. P.; Daschel, H.; Zhang, W. M.; Korambath, P. P.; Baker, J.; Byrd, E. F. C.; Van Voorhis, T.; Oumi, M.; Hirata, S.; Hsu, C. P.; Ishikawa, N.; Florian, J.; Warshel, A.; Johnson, B. G.; Gill, P. M. W.; Head-Gordon, M.; Pople, J. A. *J. Comput. Chem.* **2000**, *21*, 1532-1548.

Chapter 5

Cruciform-Silica Hybrid Materials

5.1 Introduction

Functional chromophores and fluorophores are attractive as sensory and responsive materials in biology, materials science, organic electronics and analytical chemistry.[1] For deployment in biological applications such as the targeted staining of cell compartments, water soluble fluorophores appended with binding elements are highly desirable and necessary. To enable charge transport for applications in organic electronics, chromophores/fluorophores must be capable of forming high quality, ordered thin films. For many environmental and biodiagnostic sensory applications, it is desirable if the fluorophores or chromophores utilized for analysis are immobilized – temporarily or permanently – on a solid support. Such solid supports can either be just a scaffold for the dye(s) under consideration, or they can perform secondary functions such as suppressing aggregation/excimer formation or aiding in preconcentration of analytes. An elegant example of this approach is the work by Rakow and Suslick, who investigated the response of an array of immobilized porphyrin dyes towards a battery of different analytes.[2] The success of their colorimetric approach was rooted in the immobilization of their dyes onto hydrophobic silanized silica gel which helped to pre-concentrate gaseous

or liquid analytes either from the gas phase or from the aqueous phase onto their solid support, where it could react with the dye under consideration.

Coordination of metal cations to XFs results in either red- or blue-shifted emission if pyridines or dialkylanilines are incorporated.[3] If both are present, a two-stage mechanism, where there is first a blue shift followed by a red shift is observed that results from the complexation of an XF such as **5.5** with increasing amounts of zinc or magnesium ions. If we incorporate hydroxyl groups into the π-system of these functional fluorophores, we observe fluorescence shifts upon deprotonation. These compounds can also serve as fluorescent probes for the differentiation of amine bases.[5]

In this chapter, we examine the interaction of XFs **5.1**-**5.7** with mesoporous SBA-15 silica materials **A**-**D** containing acidic sites (**A**), basic sites (**B**), hydrophobic trimethylsilyl sites (**C**), and bare, unfunctionalized silica containing silanols (**D**) (Scheme 5.1). We investigate the resulting cruciform-silica hybrid materials by optical and fluorescent spectroscopies. It was of great interest to examine the interactions between the various XFs and the different mesoporous silica samples, establish what emission responses would be observed, whether support of XFs on silica would allow the XFs to maintain their fluorescence properties in the solid state, and if these solid-state adsorbed XFs could be used to detect amines or organic acids in the gas phase.

5.2 Results and Discussion

5.2.1 Synthesis of Mesoporous Silica Supports.

Mesoporous silica SBA-15 was identified as a good candidate for a porous host material.[6] SBA-15 can be easily prepared via block copolymer templating methods and the size of the mesopores can be controlled. In this work, SBA-15 with an average pore

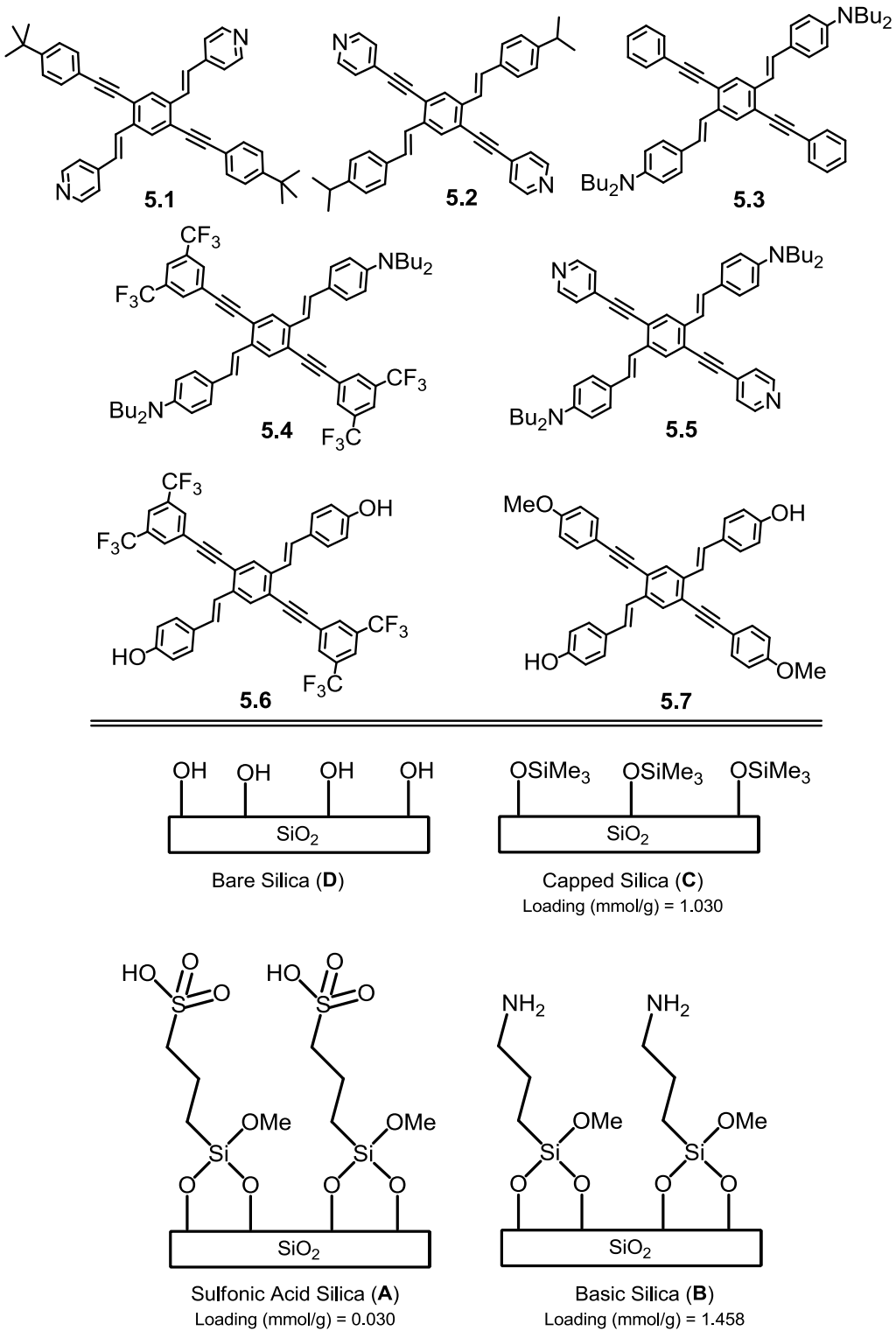

Scheme 5.1. Structure of XFs **5.1-5.7** and a schematic representation of the surface functionality of silicas **A-D.**

diameter of 57 Å and a surface area of ~700 m^2/g was prepared via standard methods.[7] After calcination to remove the block copolymer template, the material was functionalized by standard silane grafting techniques to introduce Lewis basic aminopropyl groups,[8] Brønsted acidic sulfonic acid groups,[9] or hydrophobic trimethylsilyl groups.[10] Changes in surface properties were verified by nitrogen physisorption and thermogravimetric analysis.

5.2.2. Spectroscopic Properties of the XFs 5.1-5.7 in the Presence of Microstructured Functionalized Silica Supports.

XFs **5.1-5.7** emit vibrantly in organic solutions. We have detailed their sensory responses towards metal cations, protons, and amines.[3, 5] Emissions of the XFs in the solid state are generally red shifted, broadened, and less intense, limiting their potential use as sensory materials in the solid state (Figure 5.1). A possible method to overcome these limitations is to employ the fluorophore immobilized on a solid support for potential environmental and biodiagnostic applications. Solid supports serve as scaffolds for the dye(s) under consideration; they may also suppress aggregation/excimer formation or preconcentrate analytes.

XFs **5.1-5.7** were dissolved in toluene and dry mesoporous silica was added. The resulting suspensions were incubated in the dark for 24 hours, at which point the samples were photographed under UV light (ex = 365 nm) to qualitatively examine the resulting fluorescence of the cruciform-silica hybrid materials. As Figure 5.2 shows, the solid silica settled to the bottom of the vials and was highly fluorescent. To more quantitatively assess the fluorescent of these XF-silica hybrid materials, we recorded the fluorescence spectra of suspensions of these hybrid materials in toluene using a triangular cuvette to minimize scattering (Figure 5.3 and Table 5.1). When compounds **5.1-5.7** are

exposed to capped silica, the emission of the XF-silica hybrids ranges from 424 (XF **5.7**) to 548 (XF **5.4**) nm. In addition, the intensity and shape of the observed emissions are reminiscent of those observed in solution, not those observed in the solid state. Thus, mesoporous SBA-15 silica appears to be a promising platform to enhance and/or modulate XF fluorescence.

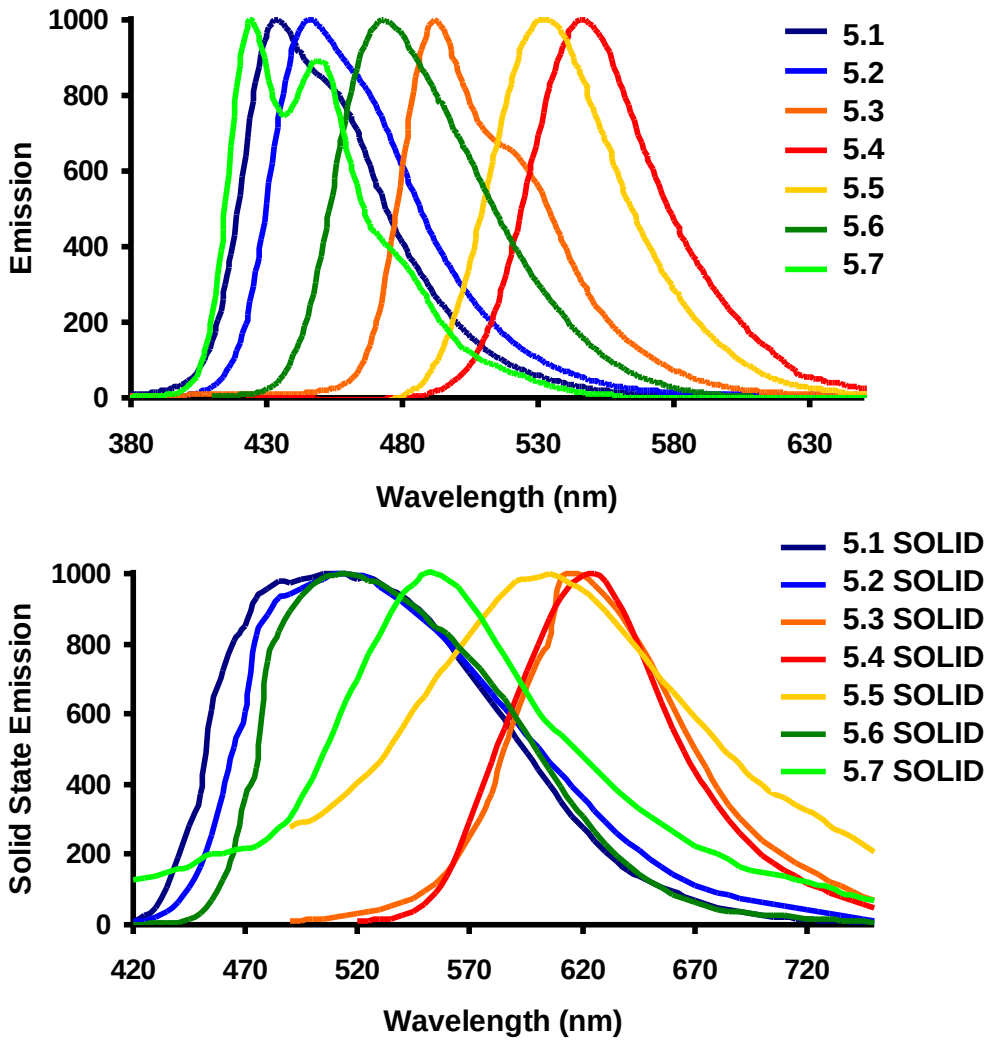

Figure 5.1. Normalized emission spectra of **5.1-5.7** in toluene (top) and the solid state (bottom). In the solid state, spectra are broadened, redshifted, and of dramatically decreased intensity compared to in solution. Spectra of XFs in the solid state are noisy due to scattering off of the powdered solid as well as relatively low fluorescence intensity.

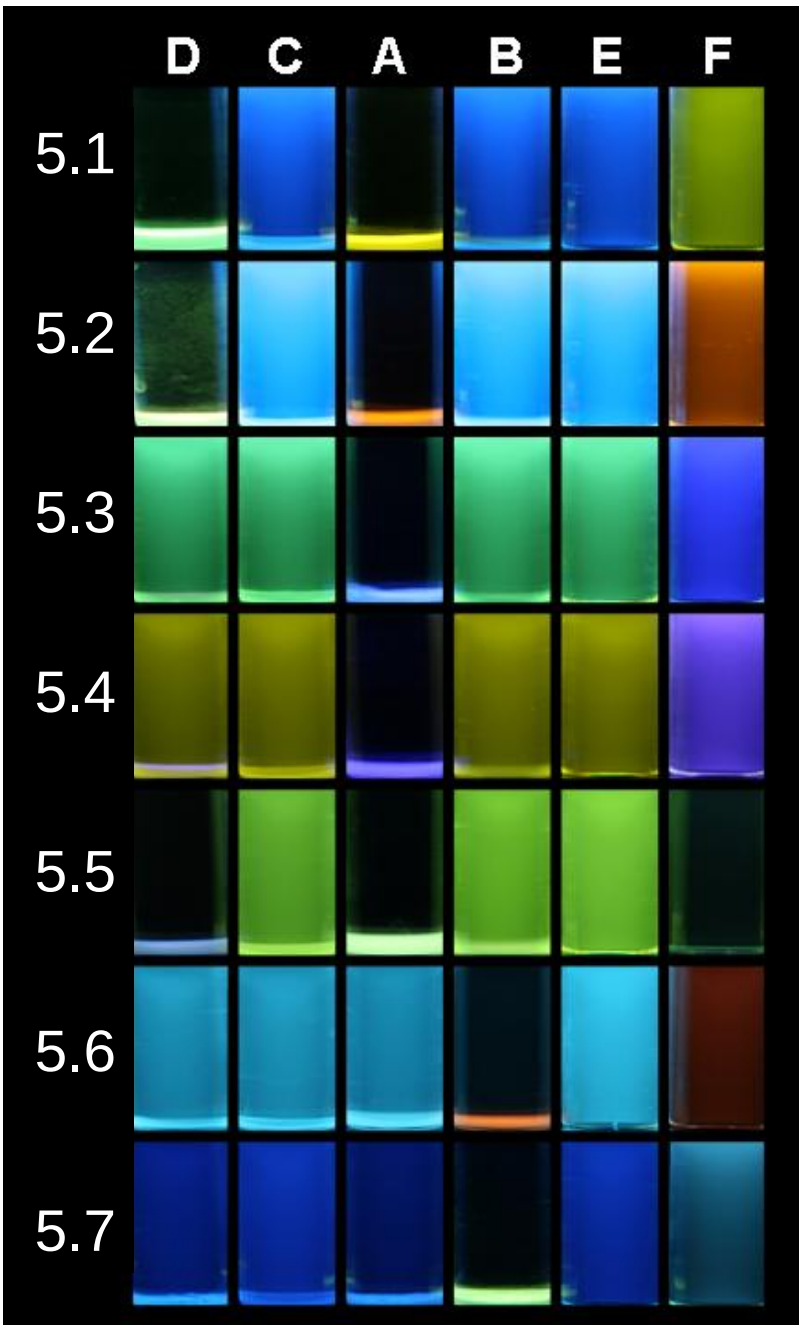

Figure 5.2. Vials containing XFs **5.1-5.7** in toluene incubated with silicas (**D** = Bare silica, **C** = Capped Silica, **A** = Acidic Silica, **B** = Basic Silica) for 24 hours. For comparison, column F shows XFs **5.1-5.7** in toluene exposed to trifluoroacetic acid (**5.1-5.5**) or *n*-hexylamine (**5.6, 5.7**). Column E shows XFs **5.1-5.7** in a toluene solution. Photos were taken under blacklight (ex = 365 nm) and photographed using a Canon EOS Digital Camera equipped with an EFS 18-55mm lens.

Table 5.1. Tabulated emission data of XFs **5.1**-**5.7** in the solid state, solution, and complexed with functionalized silica. For reference, emissions of **5.1**-**5.7** upon exposure to trifluoroacetic acid and n-hexylamine in toluene solution are included. All λ_{max} emission values are reported in nm.

XF	Solid	Toluene	Bare	Capped	Acidic	Basic	TFA	Hexylamine
5.1	515	434	508	434	537	434	530	n/a
5.2	515	446	513	446	555	446	555	n/a
5.3	615	492	426, 492	492	427	492	424	n/a
5.4	625	547	428, 547	548	433	546	432	n/a
5.5	605	531	468	531	523	531	532	n/a
5.6	515	473	475	475	473	476, 550	n/a	561
5.7	550	424	425	424	426	513	n/a	454, 497

XFs **5.1**-**5.5** – all of which possess Lewis base moieties – show large shifts in fluorescence upon exposure to acidic silica. These shifts can be rationalized by assuming protonation of **5.1**-**5.5** occurs upon exposure to the sulfonic acid moieties present on these silica particles. We have previously established that upon donor and/or acceptor substitution, XFs can display spatially separated FMOs. In the case of **5.1** and **5.2**, the LUMO is localized primarily on the acceptor-substituted axis of the molecule while the HOMO resides on the 'non-substituted' branch of the XF. Upon protonation of the pyridine, the LUMO is stabilized while the HOMO remains largely unaffected, resulting in large bathochromic shifts in **5.1** (434 to 537 nm) and **5.2** (446 to 555 nm) in emission (Figure 7.4, A).

In the case of **5.3** and **5.4**, we observe large hypsochromic shifts upon protonation. Upon incubation with acidic silica, we oberve blue shifts in the emission of

5.3 (492 to 427 nm) and **5.4** (547 to 433 nm). This is a consequence of the FMO structure of these donor/acceptor-substituted XFs. In XFs **5.3** and **5.4**, the HOMO is

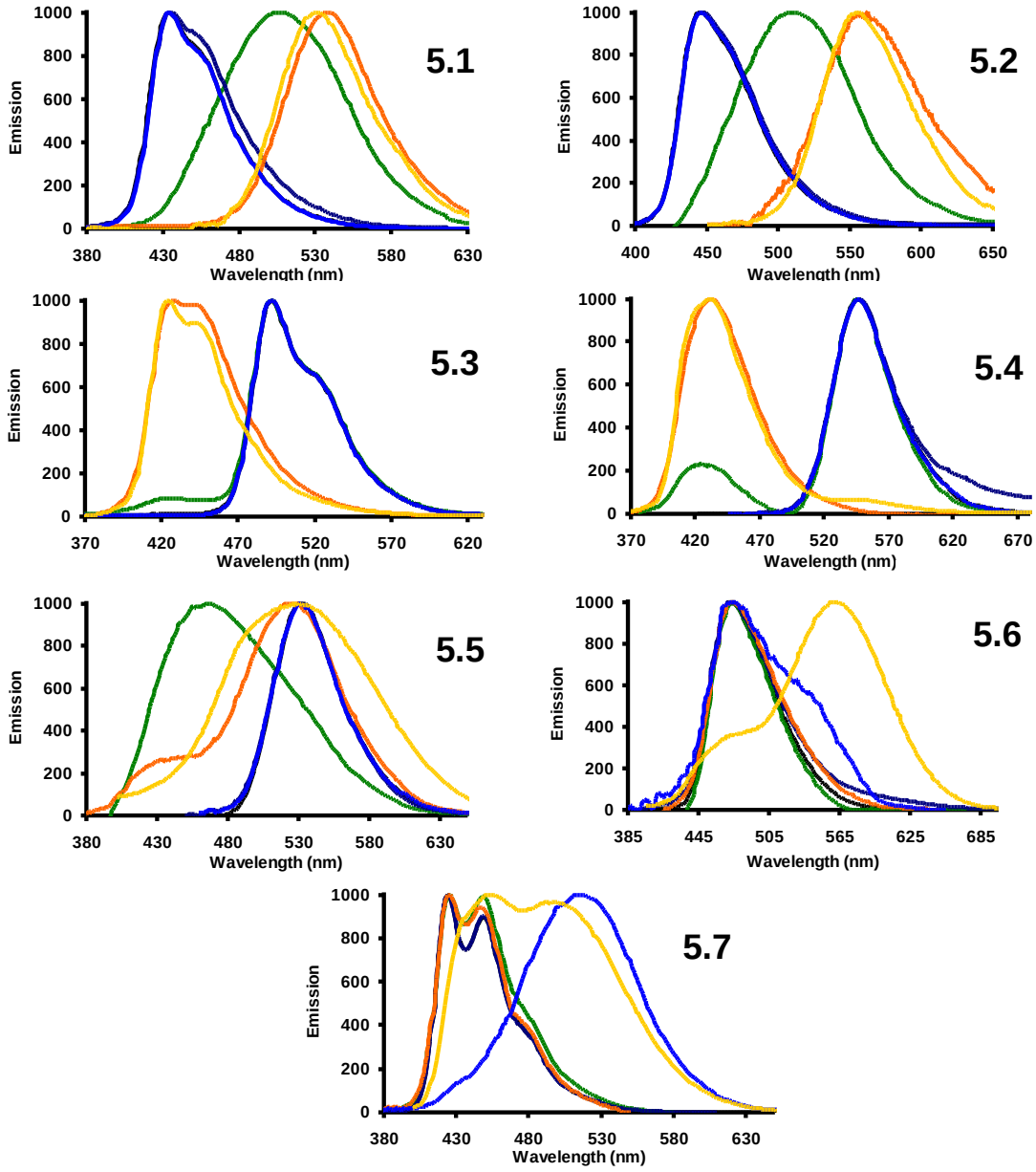

Figure 5.3. Normalized emission spectra of **5.1**-**5.7** supported on bare (green), capped (dark blue), acidic (orange), and basic (light blue) silica. For comparison, the emission of XFs **5.1**-**5.7** in toluene (black), **5.1**-**5.5** with trifluoroacetic acid (yellow), and **5.6**-**5.7** with *n*-hexylamine (yellow) are shown in black. Spectra were taken of the suspended silica particles in toluene using a triangular cuvette. Emission maxima are shown in Table 5.1.

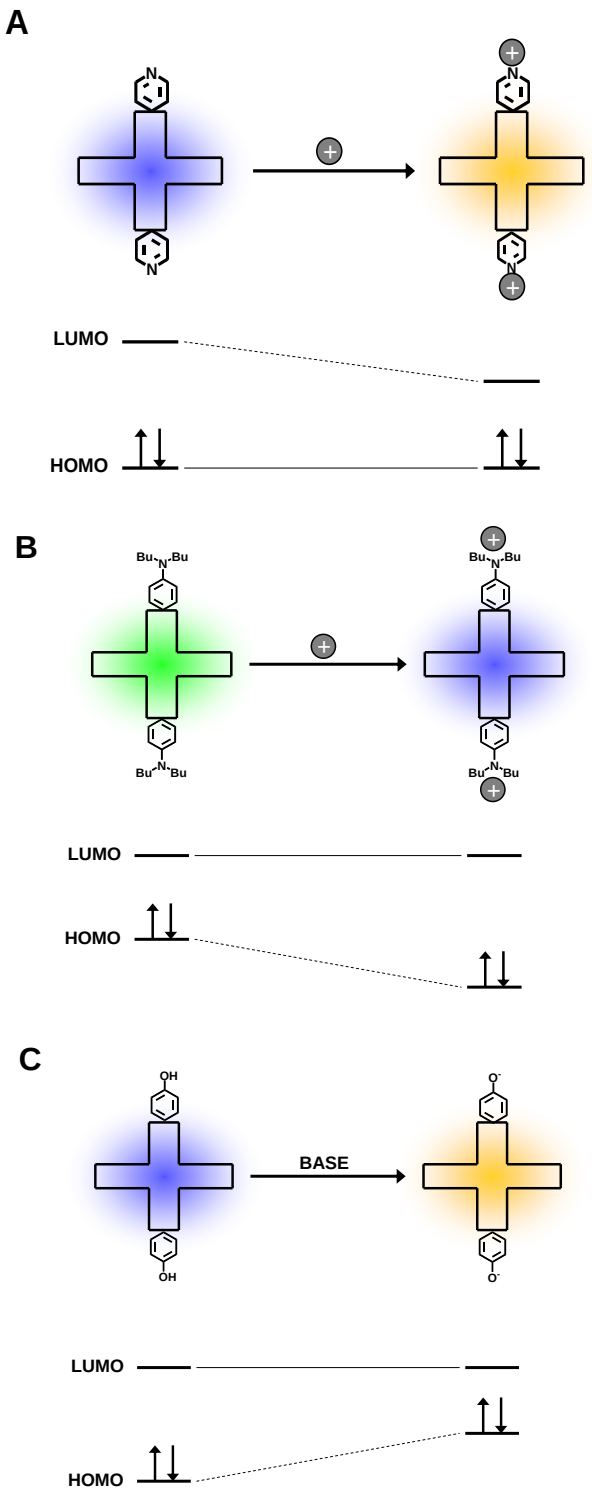

Figure 5.4. Schematic representation of the effect of protonation upon the FMOs and emission of XFs **5.1** (A, top left) and **5.3** (B, top right). C (bottom) shows the effect of deprotonation on the FMOs and emission of **5.6**.

localized on the electron-rich distyryl axis of the XF while the LUMO lies on the arylethynyl arms. Protonation of the alkylaniline functionalities stabilizes the HOMO while the LUMO remains unaffected, resulting in a blue shift (Figure 5.4, B).

We also observe a small blue shift (531-523 nm) upon incubation of **5.5** with acidic silica. We are able to rationalize this slight blue shift as the consequence of the two-stage fluoresence response previously observed upon reaction of **5.5** with trifluoroacetic acid.[3a-b] In the case of **5.5**, the HOMO lies on the donor-substituted distyryl axis of **5.5**, while the LUMO is localized primarily on the arylethynyl branch of the XF. Upon exposure to acidic silica, the protonation of all four nitrogens stabilizes both the HOMO and the LUMO, resulting in a slight net blue shift. As the digital photograph indicates, the toluene supernatant was completely non-fluorescent upon incubation of **5.1-5.5** with **A**, presumably because the acidic support adsorbs all the basic XFs from solution. In all cases, the emissions observed for complexes of **5.1-5.5** with **A** are similar to emissions recorded upon addition of excess trifluoroacetic acid to **5.1-5.5**; **5.6** and **5.7** show no change in emission upon exposure to **A**. This can be rationalized by assuming that the hydroxy functionalities present in these XFs do not react with the acidic functional groups of the silica particles. As a result, the emission of the resulting composites are roughly identical to the emissions observed upon complexation with capped silica.

Upon exposure of **5.1-5.7** to basic silica, an opposite response is observed. The composites of Lewis basic substituted XFs **5.1-5.5** with basic silica **B** display the same emission as **5.1-5.5** with **C**. This is readily rationalized by assuming that the basic surface functionality of **B** does not interact with these XFs and affect the photophysics of

5.1-**5.5**. In the case of **5.6** and **5.7**, the chromophores possess hydroxy substituents which interact with the amino-functionalized surface of **B**. We have previously reported that hydroxy-functionalized XFs such as **5.6** and **5.7** can display shifts in emission upon exposure to amines and other bases. Similar effects are observed here upon complexation of **5.6** and **5.7** with **B**. Reaction with **B** deprotonates the hydroxy functionalities, destabilizing the HOMO of **5.6** and **5.7** while the LUMO remains relatively unperturbed (Figure 5.4, C). As a result, bathochromic shifts are observed upon complexation of hydroxy-functionalized XFs with **B**. In the case of **5.6**, a large redshift is readily visible in Figure 5.2; this is observed as a large shoulder in the emission of **5.6•B** centered near 550 nm. Some of the unreacted XF **5.6** also remains in the silica, which appears dominant due to the relatively low emission intensity of the sample as well as the higher quantum yield of the blue species relative to the red species. Upon exposure of **5.7** to **B**, we observe a similar redshift from 424 nm to 513 nm.

Complexation of XFs **5.1**-**5.7** with bare silica **D** also generates fluorescent hybrid materials. The surface chemistry of **D** is mildly acidic; therefore, one might expect to observe similar responses to those observed for the sulfonic acid functionalized silica **A**. Upon exposure of **5.6** and **5.7** to bare silica, solids are formed which retain the fluorescence of **5.6** and **5.7** in solution. As in the case of **A**, no large shifts in emission are observed upon formation of **5.6•D** and **5.7•D**. In the case of the complex of **5.3** with **D**, we observe little change in emission qualitatively. Spectroscopic examination of **5.3•D** reveals a small amount of a blueshifted species present in the hybrid material at 426 nm, corresponding to the emission of the protonated XF **5.3**. However, the majority of the XF is deposited in the complex as the native unprotonated **5.3**, responsible for the

dominant emission at 492 nm. A similar result is observed in the case of **5.4•D**. Here we observe a dominant emission at 547 nm originating from unprotonated **5.4**; however, a small blueshifted band is observed at 428 nm, contributed by protonated **5.4**.

Upon reaction of XF **5.5**, containing both alkylamino substituents and pyridyl substituents, with bare silica particles, we observe a large hypsochromic shift from 531 nm to 468 nm. This emission is attributed to the bisprotonated state of **5.5** and is consistant with the emission observed in previous titrations of **5.5** with trifluoroacetic acid. When **5.1** and **5.2** are exposed to bare silica, bathochromic shifts are observed upon formation of hybrids **5.1•D** and **5.2•D**. In the case of **5.1**, a shift from 434 to 508 nm is observed; in **5.2**, the emission shifts from 446 to 513 nm. These bathochromic shifts are consistent with an interaction which stabilizes the LUMOs of the XFs while leaving the HOMOs unpreturbed (i.e. protonation); however, the magnitude of the shift is considerably smaller in both cases as compared with shifts observed upon addition of sulfonic-acid functionalized silica or trifluoroacetic acid. We attribute this to hydrogen bond formation rather than true protonation. It is interesting to note that while the alkylamino functionalities are considerably more basic than the pyridine moieties, the experimental results suggest that protonation of the pyridine nitrogens in **5.1•D** and **5.2•D** appears more favorable than protonation of the alkylamino nitrogens in **5.3•D** and **5.4•D**. We attribute this to the steric effects of the dibutyl chains which limit the interaction of the aniline nitrogens with the silica surface.

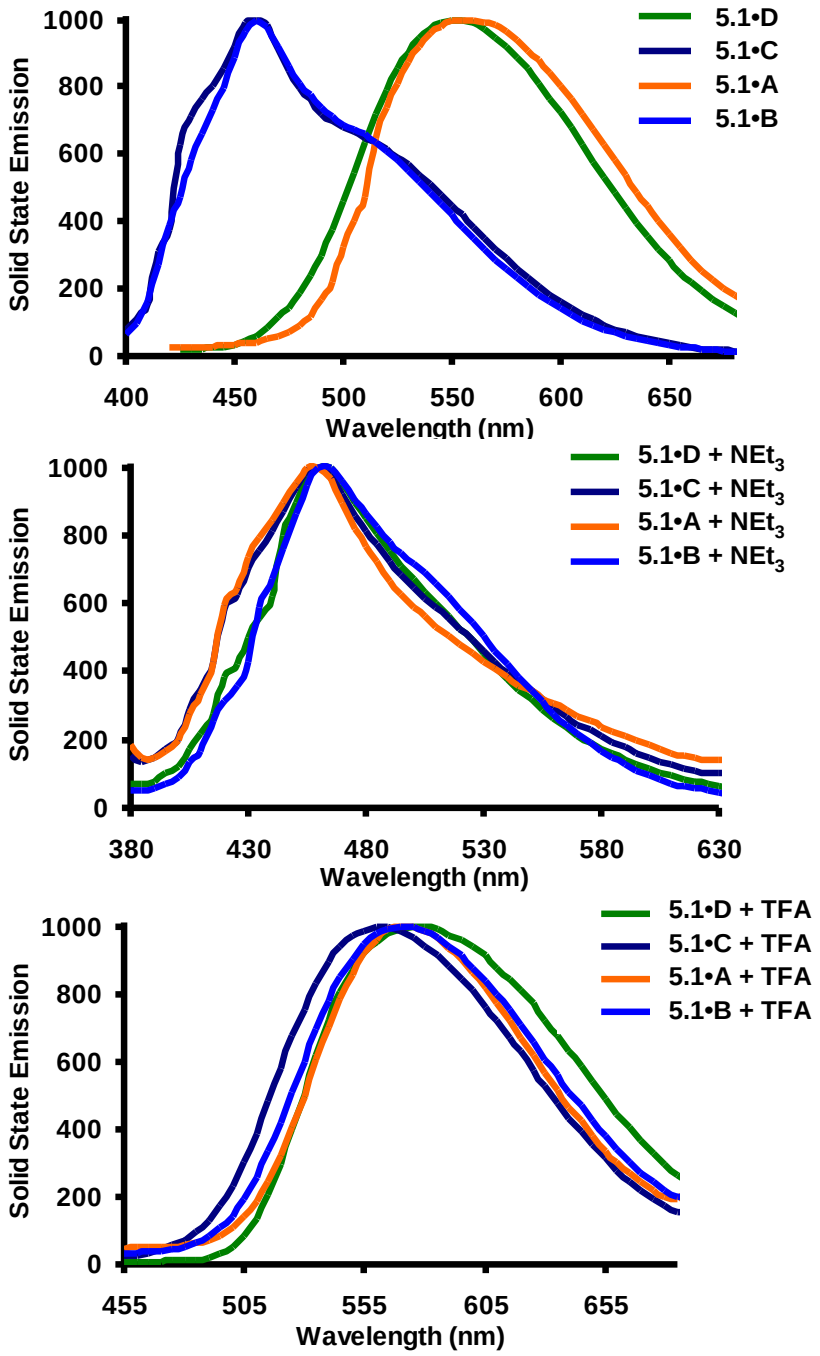

Figure 5.5. Fluorescence response of **5.1** supported on functionalized silica scaffold upon exposure to vapor analytes. The top spectra displays the emission of **5.1** supported on bare (green), caped (dark blue), acidic (orange), and basic (blue) silicas. Upon exposure to NEt_3 (middle) and trifluoroacetic acid (bottom) vapors, notable fluorescence responses are observed.

5.2.3. Sensory Responses of XF-functionalized Silica Microstructures Towards Representative Volatile Organic Compounds (VOCs).

Functionalized mesoporous silica microstructures provide an attractive platform for the solid-phase support of XFs. We were anxious to assess the potential of these fluorophores to respond to the presence of vapor-phase analytes. We exposed **5.1** supported on all four functionalized silicas to representative vapor phase analytes of interest. This proof-of-principle sensing experiment was conducted using dried XF-silica hybrids. After incubation of the desired XF dye with the functional silica scaffold of choice, evaporation of the solvent in vacuo yields dry, vibrantly fluorescent solids (Figure 5.5, A).

Figure 5.5 shows the responses observed upon exposure of **5.1** (A) to triethylamine (B) and trifluoroacetic acid (C) vapors. In the dry solid state, the hybrid materials resulting from the exposure of XF **5.1** to both basic and capped silica display emissions of approximately 460 nm. Incorporation of **5.1** into/onto bare and acidic particles generates materials with emissions of 550 and 555 nm respectively. Upon exposing these solids to NEt_3 vapors for five minutes, large hypsochromic shifts in the emission of the acidic and bare hybrid materials are observed while the emission of the capped and basic materials remain largely unchanged; the result is nearly identical emissions of between 460 and 465 nm for all materials. Upon exposure to trifluoroacetic acid, a large red shift in the emission of the capped and basic hybrid materials is observed. However, the emission of the acidic and bare composites remain largely intact, resulting similar emissions – ranging from 560 to 580 nm – in all four cases.

These responses can be rationalized by considering the protonation states of XF **5.1** when deposited on silica scaffolds and when exposed to vapor-phase analytes. The

emissions of hybrids **5.1•C** and **5.1•B** centered at 460 nm indicate the presence of the nonprotonated XF **5.1**. Emissions of 550 and 555 nm recorded for **5.1•D** and **5.1•A** respectively correspond to the expected protonated form of **5.1**. Upon exposure to ambient NEt_3 vapors, we observe large bathochromic shifts in **5.1•A** and **5.1•D** while the emissions of the capped and basic hybrids remain unchanged; after exposure, the emissions of all four species appear between 460 and 465 nm. This can be explained by assuming exposure to NEt_3 vapor causes the deprotonation of **5.1** supported in/on **5.1•A** and **5.1•D**, restoring their emission to the native form. A similar but opposite effect is observed upon exposure to trifluoroacetic acid vapors. Upon exposure, the bathochromic shift is observed in the case of **5.1•B** (460-570 nm) and **5.1•C** (460-560 nm) while acidic and bare hybrids of **5.1** remain unchanged. This finding is consistent with the protonation of **5.1** in the basic and capped hybrids, resulting in the observed redshift in these samples.

The shifts observed upon exposure of these XF-silica hybrids are not readily reversed upon incubation of the reacted solids under a flow of air. Over 1 hour, no reversal of these shifts is observed in the emission spectra of the reacted hybrids. In this application, the silica scaffolds serve two functions. First, the porous particles preserve the desirable solution properties of the XFs in the solid state hybrids, rendering them potentially useful for a wider variety of environmental and biodiagnostic assays. In addition, the functionality of these particles modulates the photophysics of the XFs as well as their reactivity towards the simple VOCs employed in this proof-of-principle assay.

5.3. Conclusions

Microstructured mesoporous silica possessing varied functionalities were successfully employed as scaffolds for the support of XFs. Whereas crystalline XFs frequently display weak emission in the solid state, immobilization of XFs in/on these particles yields solids which retain the highly fluorescent character of the parent cruciforms. Functionality integrated into the silica scaffold can be utilized to modulate the photophysical behavior of the incorporated dyes. The resulting XF-silica hybrid materials display reactivity towards representative amines and organic acids which is modulated by the functionalization present on the silica scaffold. Future contributions will more thoroughly examine the potential of silica-supported XFs – as well as the hybrid materials generated from the XFs metallated and protonated analogues – as fluorescent dyes for the detection of a variety of volatile organic compounds. Such materials may prove useful in the future development of fluorescent differential sensory arrays for the detection of VOCs in the gas phase as well as in aqueous solution.

5.4. Experimental

General Methods. All chemicals were purchased from Aldrich Chemical, Acros, TCI America, or Fischer Scientific and used without purification unless otherwise specified. Column chromatography was performed using Standard Grade silica gel 60 Å, 32-63 μm (230 x 450 mesh) from Sorbent Technologies and the indicated eluent. Elution of cruciforms was readily monitored using a handheld UV lamp (365 nm). Melting points were obtained using a Mel-Temp apparatus fitted with a Fluke 51K/J digital thermometer. All IR spectra were obtained using a Simadzu FTIR-8400s spectrometer.

Unless otherwise specified, NMR spectra were recorded at 298 K on a Varian Mercury spectrometer (300 MHz). Chemical shifts are reported in parts per million (ppm), using residual solvent (chloroform-*d*) as an internal standard. Data Reported as follows: chemical shift, multiplicity (s = singlet, d = doublet, t = triplet, q = quartet, m = multiplet), coupling constant, and integration. Mass spectral analyses were provided by the Georgia Institute of Technology Mass Spectrometry Facility.

All absorption spectra were collected using a Shimadzu UV-2401PC spectraphotometer. The emission spectra of solutions and suspensions were acquired using a Shimadzu RF-5301PC spectrofluorophotometer or a PTI QuantaMaster spectrofluorophotometer outfitted with a xenon arc lamp and series 814 PMT detector. To minimize scattering, spectra of silica suspensions were obtained using a triangular cuvette. Scattering peaks were removed by subtracting a fluorescence spectra of suspended silica with no added fluorophores from all spectra. Solid state emission spectra of XFs and dried functionalized silica materials were acquired using a Spectra Max M2 plate reader from Molecular Devices.

Synthesis of Mesoporous Silica Materials. SBA-15 was prepared similarly to reported literature procedures.[7] A copolymer template of poly(ethylene oxide)-block-poly(propylene oxide)-block-poly(ethylene oxide) (18 g) was dissolved in a solution of cHCl (103.5 g) and deionized water (477 g). Tetraethyl orthosilicate (38.4 g) was added to the solution which was subsequently stirred for 20 h at 35 °C, heated to 80 °C, and held for 24 h at 80 °C. At the end of this period, the reaction was quenched with deionized water, and the solid was filtered and washed with several portions of deionized water to remove residual copolymer and give SBA-15 as a white powder. The material

was dried for 3 h at 50 °C and then calcined as follows: ramp to 200 °C at 1.2 °C/min, hold at 200 °C for 1 h, ramp to 550 °C at 1.2 °C/min, and hold at 550 °C for 6 h. The calcined SBA-15 was then heated under vacuum at 200 °C for three hours and yielded approximately 12 g of SBA 15. Nitrogen physisorption experiments showed the material to have a BET surface area of 687 m^2/g and a BJH adsorption pore diameter of 57 Å.

Synthesis of capped SBA-15. In order to remove surface silanol groups and reduce surface acidity, 1,1,1,3,3,3-hexamethyldisilazane (1.0 g) was added to a solution of calcined SBA 15 (1.0 g) in hexanes. The solution was stirred overnight and then filtered. The solid material was washed with copious amounts of hexanes and dried under vacuum at 50 °C. Thermogravimetric analysis indicated a capping of 1.6 mmol silanols/g SiO_2. Nitrogen physisorption experiments showed the material to have a BET surface area of 332 m^2/g and a BJH adsorption pore diameter of 49 Å.

Synthesis of sulfonic acid functionalized SBA-15. The sulfonic acid functionalized SBA-15 was prepared similarly to reported literature procedures.[8] 3-mercaptopropyltrimethoxysilane (1.0 g) was added to a solution of calcined SBA 15 (1.0 g) in toluene. The solution was stirred overnight and then filtered. The solid material was washed with copious amounts of toluene and hexanes and dried under vacuum at 50 °C. Thermogravimetric analysis indicated a loading of 0.57 mmol SH/g SiO_2. The residual surface silanols groups on the thiol functionalized SBA-15 were capped by adding the material (1.0 g) to 1,1,1,3,3,3-hexamethyldisilazane (1.0 g) in hexanes and stirring overnight. The capped, thiol functionalized material was then filtered, washed with hexanes, and dried under vacuum at 50 °C. Thermogravimetric analysis indicated a capping of 0.55 mmol silanols/g SiO_2. Finally, the capped, thiol functionalized material

(1.0 g) was oxidized by adding it to a solution of methanol (10 g) and 30% H_2O_2 (20 g). The solution was stirred overnight and filtered. The solid material was washed with deionized water and dried under vacuum at 50 °C. Nitrogen physisorption experiments showed the material to have a BET surface area of 450 m^2/g and a BJH adsorption pore diameter of 50 Å.

Synthesis of amine functionalized SBA-15. The amine functionalized SBA-15 was prepared similarly to reported literature procedures.[11, 12] 3-aminopropyltrimethoxysilane (1.0 g) was added to a solution of calcined SBA 15 (1.0 g) in toluene. The solution was stirred overnight and then filtered. The solid material was washed with copious amounts of toluene and hexanes and dried under vacuum at 50 °C. Thermogravimetric analysis indicated a loading of 1.7 mmol NH_2/g SiO_2. Nitrogen physisorption experiments showed the material to have a BET surface area of 180 m^2/g and a BJH adsorption pore diameter of 38 Å.

Silica material characterization. Thermogravimetric analyses (TGA) were conducted on a Netzsch STA409. Samples were heated from 30 °C to 900 °C at 10 °C/min under an air blanket. The organic loading was determined from weight loss occurring between 200 °C and 750 °C. Nitrogen physisorption measurements were performed on a Micromeritics ASAP 2010 at 77 K. SBA-15 samples were degassed at 150 °C under vacuum overnight prior to analysis, and functionalized SBA-15 samples were degassed at 50 °C under vacuum overnight prior to analysis. Analysis of the porosity of the organic-inorganic hybrid materials before and after XF adsorption showed minimal loss of porosity, indicating that the XFs adsorbed primarily on the outer surface of the particles or in the pore mouths.

Synthesis of XF 5.7. Scheme 5.2 outlines the general synthetic approach used to obtain XF **5.7**. From the previously reported diiodide **5.8**,[5] a Sonogashira coupling is utilized to affix the arylethynyl substituents. Incorporation of hydroxy functionality requires tetrahydropyran (THP) protection of 4-hydroxybenzaldehyde prior to the Horner olefination used to synthesize **5.8**. Following the Sonogashira coupling, deprotection with trifluoroacetic acid readily yields **5.7** from **5.10** 91% yield. The synthesis of XFs **5.1-5.6** have been previously reported.[3a,b, 4, 5a]

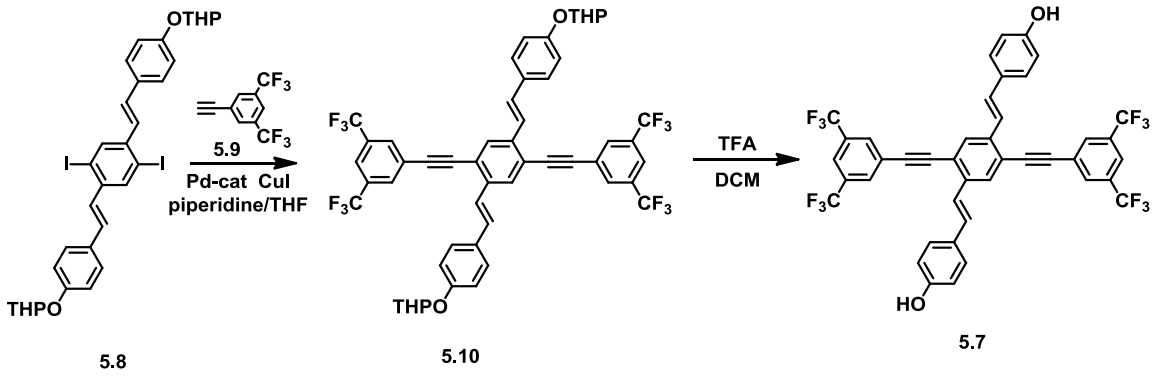

Scheme 5.2. Synthetic route for XF **5.7**.

Synthesis of compound 5.10. 5.8 (0.450 g, 0.613 mmol) was combined with **5.9**[4] (0.572 g, 1.84 mmol), $(PPh_3)_2PdCl_2$ (5 mg, 7.1 μmol), CuI (5 mg, 33 μmol), KOH (0.500 g, 8.90 mmol) and dissolved in piperidine (5 mL), EtOH (10 mL) and THF (25 mL) in a nitrogen purged Schlenk flask. The solution was degassed, capped with a septum and allowed to stir at room temperature for 24 h. The product was extracted with dichloromethane (100 mL), washed three times with water (100 mL), dried with magnesium sulfate and reduced until a yellow powder formed, which was purified by chromotagraphy eluting with 70:30

dichloromethane and hexanes, yielding 252 mg of yellow crystals. Yield: 53%. *MP:* 242 ºC. *IR:* 2929, 2852, 2214, 1507, 1374, 1280, 1245, 1181, 1130 cm^{-1}. *^{1}H NMR (500 MHz, $CDCl_3$):* δ = 8.05 (s, 4H, Ar-H), 7.94 (s, 2H, Ar-H), 7.90 (s, 2H, Ar-H), 7.53 (d, 2H, Ar-H, JH,H = 8.5 Hz), 7.49 (d, 2H, C=C-H, JH,H =16.5 Hz), 7.27 (d, 2H, C=C-H, JH,H =16.5 Hz), 7.11 (d, 4H, Ar-H, JH,H = 8.5 Hz), 5.49 (s, 2H, α-C-H), 3.95 (m, 2H, ε-C-H), 3.65 (m, 2H, ε-C-H), 2.05 (m, 2H, β-CH), 1.91 (m, 4H, γ-C-H) 1.72 (m, 4H, δ-C-H), 1.65 (m, 2H, β-C-H). *^{13}C NMR (125 MHz, $CDCl_3$):*δ =157.87, 138.25, 132.65 (m), 131.76, 131.58, 130.80, 129.36, 128.41, 126.60, 125.78, 124.43 123.26, 122.26, 121.84, 117.24, 96.71, 92.82, 91.60, 62.53, 30.71, 25,59, 19.10

Synthesis of XF 5.7. 5.10 (0.095 g, 0.166 mmol) was dissolved in dichloromethane (50 mL) and trifluoroacetic acid (2 mL) was added into a 100 mL round bottom flask kept in a dry ice acetone bath. The solution was allowed to stir at -78 °C for 2h and then thawed to room temperature. The reaction mixture was extracted with diethyl ether (100 mL), washed three times with water (100 mL), dried with magnesium sulfate, filtered and reduced until an orange powder was formed. The powder was recrystallized by dissolving in hot methanol, yielding yellow crystals (76.4 mg). Yield: 91%. *MP:292* ºC. *IR:* 3356, 2923, 2858, 2213, 1606, 1514, 1373, 1280, 1126 cm^{-1}. *^{1}H NMR (500 MHz ,THF-d_8):* δ = 8.53 (s, 2H, Ar-H), 8.30 (s, 4H, Ar-H), 8.12 (s, 2H, Ar-OH), 8.09 (s, 2H, Ar-H), 7.57 (d, 2H, C=C-H, $J_{H,H}$ = 16.5 Hz), 7.52 (d, 4H, Ar-H, $J_{H,H}$ = 8.5 Hz), 7.39 (d, 2H, C=C-H, $J_{H,H}$ = 16.5 Hz), 6.81 (d, 4H, Ar-H, $J_{H,H}$ = 8 Hz)**.** *^{13}C NMR (125 MHz, THF-d_8):* δ = 157.03, 136.50, 130.18 (m), 127.17, 126.90, 126.67, 125.04, 124.19, 122.88, 120.71, 120.47, 119.81, 119.62, 118.58 114.07, 90.70, 89.65.

5.5. References and Notes

1. (a) Pond, S. J. K.; Tsutsumi, O.; Rumi, M.; Kwon, O.; Zojer, E.; Bredas, J. L.; Marder, S. R.; Perry, J. W. *J. Am. Chem. Soc.* **2004**, *126*, 9291-9306. (b) Wang, B.; Wasielewski, M. R. *J. Am. Chem. Soc.* **1997**, *119*, 12-21. (c) Bangcuyo, C. G.; Rampey-Vaughn, M. E.; Quan, L. T.; Angel, S. M.; Smith, M. D.; Bunz, U. H. F. *Macromolecules* **2002**, *35*, 1563-1568. (d) Pautzsch, T.; Klemm, E. *Macromolecules* **2002**, *35*, 1569-1575. (e) Nielsen, M. B.; Diederich, F. *Chem. Rev.* **2005**, *105*, 1837-1867. (f) Kivala, M.; Diederich, F. *Acc. Chem. Res.* **2009**, *42*, 235-248. (g) Iyer, P. K.; Beck, J. B.; Weder, C.; Rowan, S. J. *Chem. Commun.* **2005**, 319-321. (h) Knapton, D.; Rowan, S. J.; Weder, C. *Macromolecules* **2006**, *39*, 651-657. (i) Beck, J. B.; Ineman, J. M.; Rowan, S. J. *Macromolecules* **2005**, *38*, 5060-5068.

2. (a) Rakow, N. A.; Suslick. K. S. *Nature* **2000**, *406*, 710-713. (b) Rakow, N. A.; Sen, A.; Janzen, M. C.; Ponder, J. B.; Suslick, K. S. *Angew. Chem. Int. Ed.* **2005**, *44*, 4528-4532. (c) Suslick, K. S.; Rakow, N. A.; Sen, A. *Tetrahedron* **2004**, *60*, 11133-11138. (d) M. C. Janzen, J. B. Ponder, D. P. Bailey, C. K. Ingison, K. S. Suslick. *Anal. Chem.* **2006**, *78*, 3591-3600. (e) Zhang, C.; Suslick, K. S. *J. Am. Chem. Soc.* **2005**, *127*, 11548-11549. (f) Zhang, C.; Suslick, K. S. *J. Agric. Food Chem.* **2007**, *55*, 237-242. (g) Zhang, C.; Bailey, D. P.; Suslick, K. S. *J. Agric. Food Chem.* **2006**, *54*, 4925-4931.

3. (a) Wilson, J. N.; Bunz, U. H. F. *J. Am. Chem. Soc.* **2005**, *127*, 4124-4125. (b) Zucchero, A. J.; Wilson, J. N.; Bunz, U. H. F. *J. Am. Chem. Soc.* **2006**, *128*, 11872-11881. (c) Tolosa, J.; Zucchero, A. J.; Bunz, U. H. F. *J. Am. Chem. Soc.* **2008**, *130*, 6498-6506. (d) Brombosz, S. M.; Zucchero, A. J.; Phillips, R. L.; Vazquez, D.; Wilson, A.; Bunz, U. H. F. *Org. Lett.* **2007**, *22*, 4519-4522. (e) Hauck, M.; Schönhaber, J.; Zucchero, A. J.; Hardcastle, K. I.; Müller, T. J. J.; Bunz, U. H. F. *J. Org. Chem.* **2007**, *72*, 6714-6725. (f) Wilson, J. N.; Hardcastle, K. I.; Josowicz, M.; Bunz, U. H. F. *Tetrahedron.* **2004**, *60*, 7157-7167. (g)

4. (a) Wilson, J. N.; Josowicz, M.; Wang, Y.; Bunz, U. H. F. *Chem. Commun.* **2003**, 2962-2963.

5. (a) McGrier, P. L.; Solntsev, K. M.; Miao, S.; Tolbert, L. M.; Miranda, O. R.; Rotello, V. M.; Bunz, U. H. F. *Chem. Eur. J.* **2008**, *14*, 4503-4510. (b) McGrier, P. L.; Solntsev, K. M.; Schönhaber, J.; Brombosz, S. M.; Tolbert, L. M.; Bunz, U. H. F. *Chem. Commun.* **2007**, 2127 –2129.

6. Zhao, D.; Feng, J.; Huo, Q.; Melosh, N.; Fredrickson, G. H.; Chmelka, B. F.; Stucky, G. D. *Science* **1998**, *279*, 548-552.

7. Zhao, D.; Huo, Q.; Feng, J.; Chmelka, B. F.; Stucky, G. D. *J. Am. Chem. Soc.* **1998**, *120*, 6024-6036.

8. Yokoi, T.; Yoshitake, H.; Tatsumi, T. *J. Mater. Chem.* **2004**, *14*, 951-957.

9. (a) Van Rhijn, W. M.; De Vos, D. E.; Sels, B. F.; Bossaert, W. D. *Chem. Commun.* **1998**, 317-318. (b) Wilson, B. C.; Jones, C. W. *Macromolecules* **2004**, *37*, 9709-9714.

10. Anwander, R.; Nagl, I.; Widenmeyer, M.; Engelhardt, G.; Groeger, O.; Palm, C.; Röser, T. *J. Phys. Chem. B* **2000**, *104*, 3532-3544.

11. Stein, A.; Melde, B. J.; Schroden, R. C. *Adv. Mater.* **2000**, *12*, 1403-1419.

12. Kallury, K. M. R.; Macdonald, P. M.; Thompson, M. *Langmuir* **1994**, *10*, 492-499.

Chapter 6

Acidochromicity of Bisarylethynylbenzenes: Hydroxy versus Dialkylamino Substituents

6.1 Introduction

Reactive chromophores or fluorophores that change color, emission wavelength, and/or emission intensity upon exposure to analytes and are potentially useful as sensors. They contain a chromophoric π-conjugated core with embedded functionality possessing free electron pairs before or after addition of an analyte.[1] The interaction of the free electron pairs of functional fluorophores with suitable analytes or stimuli influences the position of the HOMO, the LUMO, or both and elicits changes in absorption and emission.

The concept of isolobality of molecules was set forth by Hoffmann[2] and asserts that molecules of similar Frontier Molecular Orbital (FMO) structure geometry and electron count display similar reactivity and properties. It is a qualitative model that guides the understanding of properties and reactivities of analogous molecules. One should be able to use the isolobal principle to predict – at least qualitatively – the expected responses of classes of consanguine fluorophores towards change of pH or metal coordination. Superficially, one might expect hydroxy substituents should be isolobal to amino groups. However, a simple application of the isolobal principle will not always suffice in such organic systems, as the relative orbital ordering results in systems where (in a formal sense) free electron pairs interact predominately with either the σ- or the π-system. If the free electron pairs are energetically low lying, we expect them to interact predominately with the σ-system, while energetically higher lying electron pairs should have a larger interaction with the π-system.

A simple test bed for this hypothesis would be compounds **6.4** and **6.5**, bis(arylethynyl)benzenes functionalized with dibutylamino and hydroxy groups, respectively. Though synthetically simple, their sensory responses have not been examined.[3] Comparison of **6.4** and **6.5** with their analogous distyrylbenzenes[4] **6.6** and **6.7** permit the expansion of this study to investigate differences that arise when alkenyl groups are exchanged for alkynyl groups. Probing the acidochromicity and photophysical properties of **6.4-6.7** should offer insight into the application of the isolobal principle and provide an understanding of fundamental physical-organic issues in these systems.

6.2 Results and Discussion

6.2.1 Synthesis of Bisarylethynylbenzenes

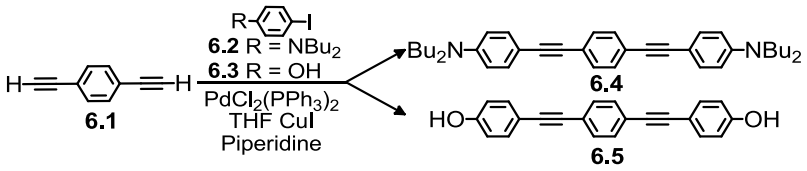

Scheme 6.1. Synthesis of compounds **6.4** and **6.5** from **6.1** via Sonogashira coupling of substituted *p*-iodobenzenes **6.2** and **6.3**.

Distyrylbenzene compounds **6.6** and **6.7** were synthesized according to literature procedures.[5,6] Surprisingly, **6.5** [7] has been reported only once and **6.4** is unreported, although the dimethyl-[8] and dihexyl-substituted[9] compounds are known. Heck-Cassar-Sonogashira-Hagihara (HCSH) coupling of **6.2** to **6.1** furnishes **6.4**. Similarly, **6.5** was synthesized from the HCSH coupling of **6.3** with **6.1** (Scheme 6.1).[10] Upon protonation with trifluoroacetic acid or deprotonation with tetrabutylammonium hydroxide, compounds **6.4a-6.7a** are obtained.

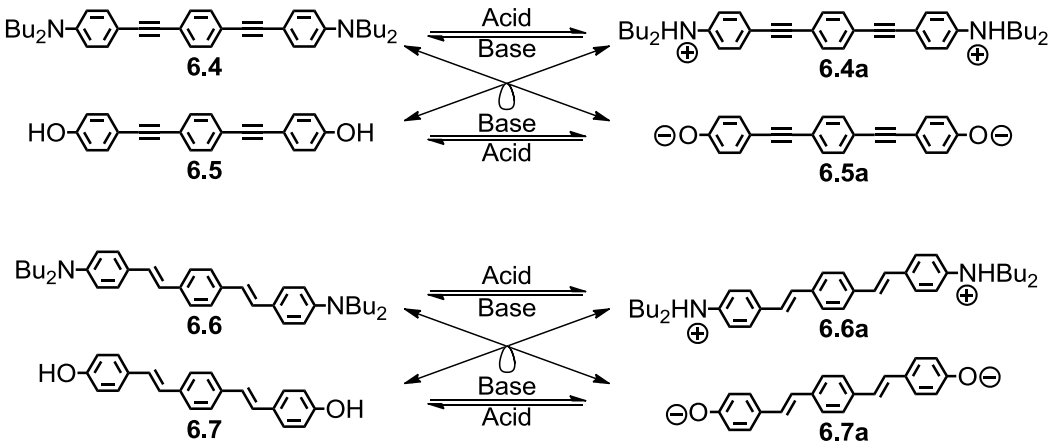

Figure 6.1. Acid/Base equilibrium relationships of **6.4**-**6.7a** are shown. Diagonal isolobal relationships are indicated.

6.2.2 Spectroscopic Properties of Hydroxy/Dialkylamino Bisarylethynylbenzenes and Distyrylbenzenes

For ease of discussion, isolobal pairs have been placed into sets (**A**-**D**, Figure 6.2). These compounds were examined through UV-vis and fluorescence spectroscopy (dilute solutions in diethyl ether, 1,4-dioxane, chloroform, dichloromethane, methanol, ethanol, isopropanol, *tert*-butyl alcohol, acetonitrile, dimethylformamide, and dimethylsulfoxide; (Figure 6.2). Figure 6.2 displays the absorption and emission of sets **A**-**D** in four representative solvents to permit a qualitative examination of solvent effects upon each compound. Diethyl ether, methanol, acetonitrile and dimethylsulfoxide were chosen because they represent non-polar, polar protic, and polar aprotic solvents. In the case of sets **C** and **D**, with the exception of **6.5** in the very polar solvent DMSO, the absorption spectra for both compounds are nearly each superimposable in a range of solvents. The absorption spectra of **6.4a** and **6.5** are only ~10 nm apart and display similar vibronic features.

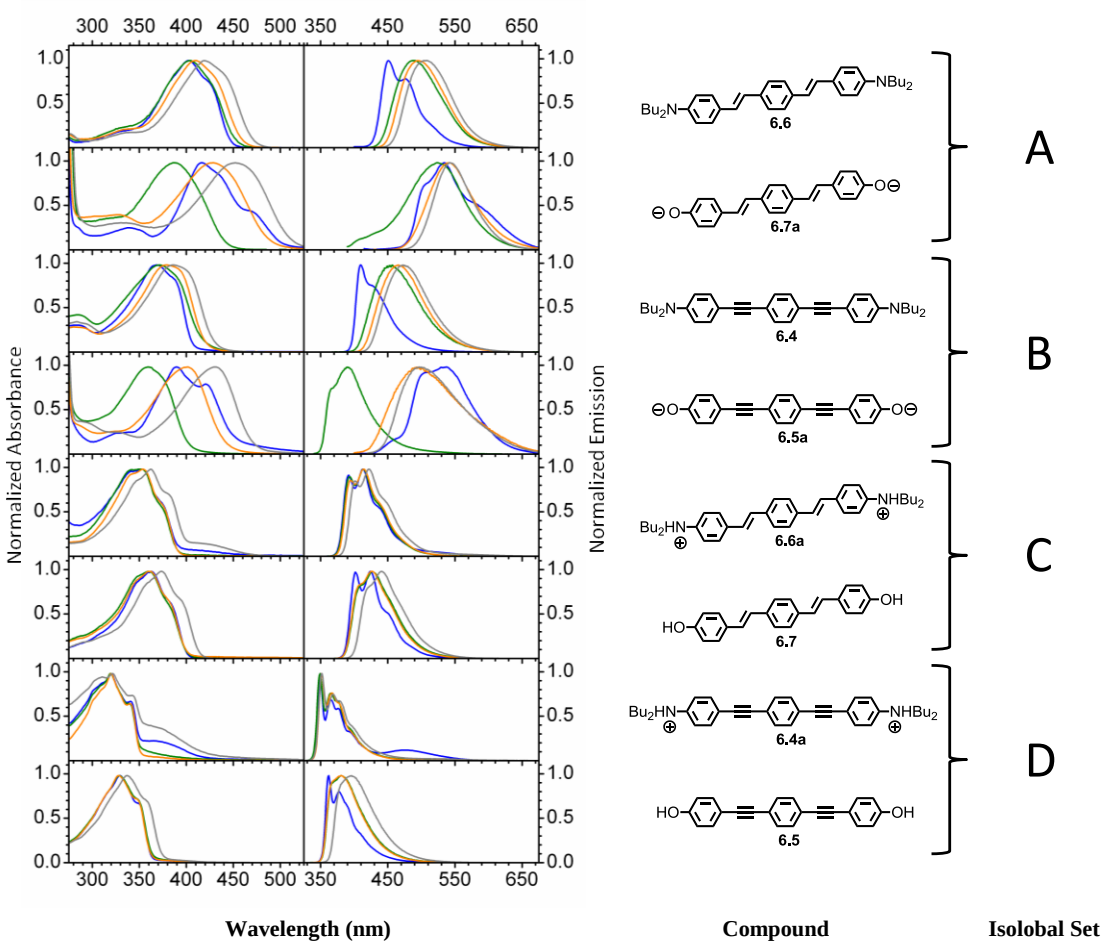

Figure 6.2. Absorption (left) and emission (right) spectra of **6.4**-**6.7a** in diethyl ether (blue), methanol (green), acetonitrile (orange) and dimethylsulfoxide (grey). Compounds are grouped by electronic structure into isolobal sets **A**-**D** (far right).

Similarities are also observed in the emission spectra of set **D**; **6.4a** displays nearly overlaped, highly structured emissions in a range of solvents. **6.5** exhibits a similarly featured emission in diethyl ether; however, as solvent polarity increases, the vibronic features give way to a broadened, smooth lineshape. Once again, the emission λ_{max} of **6.5** is similar to that of **6.4a**. Set **C** behaves in a nearly identical fashion to **D**; however, the absorption and emission spectra are red-shifted approximately by 30 and 40 nm, respectively. In sets **C** and **D**, the chromophores lack available lone pairs; as a result, we

would expect little solvent dependence in their absorption or emission λ_{max}. Furthermore, the isolobal principle suggests all four chromophores should exhibit similar photophysical properties. Indeed, this is what is observed. Surprising differences were observed in sets **A** and **B**, where the chromophores possess available lone pairs. The isolobal principle predicts that pairs **6.6** and **6.7a** and **6.4** and 6.**5a** should exhibit similar photophysical properties; furthermore, we expect sets **A** and **B** to behave in a similar fashion. While sets **A** and **B** are similar, differences appear in the pairs **6.6** and **6.7a** and **6.4** and **6.5a**. In the case of dibutylamino-functionalized **6.6** and **6.4**, the absorption spectra in variety of solvents are similarly featured and exhibit a minimal (~ 25 nm) solvent dependence. Greater solvent dependence is observed in the emission spectra. The emission of **6.6** and **6.4** in ether is highly featured; as solvent polarity increases, the emission is redshifted (~ 60 nm) and vibronic definition disappears.

In **6.7a** and **6.5a**, methanol exhibits the highest energy absorption, and dramatic solvent dependence (~80 nm) is observed in the absorption maxima. Divergence is also observed in the emission spectra. The emission of **6.7a** and **6.5a** in diethyl ether is considerably redshifted relative to their alkylamino counterparts (~ 80-100 nm). Little solvent dependence is observed in the emission of **6.7a** (~ 20 nm), while in the case of **6.5a**, a large solvent effect is seen. Here, the emission of **6.5a** varies by more than 150 nm, ranging from MeOH at the highest energy to ethyl ether at the lowest energy.

The compounds in sets **C** and **D** behave as isolobal pairs; however, the suprising lack of 'isolobility' in the case of **A** and **B** requires an explanation. Previously, we have analyzed solvent dependent absorption and emission spectra of similar compounds utilizing the Lippert-Mataga equation:[6a] A solvent's dielectric constant and refractive index are

used to calculate an orientation polarizability value (Δf) for a given solvent; Δf is then plotted against the energy of the Stokes shift for each measured solvent.[11] Generally, a linear plot is obtained with the magnitude of the slope reflecting the change in a fluorophore's dipole moment upon excitation.

A Lippert-Mataga analysis of **6.4-6.7a** proved difficult; whereas the dibutylamino compounds (**6.4**, **6.4a**, **6.6**, and **6.6a**) were well correlated, the phenolic compounds (**6.5**, **6.5a**, **6.7**, and **6.7a**) showed no meaningful relationship. The Lippert-Mataga equation only considers non-specific effects related to solvent reorganization. Solvent-fluorophore interactions may, however, play a critical role in understanding the behavior of the phenolates.

6.2.3 Kamlet-Taft Analysis of Hydroxy/Dialkylamino Bisarylethynylbenzenes and Distyrylbenzenes

We subjected **6.4-6.7a** to a Kamlet-Taft (KT) solvent analysis accounting for solvent-specific interactions due to hydrogen bonding or acid/base reactions.[12] KT relies on a multivariate linear regression analysis of the absorption λ_{max} of a chromophore in a variety of solvents (Eq. 1).

Eq 1. Kamlet-Taft multivariate approach:

$$\nu \text{ (1000/cm)} = \nu_0 + s \cdot \pi^* + a \cdot \alpha + b \cdot \beta$$

The KT approach correlates the solvent-dependent spectral shifts observed (ν) for a chromophore with three solvent-dependent parameters (α, β, and π*). Here, ν_0 corresponds to the absorption or emission energy of the chromophore in a vacuum while *s*, *a*, and *b* are fitted coefficients obtained from the linear regression analysis (see 6.4 experimental). The index π* expresses the ability of the solvent to stabilize the chromophore's charge and/or

dipole via nonspecific dielectric interactions. α and β incorporate solvent-solute interactions; β describes the proton accepting character of the solvent while α corresponds to the hydrogen donating character of the solvent. By analyzing the coefficients, it is possible to determine the degree to which each mode of interaction (α, β, and π*) affect the absorption λ_{max} of a chromophore.

Table 6.1 shows the results of the Kamlet-Taft analysis. The calculated ν_0 values range from 25.1 to 31.2 x 10^3 cm^{-1}; the compounds within isolobal set **A** have similar ν_0 values as do those in sets **B**, **C** and **D**. As one would expect, the values of ν_0 for the styryl isolobal set **A** are slightly lower, indicating a redshift in the gas phase absorption relative to their arylethynyl congeners in set **B**. The red shift is a consequence of the hybridization change ($sp \rightarrow sp^2$) in the bridge carbons when going from alkynes to alkenes. This more electron-rich system allows the phenyl groups to interact somewhat more strongly through the conjugative bridge. The same relationship holds true for the styryl compounds in **C** relative to their arylethynyl analogues in **D**.

Table 6.1. Coefficient Values Obtained from Kamlet-Taft Analysis

Isolobal Sets	A		B		C		D	
Compound	6.6	6.7a	6.4	6.5a	6.6a	6.7	6.4a	6.5
ν_0[a]	25.1	25.4	27.4	26.8	28.8	27.9	31.2	30.7
S	-1.2	-1.4	-1.5	-2.5	-0.76	-0.76	-0.26	-0.52
A	0.29	2.7	0.17	2.9	0.60	0.52	-0.07	0.32
B	0.16	-2.7	0.14	-1.5	-0.63	-0.31	0.30	-0.55
R[b]	0.95	0.90	0.95	0.80	0.83	0.77	0.58	0.80

[a] Units of ν_0 are in 10^3 cm^{-1}. [b] R is the correlation coefficient.

The *s* coefficient of the π* term reflects the contribution of nonspecific dielectric interactions of the solvent with the fluorphore and is somewhat analagous to the slope obtained from a Lippert-Mataga analysis; it is related to the fluorophore's dipole. In all cases, this term is negative, inducing a spectral redshift. Isolobal pairs behave similarly and as we would expect. In sets **C** and **D**, electron pairs are involved in proton bonding. As a consequence, *s* is less significant, suggesting a smaller dipole. In sets **A** and **B**, where free electron pairs are more available, *s* is larger, suggesting a greater dipole.

The *a* and *b* coefficients for the isolobal sets **C** and **D** are modest. The lack of availabile free electron pairs results in minimal solvent-specific interaction. Similarly, in the case of dibutylamino compounds **6.4** and **6.6**, the *a* and *b* values are also relatively small. The *s* term is the predominant influence on the observed absorption. However, in the case of the deprotonated phenols **6.5a** and **6.7a**, *a* and *b* become significant, with *a* inducing a hypsochromic shift and *b* resulting in a bathochromic shift. This results in the divergent photophysical behavior observed in **6.5a** and **6.7a** relative to their isolobal counterparts.

Why is this pronounced solvent effect observed exclusively in **6.5a** and **6.7a** and not in their isolobal counterparts **6.4** and **6.6**? One might attribute this differential behavior to the increased basicity of a phenolate ($pK_a \sim 10$)[13] as compared to a dialkylamino group ($pK_a \sim 6.6$).[1] A look into the Hammett σ-values is instructive, as here the σ-values[14] of $-O^-$, $-N(C_3H_7)_2$, -OH and $-NMe_2H^+$ are $\sigma = -0.81$, $\sigma = -0.93$, $\sigma = -0.37$, and $\sigma \approx 0.70$, respectively.[15] The Hammett values testify to the apparent electronic similarity of the

phenolate to the dialkylamino groups but of course do not take into account the hydrogen bonding contributions that will undoubtly be much stronger in the case of a phenolate than in a neutral amine. More surprising is the similarity of the spectroscopic properties of the phenols and the ammonium salts (where hydrogen bonding apparently does not play a significant role), given the larger differences in their respective Hammett parameters. While the correlation with Hammet σ_p parameters is appealing and correct, they clearly cannot explain the subtleties in this interesting system.

An important additional point are the quantum yields of these eight compounds, which we determined in acetonitrile. Generally, in the pairs **A** and **B**, the aniline always has a significantly higher quantum yield than the phenolate. In the case of **6.5a**, the quantum yield is below 0.01. For the pairs **C** and **D**, the differences are much smaller and the quantum yields are generally quite substantial. In both cases, the ammonium species display a higher quantum yield than the phenols. The differences in the quantum yields are somewhat intransparent, as it is often observed, the only rough trend is that the higher the emission wavelength, the lower the emission quantum yield is; a notable exception is **6.5a** with its vanishing emission. Generally, the amines do better with respect to emission quantum yield than the phenols and phenolates, for subtle reasons that are not easily divined.

6.4 Conclusions

We have examined the photophysical properties and acidochromicity of hydroxy- and dibutylamino-functionalized distyrylbenzenes and arylethynylbenzenes. While sets **C** and **D** exhibit similar photophysical behavior as expected, and do not possess effective lone

pairs, sets **A** and **B** – possessing lone pairs that interact effectively with the π-system of the fluorophore– show different behavior in absorption and emission. These differences stem from fluorophore-solvent interactions which disproportionally affect the phenolate-substituted dyes.

The true electronic similarity of **6.4**-**6.7a** can be appreciated when viewing their absorption and emission in acetonitrile – a solvent possessing small and similar α and β parameters (Figure 6.3, Table 6.2). The contribution of solute-specific effects is minimized; the isolobal similarity of **A** and **B** as well as **C** and **D** becomes readily apparent. Although the phenolate and dibutylamino groups are isolobal, the difference in their pK_a and the presence of the ionic phenolate results in dyes that are electronically isolobal. However, they behave very differently in practice, particularly in hydrogen bonding solvents.

Table 6.2. Selected photophysical data of compounds **6.4**-**6.7a** in CH_3CN.

Isolobal Sets	A		B		C		D	
Compound	6.6	6.7a	6.4	6.5a	6.6a	6.7	6.4a	6.5
λ_{max} Absorption (nm)	410	431	378	408	353	364	321	328
λ_{max} Emission (nm)	494	542	466	496	414	426	351	380
E ($M^{-1}\cdot cm^{-1}$)	7774	17515	6799	9632	4712	24191	6089	10230
Φ	0.60[a]	0.13	0.51	<0.01	0.73	0.43	0.54	0.43

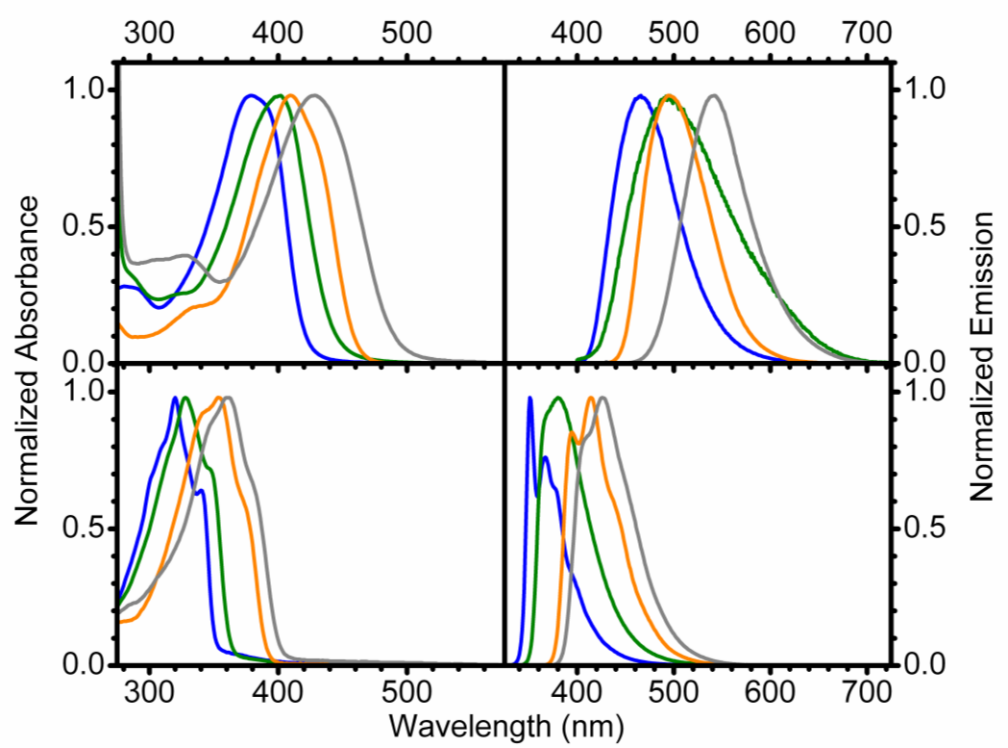

Figure 6.3. Absorption (left) and emission (right) spectra of **6.4**-**6.7a** in acetonitrile. Top: **6.4** (blue), **6.5a** (green), **6.6** (orange), **6.7a** (grey). Bottom: **6.4a** (blue), **6.5** (green), **6.6a** (orange), **6.7** (grey).

Interesting and somewhat unexpected is the finding that free electron pairs in the hydroxy compounds **6.5** and **6.7** are *not* available for conjugation with the π-system. Apparently, these electrons are too low in energy to permit efficient interaction. The other, somewhat expected trend is that dyes containing alkene bridges display redshifted spectral features when compared to analogous fluorophores featuring alkyne groups. We note that the change in hybridization ($sp \rightarrow sp^2$) increases the electron donating character of the distyryl compounds as compared to the bisarylethynyl compounds. While the gas phase absorption, ν_0, is redshifted in all of the alkene compounds relative to the corresponding alkyne compounds, the degree to which a solvent effects the absorption of a molecule is nearly identical among an alkene-alkyne pair as can be seen through similar

values of *s*, *a*, and *b*. Therefore, we recommend acetonitrile as the preferred solvent for the comparison of a series of consanguine fluorophores. In addition, our study gives design guidelines showing how to engineer absorption and emission wavelengths in distyrylbenzene and bisarylethynylbenzene-like dyes.

6.3 Experimental

Materials and Methods: All chemicals were purchased from Aldrich Chemical, Acros, or Fischer Scientific and used without purification unless otherwise specified. Column chromatography was performed using Standard Grade silica gel 60 Å, 32-63 μm (230 x 450 mesh) from Sorbent Technologies and the indicated eluent. Elution of cruciforms was readily monitored using a handheld UV lamp (365 nm). Melting points were obtained using a Mel-Temp apparatus fitted with a Fluke $51^{K/J}$ digital thermometer. All IR spectra were obtained using a Shimadzu FTIR-8400s spectrometer. Unless otherwise specified, NMR spectra were recorded at 298 K on a Bruker DRX spectrometer (500 MHz). Chemical shifts are reported in parts per million (ppm), using residual solvent (chloroform-*d*, DMSO-*d*6 or THF-*d*8) as an internal standard. Data Reported as follows: chemical shift, multiplicity (s = singlet, d = doublet, t = triplet, q = quartet, m = multiplet), coupling constant, and integration. Mass spectral analyses were provided by the Georgia Institute of Technology Mass Spectrometry Facility. All absorption spectra were collected using a Shimadzu UV-2401PC spectrophotometer. The emission spectra of solutions were acquired using a PTI QuantaMaster spectrofluorophotometer outfitted with a xenon arc lamp and series 814 PMT detector.

Synthesis of 6.4: To a stirring solution of 0.150 g of 1,4-diethynylbenzene (**6.1**) (1.19 mmol, 1 eq.) in 10 mL of degassed THF/Piperidine (3:1 v/v) under nitrogen was added 0.867 g of 6.2 (2.62 mmol, 2.2 eq.), 8.3 mg of $PdCl_2(PPh_3)_2$ (0.012 mmol, 0.01 eq.) and 2.3 mg of CuI (0.012 mmol, 0.01 eq.). The vessel was sealed and allowed to stir for 24 hours. The solution was then poured into dichloromethane, followed by extraction with brine (X2) and water (X2). The organic layer was dried with magnesium sulfate, filtered and concentrated under reduced pressure. The crude compound was then purified by column chromatography utilizing DCM:Hexane (2:3) furnishing 6.4 in 54% yield (0.342 g, 0.643 mmol). ^{1}H-NMR (500 MHz, $CDCl_3$) d 0.96 (t, 12H J=9 Hz), 1.36 (m, 8H), 1.57 (m, 8H), 3.28 (t, 8H J=12 Hz), 6.57 (d, 4H J=9 Hz), 7.35 (d, 4H J=9 Hz), 7.42 (s, 4H); ^{13}C-NMR (125 MHz, $CDCl_3$) 114.41, 20.74, 51.10, 87.61, 92.87, 108.99, 111.60, 123.53, 131.43, 133.29, 148.41; IR (KBr) $\tilde{\nu}$ 3798 (w), 3333 (w), 3196 (w), 3092 (w), 3043 (w), 2953 (s), 2868 (s), 2727 (w), 2561 (w), 2207 (s), 2160 (m), 1902 (w), 1884 (w), 1688 (w), 1609 (s), 1523 (s), 1468 (m), 1400 (m), 1371 (m), 1285 (m), 1198 (m), 1144 (s), 1109 (m), 926 (m), 833 (s), 814 (s), 525 (m).

Spectroscopic Data of Compounds 6.4-6.7a.

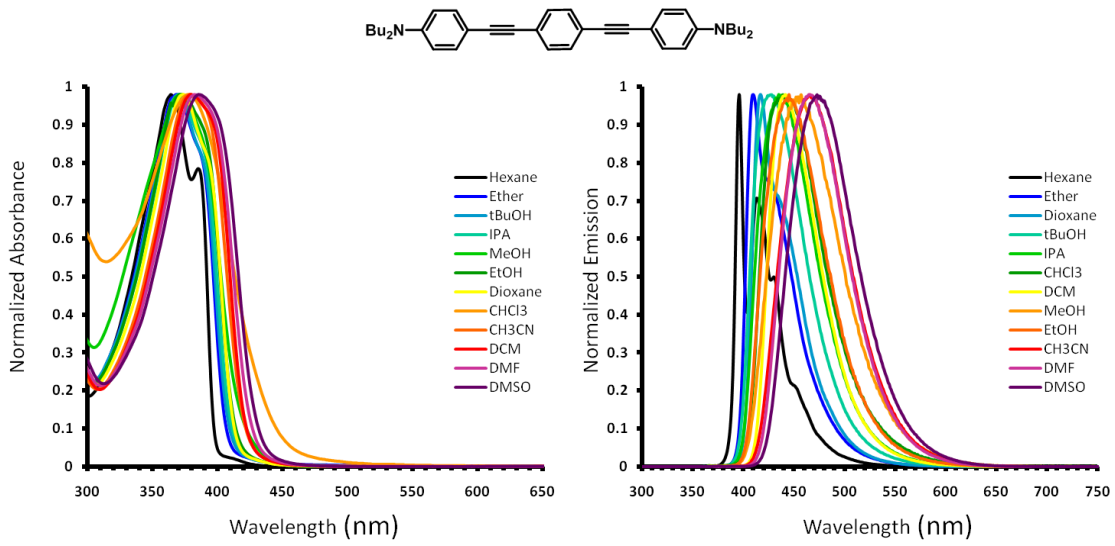

Figure 6.4. Absorption (left) and emission (right) spectra of **6.4** in a variety of solvents.

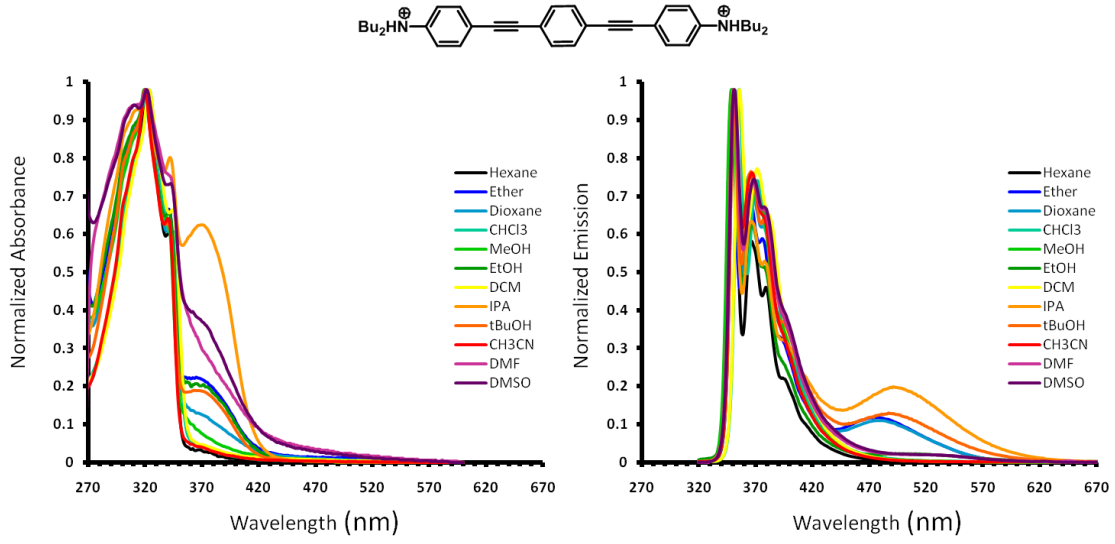

Figure 6.5. Absorption (left) and emission (right) spectra of **6.4a** in a variety of solvents.

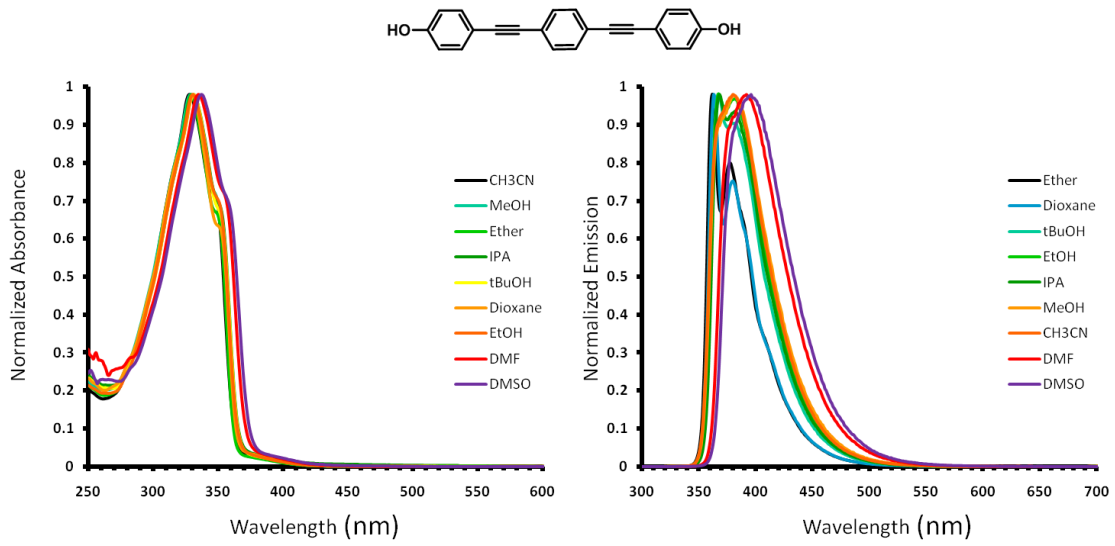

Figure 6.6. Absorption (left) and emission (right) spectra of **6.5** in a variety of solvents.

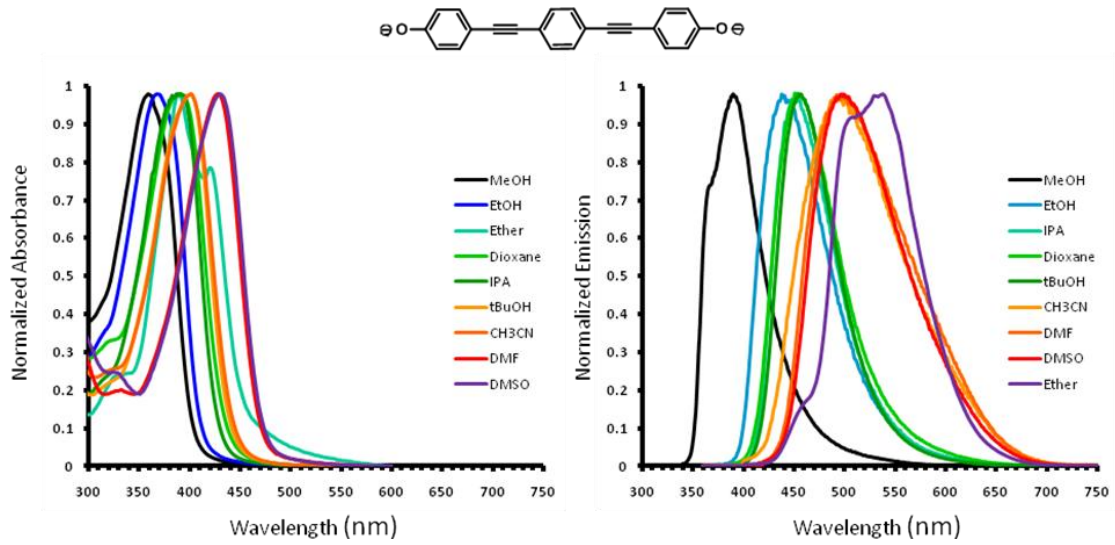

Figure 6.7. Absorption (left) and emission (right) spectra of **6.5a** in a variety of solvents.

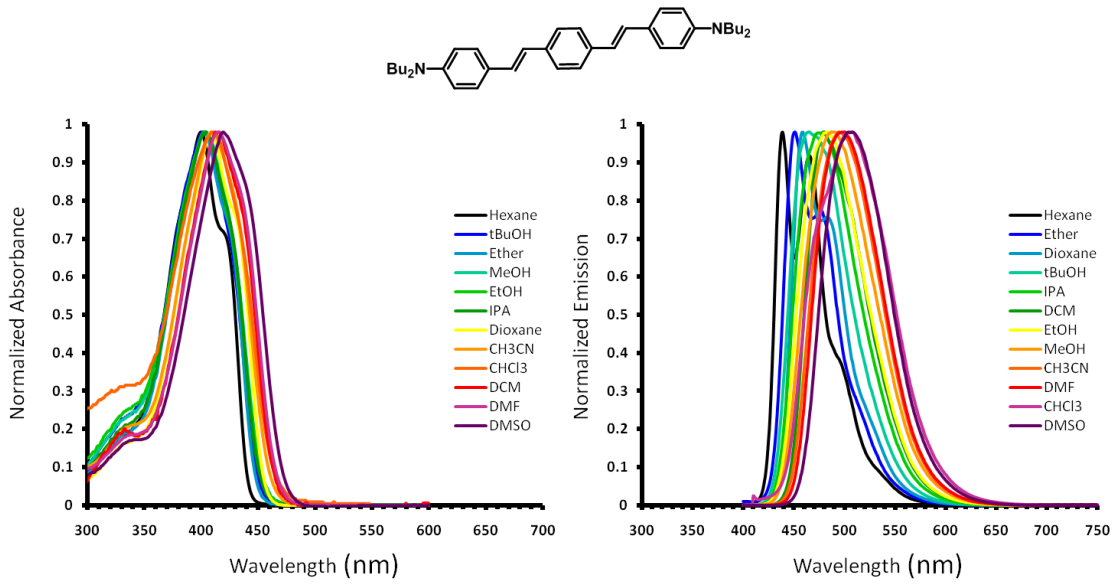

Figure 6.8. Absorption (left) and emission (right) spectra of **6.6** in a variety of solvents.

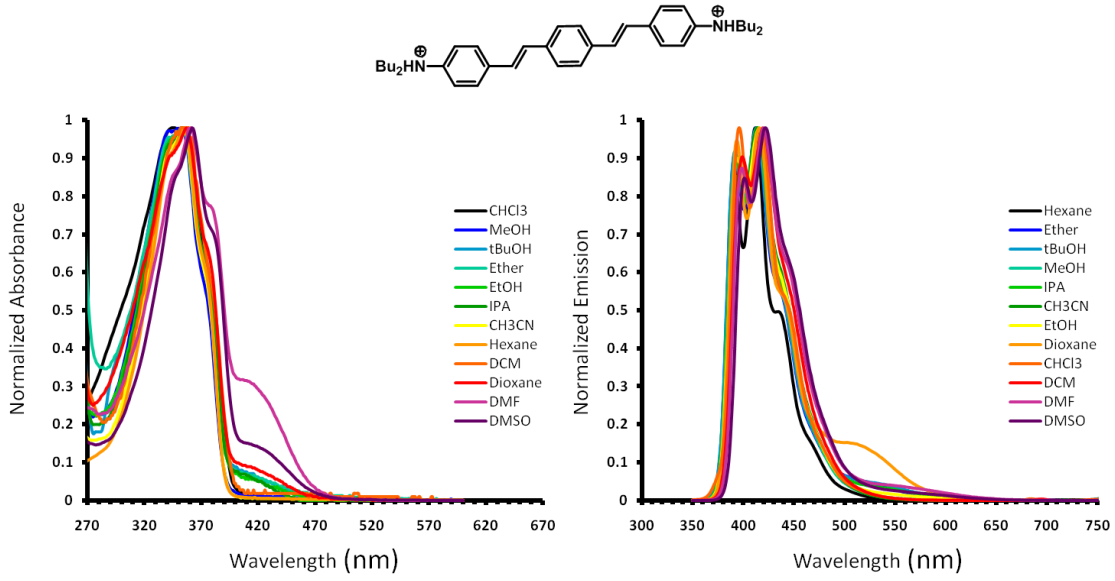

Figure 6.9. Absorption (left) and emission (right) spectra of **6.6a** in a variety of solvents.

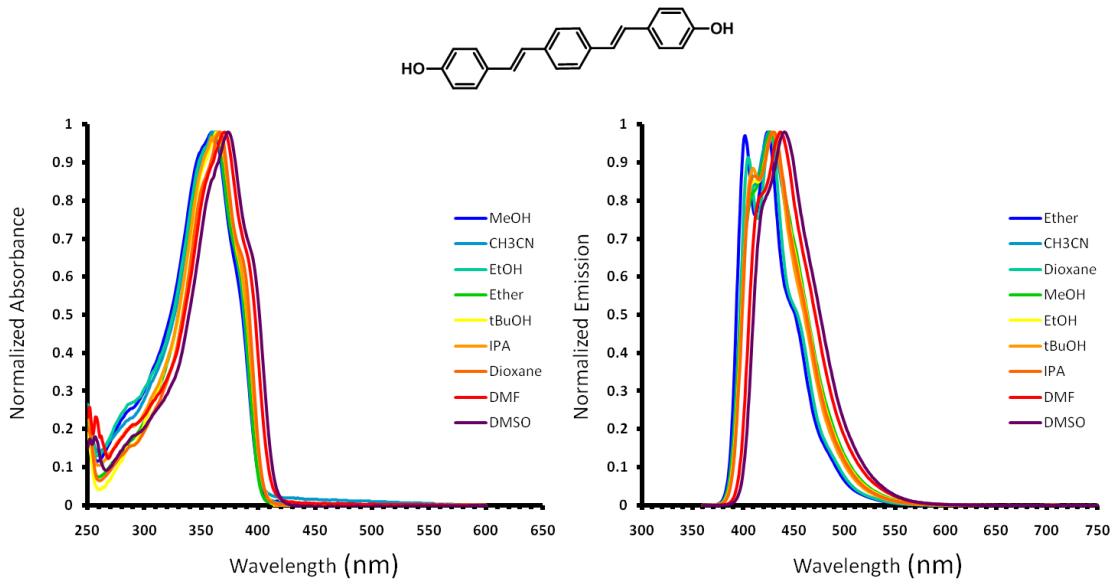

Figure 6.10. Absorption (left) and emission (right) spectra of **6.7** in a variety of solvents.

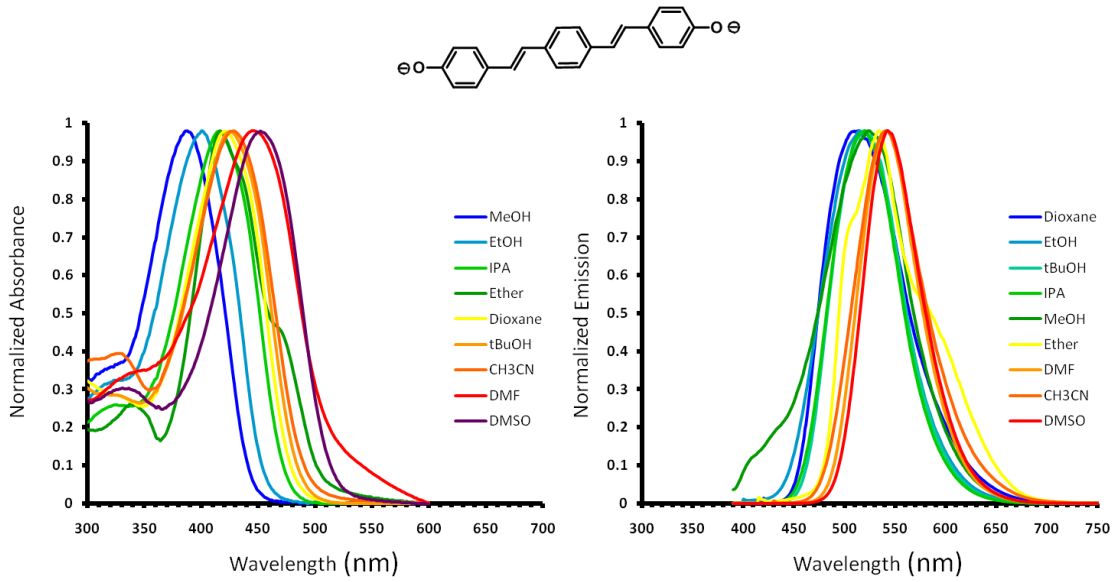

Figure 6.11. Absorption (left) and emission (right) spectra of **6.7a** in a variety of solvents.

Kamlet-Taft Analysis Data.

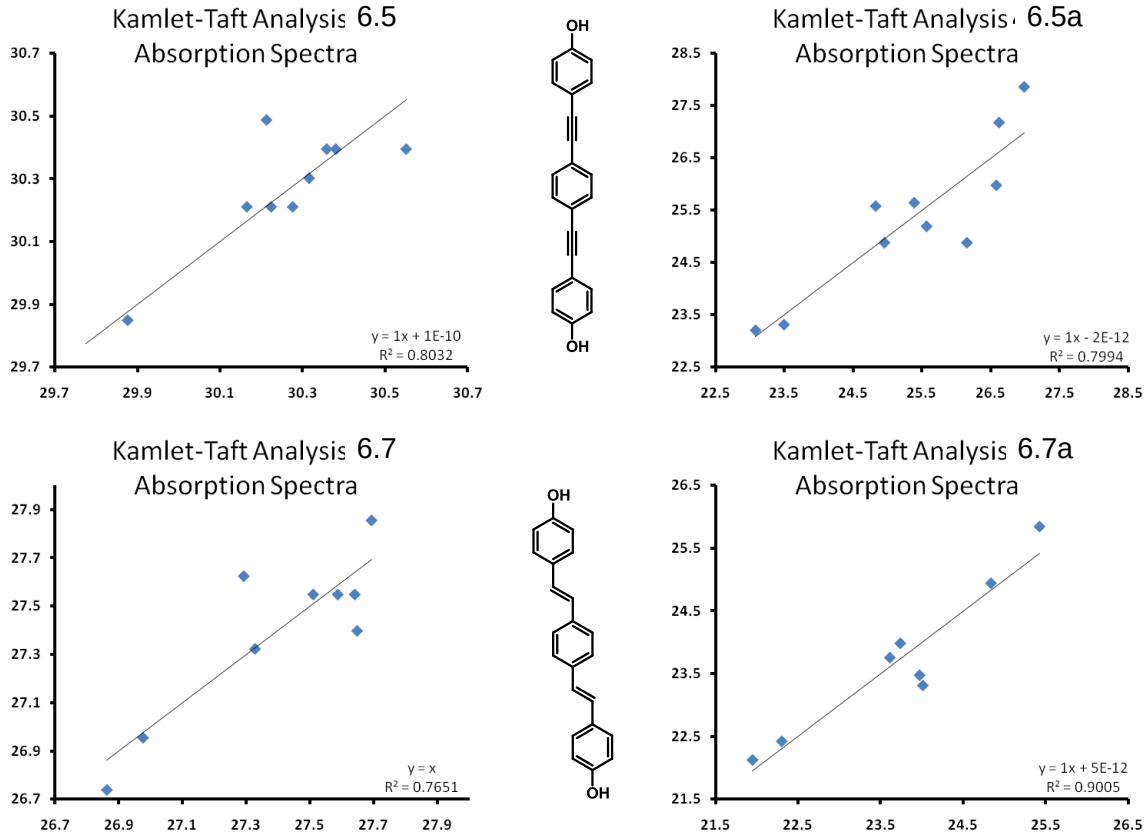

Figure 6.12. Kamlet-Taft multivariate linear regression analysis plots of **6.5** (top left), **6.5a** (top right), **6.7** (bottom left), and **6.7a** (bottom right).

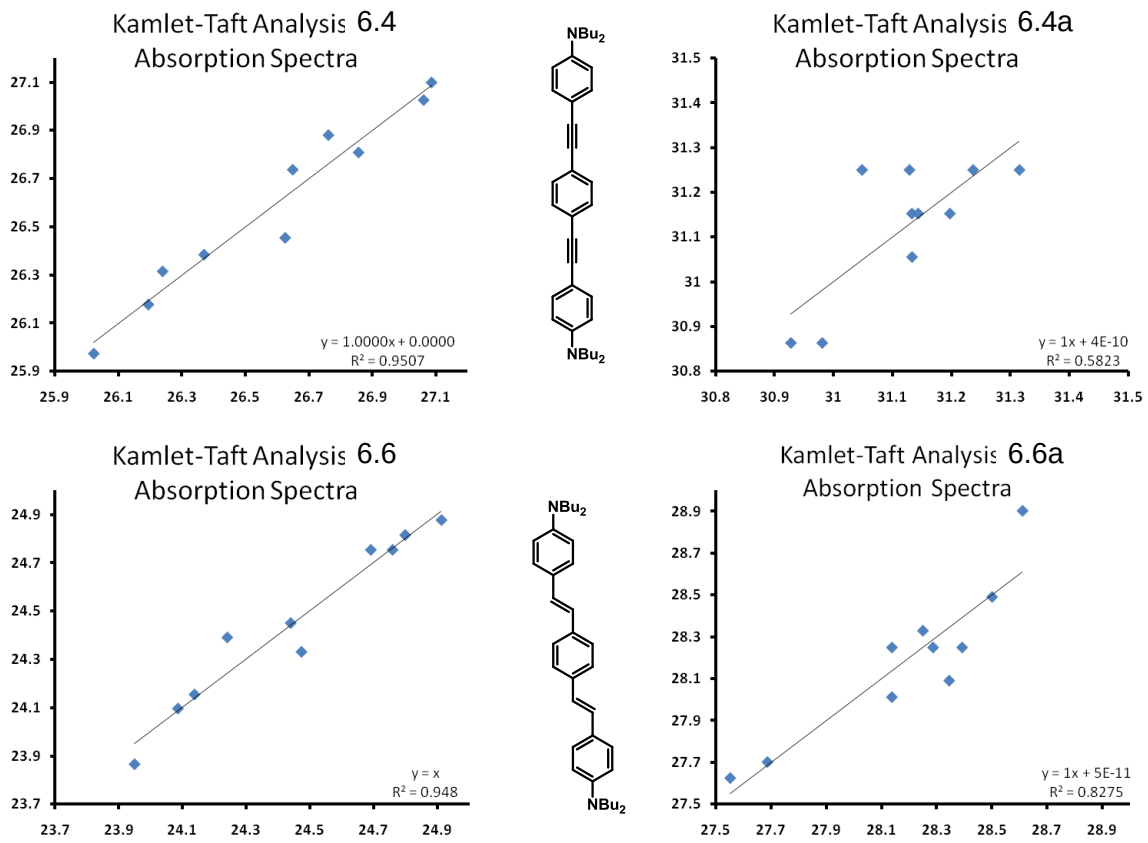

Figure 6.13. Kamlet-Taft multivariate linear regression analysis plots of **6.4** (top left), **6.4a** (top right), **6.6** (bottom left), and **6.6a** (bottom right).

6.5 References and Notes

1. Zucchero, A. J.; Wilson, J. N.; Bunz, U. H. F. *J. Am. Chem. Soc.* **2006**, *128*, 11872–11881.

2. (a) Hoffmann, R. *Angew. Chem., Int. Ed. Engl*. **1982**, 21, 711–724. (b) Evans, D. G.; Mingos, D. M. P. *J. Organomet. Chem.* **1982**, *232*, 171–191.

3. For the photophysics of hydroxystilbenes and aminostilbenes, see: (a) Crompton, E. M.; Lewis, F. D. *Phototochem. Photobiol. Sci.* **2004**, *3*, 660–668. (b) Lewis, F. D.; Crompton, E. M. *J. Am. Chem. Soc.* **2003**, *125*, 4044–4045. (c) Yang, J. S.; Liau, K. L.; Li, C. Y.; Chen, M. Y. *J. Am. Chem. Soc.* **2007**, *129*, 13183–13192. (d) Yang, J. S.; Chiou, S. Y.; Liau, K. L. *J. Am. Chem. Soc.* **2002**, *124*, 2518–2527.

4. (a) Schmitt, V.; Glang, S.; Preis, J.; Detert, H. *Sensor Lett.* **2008**, *6*, 524–530. (b) Detert, H.; Sugiono, E.; Kruse, G. *J. Phys. Org. Chem.* **2002**, *15*, 638–641. (c) Detert, H.; Sugiono, E. *J. Lumin.* **2005**, *112*, 372–376.

5. (a) Solntsev, K. M.; McGrier, P. L.; Fahrni, C. J.; Tolbert, L. M.;

Bunz, U. H. F. *Org. Lett.* **2008**, *10*, 2429–2432. (b) McGrier, P. L.; Solntsev, K. M.; Miao, S.; Tolbert, L. M.; Miranda, O. R.; Rotello, V. M.; Bunz, U. H. F. *Chem.Eur. J* **2008**, *14*, 4503–4510.

6. (a) Zucchero, A. J.; Tolosa, J.; Tolbert, L. M.; Bunz, U. H. F. *Chem. Eur. J* **2009**, *15*, 13075-13081. (b) Albota, M.; Beljonne, D.; Bredas, J.-L.; Ehrlich, J. E.; Fu, J.-Y.; Heikal, A. A.; Hess, S. E.; Kogej, T.; Levin, M. D.; Marder, S. R.; McCord-Maughon, D.; Perry, J. W.; Rockel, H.; Rumi, M.; Subramaniam, G.; Webb, W. W.; Wu, X.-L.; Xu, C. *Science* **1998**, *281*, 1653–1656. (c) Cumpston, B. H.; Ananthavel, S. P.; Barlow, S.; Dyer, D. L.; Ehrlich, J. E.; Erskine, L. L.; Heikal, A. A.; Kuebler, S. M.; Lee, I.-Y. S.; McCord-Maughon, D.; Qin, J.; Rockel, H.; Rumi, M.;Wu, X.-L.; Marder, S. R.; Perry, J.W. *Nature* **1999**, *398*, 51–54. (d) Rumi, M.; Ehrlich, J. E.; Heikal, A. A.; Perry, J. W.; Barlow, S.; Hu, Z.; McCord-Maughon, D.; Parker, T. C.; Roeckel, H.; Thayumanavan, S.; Marder, S. R.; Beljonne, D.; Bredas, J.-L. *J. Am. Chem. Soc.* **2000**, *122*, 9500– 9510.

7. Yam, C. M.; Kakkar, A. K. *Langmuir* **1999**, *15*, 3807–3815.

8. (a) Kivala, M.; Boudon, C.; Gisselbrecht, J.-P.; Seiler, P.; Gross, M.; Diederich, F. *Chem. Commun.* **2007**, 4731–4733. (b) Nguyen, P.; Yuan, Z.; Agocs, L.; Lesley, G.; Marder, T. B. *Inorg. Chim. Acta* **1994**, *220*, 289–296.

9. (a) Michinobu, T.; Boudon, C.; Gisselbrecht, J.-P.; Seiler, P.; Frank, B.; Moonen, N. N. P.; Gross, M.; Diederich, F. *Chem .Eur. J* **2006**, *12*, 1889–1905. (b) Liu, B.; Liu, J.; Wang, H.-Q.; Zhao, Y.-D.; Huang, Z.-L. *J. Mol. Struct.* **2007**, *833*, 82–87.

10. (a) Negishi, E.; Anastasia, L. *Chem. Rev.* **2003**, *103*, 1979–2017. (b) Sonogashira, K. *J. Organomet. Chem.* **2002**, *653*, 46–49. (c) Bunz, U. H. F. *Chem. Rev.* **2000**, 100, 1605–1645. (d) Bunz, U. H. F. *Macromol. Rapid Commun.* **2009**, *30*, 772–805.

11. (a) Von Lippert, E. Z. *Electrochem.* **1957**, *61*, 962–975. (b) Mataga, N.; Kaifu, Y.; Koizumi, M. *Bull. Chem. Soc. Jpn.* **1956**, *29*, 465–470.

12. (a) Kamlet, M. J.; Abboud, J.-L.; Abraham, M. H.; Taft, R. W. *J. Org. Chem.* **1983**, 48, 2877–2887. (b) Dong, J.; Solntsev, K. M.; Tolbert, L. M. *J. Am. Chem. Soc.* **2006**, 128, 12038–12039. (c) Wu, Y.; Lawson, P. V.; Henary, M. M.; Schmidt, K.; Brédas, J.-L.; Fahrni, C. J. *J. Phys. Chem. A* **2007**, *111*, 4584–4595.

13. For comparison, the pKa values of methanol and ethanol are 15.5 and 16.0, respectively. Additional pKa values for the solvents used in this study are listed in the Supporting Information.

14. (a) Hammett, L. P. *Chem. Rev.* **1935**, 17, 125–136. (b) Hansch, C.; Leo, A.; Taft, R. W. *Chem. Rev.* **1991**, *91*, 165–195.

15. Interpolated from the σ_p values for-NH_3^+ (0.60) and NMe_3^+ (0.82); the other values are directly from Table 1 in ref 14b.

Chapter 7

Hydroxy-Dialkylamino Cruciforms: Dual Response to Protons, Base, Selected Metal Ions and Amines

7.1 Intoduction

In this chapter, we investigate the photophysical, amine and metalloresponsive properties of hydroxy-dibutylaniline cruciforms (XFs) **7.6** and **7.7**. Metalloresponsive fluorophores are of interest as it may be possible for them to detect metal cations in compartmentalized biological systems such as eukaryotic cells.[1] Metal cations such as Zn^{2+}, Mg^{2+}, Ca^{2+}, and Mn^{2+} exhibit important biological functions in cells.[2] The detection and quantification of amines is critical in food safety as the prescence of amines can indicate spoilage. Because amines are commonly used in the preparation of pharmaceuticals, surfactants, and fertilizers, they often become pollutants in landfills and the aqueous environment. The detection amines have been achieved by antibodies,[3] molecularly imprinted polymers,[4] enzymes,[5] single-molecule and array sensors,[6] and chromatographic methods.[7] However, most of these methods are costly and a more efficient approach for detection is desired.

Up to now, XFs have been reported containing basic nitrogens, pyridines, or phenolates as functional appendages attached to a perpendicular distyryl or an arylethynyl branch both connected to a central benzene core. If pyridines or dialkylanilines are incorporated, either a red or blue color change in emission is observed upon coordination of metal cations. If both functional groups are present, a two-stage metalloresponsive fluorophore results as a blue-shift is observed upon addition of Zn^{2+} followed by a red-shift upon addition of excess Zn^{2+}.[8] If hydroxyl groups are

incorporated into the π-system, spectroscopic changes are observed upon deprotonation; particularly upon exposure to amine bases.[9]

The following work focuses on incorporating dialkylaniline and hydroxyl substituents onto one XF in an effort to create a two-stage probe that is responsive not only to protons and base, but also to metal cations and amines. The changes in absorption and emission elicited by these analytes are induced by the destabilization and stabilization of the HOMO of the XFs, respectively. In principal, the approach of using one fluorophore to detect such analytes would be more feasible than using multiple fluorophores. Surprisingly, there is no published literature on chromophores or fluorophores that exhibit this two-stage responsive capability. The specifically engineered FMOs of hydroxy-dibutylanline XFs allow protons and metal cations to interact with the free electron pairs of the dibutylanilines, and the phenols to exhibit hydrogen bonding or proton transfer to amines, all resulting in attractive spectroscopic changes.

7.2 Results and Discussion

7.2.1 Synthesis of Hydroxy-Dialkylamino XFs

The synthesis of hydroxy-dibutylaniline XFs **7.6** and **7.7** begins with a Horner reaction of **7.2a** or **7.2b** to produce the distyrylbenzene derivatives **7.3a** and **7.3b** in 77 and 71 % yield, respectively after recrystallization (Scheme 7.1). Subsequently, a Sonogashira coupling with either **7.4a** or **7.4b** gave rise to the formation of **7.5a** and **b** at 66% yield. At a temperature of -78 °C with trifluoroacetic acid (TFA) **7.5a** and **7.5b** were deprotected to afford XFs **7.6** and **7.7** at 84 and 82 % yield, respectively.

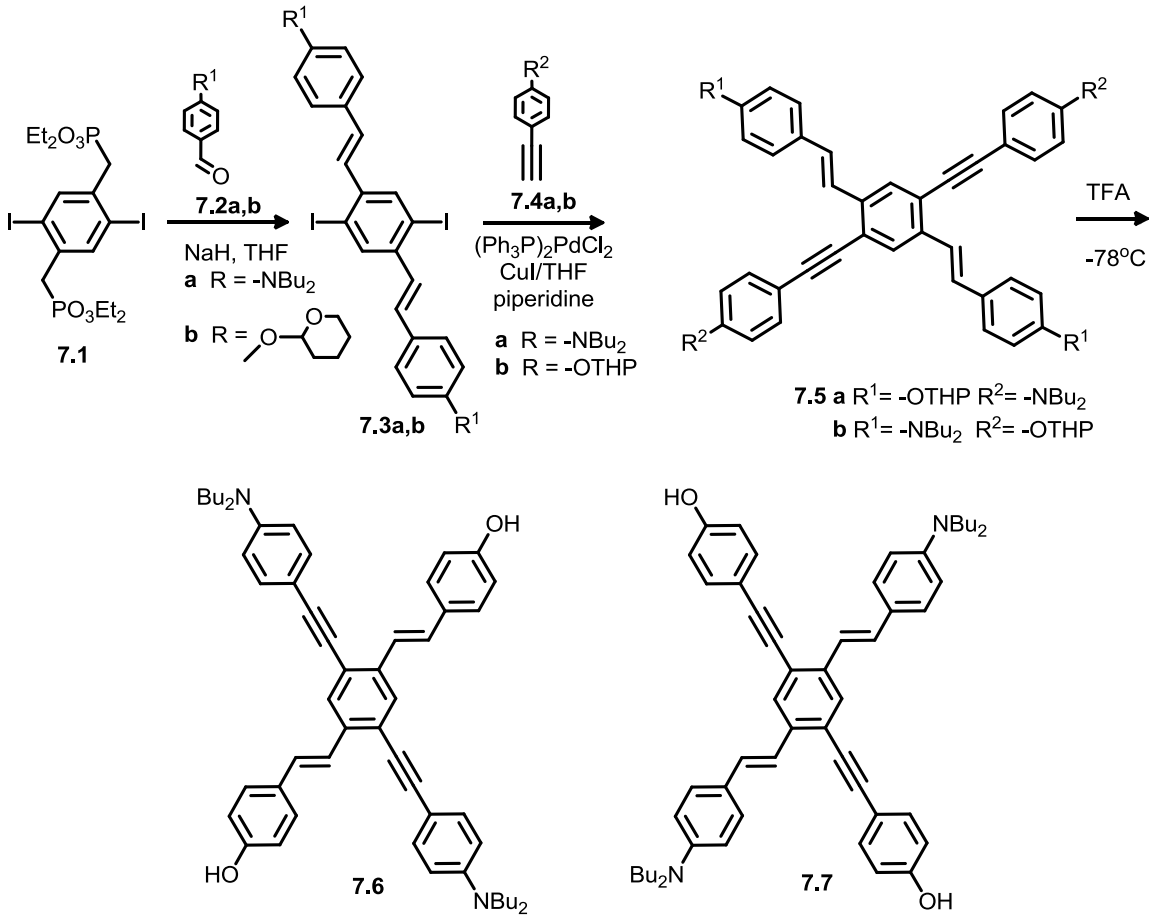

Scheme 7.1. Synthesis of hydroxy-dibutylamino XFs **7.6** and **7.7**.

7.2.2 Spectroscopic Properties of Hydroxy-Dialkylamino XFs

Figures 7.1 and 7.2 display the absorption and emission spectra of both XFs in different solvents. The absorbance spectra of **7.6** display broad absorption maximums ranging from 359-372 nm. XF **7.7** exhibits a significant charge transfer band in all solvents around 423-445 nm and a single more intense absorption at ~ 338 nm. The absorbance spectra for both compounds depend weakly on solvent polarity indicating a small ground-state dipole moment. However, the emission spectra of both XFs display stronger bathochromic shifts in polar solvents due to the increase in the dipole moment upon excitation. The emission spectra of the XFs are broad and featureless and range

from 461 to 540 nm. The only exception is **7.7** in the presence of ether and toluene, which display vibronic progressions at 992 and 1177 cm^{-1}, respectively. We assume that the large bathochromic shifts observed in the more polar solvents is attributed to hydrogen bonding with the hydroxyl groups of the chromophores, especially with the more basic solvents DMF and DMSO. The fluorescence quantum yield in methanol was ~ 14% for both compounds. XF **7.6** exhibited the longest emissive lifetime at 5.56 ns (Table 7.3).

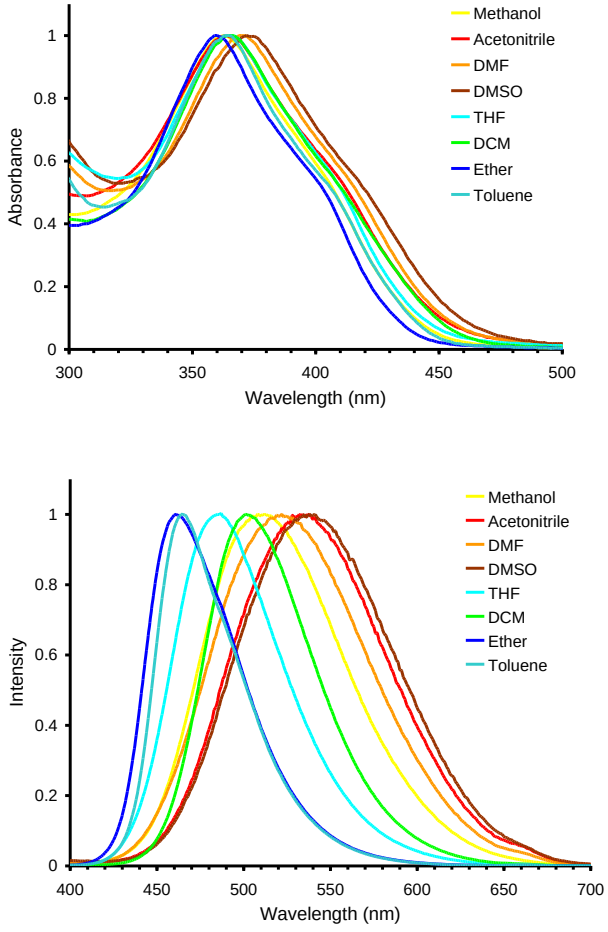

Figure 7.1. Absorption (top) and emission (bottom) spectra of **7.6** in different solvents.

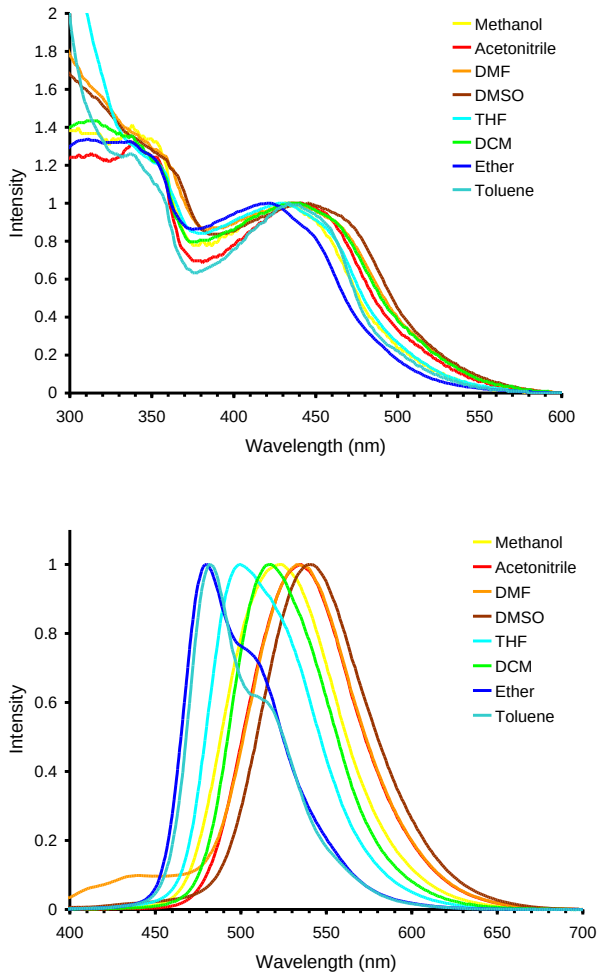

Figure 7.2. Absorption (top) and emission (bottom) spectra of **7.7** in different solvents.

Table 7.1. Absorption and emission maximums for **7.6** in various solvents.

Solvent	**λ_{max} abs (nm)**	**λ_{max} em (nm)**	**Stokes Shift (cm^{-1})**	**Vibronic Progression (cm^{-1})**
Methanol	363	508	7863	-
Acetonitrile	364	537	8851	-
DMF	369	521	7906	-
DMSO	372	538	8294	-
THF	364	485	6853	-
DCM	364	501	7512	-
Ether	359	461	6163	-
Toluene	363	464	5996	-

Table 7.2. Absorption and emission maximums for **7.7** in various solvents.

Solvent	λ_{max} abs (nm)	λ_{max} em (nm)	Stokes Shift (cm^{-1})	Vibronic Progression (cm^{-1})
Methanol	339, 431	523	10378, 4081	-
Acetonitrile	340, 440	535	10720, 4035	-
DMF	339, 434	533	10736, 4279	-
DMSO	340, 445	540	10893, 3953	-
THF	337, 430	499	9633, 3215	-
DCM	339, 433	517	10156, 3752	-
Ether	337, 423	480, 504	8840, 2807	992
Toluene	338, 433	482, 511	8838, 2347	1177

Table 7.3. Photophysical data of **7.6** and **7.7** in methanol

Compound	7.6	7.7
Abs (nm)	363	339, 431
Em (nm)	508	523
Φ_{fl} (quantum yields)	0.14	0.13
τ (ns)	5.56	1.45

7.2.3 Acid-Base and Titration Studies of Hydroxy-Dialkylamino XFs

To see if XFs **7.6** and **7.7** display changes in absorption and emission upon the addition of acid and base, we performed qualitative studies by adding an excess of TFA and tetrabutylammonium hydroxide (TBAOH) to both compounds in different solvents. Figures 7.3 and 7.4 show real-color photographs of both XFs upon the addition of TFA and TBAOH. In the case of **7.6,** a two-stage response in absorption and emission is observed in methanol, acetonitrile, and dichloromethane (Figure 7.5). In methanol, the absorbance maximum experiences a small red-shift from 363 nm to 377 nm upon the addition on TBAOH. The addition of excess TFA causes a blue-shift to 330 nm accompanied by a shoulder at ~ 368 nm. In the emission spectra, we observe a vibrant green emission at 507 nm followed by a blue-shift to 481 nm then a red-shift to 545 nm

upon the addition of TFA and TBAOH, respectively. We attribute these shifts to the stablization of the HOMO upon protonation of the dialkylanilines attached to the arylethynyl branch, and destablization of the HOMO upon deprotonation of the phenols attached to the distyryl branch (Scheme 7.2). Similar spectroscopic changes are observed in the absorbance spectra of acetonitrile and dichloromethane, but to a much greater extent in the emission spectra as the addition of TBAOH leads to a red emission (~ 600 nm) in acetonitrile, and an orange emission in dichloromethane (~ 585 nm). XF **7.6** also displays red emissions in DMSO and DMF upon addition of TBAOH, but no change in emission color is observed upon addition of excess TFA. For XF **7.7**, we observe quenching upon the addition of excess TBAOH in all solvents. We have shown that simple hydroxy-substituted bisarylethynylbenzenes typically display weak emissions in organic solvents upon deprotonation.[10] This premise may be explained by a change in hybridization that occurs when transitioning from an alkene bridge (sp^2) to an alkyne bridge (sp), which decreases the electron donating character. In most cases, this event dramatically changes the excited-state properties of these compounds and leads to quenching upon deprotonation. However, the addition of excess TFA to **7.7** leads to blue shifts in methanol, acetonitrile, ether, and toluene. In DMSO and DMF, addition of excess TFA leads to a red shift in emission possibly due to competition with the more basic solvents leading to monoprotonation of the dialkylanilines. This situation leads to a donor-acceptor system, which typically displays red-shifted emissions. [15]

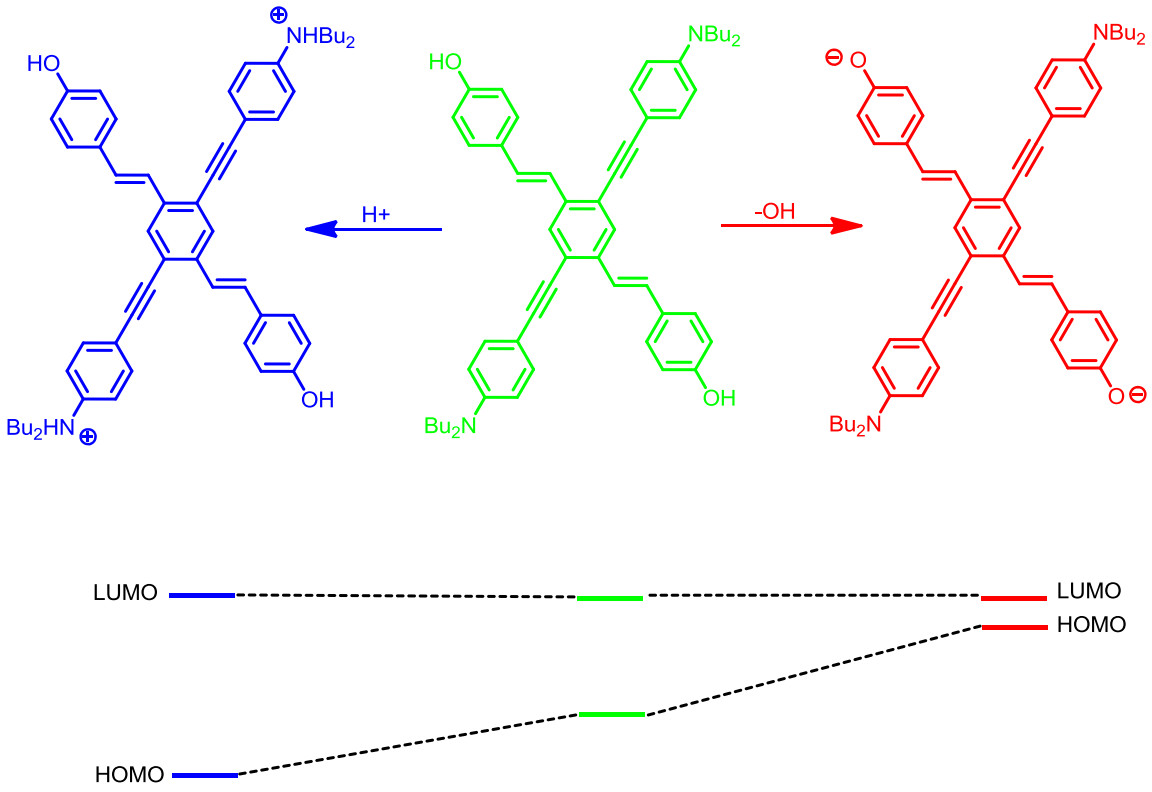

Scheme 7.2. Modulation of HOMO-LUMO gap in hydroxy-dialkylamino XFs by interaction with acid and base.

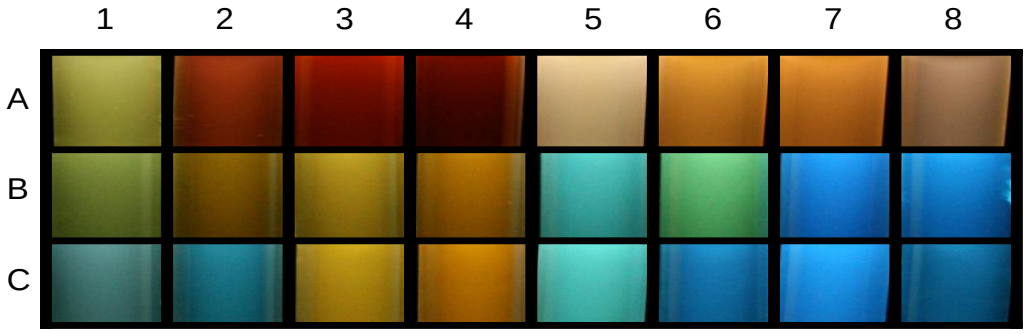

Figure 7.3. Exposure of **7.6** to acid and base in various solvents. Top to Bottom: A) tetrabutylammonium hydroxide, B) **7.6**, C) trifluoroacetic acid. Left to Right: 1.) methanol, 2.) acetonitrile, 3.) DMF, 4.) DMSO, 5.) THF, 6.) DCM, 7.) diethyl ether, and 8.) toluene. The samples were excited by using a hand-held UV-lamp at an emission wavelength of 366 nm.

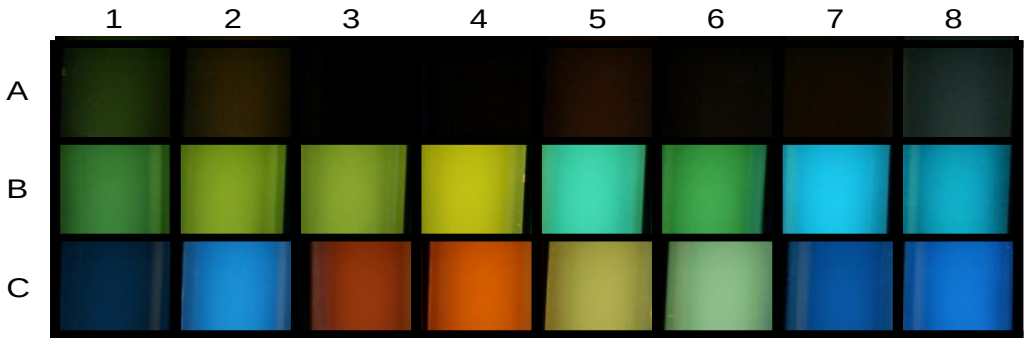

Figure 7.4. Exposure of **7.7** to acid and base in various solvents. Top to Bottom: A) tetrabutylammonium hydroxide, B) **7.7**, C) trifluoroacetic acid. Left to Right: 1.) methanol, 2.) acetonitrile, 3.) DMF, 4.) DMSO, 5.) THF, 6.) DCM, 7.) diethyl ether, and 8.) toluene. The samples were excited by using a hand-held UV-lamp at an emission wavelength of 366 nm.

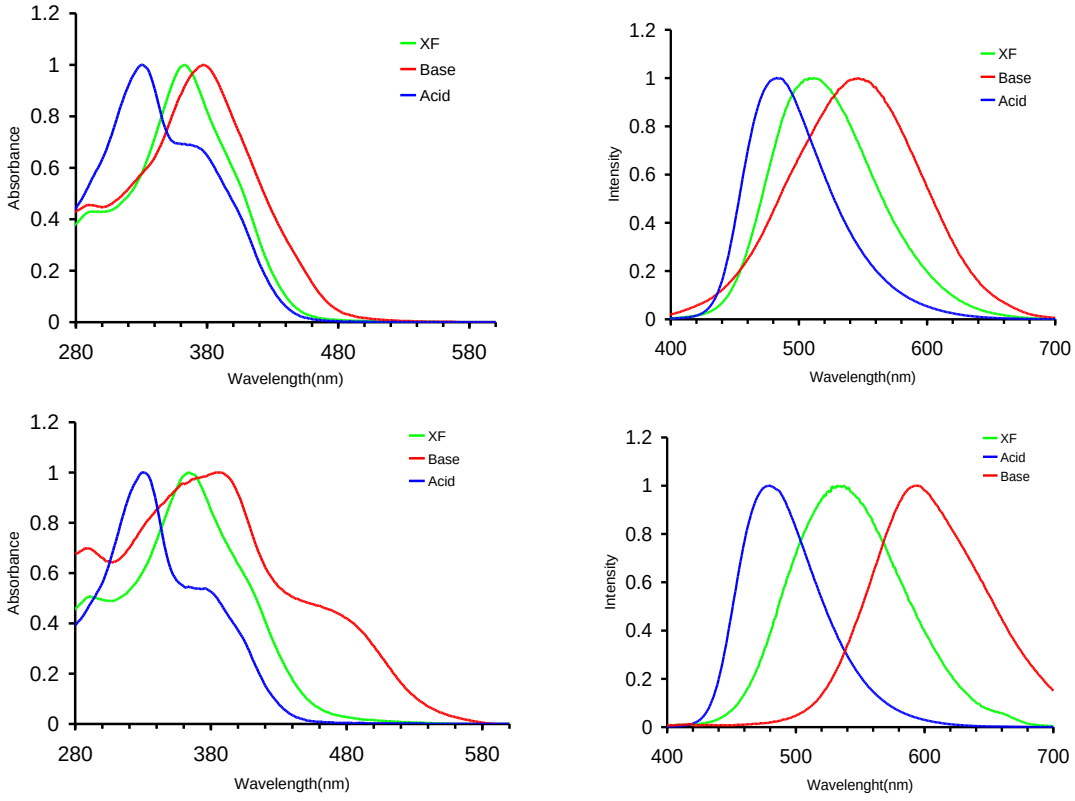

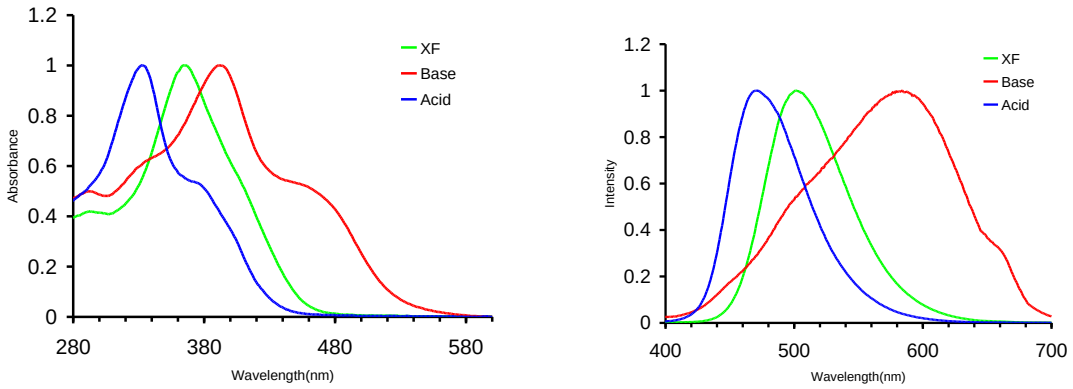

Figure 7.5. Normalized absortion (left) and emission (right) of **7.6** upon the addition of TFA and TBAOH in methanol (top), acetonitrile (middle), and dichloromethane (bottom).

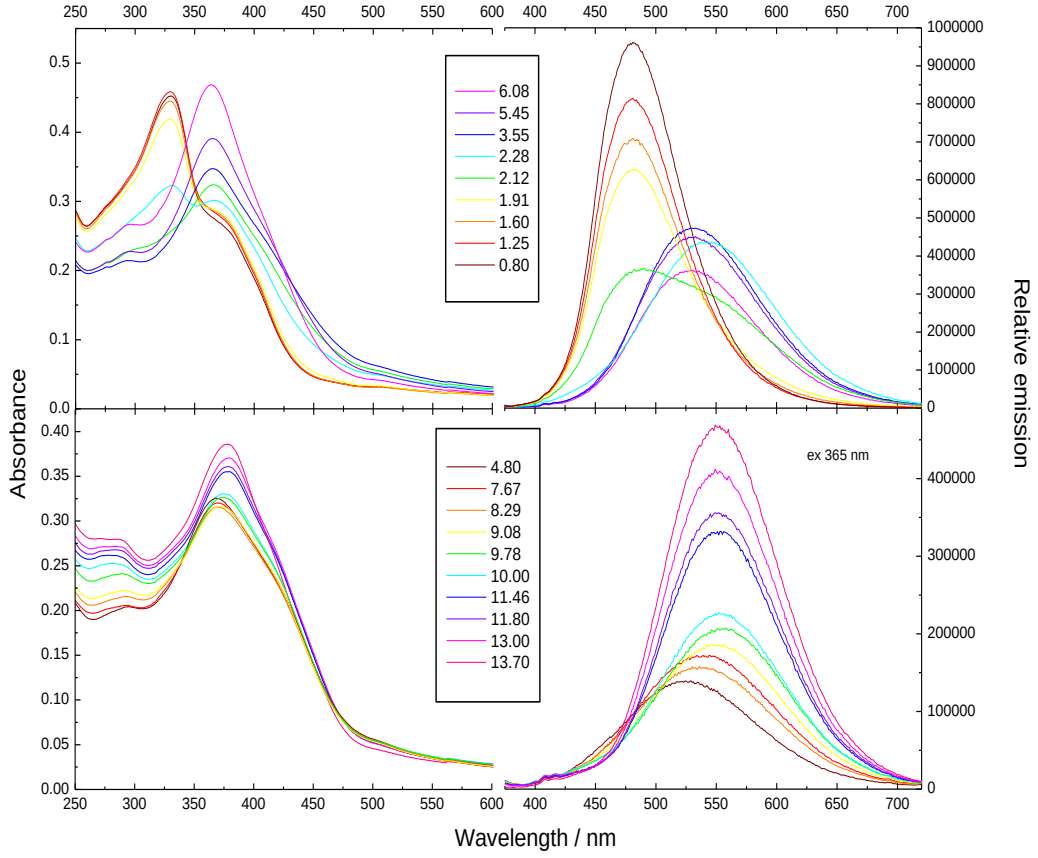

Figure 7.6. Absorption (left) and emission (right) of **7.6** in 2:1 vol. methanol water mixtures at different pH.

XFs **7.6** and **7.7** were poorly soluble in pure water at neutral pH. In order to further investigate their acid-base behavior, we elected to perform titrations of both compounds in a 2:1 volume ratio of methanol/water. Titrations of XF **7.7** proved ineffective due to poor solubility in 2:l methanol/water mixtures . Although **7.6** displayed moderate solubility, spectrophotometric titration data for the compound was attainable. However, one should proceed with caution as the data reflects not only protonation and deprotonation, but also the dissolution of its aggregates (Figure 7.6). Upon protonation with aqueous hydrochloric acid (HCl), **7.6** experiences a hypsochromic shift in absorption and emission. A new band emerges at 330 nm along with a shoulder at ~370 nm. In the emission spectrum, a new fully developed band emerges at pH 0.80 (479 nm), while the band at pH 6.08 (531 nm) disappears due to full ground state protonation of the dialkylanilines. Upon the addition of aqueous KOH, there is no significant change in the absorption spectrum of **7.6**. The small bathochromic shifts in absorption is surprising and persists upon addition of excess KOH. Similar behavior is observed in the emission spectrum with a small ~20 nm shift from 529 nm (pH 4.80) to a new low energy band at 549 nm (pH 13.7). This band is fully developed and does not change upon the addition of excess KOH. It is not clear why small bathochromic shifts are observed for **7.6** upon increasing amounts of base, which is atypical for hydroxy XFs.

7.2.4 Interaction of Hydroxy-Dialkylamino XFs with Metal Salts

The exposure of hydroxy-dibutylaniline XFs to acid leads to hypsochromic shifts in absorption and emission. With this in mind, we set out to examine the reaction of both XFs upon the addition of different metal cations. Previous investigations have shown that XFs containing pyridines, anilines, and phenothiazines[11] are capable of

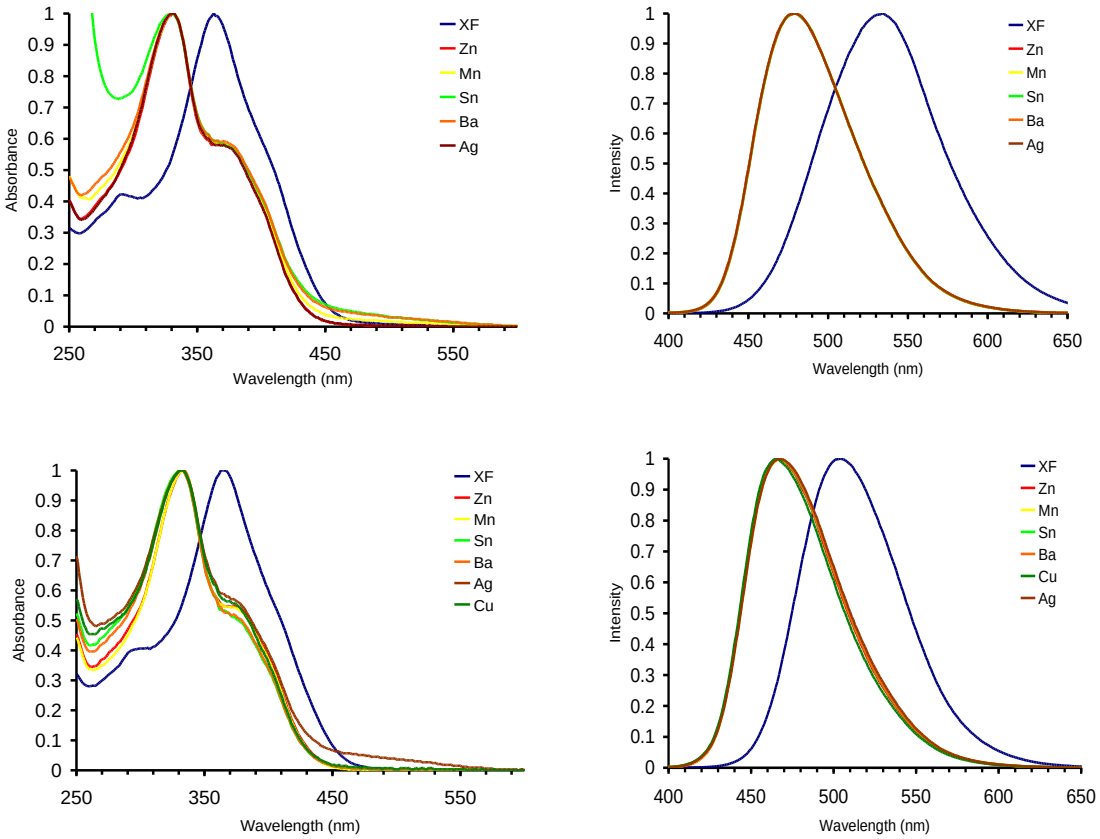

Figure 7.7. Normalized absorption (left) and emission (right) of **7.6** in acetonitrile(top) and DCM (bottom) in the presence of different metal cations.

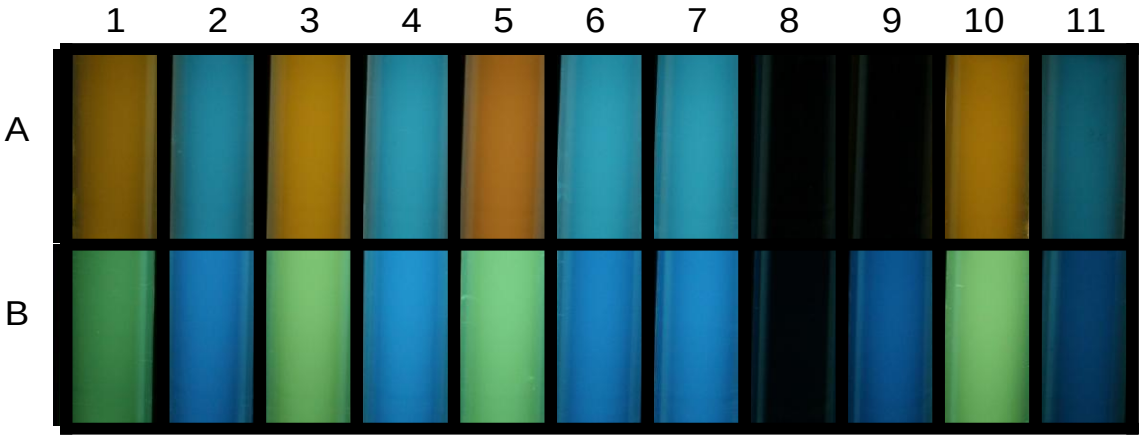

Figure 7.8. Exposure of **7.6** to different metal cations in acetonitrile and dichloromethane. Top to bottom: A) acetonitrile, and B) dichloromethane. Left to right: 1.) **7.6**, 2.) Zn^{2+} 3.) Mg^{2+},4.) Mn^{2+}, 5.) Ca^{2+}, 6.) Sn^{2+} , 7.) Ba^{2+}, 8.) Hg^{2+}, 9.) Cu^{2+}, 10.) Li^{+}, 11.) Ag^{+}.

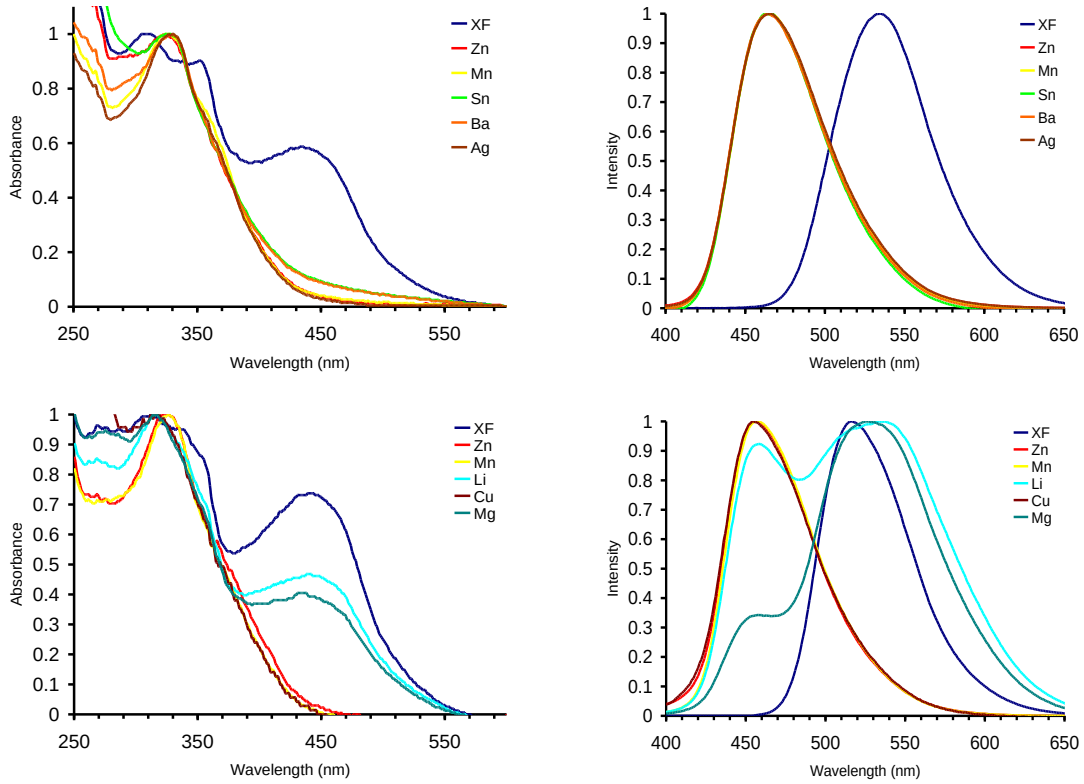

Figure 7.9. Normalized absorption (left) and emission (right) of **7.7** in acetonitrile(top) and DCM (bottom) in the presence of different metal cations.

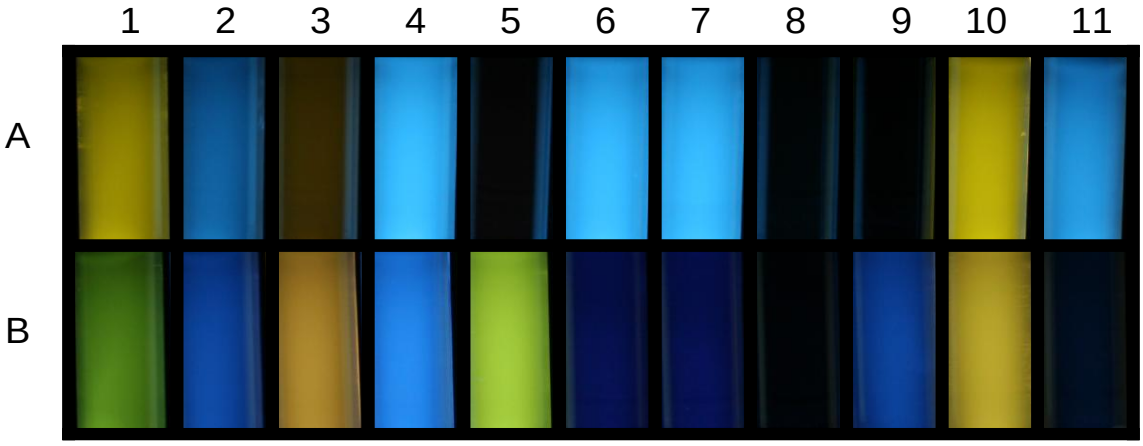

Figure 7.10 Exposure of **7.7** to different metal cations in acetonitrile and dichloromethane. Top to bottom: A) acetonitrile, and B) dichloromethane. Left to right: 1.) **7**, 2.) Zn^{2+} 3.) Mg^{2+},4.) Mn^{2+}, 5.) Ca^{2+}, 6.) Sn^{2+}, 7.) Ba^{2+}, 8.) Hg^{2+}, 9.) Cu^{2+}, 10.) Li^{+}, 11.) Ag^{+}.

coordinating metal cations with simultaneous change in emission color. Figures 7.8 and 7.10 displays photographs of both XFs before and after the addition of an excess of ten different metal triflates. The experiments were conducted in acetonitrile and dichloromethane, and the pictures were taken under black light illumination at λ= 366 nm. While the addition of Mg^{2+}, Ca^{2+}, and Li^{+} do not lead to changes in fluorescence for **7.6**, all the other metal cations exhibit changes in emission. For XF **7.7**, all cations lead to either quenching or changes in emission color with the exception of Li^{+} in acetonitrile. The fluorescence changes shown in both figures are qualitatively similar to those observed upon protonation, but do not occur for each XF with every metal.

Figure 7.8 displays the absorption and emission spectra of **7.6**. In acetonitrile, Zn^{2+}, Mn^{2+}, Sn^{2+}, Ba^{2+}, and Ag^{+} all display a blue-shift in emission. The addition of Hg^{2+}, and Cu^{2+} fully quench the emission of **7.6**. In the case of Hg^{2+}, quenching of fluorescence is possibly due to the heavy atom effect. Cu^{2+} quenches possibly due to excited-state decomplexation in acetonitrile. Similar spectroscopic properties are observed in dichloromethane with the exception of Cu^{2+}, which exhibits a blue-shift in emission. In the case of **7.7**, the fluorescence changes are slightly different from its inverse congener **7.6** (Figures 7.9 and 7.10). In acetonitrile, Zn^{2+}, Mn^{2+}, Sn^{2+}, and Ba^{2+} exhibit a blue-shift in emission, while Mg^{2+}, Ca^{2+}, Hg^{2+} and Cu^{2+} fully quench fluorescence. In dichloromethane, Zn^{2+}, Mn^{2+}, and Cu^{2+} are the only cations that display blue-shifts in emission. Mg^{2+} and Li^{+} display orange and yellow emissions, respectively. This is possibly due to a dual emission that occurs between the complexed and uncomplexed forms of cations coordinated to the lone pairs of the dibutylanilines.

7.2.5 Amine Sensing with Hydroxy-Dialkylamino XFs

After examining the photophysics of hydroxy-dibutylaniline XFs upon the addition of metal cations, we set out to explore the fluorescence change of XF **7.6** upon exposure to amine bases. Since the fluorescence of XF **7.7** quenches in the prescence of base, we decided to investigate the photophysics of **7.6**, which undergoes vibrant emission color changes upon deprotonation. We prepared 10 micromolar solutions of **7.6** in eight different solvents. These solutions were then distributed into 11 vials each to obtain a matrix of 10 amines plus the reference in eight solvents to give 88 samples. The amine (0.1 mL per sample, which corresponds to a 0.7-7.2 mM concentration range) was then added and a picture of the samples was taken. Figure 7.11 shows real-color photographs of the samples taken in the dark upon irradiation with a hand-held UV-lamp at λ= 366 nm.

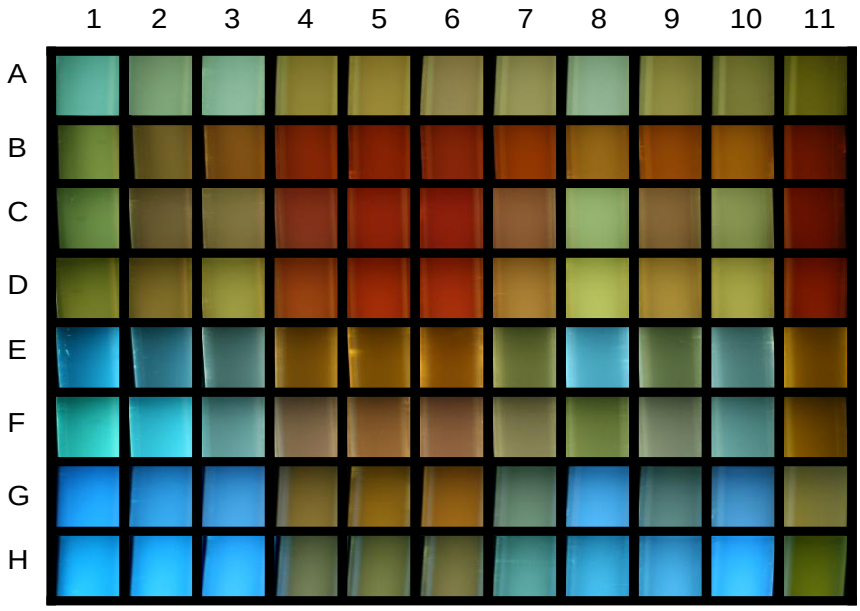

Figure 7.11. Exposure of **7.6** to different amines in various solvents. Top to bottom**:** A) methanol, B) acetonitrile, C) DMF, D) DMSO, E) THF, F) DCM, G) ether, and H) toluene respectively. Left to right**:** 1.) **7.6**, 2.) morpholine (8.33), 3.) piperazine (9.83), 4.) putrescine (9.90), 5.) 1,3-diaminopropane (10.47), 6.) ethylenediamine (10.70) , 7.) piperidine (10.80), 8.) triethylamine

(10.80), 9.) diethylamine (11.00), 10.) diisopropylamine (11.10), 11.) 1,8-diazabicyclo[5.4.0]undec-7-ene (DBU~12). The numbers in parentheses are the pKa values of the corresponding ammonium ions.

XF **7.6** displayed spectacular changes in emission color upon addition of amines ranging from blue to red traversing yellow and green, covering the full visible spectral range. Previous studies have shown that the reason for these changes in fluorescence is due to the ground- and excited-state acid-base interactions between the hydroxy XFs and amines. In the ground state, hydroxy XFs form hydrogen-bonded complexes with amines, which upon excitation are disrupted to promote excited state proton transfer (ESPT) to the more basic amines (Figure 7.12).[9] This event leads to a fully deprotonated (ion pair) state, which displays vibrant emission colors that can be tuned by choice of the solvent. Hydroxyaromatic molecules typically display enhanced photoacidity in the excited state.[16] However, if the amine under consideration is not very basic, such is the case with morpholine and piperazine, then there is no change in fluorescence,. Putrescine, 1,3-diaminopropane, ethylenediamine, and DBU give the most spectacular changes in fluorescence in all solvents.

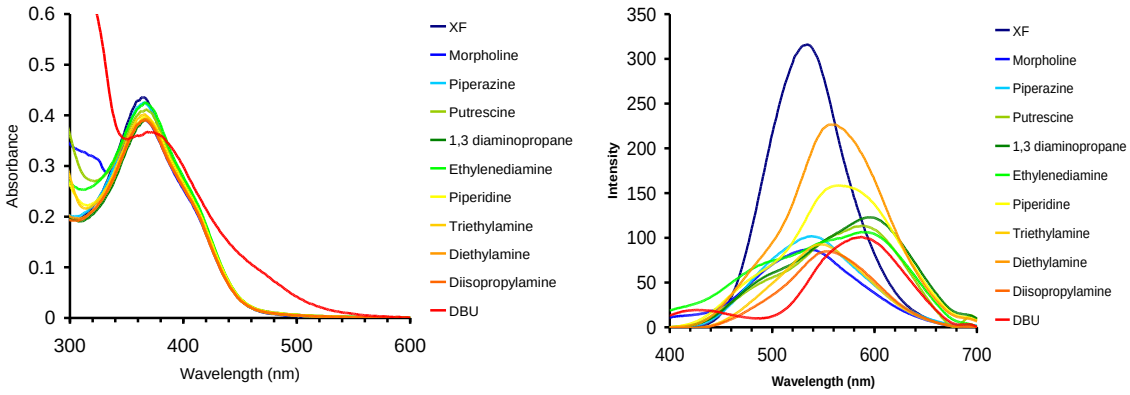

Figure 7.12. Absorption and emission of XF **7.6** upon the addition of different amines in acetonitrile.

Although the spectral data and photographs give a good indication to discern the amines, they do not adequately explain the spectral shifts that are observed for each amine. The data shows no correlation between the magnitude in shift and pK_a values of the amines. Due to this, we decided to convert the color from the amine panel into RGB values and substract the RGB values from the reference using the program Contrast Analyzer.[12] This data was then subjected to an LDA analysis using the program SYSTAT.[13] Using 20 different data points for each amine, SYSTAT is able to reduce the data into a 2D LDA plot containing only two factors. In doing so, all 10 amines are cleanly separated based on the analysis of their RGB values (Figure 7.13). The plot shows the di-amines (green) grouped together in the top left corner, while the secondary amines such as diethylamine and diisopropylamine (yellow-orange) are grouped together on the bottom right corner with the exception of piperidine.

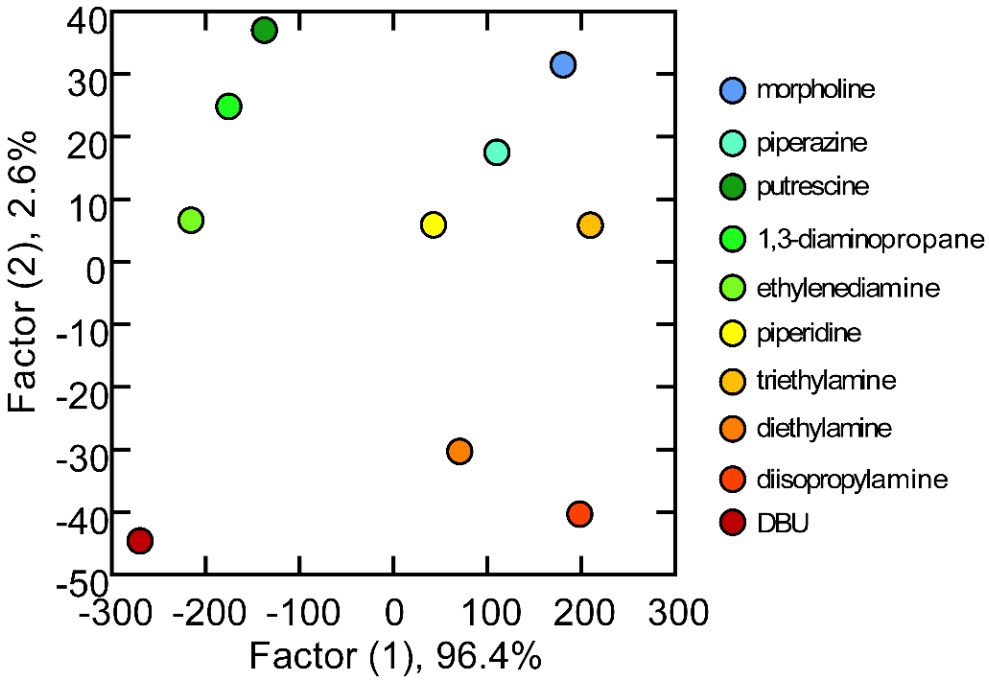

Figure 7.13. LDA anlaysis of the differential RGB values of **7.6** obtained from Figure 7.11.

7.3 Conclusions

In conclusion, we have synthesized two hydroxy-dibutylaniline XFs **7.6** and **7.7.** XF **7.6** displays red- and blue-shifted absorption and emission upon protonation and deprotonation, while XF **7.7** displays similar properties with the exception of fluorescence quenching in the presence of base. Both compounds exhibit changes in emission upon the addition of various metal cations. XF **7.6** was investigated for its properties as a potential amine sensor, and demonstrated the ability to discern 10 amines by the specific fluorescence response based on ESPT in eight different solvents. These experiments imply that a fluorophore constructed with strategically positioned phenolic and dialkylaniline functional groups can posses the ability to probe not only metal cations, but also amines. In doing so, one fluorophore can be designed to constitute a small sensor array for probing amines in different chemical environments, or distinguishing between which metal cations are present in solution. Such design principles could also be used to construct solid state materials that change emission color upon exposure to amines and acid in air or water. Such investigations are underway and will be reported in the future.

7.4 Experimental

Materials and Methods: All chemicals were purchased from Aldrich Chemical, Acros, TCI America, or Fisher Scientific and used without purification unless otherwise specified. Column chromatography was performed using Standard Grade silica gel 60 Å, 32-63 μm (230 x 450 mesh) from Sorbent Technologies and the indicated eluent. Elution of cruciforms was readily monitored using a handheld UV lamp (365 nm). Melting points

were obtained using a Mel-Temp apparatus fitted with a Fluke 51K/J digital thermometer. All IR spectra were obtained using a Simadzu FTIR-8400s spectrometer. Unless otherwise specified, NMR spectra were recorded at 298 K on a Bruker (500 MHz). Chemical shifts are reported in parts per million (ppm), using residual solvents (chloroform-*d*) or (DCM-*d2*) as an internal standard. Data are reported as follows: chemical shift, multiplicity (s = singlet, d = doublet, t = triplet, q = quartet, m = multiplet), coupling constant, and integration. Mass spectral analyses were provided by the Georgia Institute of Technology Mass Spectrometry Facility.

All absorption spectra were collected using a Shimadzu UV-2401PC spectrophotometer. All emission spectra were acquired using a Shimadzu RF-5301PC spectrofluorophotometer. Lifetime data were collected using a Lifespec-ps (Edinburgh Instruments), pulsed diode laser (PicoQuant, 372 nm excitation), and PMT detector (Hamamatsu). Data were fit to single exponential decay so as to optimize chi-squared values. Quantum yields for all cruciforms were measured using standard procedures. [14] In all cases, quinine sulfate was used as a standard.

Compounds 7.5a-b:

Compounds **7.5a** and **7.5b** were produced by the Sonogashira coupling of **7.4a** or **7.4b**. The reaction progress could be monitored by the development of the fluorescent products which were isolated by precipitating twice in non solvents.

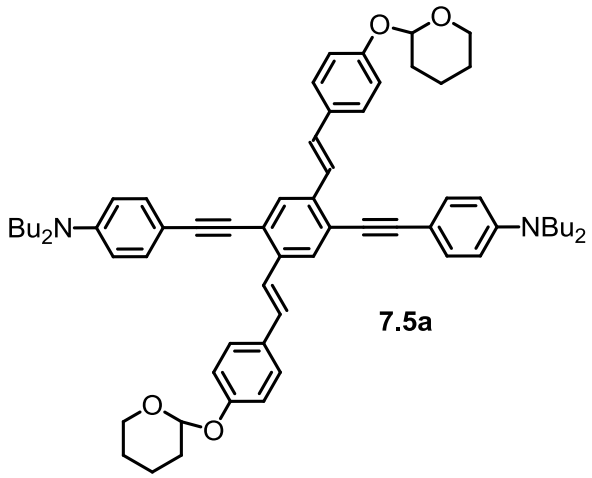

7.5a

Compound 7.5a: 7.3b (0.312 g, 0.333 mmol) was combined with **7.4a** (0.385 g, 1.28 mmol), $(PPh_3)_2PdCl_2$ (5 mg, 7.1 μmol), CuI (5 mg, 33 μmol) KOH (0.500 g, 8.90 mmol) and dissolved in piperidine (5 mL), EtOH (10 mL) and THF (25 mL) in a nitrogen purged Schlenk flask. The solution was degassed, capped with a septum and allowed to stir at room temperature for 24 h. The product was extracted with dichloromethane (100 mL), washed three times with water (100 mL), dried with magnesium sulfate and reduced until a light orange powder formed. The product was purified by chromatography eluting with 70:30 dichloromethane/hexanes yielding bright orange crystals. Yield: 66 %. *MP:* 205 ºC. *IR:* 3442.7, 3419.5, 2952.8, 2929.6, 2870.3, 2196.4, 1604.6, 1519.8, 1367.4, 1238.2, 962.41 cm^{-1}. *^{1}H NMR (500 MHz, $CDCl_3$):* δ = 7.85(s, 2H, Ar-H), 7.60 (d, 2H, C=C-H, $J_{H,H}$ = 16.5 Hz), 7.54 (d, 4H, Ar-H, $J_{H,H}$ = 9 Hz), 7.46 (d, 4H, Ar-H, $J_{H,H}$ = 9 Hz), 7.24 (d, 2H, C=C-H, $J_{H,H}$ = 16.5 Hz), 7.10(d, 4H, Ar-H, $J_{H,H}$ = 9 Hz), 6.65 (d, 4H, Ar-H, $J_{H,H}$ = 9 Hz), 5.49 (s, 2H, α-C-H), 3.94 (m, 2H, ε-C-H), 3.66 (m, 2H, ε-C-H), 3.34 (d, 8H, $J_{H,H}$= 7.5), 2.04 (m, 2H, β-C-H), 1.91 (m, 4H, γ-C-H), 1.71 (m, 4H, δ-C-H), 1.64 (m, 2H, β-C-H), 1.63 (m, 8H) 1.41 (m, 8H), 1.01 (t, 12H, $J_{H,H}$= 7.5). *^{13}C NMR (125 MHz, $CDCl_3$):* δ =157.24, 148.49, 137.17, 133.27, 131.72, 129.76, 128.47, 128.28, 124.90, 122.65,

117.09, 111.69, 109.17, 97.19, 96.72, 86.42, 62.45, 51.15, 30.76, 29.82, 25.64, 20.76, 19.16, 14.44.

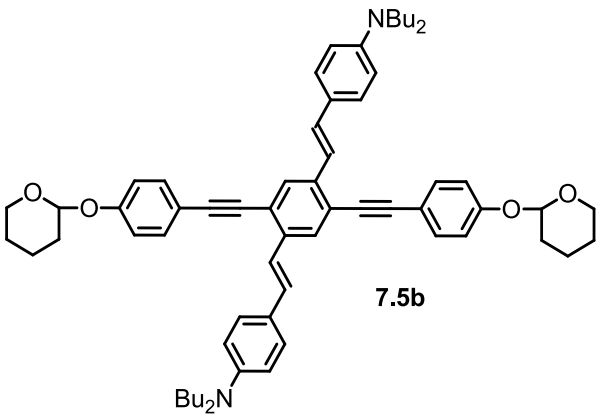

7.5b

Compound 7.5b: 7.3a (0.282 g, 0.301 mmol) was combined with **7.4b** (0.217 g, 1.07 mmol), $(PPh_3)_2PdCl_2$ (5 mg, 7.1 μmol), CuI (5 mg, 33 μmol) and dissolved in THF (50 mL) and piperidine (5 mL) in a nitrogen purged schlenk flask. The solution was degassed, capped with a septum and allowed to stir at room temperature for 24 h. The product was extracted with dichloromethane (100 mL), washed three times with water (100 mL), dried with magnesium sulfate and reduced until a red powder formed. The product was purified by chromatography eluting with 70:30 dichloromethane/hexanes yielding red crystals. Yield: 66 %. *MP:* 201 ºC. *IR:* 3444.6, 3398.3, 2954.7, 2931.6, 2856.4, 2204.5, 1600.8, 1519.8, 1367.4, 1238.21, 1184.21, 960.5 cm^{-1}. *^{1}H NMR (500 MHz, CD_2Cl_2):* δ = 7.84 (s, 2H, Ar-H), 7.56 (d, 4H, Ar-H, $J_{H,H}$ = 9 Hz), 7.43 (d, 4H, Ar-H, $J_{H,H}$ = 9 Hz), 7.42 (d, 2H, C=C-H, $J_{H,H}$ = 16.5 Hz), 7.19 (d, 2H, C=C-H, $J_{H,H}$ = 16.5 Hz), 7.09 (d, 4H, Ar-H, $J_{H,H}$ = 9 Hz), 6.66 (d, 4H, Ar-H, $J_{H,H}$ = 9 Hz), 5.48 (s, 2H, α-C-H), 3.89 (m, 2H, ε-C-H), 3.62 (m, 2H, ε-C-H), 3.31 (d, 8H, $J_{H,H}$= 7.00), 2.01 (m, 2H, β-C-H), 1.87 (m, 4H, γ-C-H), 1.68 (m, 4H, δ-C-H), 1.64 (m, 2H, β-C-H), 1.59 (m, 8H), 1.38 (m, 8H), 0.97 (t, 12H, $J_{H,H}$= 7.50). *^{13}C NMR (125 MHz, CD_2Cl_2):* δ = 157.83, 148.63,

137.49, 133.27, 130.78, 128.44, 128.23, 124.70, 121.89, 120.54, 116.99, 116.67, 112.06, 96.84, 95.35, 87.53, 62.56, 51.15, 30.70, 29.90, 25.61, 20.76, 19.21, 14.24.

Compounds 7.6 and 7.7

Compounds **7.5a-b** were deprotected by trifluoroacetic acid in a dry ice acetone bath. The products were obtained by extracting with dichloromethane or ethyl ether. The yields reported reflect the amount of pure material that was recovered after deprotection and recrystallization.

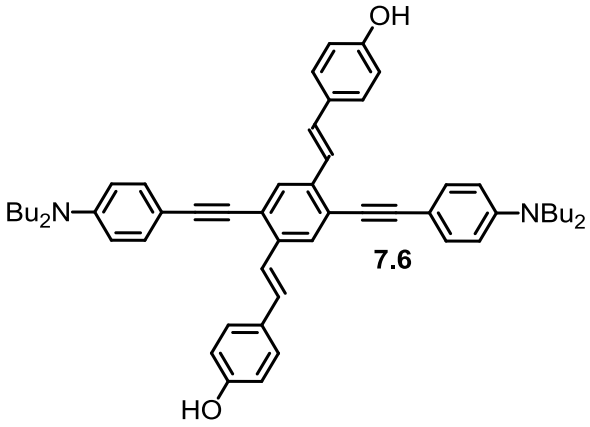

7.6

Compound 7.6: **7.5a** (0.150 g, 0.195 mmol) was dissolved in dichloromethane (50 mL) and trifluoroacetic acid (2 mL) was added into a 100-mL round bottom flask kept in a dry ice acetone bath. The solution was allowed to stir at -78 °C for 2h and then thawed to room temperature. The reaction mixture was washed three times with water (100 mL), dried with magnesium sulfate, filtered and reduced until a dark green powder was formed. The powder was recrystallized by dissolving in hot dichloromethane and adding an excess amount of hexanes, yielding dark brown crystals (126 mg). Yield: 84%. *MP:* 196 ºC. *IR:* 3502.5, 3460.1, 3365.6, 2954.7, 2929.7, 2869.9, 2194.8, 1604.7, 1517.9, 1361.7, 813.9 cm $^{-1}$. *^{1}H NMR (500 MHz , $CDCl_3$):* δ = 7.84 (s, 2H, Ar-H), 7.57 (d, 2H,

C=C-H, $J_{H,H}$ = 16.5 Hz), 7.50 (d, 4H, Ar-H, $J_{H,H}$ = 9 Hz), 7.46 (d, 4H, Ar-H, $J_{H,H}$ = 9 Hz), 7.22 (d, 2H, C=C-H, $J_{H,H}$ = 16.5 Hz), 6.88 (d, 4H, Ar-H, $J_{H,H}$ = 8.5 Hz), 6.68 (d, 4H, Ar-H, $J_{H,H}$ = 8.5 Hz), 3.34 (d, 8H, $J_{H,H}$= 7.5), 1.63 (m, 8H) 1.41 (m, 8H), 1.00 (t, 12H, $J_{H,H}$= 7.00). *^{13}C NMR (125 MHz, THF-D_8):* δ = 156.42, 146.70, 135.26, 131.06, 128.34, 127.68, 126.36, 126.11, 121.17, 120.68, 114.01, 109.89, 107.67, 95.15, 84.20, 48.97, 27.95, 18.68, 11.93. *MS (EI, 70-SE) ($C_{54}H_{60}N_2O_2$):* m/z = 768.

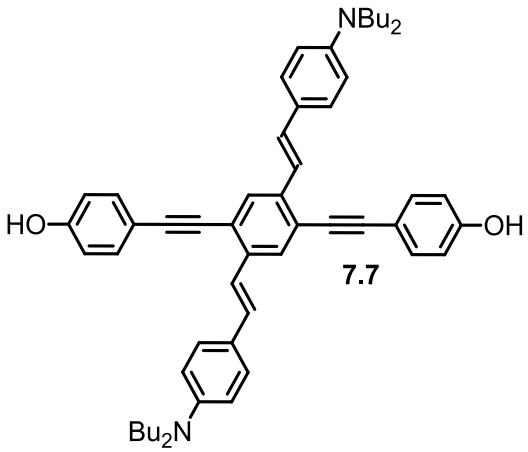

7.7

Compound 7.7: **7.5b** (0.130 g, 0.169 mmol) was dissolved in dichloromethane (50 mL) and trifluoroacetic acid (2 mL) was added into a 100-mL round bottom flask kept in a dry ice acetone bath. The solution was allowed to stir at -78 °C for 2h and then thawed to room temperature. The reaction mixture was washed three times with water (100 mL), dried with magnesium sulfate, filtered and reduced until a red powder was formed. The powder was recrystallized by dissolving in hot dichloromethane and adding an excess amount of hexanes, yielding red crystals (102 mg). Yield: 82 %. *MP:* 199 ºC. *IR:* 3386.8, 3321.5, 3271.1, 2954.7, 2929.7, 2867.9, 2196.7, 1602.7, 1515.9, 1365.5, 1184.2, 1097.4 cm^{-1}. *^1H NMR (500 MHz ,DMSO-d_6):* δ = 7.89 (s, 2H, Ar-H), 7.49 (d, 4H, Ar-H, $J_{H,H}$ = 8.5 Hz), 7.43 (d, 4H, Ar-H, $J_{H,H}$ = 8.5 Hz), 7.36 (d, 2H, C=C-H, $J_{H,H}$ = 16.5 Hz) , 7.28 (d, 2H, C=C-H, $J_{H,H}$ = 16.5 Hz), 6.88 (d, 4H, Ar-H, $J_{H,H}$ = 8.5 Hz), 6.69 (d, 4H, Ar-H, $J_{H,H}$ =

8.5 Hz), 3.34 (d, 8H, $J_{H,H}$= 7.5), 1.63 (m, 8H) 1.41 (m, 8H), 1.00 (t, 12H, $J_{H,H}$= 7.00) **.** *^{13}C NMR (125 MHz, THF-d_8):* δ = 158.6, 148.4, 137.3, 133.1, 130.6, 128.1, 127.8, 125.2, 122.0, 120.4, 115.8, 114.4, 112.0, 95.51, 86.62, 50.90, 30.07, 20.56, 13.85. *MS (EI, 70-SE) ($C_{54}H_{60}N_2O_2$):* m/z = 768.

General experimental procedure for 7.6 and 7.7 with acid and base: To evaluate the response of **7.6** and **7.7** towards acid and base, excess amounts of trifluoroacetic acid and tetrabutylammonium hydroxide was added to 10 micromolar solutions of both XFs in the following solvents: methanol, acetonitrile, dimethylformamide, dimethylsulfoxide, tetrahydrofuran, dichloromethane, ether, and toluene. After addition, the optical properties were measured. A picture of the fluorescent response of both XFs with acid and base irradiated under a UV-lamp was taken (see Figures 7.3 and 7.4.).

Absorption and Emission of 7.6 in Various Solvents with Acid and Base

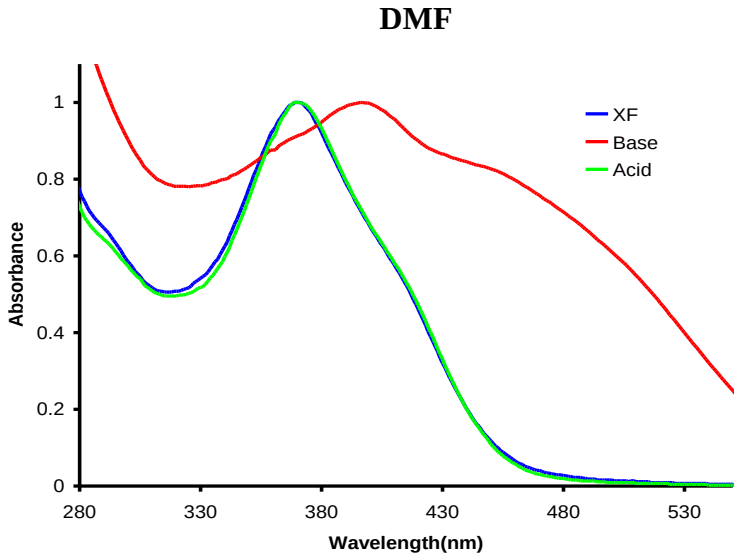

Figure 7.14. Absorption spectrum of **7.6** with acid and base in DMF.

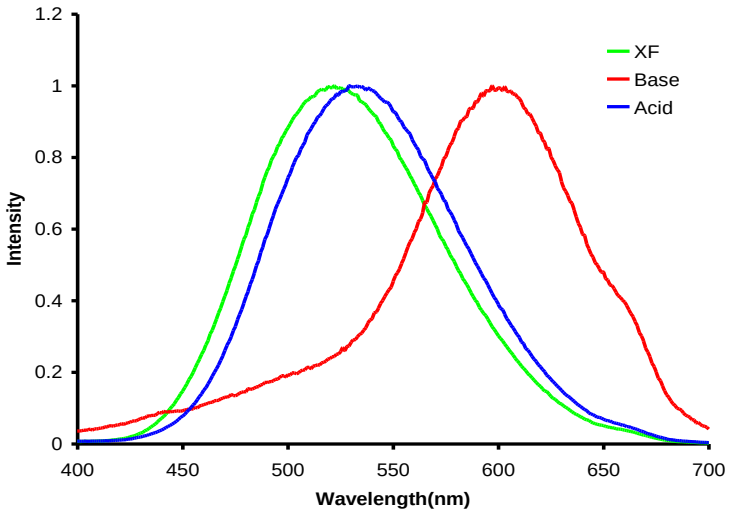

Figure 7.15. Emission spectrum of **7.6** with acid and base in DMF.

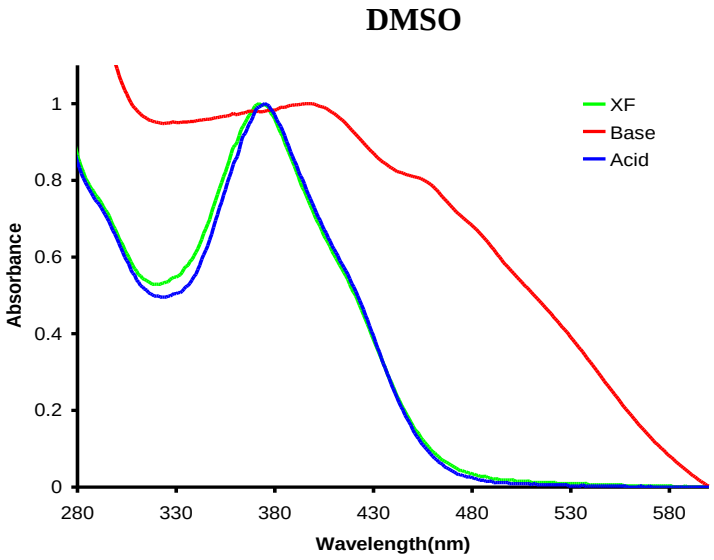

Figure 7.16. Absorption spectrum of **7.6** with acid and base in DMSO.

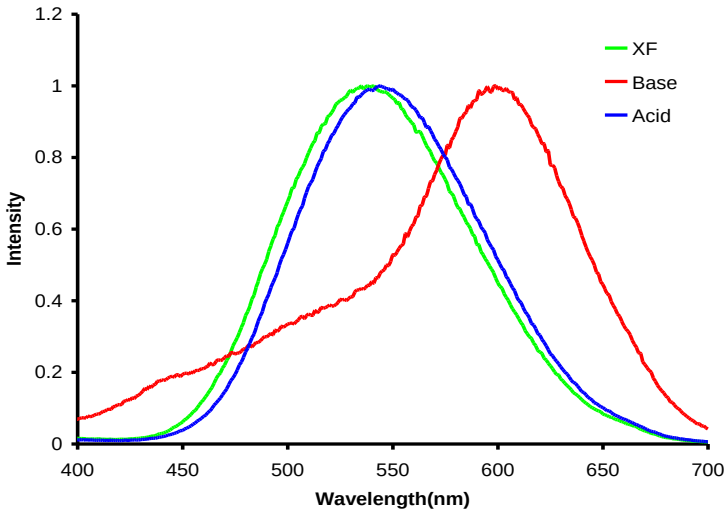

Figure 7.17. Emission spectrum of **7.6** with acid and base in DMSO.

THF

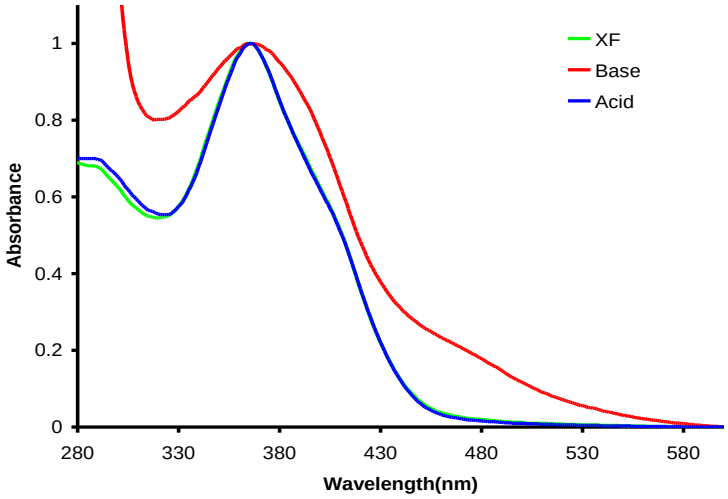

Figure 7.18. Absorption spectrum of **7.6** with acid and base in THF.

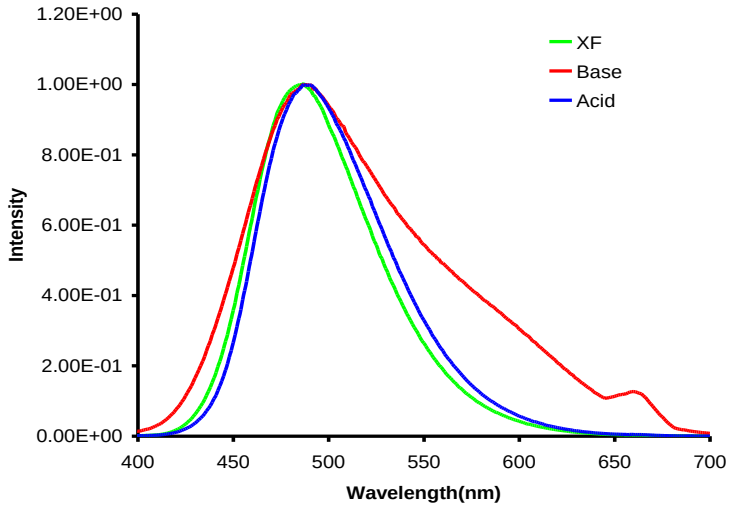

Figure 7.19. Emission spectrum of **7.6** with acid and base in THF.

Ether

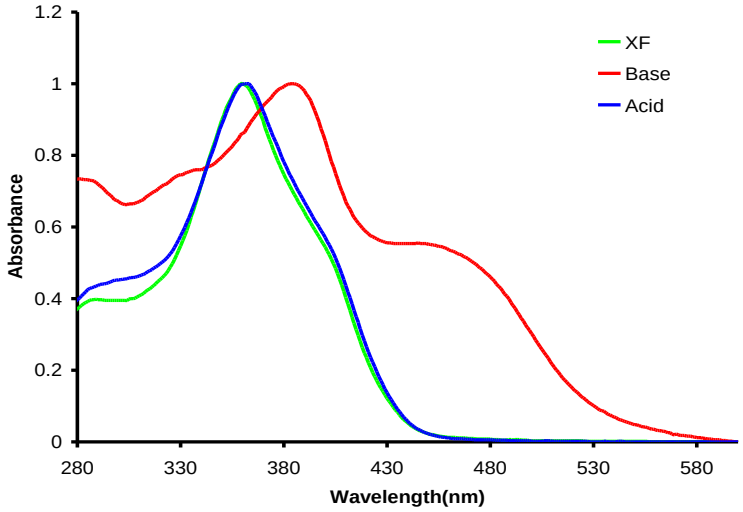

Figure 7.20. Absorption spectrum of **7.6** with acid and base in diethyl ether.

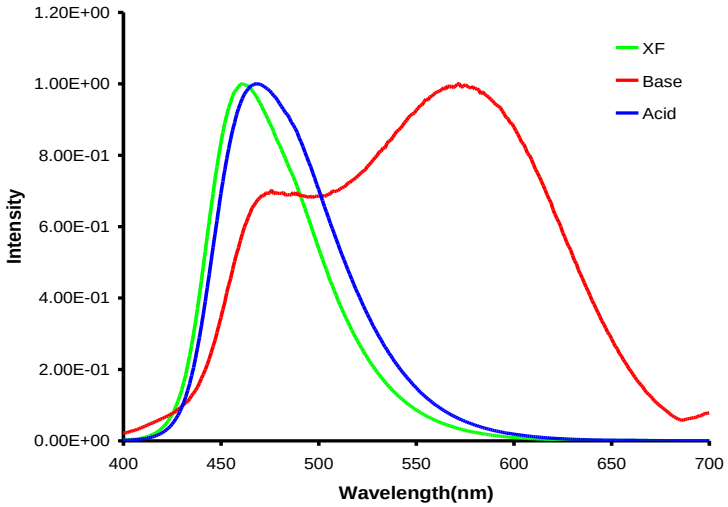

Figure 7.21. Emission spectrum of **7.6** with acid and base in diethyl ether.

Toluene

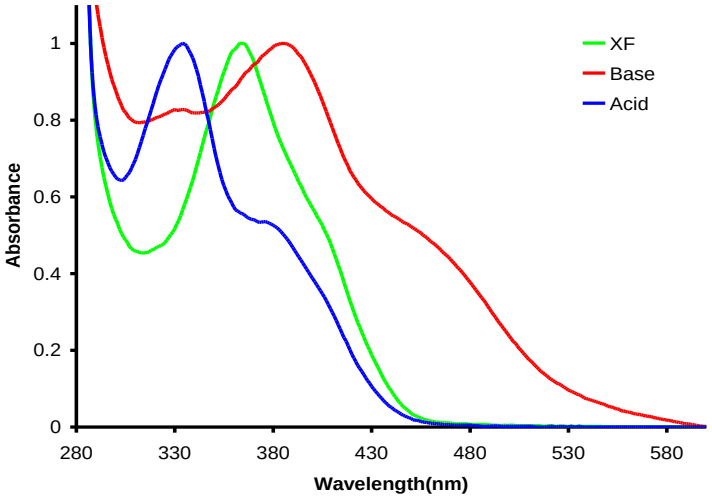

Figure 7.22. Absorption spectrum of **7.6** with acid and base in toluene.

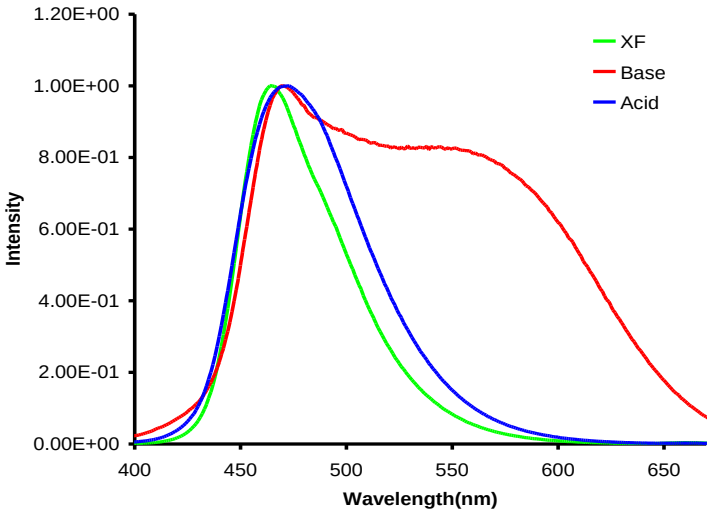

Figure 7.23. Emission spectrum of **7.6** with acid and base in toluene.

Absorption and Emission of 7.7 in Various Solvents with Acid and Base

Methanol

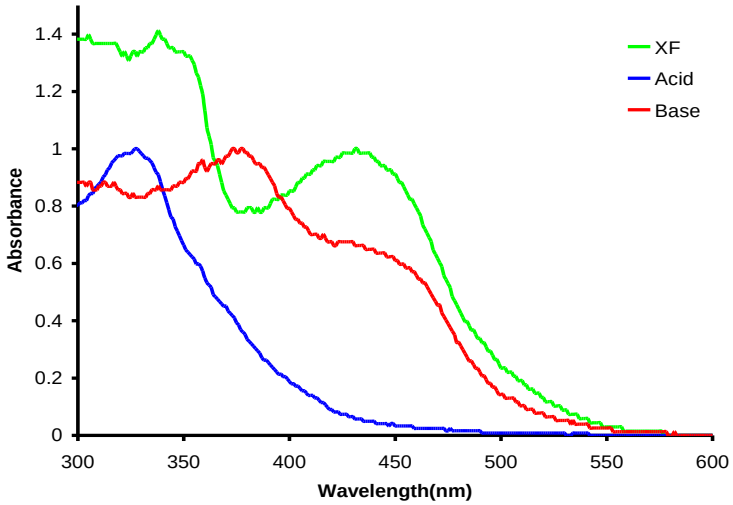

Figure 7.24. Absorption spectrum of **7.7** with acid and base in methanol.

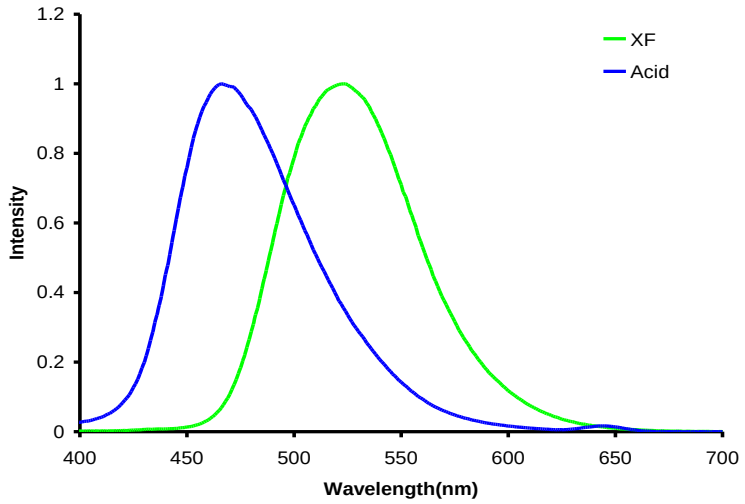

Figure 7.25. Emission spectrum of **7.7** with acid in methanol.

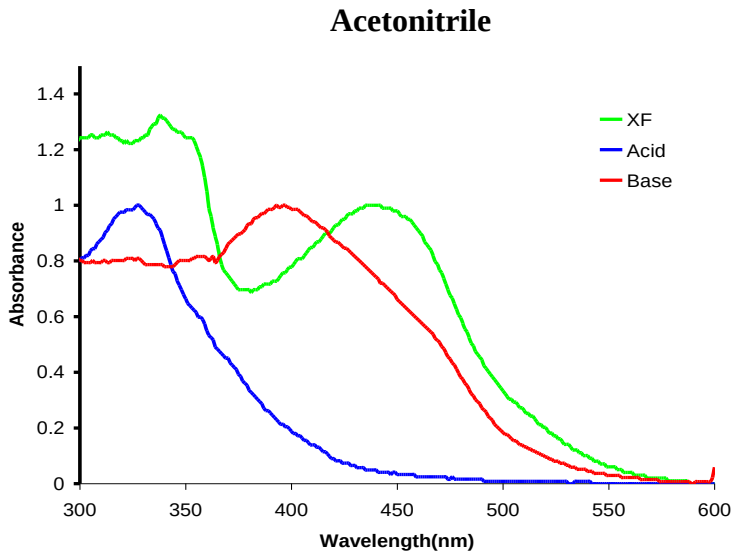

Figure 7.26. Absorption spectrum of **7.7** with acid and base in acetonitrile.

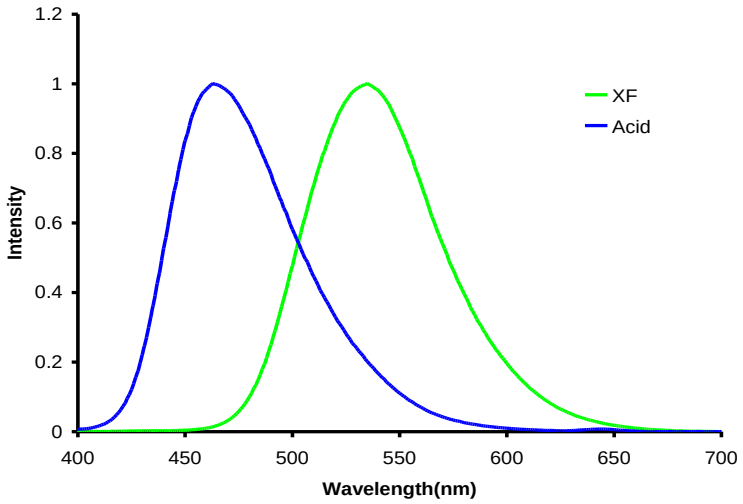

Figure 7.27. Emission spectrum of **7.7** with acid in acetonitrile.

DMF

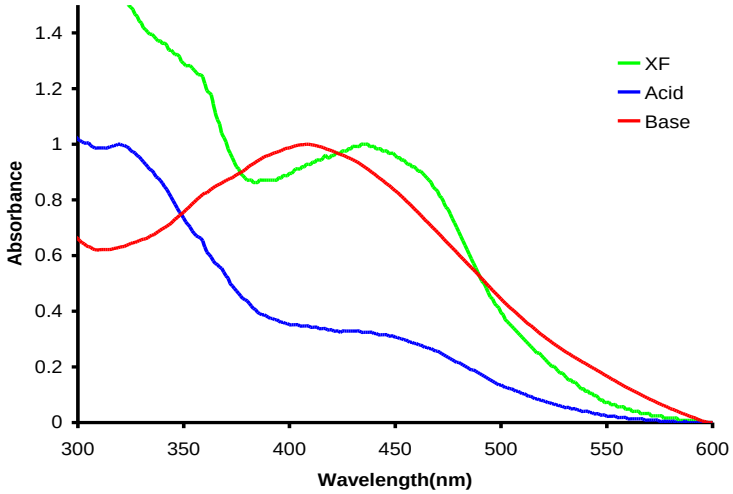

Figure 7.28.. Absorption spectrum of **7.7** with acid and base in DMF.

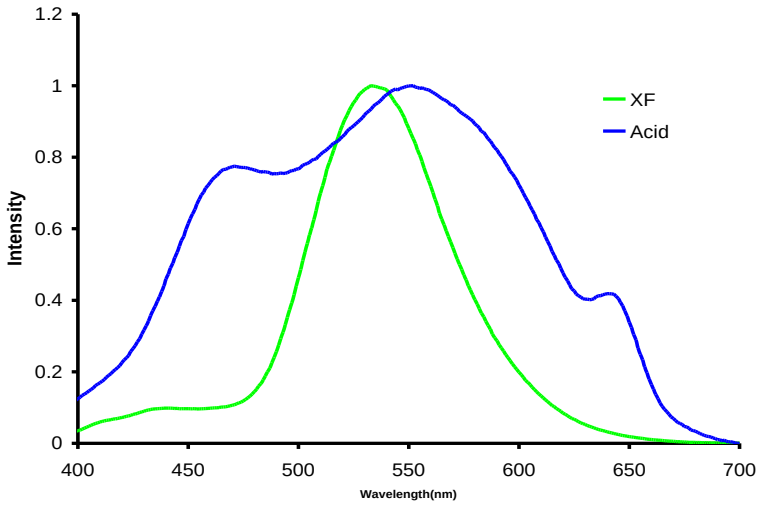

Figure 7.29. Emission spectrum of **7.7** with acid in DMF.

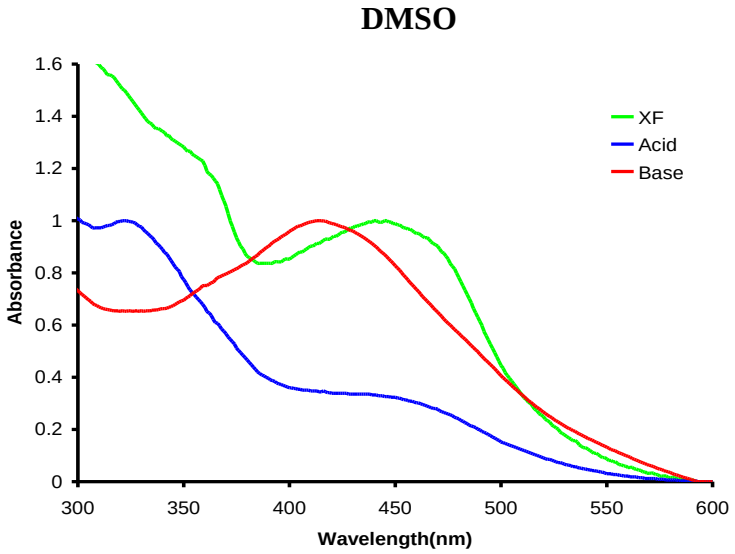

Figure 7.30. Absorption spectrum of **7.7** with acid and base in DMSO.

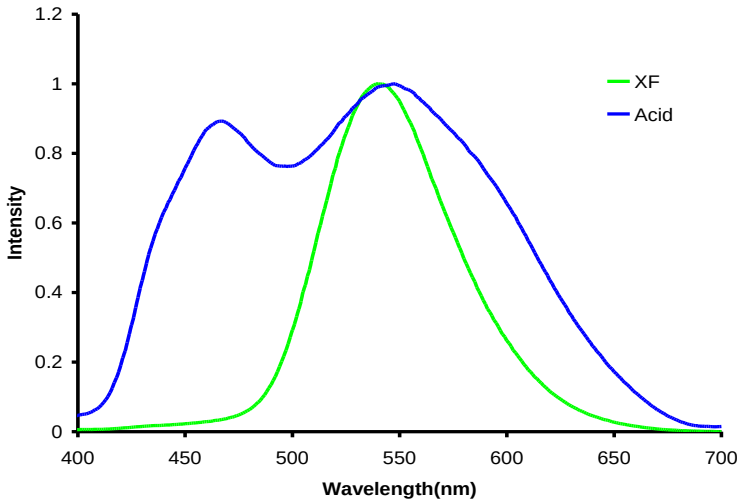

Figure 7.31. Emission spectrum of **7.7** with acid in DMSO.

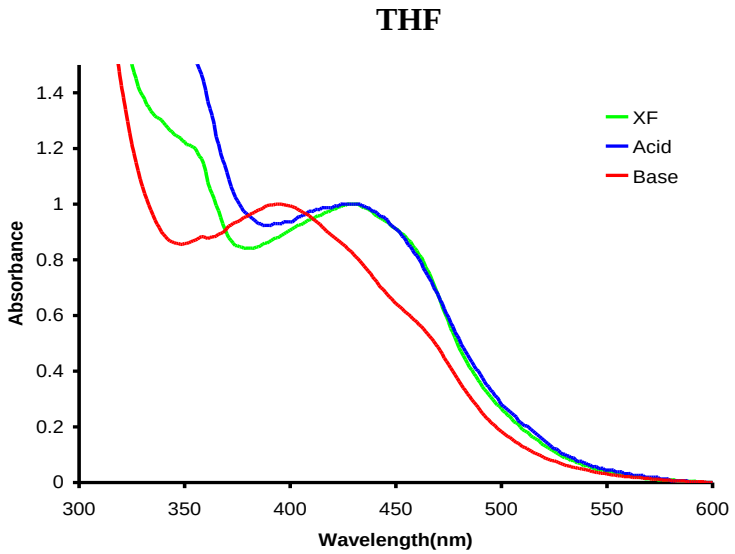

Figure 7.32. Absorption spectrum of **7.7** with acid and base in THF.

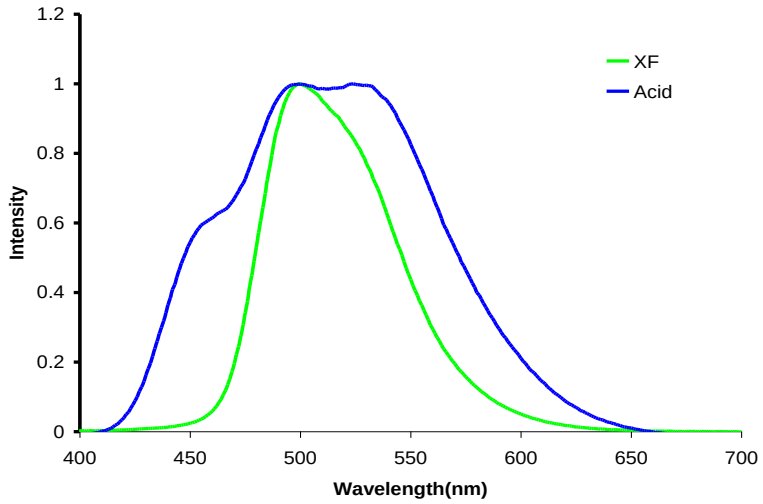

Figure 7.33. Emission spectrum of **7.7** with acid in THF.

DCM

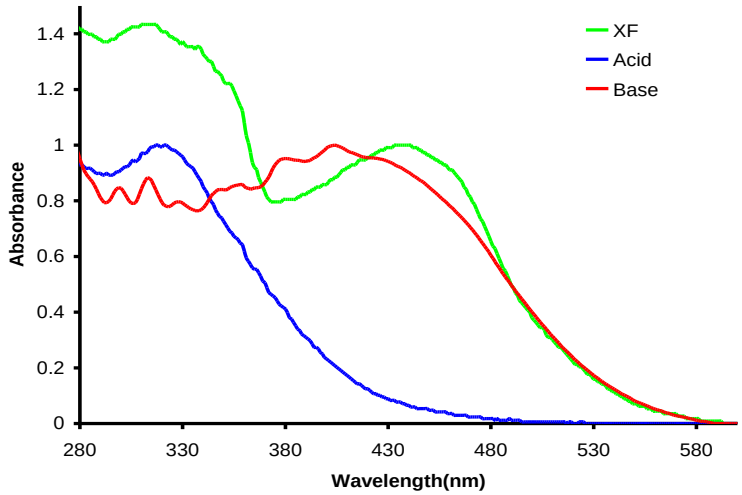

Figure 7.34. Absorption spectrum of **7.7** with acid and base in DCM.

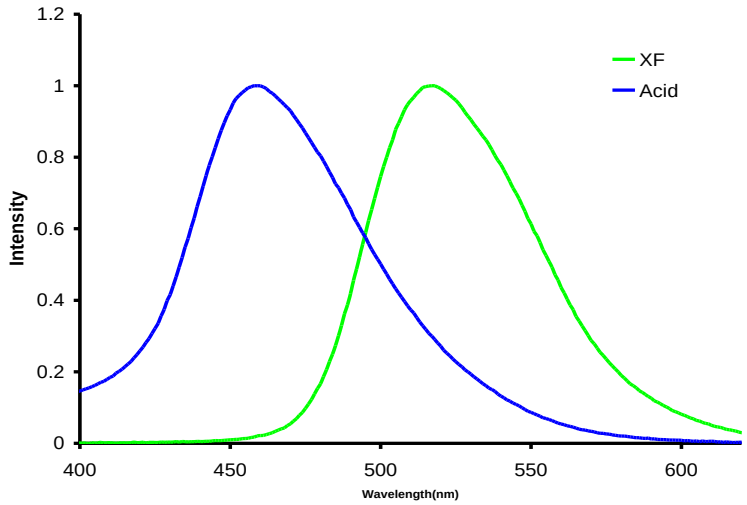

Figure 7.35. Emission spectrum of **7.7** with acid in DCM.

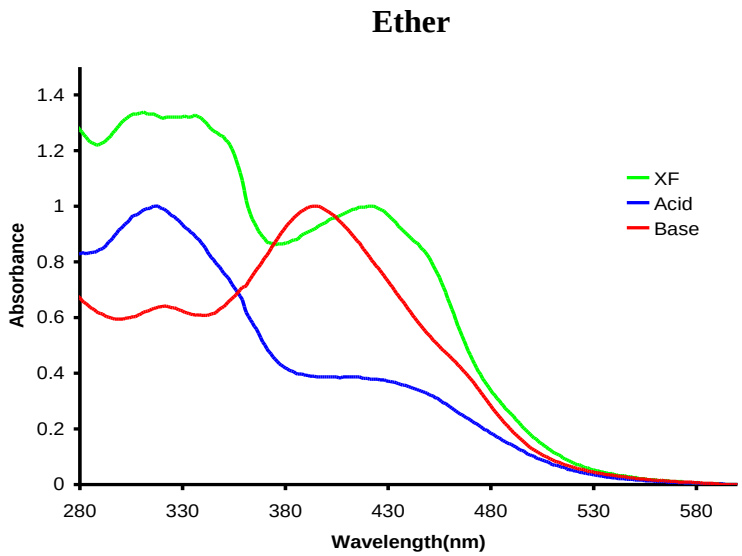

Figure 7.36. Absorption spectrum of **7.7** with acid and base in diethyl ether.

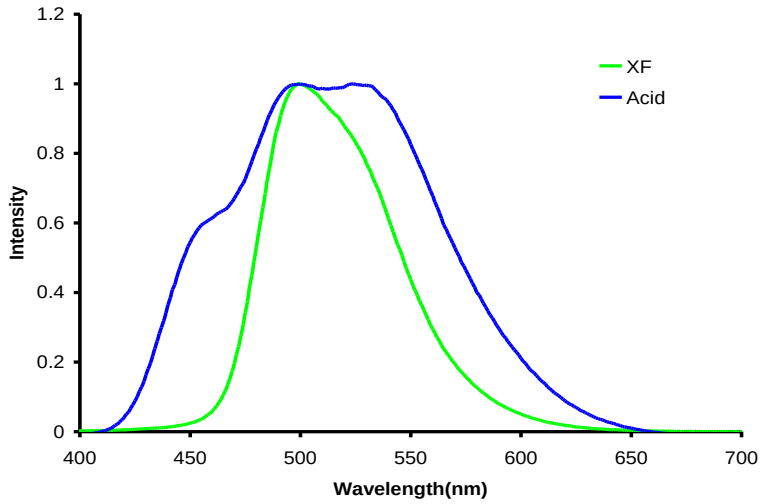

Figure 7.37. Emission spectrum of **7.7** with acid in diethyl ether.

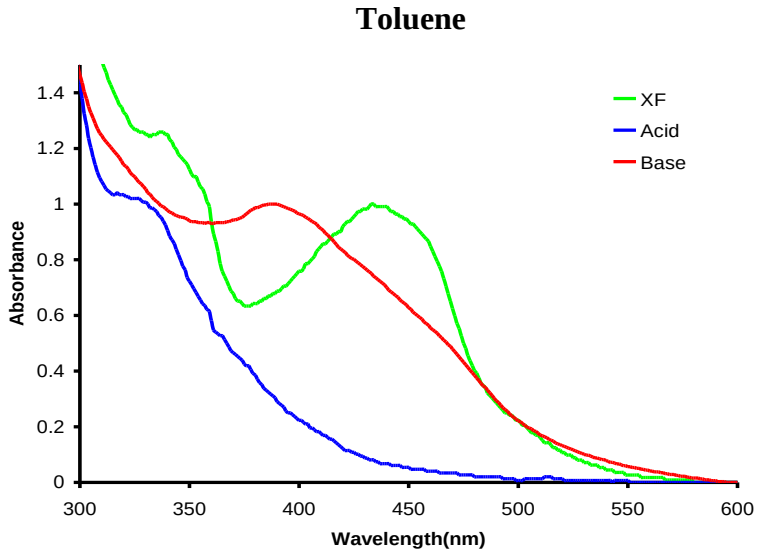

Figure 7.38. Absorption spectrum of **7.7** with acid and base in toluene.

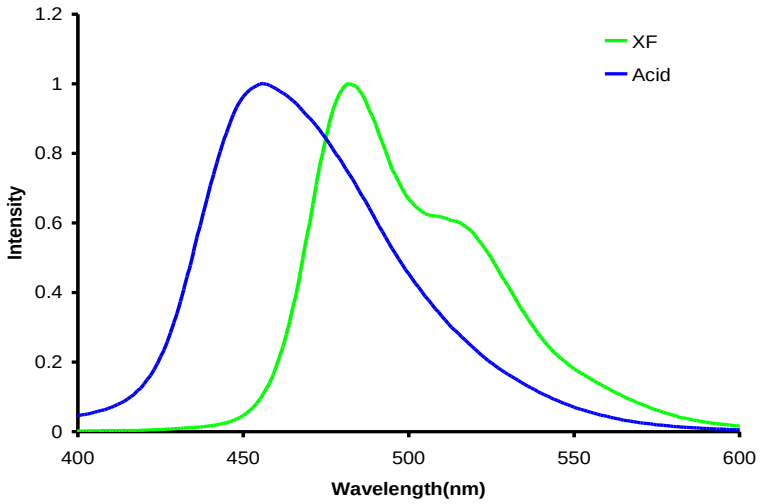

Figure 7.39. Emission spectrum of **7.7** with acid in toluene.

General experimental procedure for 7.6: To investigate the sensory ability of **7.6** towards amines, a solvatochromism study was conducted using 10 micromolar solutions the following solvents: methanol, acetonitrile, dimethylformamide, dimethylsulfoxide, tetrahydrofuran, dichloromethane, ether, and toluene. Approximately 0.1 mL (0.7-7.2 mM range) of amine was added to each 15 mL vial and its optical properties were measured. A picture of the fluorescent response of **7.6** with amines irradiated under a UV lamp is also shown in Figure 7.11.

Photophysical Response of 7.6 with Amines in Different Solvents.

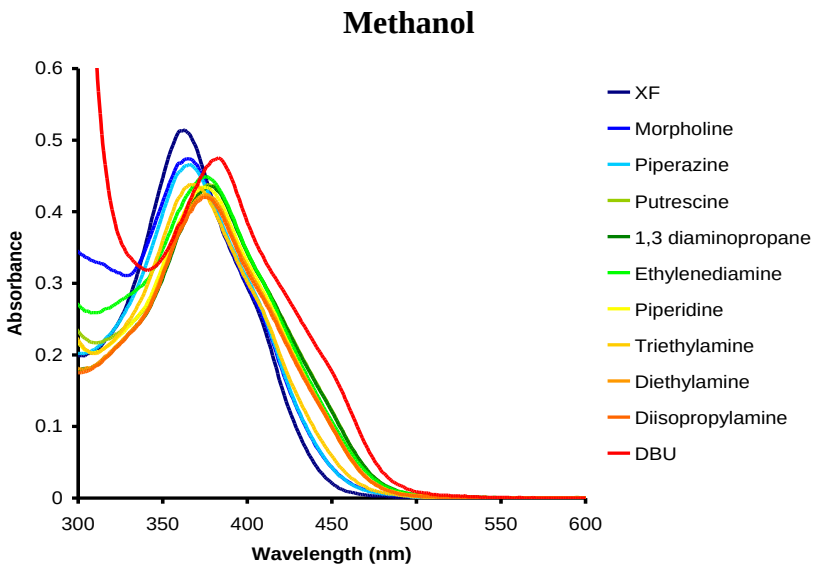

Figure 7.40. Absorption spectrum of **7.6** with amines in methanol.

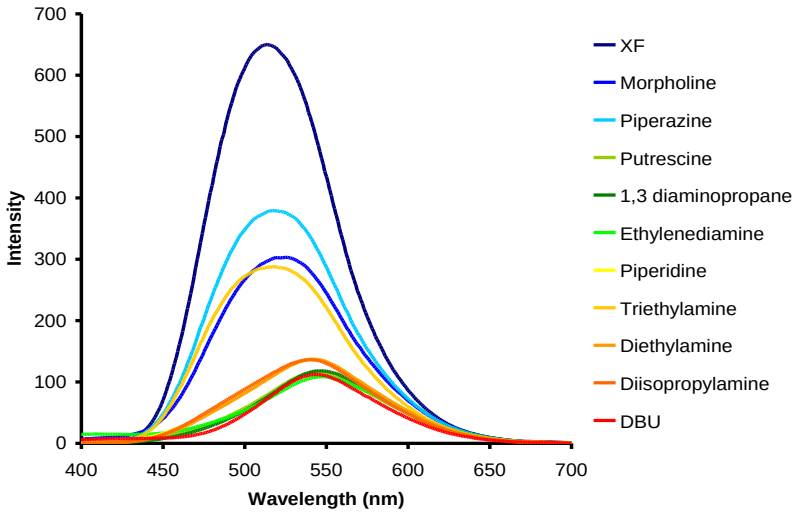

Figure 7.41. Emission spectrum of **7.6** with amines in methanol.

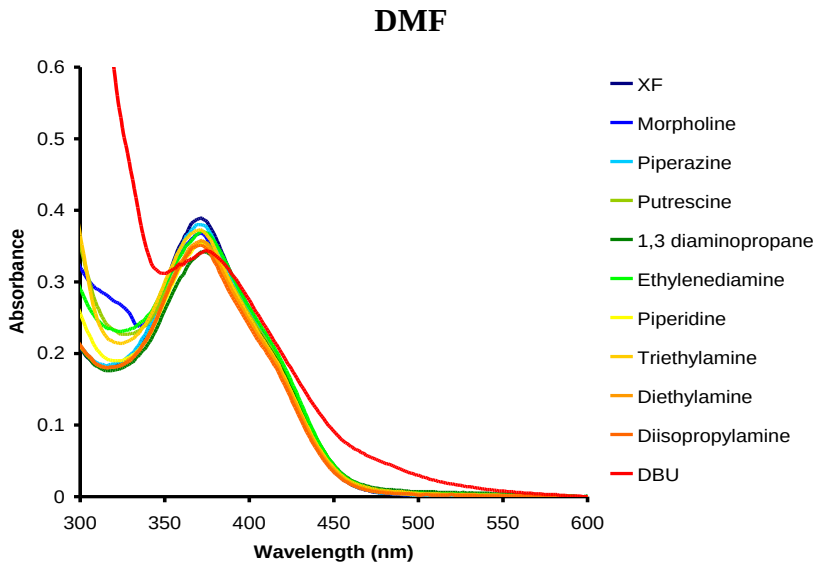

Figure 7.42. Absorption spectrum of **7.6** with amines in DMF.

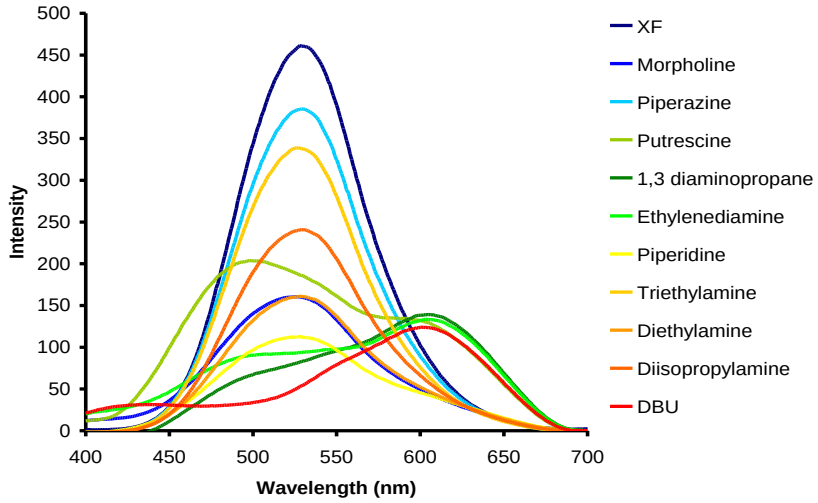

Figure 7.43. Emission spectrum of **7.6** with amines in DMF.

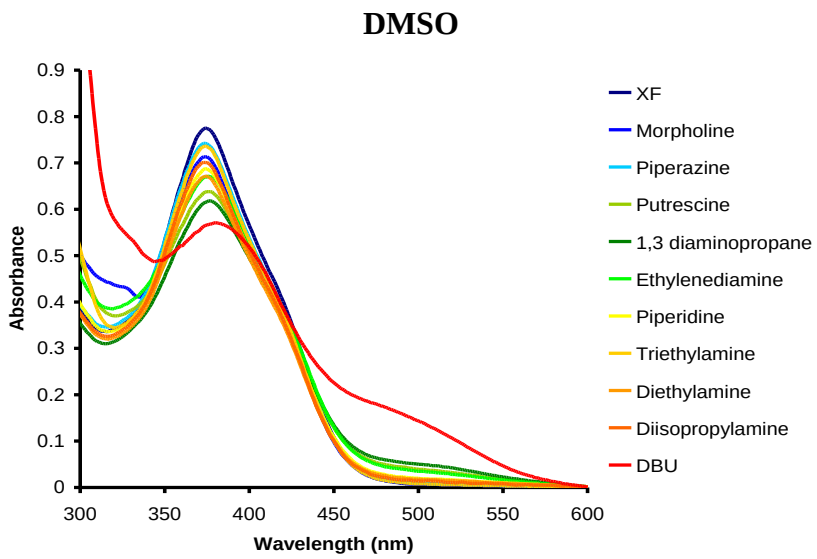

Figure 7.44. Absorption spectrum of **7.6** with amines in DMSO.

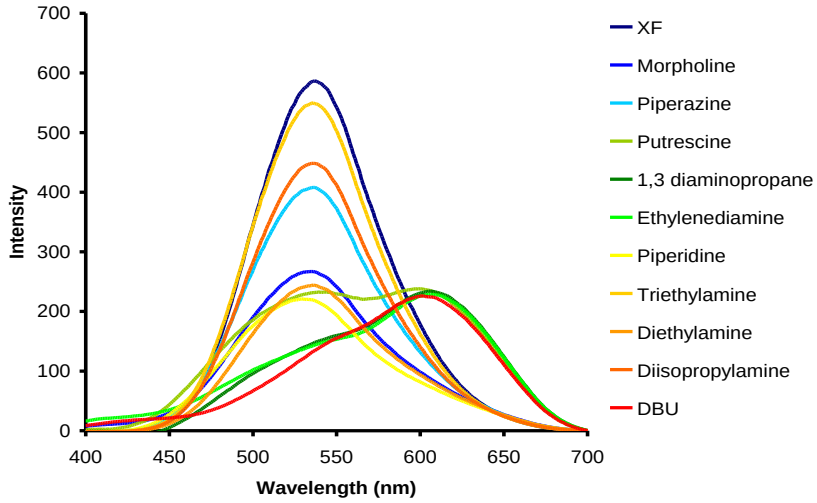

Figure 7.45. Emission spectrum of **7.6** with amines in DMSO.

THF

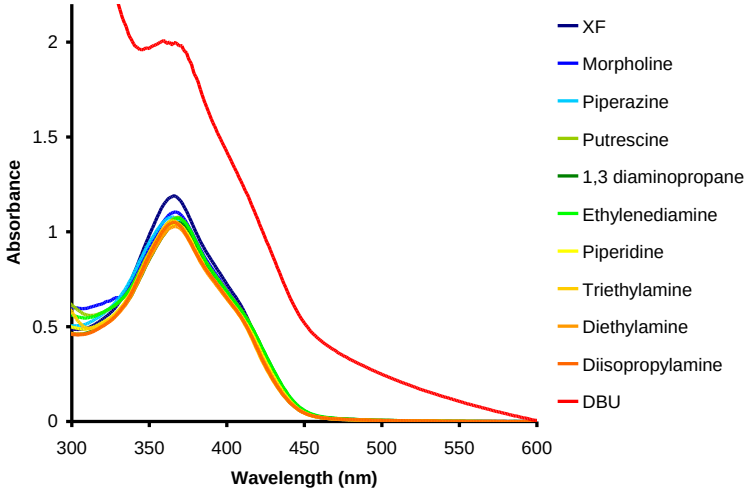

Figure 7.46. Absorption spectrum of **7.6** with amines in THF.

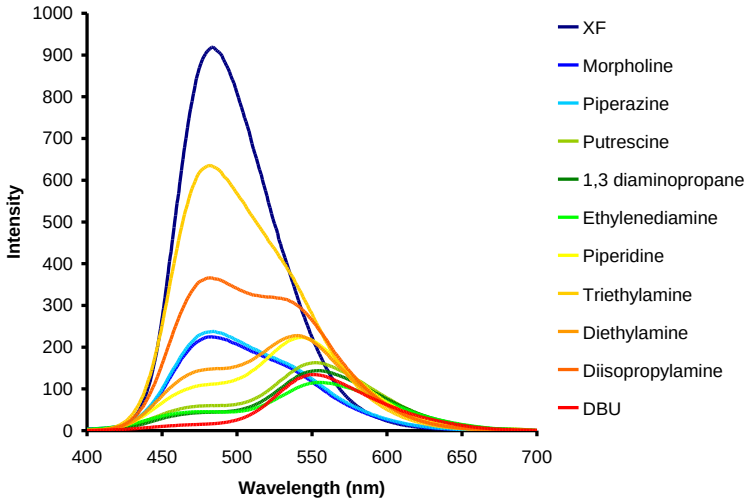

Figure 7.47. Emission spectrum of **7.6** with amines in THF.

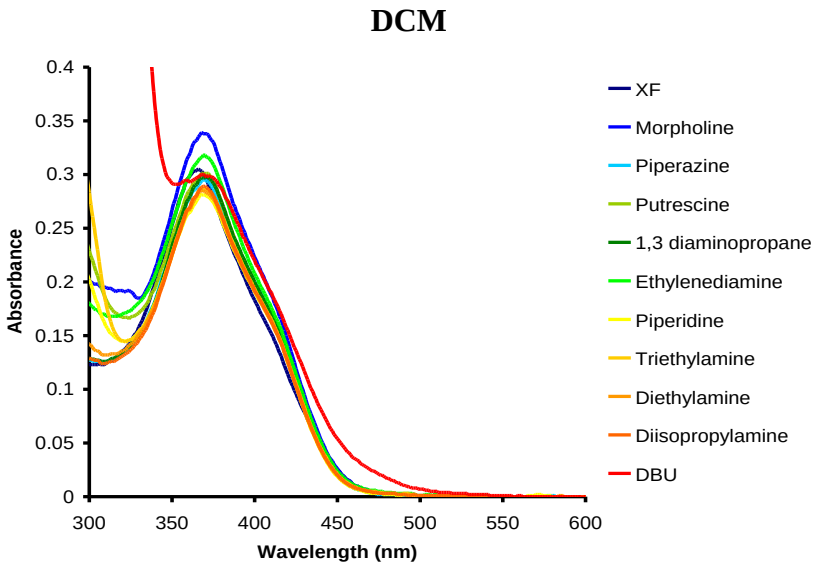

Figure 7.48. Absorption spectrum of **7.6** with amines in DCM.

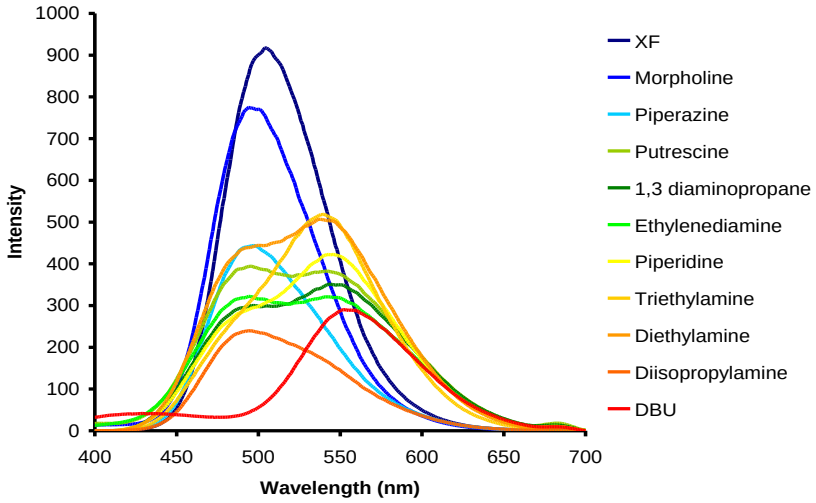

Figure 7.49. Emission spectrum of **7.6** with amines in DCM.

Ether

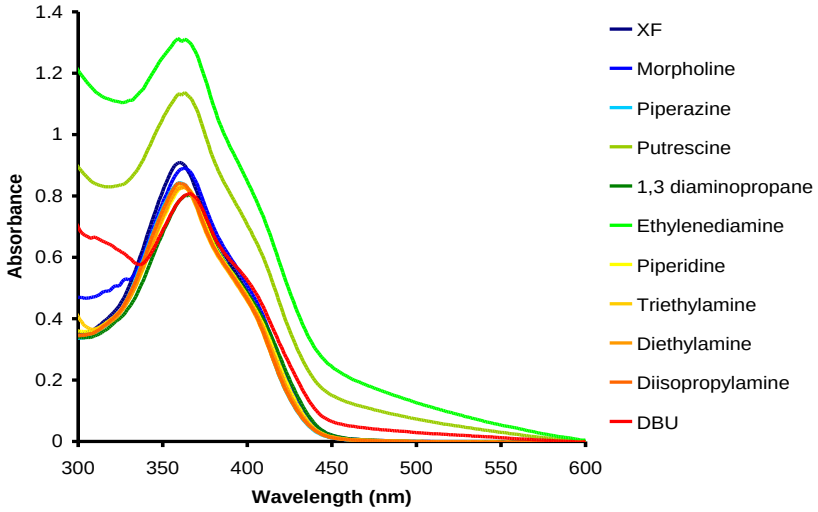

Figure 7.50. Absorption spectrum of **7.6** with amines in diethyl ether.

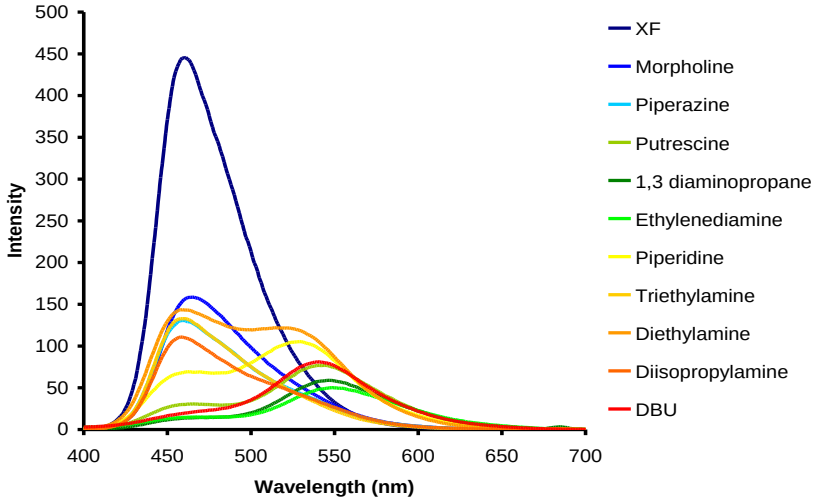

Figure 7.51. Emission spectrum of **7.6** with amines in diethyl ether.

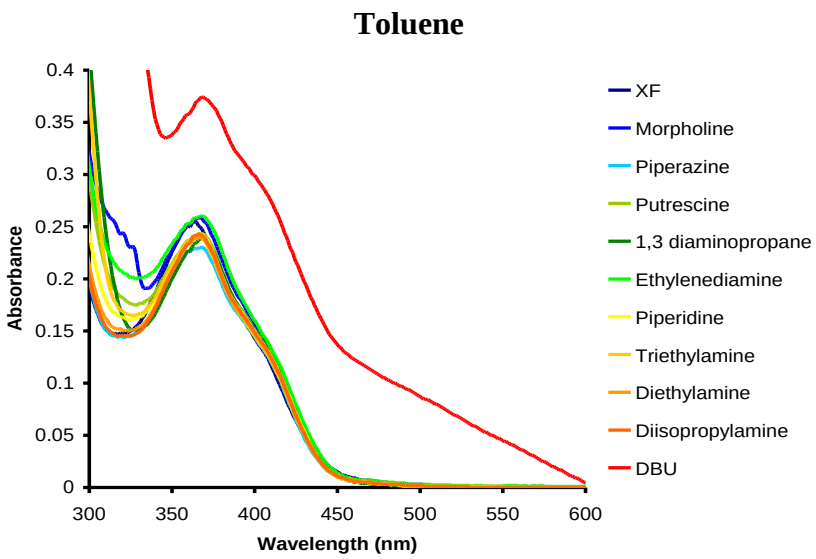

Figure 7.52. Absorption spectrum of **7.6** with amines in toluene.

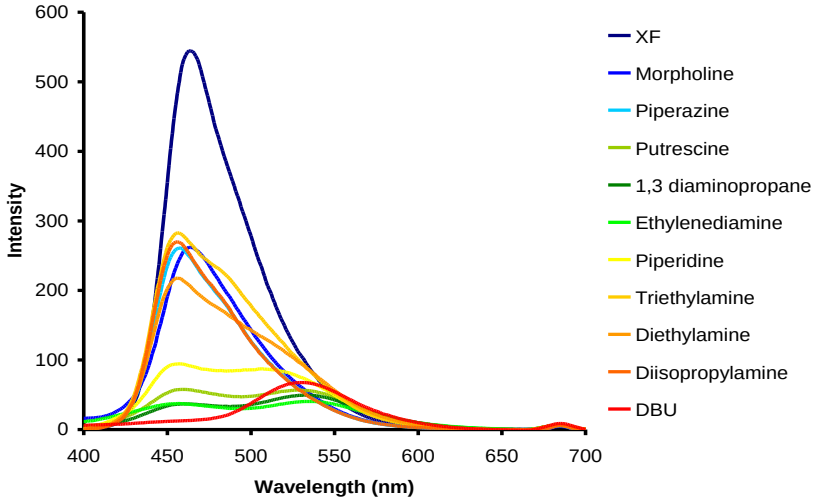

Figure 7.53. Emission spectrum of **7.6** with amines in toluene.

General experimental procedure for 7.6 and 7.7 with metals: To evaluate the response of **7.6** and **7.7** towards metal cations, excess amounts of metal trifluoromethanesulfonate salts was added to 10 micromolar solutions of both XFs in acetonitrile and dichloromethane. After addition, the optical properties were measured. A picture of the

fluorescent response of both XFs with metals irradiated under a UV-lamp is shown in Figures 7.8 and 7.10.

Absorpton and Emission Spectra of 7.6 with Metals

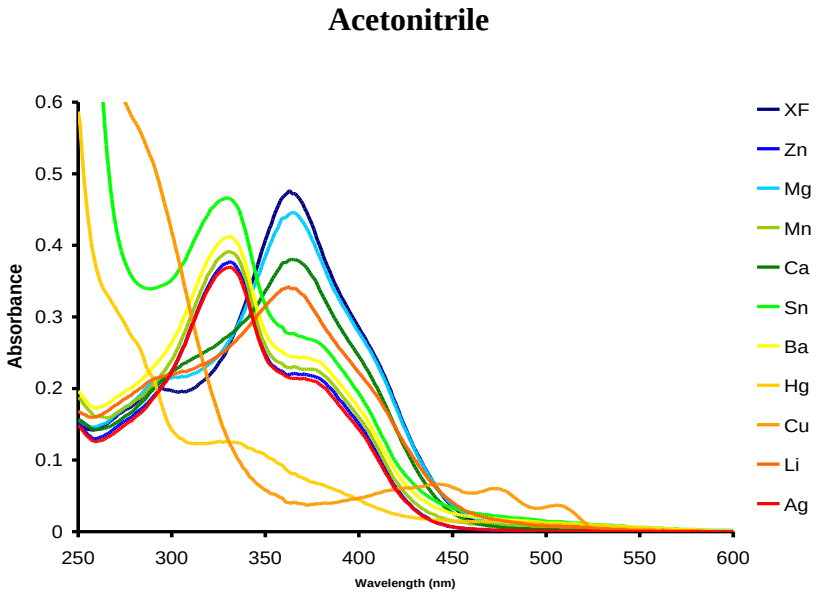

Figure 7.54. Absorption spectrum of **7.6** with metals in acetonitrile.

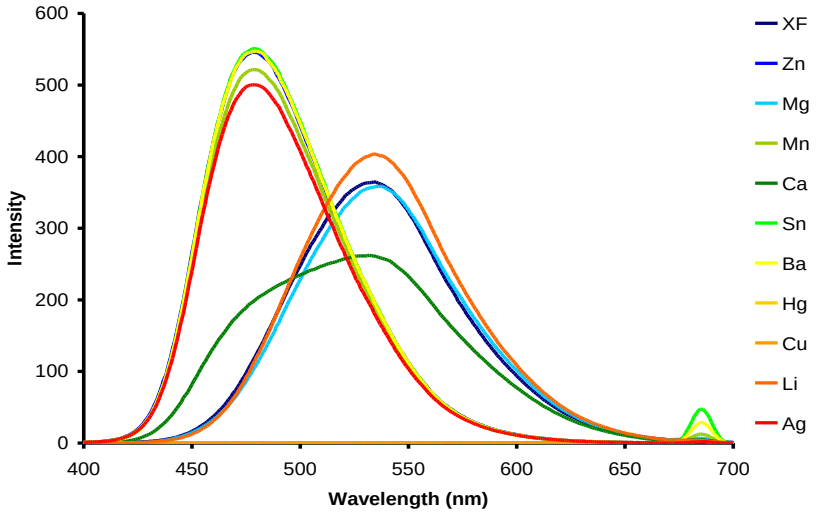

Figure 7.55. Emission spectrum of **7.6** with metals in acetonitrile.

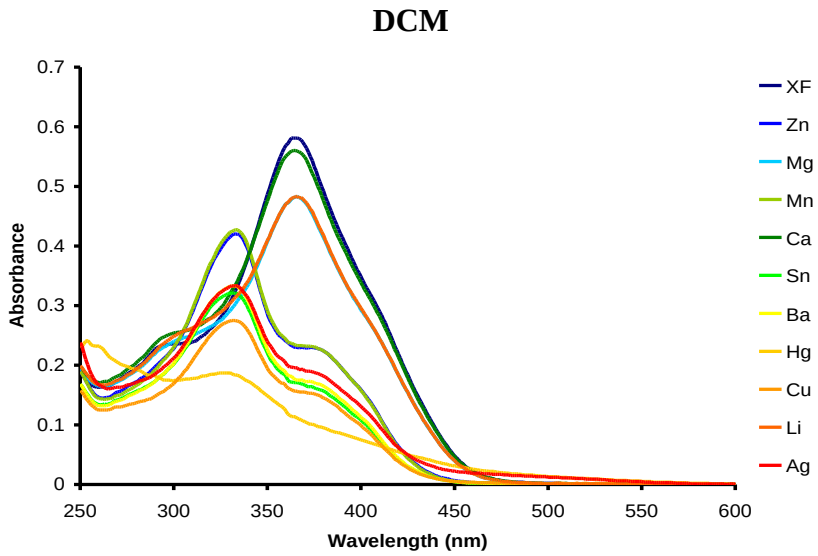

Figure 7.56. Absorption spectrum of **7.6** with metals in dichloromethane.

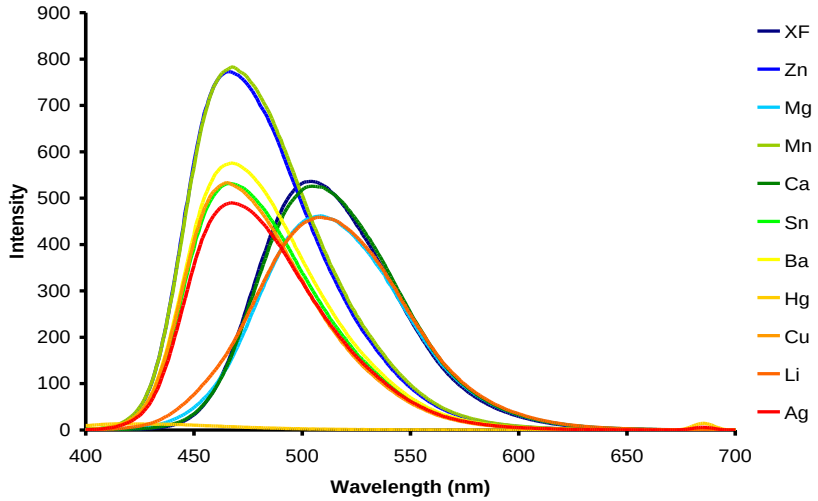

Figure 7.57. Emission spectrum of **7.6** with metals in dichloromethane.

Absorpton and Emission Spectra of 7.7 with Metals

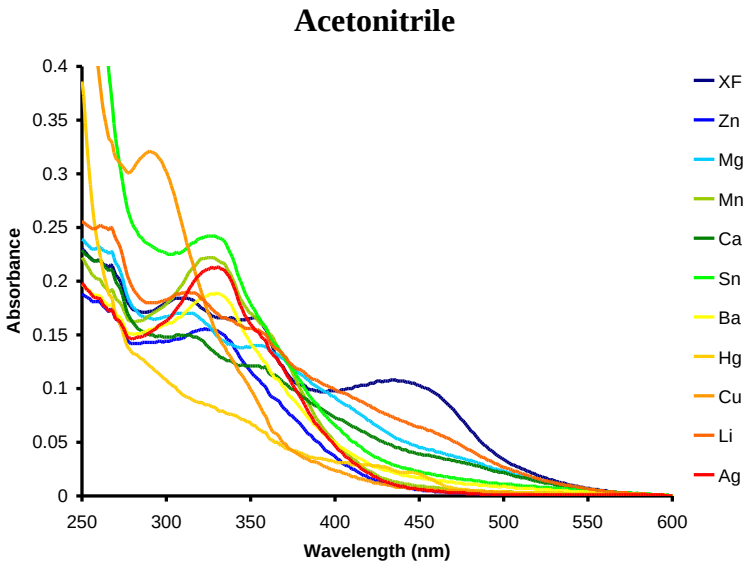

Figure 7.58. Absorption spectrum of **7.7** with metals in acetonitrile.

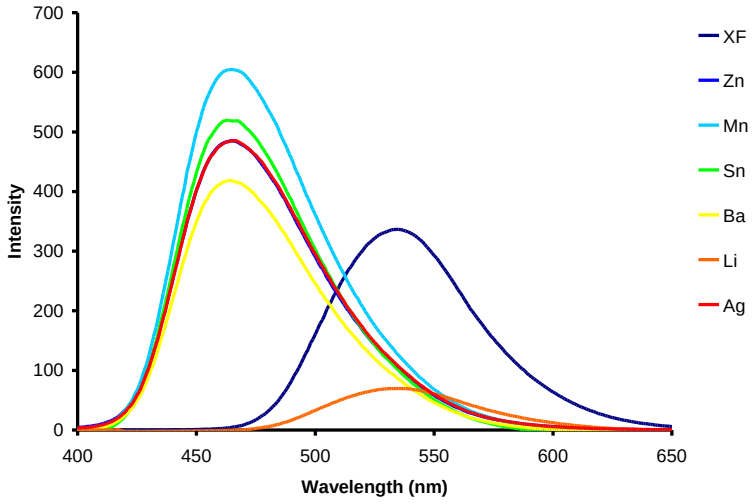

Figure 7.59. Emission spectrum of **7.7** with metals in acetonitrile.

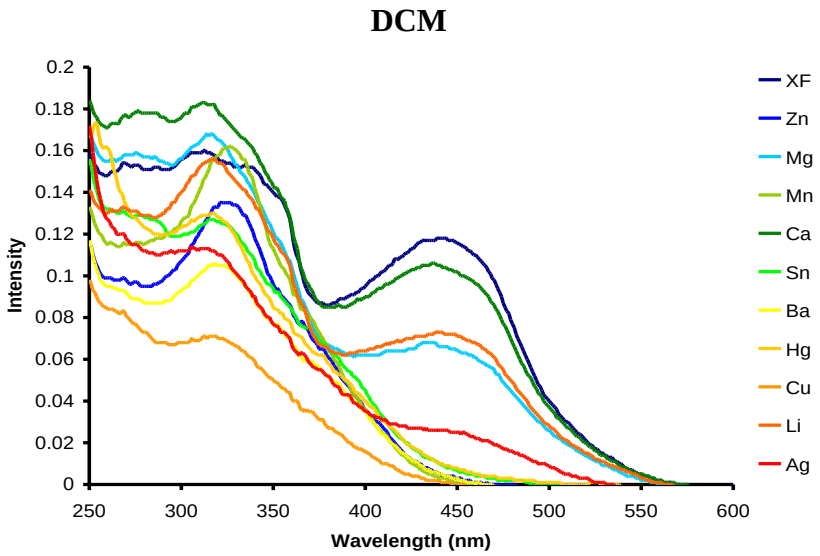

Figure 7.60. Absorption spectrum of **7.7** with metals in dichloromethane.

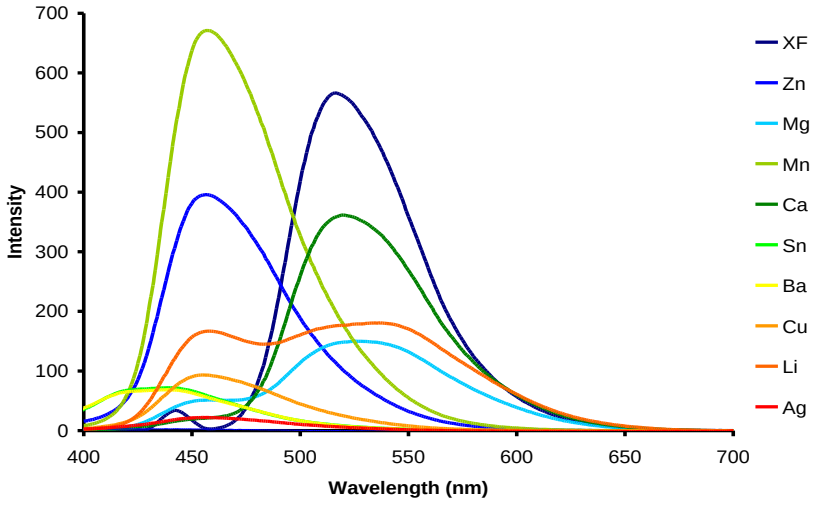

Figure 7.61. Emission spectrum of **7.7** with metals in dichloromethane.

7.5 References

1. (a) Pond, S. J. K.; Tsutsumi, O.; Rumi, M.; Kwon, O.; Zojer, E.; Bredas, J. L.; Marder, S. R.; Perry, J. W. *J. Am. Chem. Soc.* **2004**, *126*, 9291–9306. (b) Lim, N. C.; Freake, H. C.; Bru¨ckner, C. *Chem.—Eur. J.* **2005**, *11*, 38–49. (c) Pearce, D. A.; Jotterand, N.; Carrico, I. S.; Imperiali, B. *J. Am. Chem. Soc.* **2001**, *123*, 5160–5161. (d) Burdette, S. C.; Walkup, G. K.; Spingler, B.; Tsien, R. Y.; Lippard, S. J. *J. Am. Chem. Soc.* **2001**, *123*, 7831–7841. (e) Walkup, G. K.; Burdette, S. C.; Lippard, S. J.; Tsien, R. Y. *J. Am. Chem. Soc.* **2000**, *122*, 5644–5645. (f) Hirano, T.; Kikuchi, K.; Urano, Y.; Higuchi, T.; Nagano, T. *J. Am. Chem. Soc.* **2000**, *122*, 12399–12400. (g) Hirano, T.; Kikuchi, K.; Urano, Y.; Nagano, T. *J. Am. Chem. Soc.* **2002**, *124*, 6555–6562. (h) Komatsu, K.; Kikuchi, K.; Kojima, H.; Urano, Y.; Nagano, T. *J. Am. Chem. Soc.* **2005**, *127*, 10197–10204. (i) Kawabata, E.; Kikuchi, K.; Urano, Y.; Kojima, H.; Odani, A.; Nagano, T. *J. Am. Chem. Soc.* **2005**, *127*, 818-819.

2. (a) Hofer, A. M.; Machen, T. E. *Proc. Natl. Acad. Sci. U.S.A.* **1993**, *90*, 2598–2602. (b) Sensi, S. L.; Canzoniero, L. M. T.; Yu, S. P.; Ying, H. S.; Koh, J. Y.; Kerchner, G. A.; Choi, D. W. *J. Neurosci.* **1997**, *17*, 9554–9564. (c) Zhao, M. D.; Hollingworth, S.; Baylor, S. M. *Biophys. J.* **1996**, *70*, 896–916. (d) Metten, B.; Smet, M.; Boens, N.; Dehaed, W. *Synthesis* **2005**, 1838–1844. (e) Zhou, Z.; Fahrni, C. J. *J. Am. Chem. Soc.* **2004**, *126*, 8862–8863. (f) Yang, L. C.; McRae, R.; Henary, M. M.; Patel, R.; Lai, B.; Vogt,S.; Fahrni, C. J. *Proc. Natl. Acad. Sci. U.S.A.* **2005**, *102*, 11179–11184. (g) Cody, J.; Fahrni, C. J. *Tetrahedron* **2004**, *60*, 11099–11107. (h) Corradini, R.; Dossena, A.; Galaverna, G.; Marchelli, R.; Panagia, A.; Sartor, G. *J. Org. Chem.* **1997**, *62*, 6283–6289.

3. Merchant, S. G. Z. M.; Cheng, G. *Characterization of Foods: Emerging Methods* (Ed.: A. G. Gaonkar), Elsevier Science, New York, 1995, Chapter 15.

4. (a) Greene, N. T.; Shimizu, K. D. *J. Am. Chem. Soc.* **2005**, *127*, 5695 – 5700. (b) Mertz, E.; Zimmerman, S. C. *J. Am. Chem. Soc.* **2003**, *125*, 3424 – 3425.

5. Yeh, C.; Lin, S.; Hwang, D. *J. Food Drug Anal.* **2004**, *12*, 128 –132.

6. (a) Rakow, N. A.; Sen, A.; Janzen, M. C.; Ponder, J. B.; Suslick, K. S. *Angew. Chem.* **2005**, *117*, 4604 –4608; *Angew. Chem. Int. Ed.* **2005**, *44*, 4528 –4532. (b) Suslick, K. S.; Rakow, N. A.; Sen, A. *Tetrahedron* **2004**, *60*, 11133 –11138. (c) Rakow, N. A.; Suslick, K. S. *Nature* **2000**, *406*, 710 – 713. (d) Freund, M. S.; Lewis, N. S. *Proc. Natl. Acad. Sci. USA* **1995**, *92*, 2652 –2656. (e) Wright, A. T.; Anslyn, E. V. *Chem. Soc. Rev.* **2006**, *35*, 14– 28. (f) Vlasov, Y.; Legin, A.; Rudnitskaya, A. *Pure Appl. Chem.* **2005**, *77*, 1965 –1983. (g) Deisingh, A.; Stone, K.; Thompson, D. C. *Int. J. Food Sci. Tech.* **2004**, 39, 587 –604. (h) Lavigne, J. J.; Anslyn, E. V. *Angew. Chem.* **2001**, *113*, 3212 –3225; *Angew. Chem. Int. Ed.* **2001**, *40*, 3118 – 3130. Lu, G.; Grossman, J. E.; Lambert, J. B. *J. Org. Chem.* **2006**, *71*, 1769-1776.

7. (a) Rossi, S.; Lee, C.; Ellis, P. C.; Pivarnlik, L. F. *J. Food Sci.* **2002**, *67*, 2056 – 2060. (b) Ruiz-Capillas, C.; Moral, A. *J. Food Sci*. **2001**, 66, 1030 – 1032. (c) Ritchie, A. H.; Mackie, I. M. *Advances in Fish Science and Technology* (Ed.: J. J. Connell), Fishing News , Farnham (UK), **1980** pp. 489 – 494.

8. Zucchero, A. J.; Wilson, J. N.; Bunz, U. H. F. *J. Am. Chem. Soc.* **2006**, *128*, 11872 11881.

9. (a) McGrier, P. L.; Solntsev, K. M.; Schönhaber, J.; Brombosz, S. M.; Tolbert, L. M.; Bunz, U. H. F. *Chem. Commun.* **2007**, 2127 –2129. (b) McGrier, P. L.; Solntsev, K. M.; Miao, S.; Tolbert, L. M.; Miranda, O. R.; Rotello, V. M.; Bunz, U. H. F. *Chem. Eur. J.* **2008**, *14*, 4503-4510.

10. Brombosz, S.; Zucchero, A. J.; McGrier, P. L.; *J. Org. Chem.* **2009**, *74*, 8909-8913.

11. Hauck, M.; Schönhaber, J.; Zucchero, A. J.; Hardcastle, K. I.; Müller, T. J. J.; Bunz, U. H. F. *J. Org. Chem.* **2007**, *72*, 6714-6725.

12. The Contrast Colour Analyzer program is freeware and can be downloaded from http://www.visionaustralia.org.au/info.aspx?page=1985. Accessed 06/14/2010.

13. (a) Brereton, R. G. *Chemometrics: Data Analysis for the Laboratory and Chemical Plant*, Wiley, New York, 2003; (b) Albert, K. J.; Lewis, N. S.; Schauer, C. L.; Sotzing, G. A.; Stitzel, S. E.; Vaid, T. P.; Walt, D. R. *Chem. Rev.* **2000**, *100*, 2595 –2626.

14. "A Guide to Recording Fluorescence Quantum Yields." Horiba Jobin Yvon Ltd. Available online: http://www.jobinyvon.co.uk/ukdivisions/Fluorescence/plqy.htm. Accessed 06/14/2010.

15. Zucchero, A.J.; Tolosa, J.; Tolbert, L.; Bunz, U. H. F. *Chem. Eur. J.* **2009**, *15*, 13075-13081.

16. (a) Lewis, F. D.; Crompton, E. M. *J. Am. Chem. Soc.* **2003**, 125, 4044–4045. (b) Lewis,F. D.; Sinks, L. E.; Weigel, W.; Sajimon, M. C.; Crompton, E. M. *J. Phys. Chem. A*, **2005**, *109*, 2443–2451. (c) Tolbert, L. M.; Solntsev, K. M. *Acc. Chem. Res.* **2002**, *35*, 19–27. (d) Solntsev, K. M.; McGrier, P. L.; Fahrni, C. J.; Tolbert, L. M.; Bunz, U. H. F. *Org. Lett.* **2008**, *10*, 2429-2432.

Chapter 8

Conclusions and Future Work

8.1 Summary and Conclusions

This dissertation outlines our preliminary examination of hydroxy-substituted XFs, including their synthesis, investigation of their photophysical properties, and evaluation of their sensory responses upon exposure to aliphatic amines. This work highlights the benefits of utilizing the two-dimiensional cross-conjugated architecture of XFs for sensory applications.[1] However, XFs have also been employed as building blocks in supramolecular coordination assemblies[2] and used in the development of molecular electronics.[3]

The foundation for hydroxy XFs began with the synthesis of *para*- and *meta*-substituted hydroxy XFs and examination of their photophysical properties (Chapter 2). These investigations demonstrated that the deprotonation of *meta*-substituted hydroxy XFs leads to quenching, while a red-shifted absorption and emission is observed in the case of the *para*-substituted compound. This is explained by their spatially separated FMOs, which allows the HOMO and LUMO to localize on the orthogonal arms of XFs. In the case of *para*, the HOMO and LUMO show spatial overlap in the central ring. In the case of *meta*, the HOMO is localized only on the two phenolate rings, thus explaining the quenching of fluorescence. We also discovered that hydroxy XFs are responsive to amines.

In Chapter 3, we reported the synthesis and photophysical properties of bis(hydroxystyryl)benzenes. We investigated their photophysics in comparison to simple

hydroxystilbenes, which exhibit enhanced photoacidity in the case of the *meta*-substituted hydroxystilbene.[4] We discovered that although bis(hydroxystyryl)benzenes do not exhibit enhanced photoacidity in there excited-states, they do behave as weak photoacids. The photophysics of both chromophores are different not only from each other, but also from hydroxystilbenes. The photophysical properties of bis(hydroxystyryl)benzenes are also similar to those observed for hydroxy XFs.

Chapter 4 reported an extensive solvatochromic study of hydroxy XFs and their response to amines in various solvents. We explored the photophysics of di- and tetra-substituted hydroxy XFs in different polar protic, aprotic and non polar solvents. We discovered that the tetrahydroxy XF forms a sensor array in different solvents, which is based on the excited-state proton transfer (ESPT) to amines. These experiments demonstrate that one can create a "chemical nose" for amines by using only one molecule.

In Chapter 5, we utilized functionalized mesoporous silica particles as solid supports for pyridine, dialkylamino, and hydroxy substituted XFs. Since crystalline XFs display weak emission in the solid state, we decided to immobilize XFs in/on these particles. To our surprise, we discovered that not only do these XFs retain there highly fluorescent properties, but they are also responsive to amines and organic acids. This event is modulated by the functionalization present on the silica scaffold.

In Chapter 6, we investigated the photophysical properties and acidochromicity of hydroxy and dibutylamino-substituted arylethynylbenzenes. We compared their properties to hydroxy and dibutylamino-functionalized distyrylbenzenes using a Kamlet-Taft[5] analysis and solvatochromic studies. The studies show that protonated dibutylamino

bisaryethynylbenzenes and distyrylbenzenes display similar photophysical behavior to their hydroxy congeners, while deprotonated hydroxy-substituted bisaryethynylbenzenes and distyrylbenzenes display different photophysical properties from dibutylamino compounds of the like. The differences stem from each compounds interaction with the chemical environment.

Finally, in Chapter 7 we highlight the photophysics, amine and metalloresponsive properties of hydroxy-dialkylaniline XFs. We demonstrate that hydroxy and dibutylaniline functional groups can be attached to cross-conjugated architectures to elicit changes in emission color upon exposure to acid and base. The properties are mediated by the destabilization and stabilization of the HOMO and LUMO of the XFs, respectively. This allows a two-stage probe to be designed that can be used to detect amines in different chemical environments, and distinguish between which metal cations are present in solution.

These explorations have highlighted the fundamental photophysical properties of hydroxy-substituted bisarylethynylbenzenes, distyrylbenzenes, and XFs. In the case of XFs, we show that two-dimensional cross-conjugated materials offer photophysical properties that are more promising than one-dimensional molecular wire-type fluorophores.[6] These studies touch on the vast potential of the functional responsive ratiometric cores of XFs, and provide a blueprint for the development of advanced functional solid state materials for sensory applications.

8.2 Future Direction

8.2.1 Design of XF Polymer Beads for the Detection of VOCs

We have demonstrated that XFs can be supported on functionalized silicon surfaces to create materials that are responsive to external stimuli such as organic acids and amines (Chapter 5). In order to further develop this proof-of-principle essay, we have began synthesizing XFs on polymer resins to create solid state materials that are highly fluorescent and readily available in gram quantities. These materials can be synthesized starting with a commercially available formyl-substituted polystyrene resin and implementing a similar synthetic methodology used for previous XFs (Scheme 8.1). This strategy can be utilized to design a library of fluorescent solid state materials that can be used to detect volatile organic compounds (VOCs) in the gas phase.

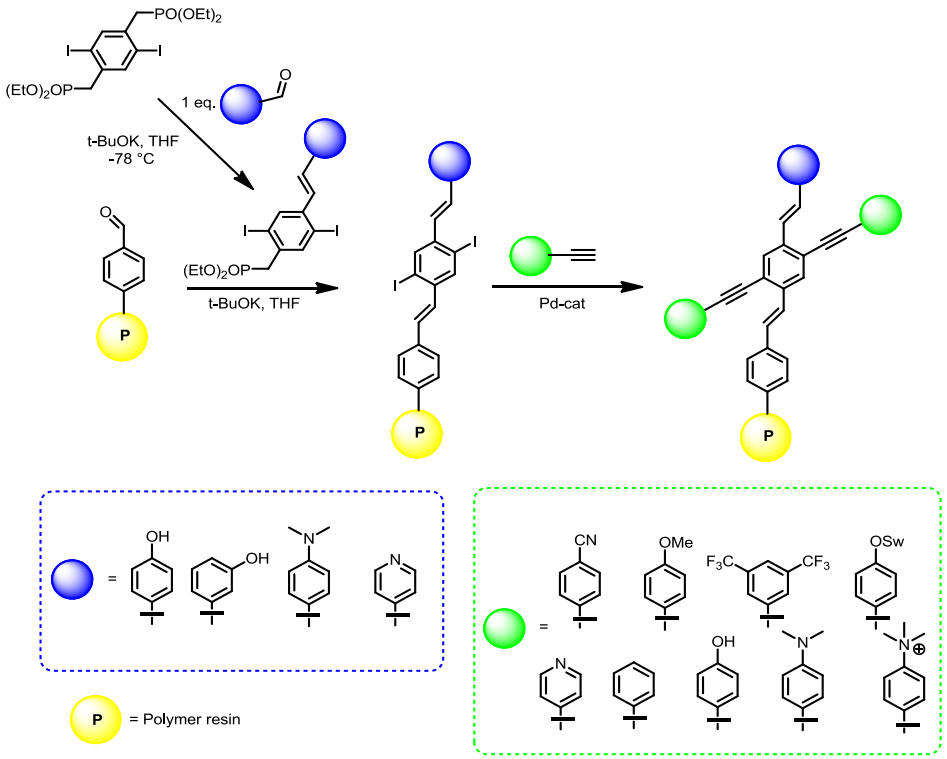

Scheme 8.1. Synthesis of XF polymer beads.

Utilizing the synthetic scheme shown in Scheme 8.1, we have been successful in making hydroxy- and dimethylamino-substitued XF polymer beads. Figure 8.1 displays the emission spectrum and fluorescent responses of both XF polymer beads upon the addition of trifluoroacetic acid (TFA) and ethylenediamine (EDA). These XF polymer beads yield materials that are highly fluorescent and responsive to acidic and amine vapors. Polymer XF **8.1** experiences a blue-shift in emission in the presence of TFA vapors, while **8.2** displays a large ~100 nm red-shift in the presence of EDA vapors. Further studies are being conducted to design various donor-donor, donor-acceptor, and acceptor-acceptor XF polymer bead systems to determine if the emission of these beads can be tuned to cover the entire visible spectrum. This work will also unveil the potential of XF polymer beads to detect the presence of different amine and acidic vapors with marked selectivity. Such investigations are currently in progress and will be reported in the future.

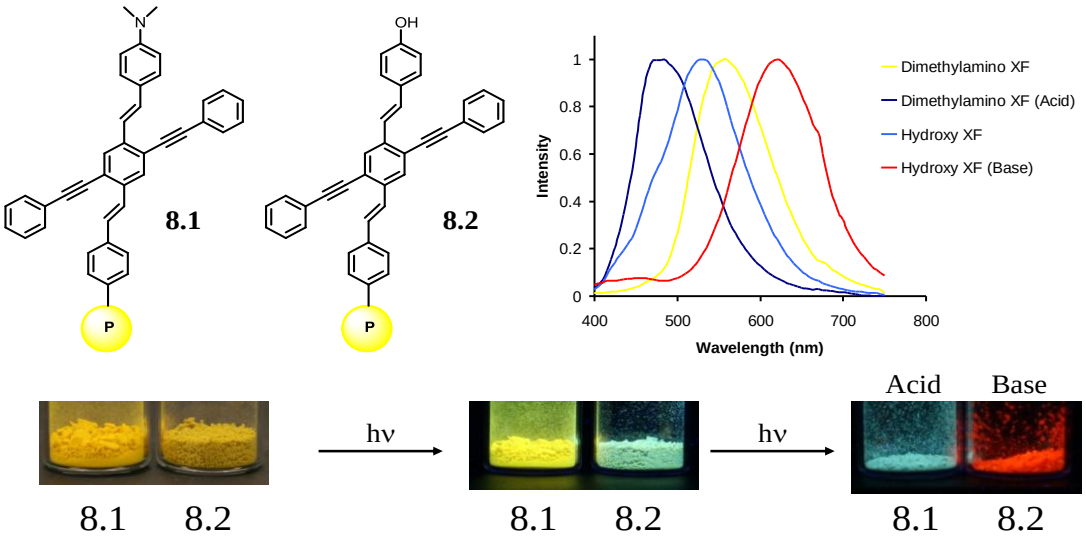

Figure 8.1. Emission spectrum and photographs of **8.1** and **8.2** XF polymer beads taken in the dark upon irradiation with a hand- held UV-lamp at λ= 366 nm before and after the addition of TFA and EDA vapors.

8.3 References and Notes

1. (a) Wilson, J. N.; Bunz, U. H. F. *J. Am. Chem. Soc.* **2005**, *127*, 4124-4125. (b) Zucchero, A. J.; Wilson, J. N.; Bunz, U. H. F. *J. Am. Chem. Soc.* **2006**, *128*, 11872-11881. (c) Tolosa, J.; Zucchero, A. J.; Bunz, U. H. F. *J. Am. Chem. Soc.* **2008**, *130*, 6498-6506. (d) Brombosz, S. M.; Zucchero, A. J.; Phillips, R. L.; Vazquez, D.; Wilson, A.; Bunz, U. H. F. *Org. Lett.* **2007**, *22*, 4519-4522. (e) Hauck, M.; Schönhaber, J.; Zucchero, A. J.; Hardcastle, K. I.; Müller, T. J. J.; Bunz, U. H. F. *J. Org. Chem.* **2007**, *72*, 6714-6725. (f) McGrier, P. L.; Solntsev, K. M.; Schönhaber, J.; Brombosz, S. M.; Tolbert, L. M.; Bunz, U. H. F. *Chem. Commun.* **2007**, 2127 – 2129. (g) McGrier, P. L.; Solntsev, K. M.; Miao, S.; Tolbert, L. M.; Miranda, O. R.; Rotello, V. M.; Bunz, U. H. F. *Chem. Eur. J.* **2008**, *14*, 4503-4510.(h) Zucchero, A.J; McGrier, P. L.; Bunz, U. H. F. *Acc. Chem. Res.* **2010**, *43*, 397-408.

2. (a) Gerhardt, W. W.; Zucchero, A. J.; Wilson, J. N.; South, C. R.; Bunz, U. H. F.; Weck, M. *Chem. Commun.* **2006**, 2141-2143. (b) Gerhardt, W. W.; Zucchero, A. J.; South, C. R.; Bunz, U. H. F.; Weck, M. *Chem. Eur. J.* **2007**, *13*, 4467-4474.

3. (a) Grunder, S.; Huber, R.; Horhoiu, V.; González, M. T.; Schönenberger, C.; Calame, M.; Mayor, M. *J. Org. Chem.* **1997**, *72*, 8337-8344.

4. (a) Lewis, F. D.; Crompton, E. M. *J. Am. Chem. Soc.* **2003**, *125*, 4044–4045. (b) Crompton, E. M.; Lewis, F. D. *Photochem. Photobiol. Sci.* **2004**, *3*, 660–668. (c) Lewis, F. D.; Sinks, L. E.; Weigel, W.; Sajimon, M. C.; Crompton, E. M. *J. Phys. Chem. A* **2005**, *109*, 2443–2451.

5. Kamlet, M. J.; Abboud, J. L. M.; Abraham, M. H.; Taft, R.W. *J. Org.Chem.* **1983**, *48*, 2877 –2887.

6. (a) Opsitnick, E.; Lee, D. *Chem. Eur. J.* **2007**, *13*, 7040-7049. (b) Galbrecht, F.; Bünnagel, T.; Bilge, A.; Scherf, U.; Farrell, T. Cruciform-Conjugated Oligomers. In *Functional Organic Materials – Syntheses, Strategies, and Applications;* Müller, T. J. J., Bunz, U. H. F., Eds.; Wiley-VCH: Heidelberg, **2007**, 83-118.